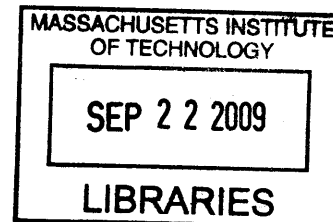


Development of Selective Peptide- and Protein-Based Reporters of Kinase Activity Utilizing Chelation-Enhanced Fluorescence

by

Elvedin Luković

B.A. Chemistry,
Haverford College, 2002



Submitted to the Department of Chemistry
in Partial Fulfillment of the Requirements for the
Degree of Doctor of Philosophy

ARCHIVES

at the

Massachusetts Institute of Technology

July 2009

© 2009 Massachusetts Institute of Technology
All rights reserved

Signature of Author: _____

✓
/ -

Department of Chemistry
July 24, 2009

Certified by: _____

Barbara Imperiali
Class of 1922 Professor of Chemistry and Professor of Biology
Thesis Supervisor

Accepted by: _____

Robert W. Field
Haslam and Dewey Professor of Chemistry
Chairman, Departmental Committee on Graduate Students

This doctoral thesis has been examined by a committee of the Department of Chemistry as follows:

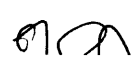
Sarah E. O'Connor
Chair

Latham Family Career Development Associate Professor of Chemistry
Massachusetts Institute of Technology



Barbara Imperiali
Thesis Supervisor

Class of 1922 Professor of Chemistry and Professor of Biology
Massachusetts Institute of Technology



Timothy F. Jamison

Professor of Chemistry
Massachusetts Institute of Technology



Development of Selective Peptide- and Protein-based Reporters of Kinase Activity Utilizing Chelation-enhanced Fluorescence

by
Elvedin Luković

Submitted to the Department of Chemistry
on July 24, 2009 in partial fulfillment of the
requirements for the Degree of Doctor of Philosophy
in Organic Chemistry

Abstract

Catalyzed by kinases, serine/threonine and tyrosine phosphorylation is a vital mechanism of intracellular regulation and is involved in nearly every aspect of normal, as well as aberrant, cell function. With more than 500 protein kinases present in the human genome, the need for probes that can *rapidly* and *selectively* report the activity of a single kinase or a discreet subset of related kinases is crucial, particularly as researchers move to increasingly complex, and more relevant, systems to study the effects of dysregulated kinase behavior.

We previously developed sulfonamido-oxine (Sox)-based fluorescent peptides following a β -turn focused (BTF) design. Upon phosphorylation of the Sox-containing peptide, the chromophore binds Mg^{2+} and undergoes chelation-enhanced fluorescence (CHEF). However, due to the BTF design limitation, only residues C- or N-terminal to the phosphorylated residue were used to specify the target kinase. To address this drawback, the recognition-domain focused (RDF) strategy, which also relies on CHEF, has been developed. In this approach, the Sox sensing moiety is introduced on the cysteine side chain (C-Sox), thereby allowing inclusion of extended kinase binding determinants, which are used to construct chemosensors for multiple Ser/Thr and Tyr kinases with greatly enhanced selectivity. Moreover, a high throughput mass spectrometry-based screening method that builds additional selectivity into RDF Sox-based probes for Ser/Thr kinases was also developed. Using this approach, it should be possible to construct short peptide probes with enhanced catalytic efficiency for virtually any kinase.

To expand the scope of CHEF-based sensors, beyond kinases that derive specificity from the short consensus sequence, a highly selective ERK sensor was prepared via semisynthesis by combining a recombinant kinase docking domain, PNT, with a synthetic sensing module that included the Sox chromophore. This probe was used to exclusively monitor ERK1/2 activity in unfractionated cell lysates in the absence of off-target kinase inhibitors. Furthermore, to improve the photophysical properties of the probes for cellular studies, we developed several oxine-based CHEF chromophores utilizing numerous approaches including the versatile click chemistry. The most promising derivative, *p*-bromophenyltriazoyl-oxine (Clk), displays a significant bathochromic shift in the excitation (15 nm) and emission (40 nm) maxima compared to Sox, and efficiently reports kinase activity when incorporated into peptides as a C-Clk residue.

Together, the results presented in this thesis indicate the power that the CHEF-based sensors have to selectively, rapidly and with great sensitivity deliver new insight into the role of in vitro and endogenous kinases in various processes and under a variety of circumstances.

Thesis Supervisor: Barbara Imperiali

Title: Class of 1922 Professor of Chemistry and Professor of Biology

Dedication/Posveta

Dragi Tata,

*Zbog tvoje neizmjerne ljubavi, doživotnog žrtvovanja i neprestane podrške,
ovu disertaciju posvećujem tebi.*

Tvoj sin, Elvedin

Acknowledgements

Most importantly, I would like to thank my advisor, Professor Barbara Imperiali, for welcoming me into the lab and for teaching me how to tackle difficult problems. Barbara, I admire your insight, your breath of knowledge and your ability to run a group with many diverse projects spanning biology and chemistry. Through my interactions with you and the incredibly gifted team of scientists that you assembled, I have learned a tremendous amount. I am particularly thankful for your support in my next step and for the compassion and understanding that you show in all matters. I also thank my chair Professor Sarah O'Connor and committee member Professor Tim Jamison, for your advice and help throughout my tenure at MIT.

The work described in this thesis would not be possible without several key people. Melissa Shults was instrumental in starting the kinase sensing project and taught me how to be a rigorous analytical chemist. Dr. Dora Carrico-Moniz was never too busy to share her vast synthetic knowledge, and Dr. Juan Antonio González Vera was always able to cheer me up as we worked late together. Beth Vogel has not only been an instrumental collaborator, but also welcomed me to Boston when I did not know anybody here. Lastly, none of my peptides would have been properly characterized without Dr. Matthieu Sainlos' willingness to run to MALDI at all hours of day or night for me. Thank you all for your help.

For the past 7 years the Imperiali lab has been home not only to me, but also to an incredible group of coworkers and friends. For accompanying me to the Muddy and keeping me sane I have to thank Mary O'Reilly, Eranthie Weerapana, Galen Loving, Matthieu Sainlos and Angelyn Larkin. My favorite Sri Lankan (aka Eranthie), I have always appreciated and tried to imitate your confidence and poise—so much that I nearly followed you to the West Coast. Mary, through the -30 Fahrenheit wind tunnel of Galileo Galilei Way to blistering heat of 28-30 Plymouth St., you've always been there on my walk home with me, even when you moved 3000 miles away. Galen, you are one of the funniest people with the best stories (despite their length). Because of you I feel bad for Rick Santorum and am excitedly trying to play the trombone (rusty or not); you made the past 6 years much more interesting. Matthieu, I admire your clear-headedness and willingness to talk about science at any time. Plus, around you I feel like I am in a French film. Angelyn, thank you for everything, from late nights at your house to HPLCing with me to much (loud) laughter. You wonder what you'll do without me, but the real question is how I will get on in med school without you?! Drs. Kathy Franz and Mark Nitz, thank you for the encouragement to pursue graduate school when I first got to MIT. Dr. Jebrell Glover, you always put life into perspective with a song recitation. Dr. Bianca Sculimbrene, no one could argue with your reasoning and your sound advice kept coming even after you left. Dr. Anne Reynolds, you are the best editor that I have ever met; thanks for all the help, from papers to personal statements. Brenda Goguen, I'm going to miss our late night conversations and ruminations on all matters—scientific and otherwise. Meredith Hartley, I truly admire your positive attitude and outlook on life. Wendy Iskenderian, thanks for all the tasty baked treats. Langdon Martin, thank you for keeping us entertained with your minimeeting slides. Dr. Jay Troutman, I appreciate your willingness to teach and to listen to Angelyn and me yammer incessantly in your pod. Dr. James Morrison, it's been fun to have a running buddy with whom I shared the agony of marathon training. Good luck with future races. Marcie Jaffee, my favorite second year, you have been an awesome pod-mate. Thanks for great, although sometimes heated, conversations. Dr. Cliff Stains, I am glad to have another Sox-mate; I know that you will keep the project going with exciting new experiments. Susana Gordo, thanks for all the fun trips—

keep them coming. Debby Pheasant, I enjoyed our many interesting lunch-time conversations. Mike Morrison and Michelle Chang, good luck in grad school, although I'm sure you won't need much of it. Of course, I have to thank Elizabeth Fong and Susan Brighton for all that you do to keep the lab and department running smoothly. To all the past members: Carlos Bosques, Maria Ufret, Debbie Rothman, Mayssam Ali, Rob Dempsey, Dr. Eugenio Vazquez, Dr. Christina Carrigan, Dr. Christian Hackenberger, Dr. Guofeng Zhang, Ryu Roshida, Dr. Nelson Olivier, Katja Barthelmes, Dr. Andreas Aemissegger Dr. Melanie Bonnekessel, Mark Chen and Seungjib Choi, it has been an absolute pleasure working with you and learning from you.

An enormous thank-you to all my eagle-eyed thesis proof-readers: Angelyn, Brenda, Matthieu, Meredith, Wendy and, of course, Barbara. You are to blame if there are spelling errors!

Outside of lab I have also been surrounded with wonderful people to whom I am forever indebted. Without my chemistry professors at Haverford College, particularly Karin Åkerfeldt and Fran Blase, who sparked my interest in organic chemistry, I would not be here. The "Asian girls," Satoko Hirai, HuiWon Choi and Sunghye Son have been with me through all the trials of first year. Our Friday lunches were highlights of my week. Thanks for making our start much more fun. Liz Young, we met during our first day of college 11 years ago and have proceeded to live in rooms next to each other for 10 of those years. We have been through the roller-coaster ride of college and grad school and I cherish our friendship. I am not sure how I will adjust to living without you! Kate Cichucki, Elena Guarinello and Karen Ballantyne, you have provided much needed support from various places in the country. Thank you for always listening to me on my long rides from Boston to NYC. To my other Bosnian, Rusmir, you made this journey so much more fun; from LOST to Salon nights all your efforts have had a captive audience. Lastly, to the Moores (Dick, Barbara, Annie, Meredith, Alec), you have always been my home away from home. With doors to your house and family always open to me, I have been able to thrive here. I cannot express enough gratitude for all that you provided, taught and showed me. Thank you from the bottom of my heart.

Michael Kieffer, I admire your easy-going nature, and appreciate your support and frankness. No matter what Beyoncé says, you are truly irreplaceable. Thank you for putting up with me.

Također se moram zahvaliti Jeleni i Faki za sve što su za mene uradili ovih godina, od vožnje na fakultet pa do širkogradnog dostavljanja organske hrane. A naravno dobrodošlicu želim mom Mukiju i njenom najnovijem dodatku našoj porodici. Napokon, svim mojim prijateljima i porodici od Majdana pa do Zavidovića, Zenice, Sarajeva, Plava, Švedske, Norveške i Njujorka moram se duboko i srdačno zahvaliti na velikom i pozitivnom doprinosu ka mom razvoju. Na kraju, naravno najveću zahvalnicu zaslužuju Mama, Tata, Dženana i Sanida. Bez vas ova disertacija ne bi bila privedena kraju, a možda ni započeta. Mama, ti si uvijek bila moja inspiracija. Tvoj trud, neprekidna volja za rad i želja za znanjem su me uvijek podsticali da doznam što višestruki stupanj obrazovanja. Nije ni čudo što ću na jesen da krenem u 23. razred! Dženi, tvoj samouvjereni duh i samostalnost su me stalno impresionirali i ponekad ostavljali bez daha. Želim da budeš sretna u životu i da pronađeš ono za čim tragaš. Dečče, tvoja ogromna odgovornost, pažnja i odanost porodici i prijateljima će te dobro služiti u bilo kojoj budućoj karijeri. Nadam se da ćeš uživati u ostatku fakultetskih godina i da ćemo se svi naći na okupu u Njujorku ubrzo. Tata, tvoj intelekt i analitički duh su naravno imali jak i konstantan uticaj na mene i moj razvoj kao naučnika. Želim ti rapidno i potpuno ozdravljenje uz svoje najbliže. Iz dubine duše sam zahvalan svima vama na neuvjetnoj ljubavi, podršci i razumijevanju.

Table of Contents

Abstract.....	3
Dedication/Posveta	4
Acknowledgements.....	5
Table of Contents.....	7
List of Figures.....	10
List of Schemes.....	12
List of Tables	13
List of Abbreviations	15
Chapter 1. Introduction	18
Protein Phosphorylation.....	19
Detection of Kinase Activity	23
Kinase Specificity	29
Dissertation Objectives.....	33
References.....	36
Chapter 2. Improving the Kinetics of Peptide-Based Kinase Substrates through Recognition-Domain Focused Design	39
Introduction.....	40
Results and Discussion	42
Synthesis of RDF Sensors.....	42
Chromophore Positioning in the RDF Design.....	44
Fluorescence Properties of RDF Probes	47
Fluorescence Intensity Dependence on [ATP] and [Mg ²⁺].....	49
Origin of Fluorescence Increase	51
Fluorescence Difference under Biochemical Assay Conditions.....	53
Fluorescence Increase Corresponds to Product Formation.....	54
Comparison of Kinetic Parameters for BTF and RDF Chemosensors	55
Conclusions.....	59
Acknowledgements.....	60
Experimental Methods.....	61
NMR spectra	88
HPLC chromatograms	91
References.....	92
Chapter 3. Development of a Mass Spectrometry-Based Method for Rapid Discovery of Selective Recognition-Domain Focused Sensors	95
Introduction.....	96
Results and Discussion	99
Sensors for Protein Kinase C Isozymes	99

Sensors for Aurora A	103
Development and Validation of the MS-based Screening Method	116
Conclusions.....	122
Future Directions	123
Acknowledgments.....	123
Experimental Methods.....	124
References.....	137

Chapter 4. Highly Selective Chimeric Reporters for ERK1/2 in Cellular Media..... 140

Introduction.....	141
Results and Discussion	145
Semisynthesis of the Sox-PNT Sensor	145
Evaluation of the Sox-PNT Probe.....	148
Studies with Crude Cell Lysates	151
Direct Titrations of Inhibitor PEA-15 into EGF-stimulated Cell Lysates	154
Immunodepletion of ERK1/2 from EGF-stimulated Lysates	154
Microinjection of Sox-PNT into PtK-1 Cells	156
Membrane-Permeable Sox-PNT-TAT ERK1/2 Sensor.....	158
Membrane-Targeted Sox-PNT-CAAX ERK1/2 Sensor.....	160
Caging the Thr Side Chain to Provide Temporal Control of Phosphorylation.....	162
Conclusions.....	166
Acknowledgements.....	168
Experimental Methods.....	169
References.....	197

Chapter 5. Toward 8-Hydroxyquinoline Derivatives with Improved Photophysical Properties as Reporter Moieties for Phosphorylation 202

Introduction.....	203
Results and Discussion	207
Fused Tricyclic Derivatives of Oxn.....	209
Bicyclic Derivatives of Oxn.....	212
Synthesis and Screening of Triazole-substituted Oxn Derivatives.....	214
Synthesis and Biophysical Evaluation of Clk-based Peptidyl Kinase Substrates.....	217
Evaluation of Clk-based Substrates in Enzymatic Assays.....	220
Conclusions.....	221
Future Directions and Perspectives.....	222
Acknowledgements.....	224
Experimental Methods.....	225
General Information.....	225
Instrumentation and Materials	225
Synthesis and Characterization of Oxine derivatives	227
General Synthesis of the Triazolyl Derivatives 77a-v	228

Peptide Synthesis	232
Stock solutions	234
Fluorescence experiments	235
NMR Spectra	239
References	252
<i>Curriculum Vitae</i>	255

List of Figures

Chapter 1

Figure 1-1.	General scheme of kinase-catalyzed phosphoryl transfer.....	20
Figure 1-2.	A dendrogram of the human kinome.	21
Figure 1-3.	A scheme summarizing known interactions between constituents of cell-matrix adhesions.	23
Figure 1-4.	Sensing strategies employed to detect kinase activity.	26
Figure 1-5.	Strategies that protein kinases employ to gain specificity in vivo.....	30
Figure 1-6.	CHEF-based chemosensors.	35

Chapter 2

Figure 2-1.	Schematic representations of the BTF and RDF designs from optimized non-fluorescent substrates.....	41
Figure 2-2.	Structures of amino acids Sox (1) and C-Sox (2) that can be used to install the Sox chromophore.	42
Figure 2-3.	The effect of [ATP] on RDF probe fluorescence.....	50
Figure 2-4.	Mg ²⁺ titration curves.	52
Figure 2-5.	HPLC chromatogram of the PKA reaction with its RDF sensor after 616 sec of reaction time.	55
Figure 2-6.	Assays of PKCβI and PKCδ enzymes with RDF and BTF chemosensors.....	58

Chapter 3

Figure 3-1.	Reaction rates (slopes) of PKCα RDF substrate, PKCβI RDF substrate, PKCδ RDF substrate, and PKCα BTF substrate with PKC isozymes.	101
Figure 3-2.	Fold fluorescence difference at 0, 0.1 and 1.1 mM ATP for AurA-S15-S21.	108
Figure 3-3.	Activation of AurA by TPX2.....	109
Figure 3-4.	The activity of AurA measured with AurA-S6 in the presence (black bars) or absence (white bars) of TPX(2-43).	110
Figure 3-5.	Qualitative comparison of reaction rates of chemosensors with AurA.	111
Figure 3-6.	AurA docking models with test peptide (H ₂ N-RFSLC(Npl)A-CO ₂ H).....	113
Figure 3-7.	MS-based screening method to design selective substrates for Ser/Thr kinases.....	118
Figure 3-8.	MALDI-TOF spectrum of the peptide library at the -3 position after its incubation with PKA for 1 h and chemical derivatization with Ba(OH) ₂ /4-MEP.	120

Chapter 4

Figure 4-1.	The mechanisms of ERK-mediated cell proliferation or apoptosis.	142
Figure 4-2.	ERK utilizes the PNT domain of its substrate Ets-1 to drive specificity.	144
Figure 4-3.	The semisynthesis of the Sox-PNT sensor via NCL.....	147
Figure 4-4.	Fluorescence spectra of phosphorylated and unphosphorylated versions of Sox-Peptide and Sox-PNT sensors.	149
Figure 4-5.	In vitro characterization of Sox-PNT.....	151
Figure 4-6.	The EGF signaling pathway results in stimulation of ERK1/2 activity.....	152

Figure 4-7.	Specificity of the Sox-PNT sensor toward ERK1/2 in unfractionated cell lysates.....	153
Figure 4-8.	Half inhibitory concentration of PEA-15 with ERK1/2.	154
Figure 4-9.	ERK1/2 activity in immunodepleted and EGF-stimulated lysates.	155
Figure 4-10.	Overlaid, false-colored images of a panel of cells microinjected with Sox-PNT and Alexa Fluor 568-labeled dextran.	157
Figure 4-11.	Overlaid raw and false-colored images of a cell microinjected with Sox-PNT and Alexa Fluor 568-labeled dextran..	157
Figure 4-12.	The semisynthesis of the Sox-PNT-TAT sensor via NCL.....	159
Figure 4-13.	The semisynthesis of the Sox-PNT-CAAX sensor via NCL.....	161
Figure 4-14.	The rate of uncaging for Sox-Isopeptide.	166
Figure 4-15.	The GST-PNT-His ₆ product.	177
Figure 4-16.	Comparison of Sox-PNT and Sox-peptide as substrates for ERK2.....	182
Figure 4-17.	Detection of ERK1/2 activity by Sox-PNT in lysates from four cell lines.....	185
Figure 4-18.	Effects of DMSO on ERK1/2 activation.	186
Figure 4-19.	Specificity of substrates for ERK.	187
Figure 4-20.	Immunodepletion of ERK1/2.....	189
Figure 4-21.	The GB1-PNT-TAT-FGT-His ₆ product.	191
Figure 4-22.	The GST-PNT-FGT-His ₆ -CAAX product.	193

Chapter 5

Figure 5-1.	Derivatives of 8-hydroxyquinoline-based amino acids used to report kinase activity.....	205
Figure 5-2.	The novel C-Clk amino acid based on the Oxn core.	207
Figure 5-3.	Visual comparison of emission wavelengths and fluorescence intensity for some Oxn derivatives when complexed with Mg ²⁺	213
Figure 5-4.	Qualitative comparison of emission wavelengths of 77a-v	216
Figure 5-5.	Spectral characterization and enzymatic evaluation of Clk-based substrates.....	220

List of Schemes

Chapter 2

Scheme 2-1.	Synthesis of RDF Chemosensors on Solid Support and Using the Building Block Approach	44
-------------	--	----

Chapter 4

Scheme 4-1.	Synthesis of Caged Thr Amino Acid	163
Scheme 4-2.	Synthesis of Backbone-Caged Sox-Peptide.....	163
Scheme 4-3.	Synthesis of Sox-Isopeptide.....	164
Scheme 4-4.	Uncaging of Sox-Isopeptide and Spontaneous O to N acyl shift to form Sox-Peptide.....	165

Chapter 5

Scheme 5-1.	A General Representation of CHEF upon Divalent Metal Binding	204
Scheme 5-2.	Synthesis and Chemical Structures of Oxn Derivatives	208
Scheme 5-3.	Synthesis of BOxn	210
Scheme 5-4.	Installation of Dimethylsulfonamide and Oxidation to Quinone upon Methoxy Deprotection	211
Scheme 5-5.	1,3-Dipolar Cycloaddition Reactions of 75 with 76a-v	215
Scheme 5-6.	Synthesis of the Clk RDF Chemosensors	218
Scheme 5-7.	Synthesis of an Alternative Tricyclic Core.....	222
Scheme 5-8.	Synthesis of 5-ArylOxn Derivatives.....	223
Scheme 5-9.	Preparation of C5 Aryl-substituted BOxn.....	223
Scheme 5-10.	Peptide Incorporation of Oxn Derivatives	224

List of Tables

Chapter 1

Table 1-1.	Consensus Phosphorylation Sites of a Representative Sampling of Protein Kinases.....	31
------------	--	----

Chapter 2

Table 2-1.	Peptide Sequences Used to Determine Optimal Positioning of the Sox Chromophore in the RDF Design	45
Table 2-2.	Fluorescence Increase and Z' Factor Values for Ser/Thr and Tyr Kinase Substrates Described in Table 2-1	46
Table 2-3.	Comparison of Substrate Sequences and Fluorescence Increases for BTF and RDF Chemosensors.....	48
Table 2-4.	Effects of ATP Concentration on Fold Fluorescence Increase of RDF Chemosensors	50
Table 2-5.	Effects of $[Mg^{2+}]$ and $[ATP]$ on Fold Fluorescence Increase ^a of RDF Tyr Kinase Chemosensors	51
Table 2-6.	Peptide Sequences, Fluorescence Differences and Dissociation Constants for Mg^{2+}	52
Table 2-7.	Fold Fluorescence Increases of RDF Chemosensors Obtained from Substrate (f_S) and Phosphopeptide (f_P) Intensities under Appropriate Assay Conditions or Standard Conditions.....	54
Table 2-8.	HPLC and ESI-MS Verification and Quantification of Product Formation Observed by Fluorescence	55
Table 2-9.	Comparison of Kinetic Parameters Obtained with BTF and RDF Substrate Sequences Presented in Table 2-3.....	57

Chapter 3

Table 3-1.	Substrate Preferences of 9 PKC Isozymes.....	97
Table 3-2.	Kinetic Parameters of PKC RDF Chemosensors and the Parent Peptides	100
Table 3-3.	The Kinetic Parameters for PKC α RDF Substrate with PKC α , PKC β I and PKC θ Isozymes.....	102
Table 3-4.	Kinetic Parameters of PKC α Substrate with PKC α , PKC β I and PKC δ	102
Table 3-5.	Sequences of RDF Chemosensors for AurA	105
Table 3-6.	Fold Fluorescence Increase for Selected AurA Chemosensors	107
Table 3-7.	Select Chemosensors were Tested for Reactivity with AurA and AurB.....	115
Table 3-8.	Kinetic Parameters of Selected Chemosensors with AurA.....	116
Table 3-9.	Peptide Libraries for PKA	119
Table 3-10.	Peptide Libraries for AurA	121
Table 3-11.	Sequences and Kinetics of Sox-substrates for AurA	122

Chapter 4

Table 4-1.	Fold Fluorescence Increase of BTF and RDF Chemosensors in the Presence and Absence of ATP.....	148
Table 4-2.	Sequences Surrounding the TP Recognition Region (Red Residues) of the Wild Type Ets-1, MBP and Sox-PNT.....	148

Chapter 5

Table 5-1.	Relevant Spectroscopic Data for Selected Oxn Derivatives that Form Fluorescent Complexes with Mg ²⁺	214
Table 5-2.	Substrate Sequences of the RDF Chemosensors and Their Fluorescence Increases.....	219

List of Abbreviations

Standard 3-letter and 1-letter codes are used for the 20 natural amino acids.

Where D precedes the amino acid code, it indicates D-chirality.

Standard 1-letter codes are used for the nucleotides.

afu	arbitrary fluorescence unit
Abl	Abelson kinase
ADP	adenosine-5'-diphosphate
AFP	<i>Aequoria victoria</i> fluorescent protein
AIBN	azobisisobutyronitrile
ATP	adenosine-5'-triphosphate
AurA	Aurora kinase A
AurB	Aurora kinase B
BME	β -mercaptoethanol
Bn	benzyl
tBu	<i>t</i> -butyl
Boc	<i>t</i> -butoxycarbonyl
BOxn	10-hydroxy-2-methylquinoline
BSA	bovine serum albumin
BTF	β -turn focused
CamK	calmodulin-dependent protein kinase
CDK	cyclin-dependent kinase
CENP-A	centromere protein A
CHEF	chelation-enhanced fluorescence
CK	casein kinase
Clk	5-(4-(4-bromophenyl)-1 <i>H</i> -1,2,3-triazol-1-yl)-2-methylquinolin-8-ol
CPEB	cytoplasmic polyadenylation element-binding proteins
CPP	cell penetrating peptides
DAG	diacylglycerol
DIC	<i>N,N</i> -diisopropylcarbodiimide
DIEA	<i>N,N</i> -diisopropylethylamine
DMAP	4-dimethylaminopyridine
DMEM	dulbecco's modified eagle medium
DMF	<i>N,N</i> -dimethylformamide
DMNB	4,5-dimethoxy-2-nitrobenzyl
DMSO	dimethyl sulfoxide
DTT	dithiothreitol
ϵ	extinction coefficient or molar absorptivity
EDT	1,2-ethanedithiol
EDTA	ethylenediaminetetraacetic acid
EGFR	epidermal growth factor receptor
EGTA	glycol-bis(2-aminoethylether)- <i>N,N,N',N'</i> -tetraacetic acid
ERK1/2	extracellular signal-regulated kinase 1/2
ESI-MS	electrospray ionization mass spectrometry
Φ	quantum yield

Fmoc	9-fluorenylmethoxycarbonyl
FPLC	fast protein liquid chromatography
FPR	fluorescence plate reader
FTase	farnesyltransferase
GB1	immunoglobulin binding domain B1 of streptococcal protein G
GGTase	geranylgeranyltransferase
GSK3	glycogen synthase kinase-3
GST	glutathione-S-transferase
HeLa	cervical cancer cell line from Henrietta Lacks
HEPES	4-(2-hydroxyethyl)-1-piperazine ethane sulfonic acid
HIV-1	human immunodeficiency virus-1
HOAt	7-aza-1-hydroxybenzotriazole
HOBt	1-hydroxybenzotriazole
HPLC	high performance liquid chromatography
HRMS	high resolution mass spectrometry
HT29	human colon adenocarcinoma grade II cell line
IC ₅₀	half inhibitory concentration
IRK	insulin receptor kinase
JNK	c-Jun N-terminal kinase
k_{cat}	catalytic constant
K_D	dissociation constant
K_i	inhibition constant
K_M	Michaelis constant
λ_{em}	emission wavelength
λ_{ex}	excitation wavelength
MALDI-TOF MS	matrix-assisted laser desorption ionization time-of-flight mass spectrometry
MeCN	acetonitrile
4-MEP	4-mercaptoethylpyridine
MESNa	2-mercaptoethane sulfonate sodium
MK2	mitogen-activated protein kinase-activated protein kinase-2
Mmt	4-methoxytrityl
NBS	<i>N</i> -bromosuccinimide
NIH-3T3	mouse fibroblast cells
Nle	Norleucine
NMR	nuclear magnetic resonance
NMP	<i>N</i> -methylpyrrolidinone
NVOC	nitroveratryloxycarbonyl
Oxn	oxnie or 8-hydroxyquinoline
Pbf	2,2,4,6,7-pentamethyldihydrobenzofuran-5-sulfonyl
PBS	phosphate-buffered saline
Pdb	protein data bank
PET	photoninduced electron transfer
Pim2	proviral integration site kinase-2
PKA	protein kinase A or cAMP-dependent protein kinase
PKB/Akt	protein kinase B (aka Akt)

PKC	protein kinase C
PKD	protein kinase D
PS	phosphatidylserine
pSer	phosphoserine
PTD	protein transduction domain
pThr	phosphothreonine
pTyr	phosphotyrosine
PtK	<i>Potorus tridactylus</i> kidney cells
PyAOP	(7-azabenzotriazol-1-yloxy)tripyrrolidinophosphonium hexafluorophosphate
PyBOP	benzotriazol-1-yl-oxytripyrrolidinophosphonium hexafluorophosphate
Ras	rat sarcoma
Rce1	ras-converting enzyme
RDF	recognition-domain focused
RP-HPLC	reverse-phase high performance liquid chromatography
RT	room temperature
SDS-PAGE	sodium dodecyl sulfate polyacrylamide gel electrophoresis
s.e.m.	standard error of measurement
Sox-Br	2-bromomethyl-8- <i>t</i> -butyldiphenylsilyloxy-5-(<i>N,N</i> -dimethyl)sulfonamidoquinoline
SPPS	solid-phase peptide synthesis
Src	sarcoma kinase
std. dev.	standard deviation
TAT	transactivator of transcription
TBDMS	<i>t</i> -butyldimethylsilyl
TBDPS	<i>t</i> -butyldiphenylsilyl
TEV	tobacco etch virus
TFA	trifluoroacetic acid
TIS	triisopropylsilane
TLC	thin-layer chromatography
TMS	tetramethylsilane
TNBS	2,4,6-trinitrobenzene sulfonic acid
t_R	retention time
Tris	2-amino-2-hydroxymethyl-propane-1,3-diol
Trt	trityl
UV-Vis	ultraviolet-visible
Xaa	used to denote any amino acid
Vmax	maximum velocity
vol%	volume percent

Chapter 1. Introduction

Protein Phosphorylation

Normal cell function heavily depends on protein phosphorylation to accurately relay multifarious cues from the extracellular environment to appropriate cellular compartments and proteins.¹ By catalyzing the transfer of the γ -phosphoryl of adenosine-5'-triphosphate (ATP) onto Ser, Thr, and/or Tyr side chains of protein substrates, kinases have emerged as crucial regulators of this ubiquitous posttranslational modification.^{2,3} Kinases are broadly classified into two major groups: Ser/Thr and Tyr kinases, which are further divided into either nonreceptor or receptor kinases. Regardless of the classification, divalent metal ions, most commonly Mg^{2+} , are necessary for catalysis as they prime the nucleotide-triphosphate for nucleophilic attack by the alcohol⁴ (Figure 1-1). Although the phosphate group is relatively small compared to the remainder of the protein, the addition of a densely negatively charged phosphate moiety can drastically alter protein conformation, biochemical function and/or binding to partner proteins. These events, in turn, lead to further propagation of the signal until the target is reached. To efficiently signal the ever-changing extracellular environment, phosphorylation needs to be highly dynamic and temporally controlled; thus, cells also employ phosphatases to rapidly remove the phosphate modification. Together with kinases, phosphatases tightly regulate this ubiquitous and reversible post-translational modification in all eukaryotes.⁵

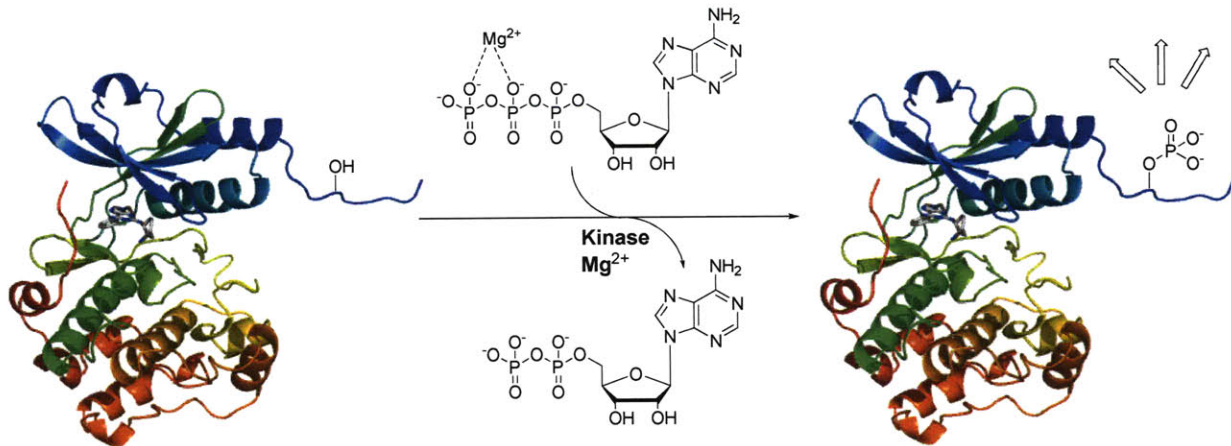


Figure 1-1. General scheme of kinase-catalyzed phosphoryl transfer. Hydrolysis occurs in the presence of Mg^{2+} , which is coordinated to the β and γ phosphates of ATP. ADP and the phosphoproduct are then released.

A recent study identified more than 500 different protein kinases encoded in the human genome (Figure 1-2), constituting nearly 2% of all genes.⁶ Ser/Thr kinases are more abundant (~400) than Tyr kinases, but not necessarily more important in cellular homeostasis. Both classes of kinases modulate aspects of protein function in many ways. They are involved in the control of subcellular localization, the degradation or stabilization of proteins, the assembly of multimeric protein complexes, and the allosteric regulation of biochemical activity (e.g., activation or repression of an enzyme or transcription factor).⁷ Because of the ubiquitous involvement of phosphoproteins in processes such as cell migration, proliferation, cell division, cell death, immunity, and learning and memory, protein kinases are also instrumental to the proper function of these listed processes as enzymes that control the generation of phosphoproteins.⁶⁻⁸ In addition, since kinases often phosphorylate proteins involved in several different biochemical pathways, their down- or up-regulation often has effects on the whole cell, rather than just a single pathway. For example, illustrated in Figure 1-3 are some of the dynamic interactions involved in cell migration that are mediated by kinases.⁹ Thus, due to the critical role

that kinases play in many aspects of cell function, it is not surprising that the misregulation of kinase activity is an underlying cause of many human diseases, from neurological disorders to cancer.¹⁰

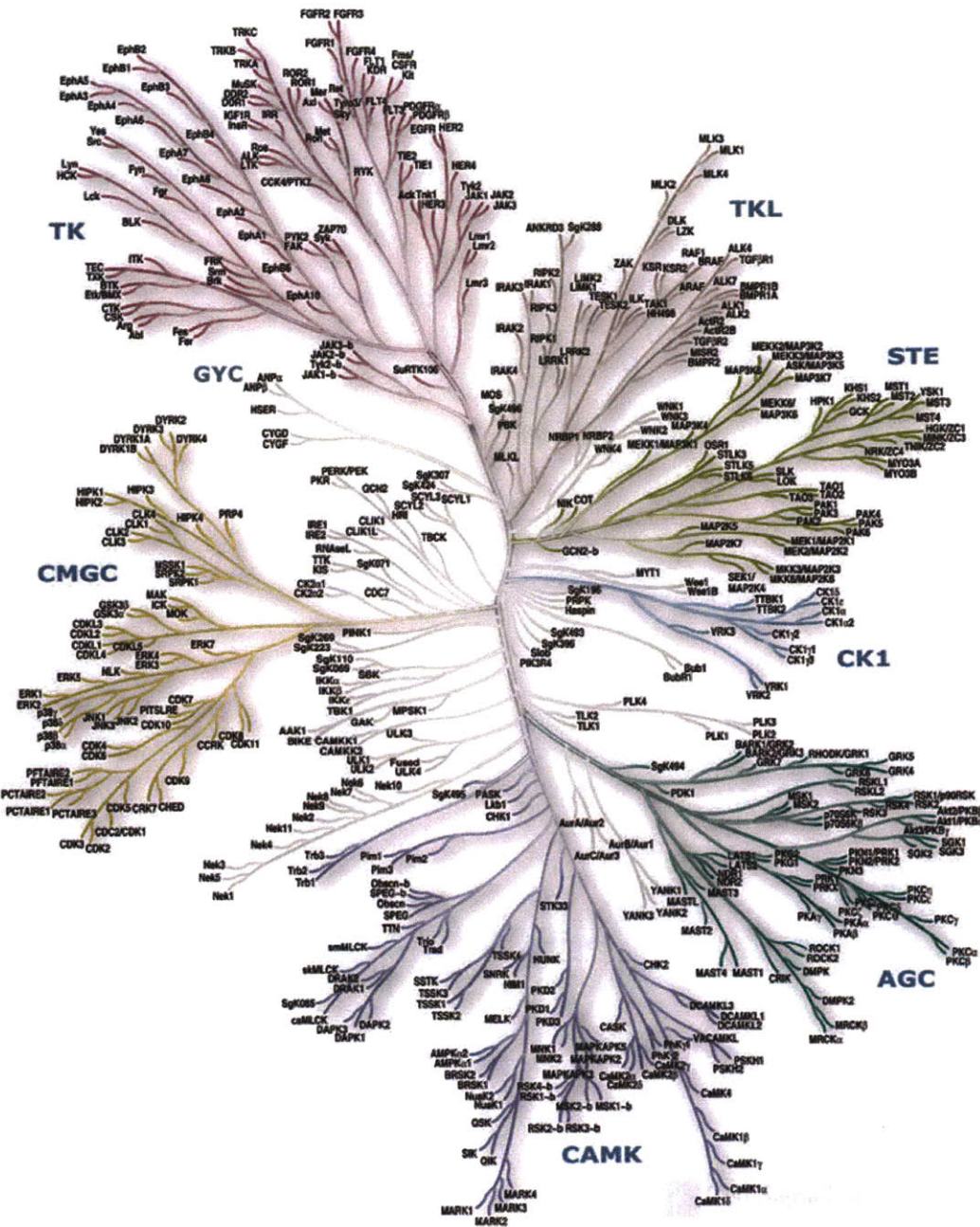


Figure 1-2. To date, the human kinome encompasses 518 Ser/Thr and Tyr kinases divided in 9 major classes. Ser/Thr kinases are the most abundant (~400), followed by Tyr kinases (~90), while only ~40 have the dual function. Dendrogram obtained from ref. 6 and www.cellsignal.com.

Recently, much effort has been put forth in the area of drug discovery to identify molecules that can modulate kinase activity for the treatment of disease. This work is partly fueled by the remarkable initial success of imatinib mesylate (also known as Gleevec and STI571) used to treat chronic myelogenous leukemia (CML), gastrointestinal stromal cell tumors (GIST) and metastatic dermatofibrosarcoma protuberans by direct inhibition of mutated Abl, c-Kit and PDGFR Tyr kinases, respectively.^{11, 12} Gleevec was the first small molecule to successfully block the constitutively active Abl kinase and also cause a marked improvement in individuals suffering from CML. Interestingly, the precursor of Gleevec was discovered by labor intensive screening of a large library of compounds for in vitro inhibition of protein kinase C (PKC), a Ser/Thr kinase.¹³ Although poor inhibitors for PKC, the Gleevec precursor showed good properties for Abl. Further elaboration led to Gleevec and its use as an inhibitor of Tyr kinases. Unfortunately, patients have started to show resistance to Gleevec, which has been attributed to a single point-mutation in the BCR-ABL gene,^{14, 15} and further drug screening and the development of follow-up compounds has been necessary.¹⁶

In light of the potential of kinases as therapeutic targets, selective, sensitive and high throughput methods to detect kinase activity are not only critical in studying the mechanisms of cellular processes, but are also necessary for the efficient search of potent inhibitors for disease treatment. As illustrated with Gleevec, kinases are attractive medical targets, but as cancer is highly adaptive, our search for a complete understanding of roles that kinases play and for more effective therapeutics is never-ending.

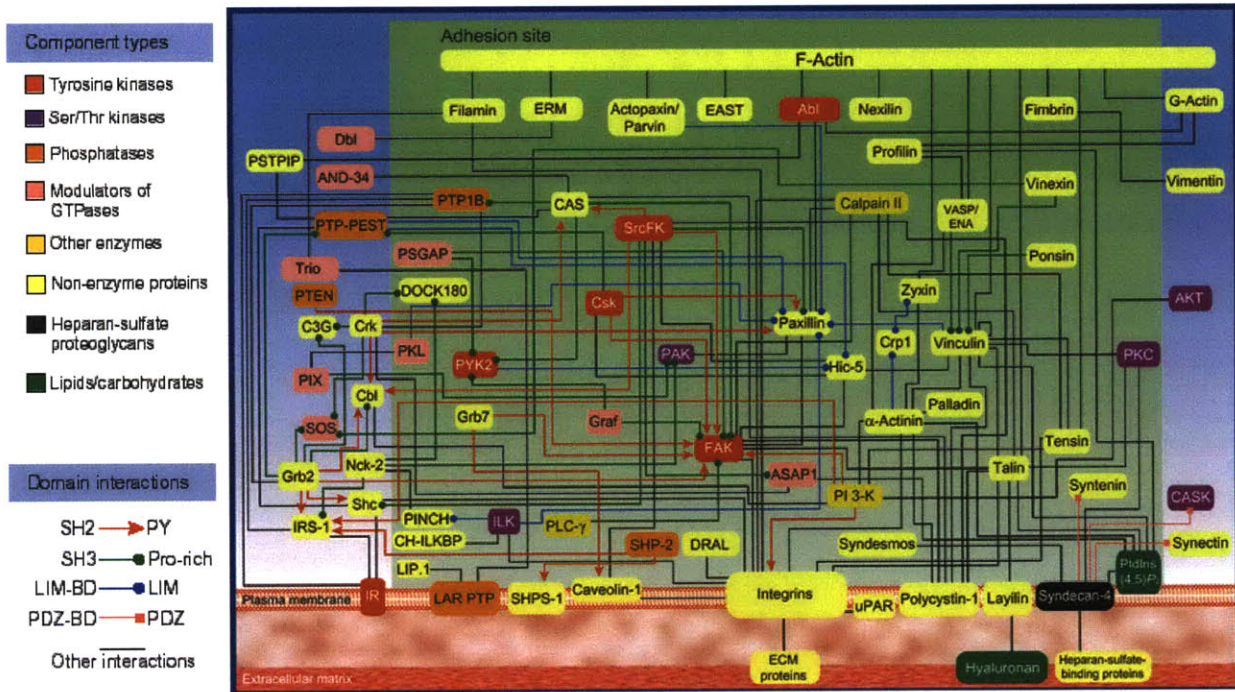


Figure 1-3. Scheme summarizing known interactions between constituents of cell-matrix adhesions, illustrating the intricacy of kinase involvement with multiple targets. Figure obtained from ref. 9 and www.cellmigration.com.

Detection of Kinase Activity

Traditional assays for kinase activity use either phosphopeptide-specific antibodies or, more commonly, $[\gamma\text{-}^{32}\text{P}]\text{ATP}$, where transfer of the radioactive γ -phosphoryl group to peptide or protein substrate is quantified by liquid scintillation counting. Although general and sensitive, $[\text{}^{32}\text{P}]$ -based assays are not compatible with physiological concentrations of ATP, real-time analysis or high-throughput kinetic determination. These assays require special handling, generate radioactive waste, and lose much of the kinetic information due to their endpoint nature. Furthermore, because $[\gamma\text{-}^{32}\text{P}]\text{ATP}$ is generally required by all kinases, this method cannot be applied in environments where multiple kinases are present.

Conversely, continuous assays that rely on fluorescence changes upon sensor phosphorylation are ideal for high throughput screening (HTS) and thus make discovery of new inhibitors and substrates with enhanced specificity much more practical. Fluorescence-based assays may also be compatible with cell lysates, living cells and physiological ATP concentrations. Existing fluorescent protein- and peptide-based sensors exploit a variety of detection methods, such as fluorescence polarization, fluorescence resonance energy transfer (FRET), fluorescence quenching, metal ion-mediated fluorescence and solvatochromism, and have been recently reviewed.^{7, 17-19} Herein we will review some of the more recent and practical approaches for sensing protein phosphorylation (Figure 1-4).

The probes that employ FRET between two *Aequorea victoria* fluorescent proteins (AFPs) are perhaps the most widely used for examining kinase activity because they can be genetically encoded and expressed within cells.²⁰ Generally, AFP-based sensors contain a kinase phosphorylation sequence, a linker region, a phosphopeptide-binding domain, and two AFP analogs with appropriate photophysical properties, such as CFP and YFP, situated on the termini of the probe (Figure 1-4a). In these sensors, phosphorylation leads to a conformational change in the protein, a result of phosphopeptide binding to its cognate recognition region, thereby altering the distance between the AFPs. Because the distance is related to the efficiency of FRET, phosphorylation produces a fluorescence response (Figure 1-4a). Accordingly, the fluorescent signal can either increase or decrease depending on the changes in distance between the AFPs upon phosphorylation, producing turn-on or turn-off sensors, respectively. Turn-off probes are less desirable since loss of signal can be mistaken for photobleaching and can affect the accuracy of readings. Genetically encoded FRET-based reporters have been developed for many kinases due to the relative ease of intracellular expression, including improved sensors for Src²¹ and

ERK.²² In addition, recent impressive optimization of the AFP-based PKA sensor now allows for small molecule inhibitor screening in cells, thus expanding the utility of these types of probes.²³ Although several AFP analogs containing complementary photophysical properties for FRET have been developed, and in theory can be applied for dual-kinase sensing, the maximal change in signal can be fairly low (~ 50%), leading to reduced sensitivity and more challenging fluorescent readouts. Additionally, the large size of the AFP-based sensors (at least 50 kDa for the two AFPs in each sensor) can be quite disruptive when studying endogenous kinases that may depend on interactions with other proteins for activity.

On the other hand, peptide-based probes offer distinct advantages over the protein counterparts, such as relatively small size, ease of large-scale synthesis, and ability to introduce unnatural elements to aid selectivity and/or sensitivity.^{17, 24} Importantly, because they generally do not depend on FRET, the maximal observed change in signal is often well above 100%. This is a significant benefit, as larger fluorescence changes allow for improved sensitivity, which is essential when studying endogenously expressed enzymes that are present in reduced amounts or may be poor catalysts.

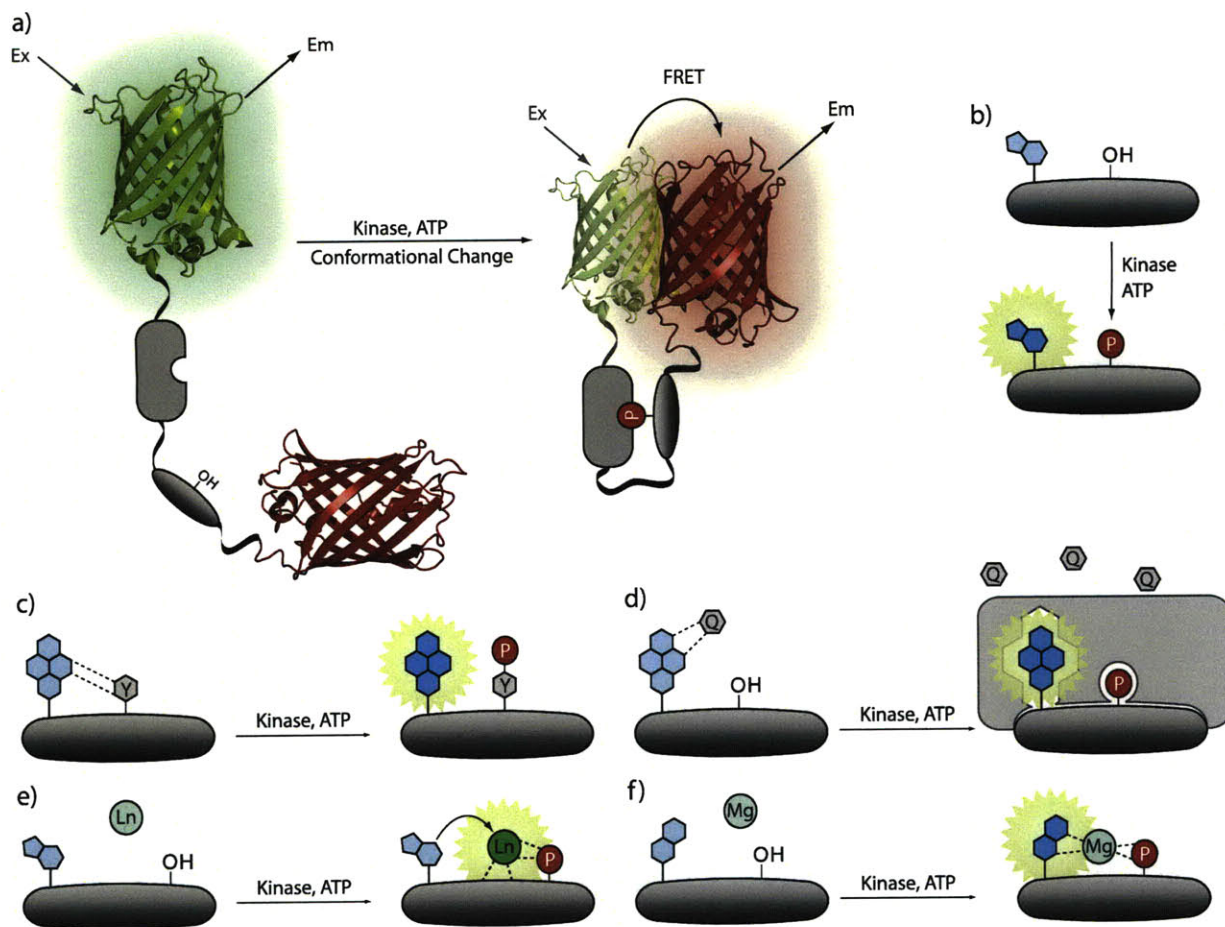


Figure 1-4. Sensing strategies employed to detect kinase activity. a) AFP-based sensors depend the change in FRET upon phosphorylation due phosphopeptide-domain binding. b) Solvatochromic chromophores experience a change in solvent polarity after phosphorylation leading to an increase in quantum yield that results in fluorescence enhancement. c) Quenching of pyrene fluorescence by a nearby Tyr residue is disrupted by phosphorylation that enables an enhancement of the fluorescent signal. d) In the “Deep Quench” method, a non-covalent quencher alters the fluorescence of pyrene. After phosphorylation, phosphopeptide-specific protein domain binds to the product and disrupts quenching, giving rise to fluorescence. e) These sensors have low affinity for Ln^{3+} , which significantly increases after the phosphate is present. A nearby antenna (i.e., Trp) can sensitize the peptide-bound Ln^{3+} , which produces a detectable, long-lived luminescence. f) Similarly, sensors bearing CHEF chromophores are silent until phosphorylation enables divalent metal binding, which causes an increase in fluorescence.

The Lawrence group has reported several types of kinase reporters, many of them utilizing solvatochromic fluorophores that exhibit changes in their fluorescence properties, such

as emission wavelength and quantum yield, due to the polarity of the immediate environment. Introduction of a phosphoryl group near the chromophore alters the local environment polarity, resulting in fluorescence change (Figure 1-4b). Notably, this strategy has been used to visualize PKC activity within live HeLa cells.²⁵ In addition, sensors employing quenching strategies have also been explored.²⁶ For example, when a pyrene moiety is positioned in close proximity to a Tyr residue, the overall fluorescence is quenched due to π - π stacking interactions, reducing fluorescence quantum yields. The size and charge of the phosphate group disrupts the pyrene-tyrosine interaction and results in a fluorescent phosphopeptide (Figure 1-4c).²⁷ However, the method is not applicable to Ser/Thr kinases, as π - π interactions do not directly contribute to diminishing pyrene fluorescence. Instead, a modified quenching strategy, called “Deep Quench” was developed by the Lawrence group for Ser/Thr kinases (Figure 1-4d). In the new system, the fluorescence was modulated using an in-solution quencher molecule, such as Rose Bengal, that bound to substrate-tethered pyrene. After phosphate installation, the peptide was sequestered by a phospho-peptide binding domain (such as 14-3-3 τ) away from the non-covalent quencher, thereby restoring fluorescence signal. Such strategy has furnished 21- to 64-fold phosphorylation-induced fluorescence enhancements, the most dramatic change reported to date.²⁸ Despite these promising results, the method has not been extended beyond PKA substrates. One reason for this may be that the probe indirectly senses phosphorylation and requires several separate components, such as the quencher and the phospho-product binding domain to be present. This may be problematic if the sensor is to be used in more complex media, such as cells and cell lysates.

Several strategies that rely on metal ion-mediated luminescence or fluorescence to detect phosphorylation have also been reported. In the unphosphorylated state, these peptides exhibit

low metal ion affinity and are predominantly non-fluorescent. However, modification with the phosphate provides two essential ligands, resulting in a significant increase in the avidity for binding to hard metal ions such as magnesium or the lanthanide ions, and a subsequent positive signal. Peptides based on this general strategy have recently been designed to bind lanthanide ions (Ln^{3+}) such as Tb^{3+} or Eu^{3+} .^{29, 30} In these cases, the obligatory nearby antenna (Trp or carbostyryl) absorbs light and sensitizes Ln^{3+} , which produces long-lived luminescence to signal kinase activity (Figure 1-4e). The peptides produce significant changes (up to 10-fold) in signal upon phosphorylation; however, the system requires the presence of free Tb^{3+} or Eu^{3+} , which might be problematic if this approach is attempted in cells due to the need for delivering the lanthanide ion into cells that may be toxic.

On the other hand, chelation-enhanced fluorescence (CHEF) sensing methods utilize biologically available metal ions, such as Ca^{2+} and Mg^{2+} , to report phosphorylation (Figure 1-4f). For example, a CHEF sensor for PKC has exploited elevated Ca^{2+} levels required for proper PKC activation and previously reported Ca^{2+} indicators.³¹ However, this approach has not been adapted for use with other ions or to monitor additional kinases.¹⁷ Alternatively, probes developed in the Imperiali laboratory contain the sulfonamido-oxine (Sox) amino acid³² that displays good fluorescence increases (4- to 12-fold) upon phosphorylation and binding of Mg^{2+} .³³ Aside from robust fluorescence changes, the use of physiological levels of Mg^{2+} (low millimolar)³⁴ makes this approach generally useful not only for multiple kinases, but also in a variety of conditions that are necessary for optimal kinase function. The method, termed the β -turn focused (BTF) design, has been successfully applied in the development of chemosensors that monitor kinases both *in vitro*³⁵ and in unfractionated cell extracts.³⁶ However, although versatile, the BTF design does not allow for exploitation of the full peptide recognition sequence

due to the limitations imposed by the requirement for a conformationally-constrained β -turn motif.

Kinase Specificity

One of the major challenges in the field of kinase analysis is sensor specificity in the presence of multiple kinases, particularly since most fluorescent sensors employ short peptide sequences to specify their target. Similar challenges are also encountered inside cells among kinases and their endogenous substrates. For instance, it has been estimated that 30% of all cellular proteins are phosphorylated on at least one residue, which translates into nearly 700,000 potential phosphorylation sites for any given kinase.³⁷⁻³⁹ Although many eukaryotic protein kinases are structurally homologous,⁴⁰ they often exhibit clear preferences for certain substrates over others. Therefore, our hope is to exploit some methods that endogenous kinases employ to select their substrates in the development of a new generation of highly targeted sensors.

In vivo substrate specificity is complex and is governed by a number of factors. The first level of specificity is dictated by the kinase active site and the consensus sequence on the substrate. Generally the catalytic clefts can either accommodate the Ser/Thr or Tyr side chain (Figure 1-5a); kinases with dual functionality are less common (~40 out of 518).³⁹ Additionally, a substantial contribution to substrate recognition comes from the residues that surround the phosphorylation site (Figure 1-5b). It has been found that typically between 4 to 8 amino acids are responsible for this substrate specificity, and several laboratories have explored the optimal consensus sequences of a variety of kinases (Table 1-1).^{37, 41-43}

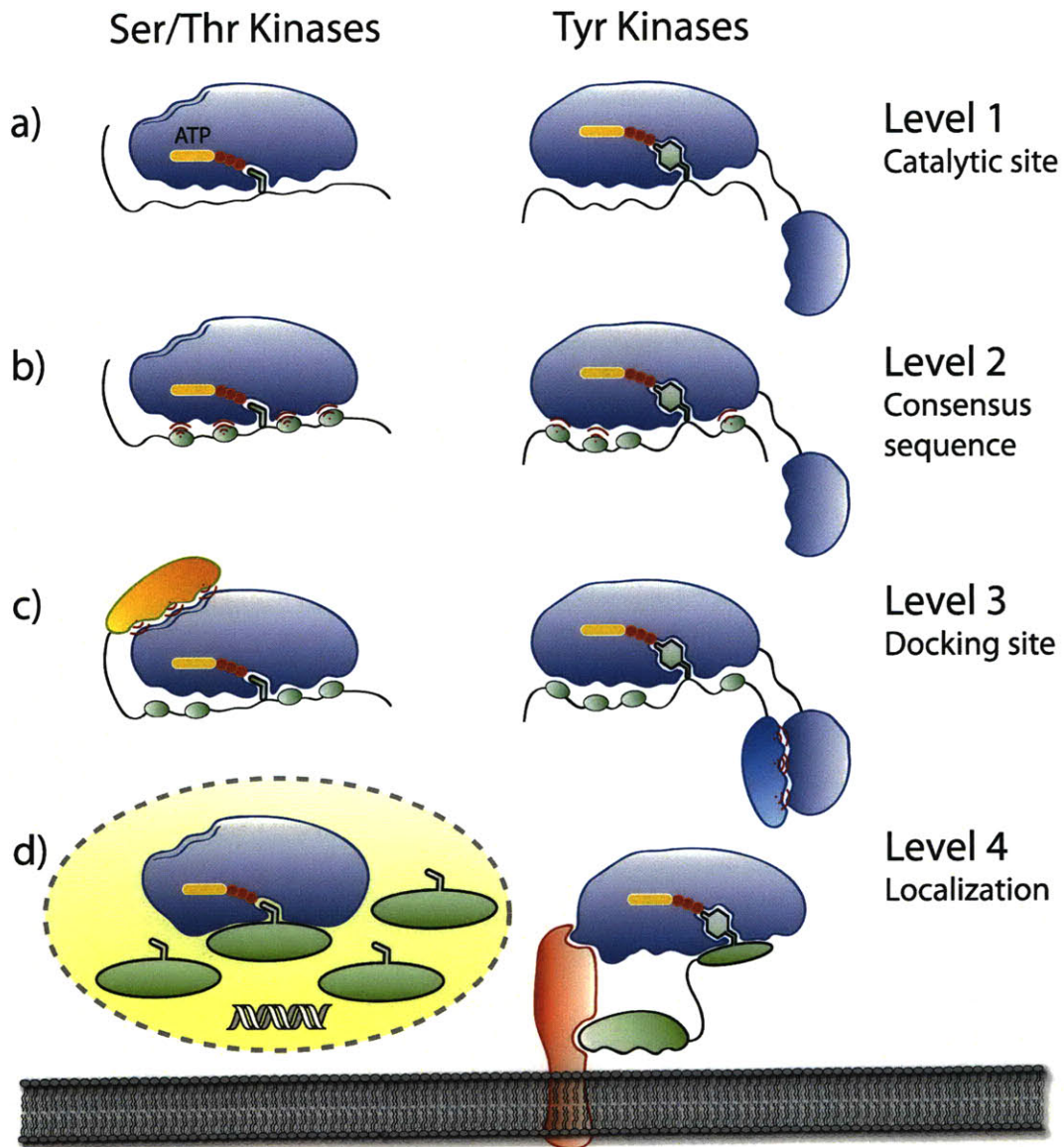


Figure 1-5. Strategies that protein kinases employ to gain specificity in vivo. a) The first level of specificity is found at the catalytic site, which can generally accommodate either Ser/Thr or Tyr side chains. Only ~40 of 518 kinases have dual, Ser/Thr and Tyr, capabilities. b) The second tier involves recognition of 4-8 residues surrounding the phosphorylatable amino acid. c) Docking domain interactions are utilized by both types of kinases when the consensus sequence is not specific enough. d) Localization, either to an organelle or to a scaffolding protein, increases the effective local concentration of enzymes and substrates, resulting in an enhanced rate of reaction.

Table 1-1. Consensus Phosphorylation Sites of a Representative Sampling of Protein Kinases^a

Kinase	Full name	Consensus sequence									
		-5	-4	-3	-2	-1	0	+1	+2	+3	+4
PKA	Protein kinase A			R	R	X	S/T	Φ			
CDK	Cyclin-dependent kinase						S/T	P	X	K/R	
ERK2	Extracellular signal-regulated kinase-2				P	X	S/T	P			
CK1	Casein kinase-1			pS	X	X	S/T				
CK2	Casein kinase-2						S/T	D/E	X	E/D	
GSK3	Glycogen synthase kinase-3						S	X	X	X	pS
CaMK2	Calmodulin-dependent protein kinase-2			R	X	X	S/T				
Abl	Abelson murine leukemia virus tyrosine kinase					I/V/L	Y	X	X	P/F	
EGFR	Epidermal growth factor receptor			E	E	E	Y	F			
Src	Rous sarcoma virus tyrosine kinase			E	E	I	Y	E/G	X	F	
IRK	Insulin receptor tyrosine kinase						Y	M	M	M	
PKB/Akt	Protein kinase B	R	X	R	X	X	S/T				
PKD	Protein kinase D	L/I	X	R	X	X	S/T				
Pim1-3	Proviral integration site kinases 1-3	R	X	R	X	X	S/T				

^a Adapted from ref. 39. X = any amino acid, Φ = hydrophobic amino acid, pS = phosphoserine.

If the consensus sequence alone cannot provide a stringent level of selectivity, often the next specificity determinant involves interactions between docking motifs on the substrate and interaction domains on the kinase (Figure 1-5c). These interaction domains are commonly short sequences of amino acid residues.⁴⁴ Such a mechanism has been identified for both Ser/Thr (JNKs, PHK, ERK, MEK, CDK2) and Tyr (TGFBR) kinases. Interestingly, Ser/Thr kinases display docking sites on the catalytic domain, while in Tyr kinases the analogous sites are generally found in modular domains that are separate from the kinase domains, such as Src-homology-2 (SH2), SH3, integrin binding, focal adhesion binding, DNA binding, or Janus tyrosine kinase (JAK) homology domains.⁴⁵ Because of the separation of docking and catalytic domains in the case of Tyr, it has been proposed that Ser/Thr phosphorylation evolved before Tyr kinases and came to rely on a simpler docking interaction strategy to discriminate among

interaction partners.⁴⁶ Conversely, because Tyr kinases evolved later, they progressed toward using multiple modular interaction domains to drive specificity (Figure 1-5c). Regardless, in both instances the function of docking motifs is thought to primarily be a mechanical method to increase the local concentration of the substrate around the kinase. For instance, within a 10 nm radius from the kinase, substrate effective concentration is proposed to reach 3 mM,⁴⁷ which would greatly accelerate the rate of phosphorylation of a scarce substrate.

Similarly, localization of the kinase to distinct cellular compartments or structures can enhance the rate of phosphorylation or promote specificity by limiting the access to the number of available substrates.^{39, 46} Additionally, some substrates and kinases also depend on adaptor or scaffold proteins, which act as dynamic organizing platforms for many molecules to bring them together (Figure 1-5d).⁴⁸ This is yet another mechanism of localization that serves to increase the substrate concentration and results in an enhanced overall rate of reaction.

In conclusion, it is evident that *in vivo* kinases-substrate recognition is a multi-tiered process that often utilizes multiple strategies in order to achieve a high level of specificity. However, current fluorescent kinase sensors generally employ short consensus sequences as selection guides. As the field moves toward cellular work, such probes may not be able to provide the requisite selectivity, and additional recognition determinants used by native kinases should be explored. For example, taking advantage of a docking domain on a kinase may turn a mediocre sensor into a species that is highly specific because it may behave more like an endogenous substrate. Moreover, a sensor for a specific kinase may be modified to localize it to a particular cellular compartment or a scaffolding protein, and could, thus, be used to define and distinguish the roles of that kinase in different processes. Thus, to effectively study these

enzymes in cellular environments, designs of kinase sensors will also need to take advantage of the different strategies that endogenous kinases employ to recognize their substrates.

Dissertation Objectives

Highly modular sensors that can quickly be adapted to take advantage of various recognition strategies that native kinases employ are of great importance in mapping kinase networks. This is particularly the case as the use of kinase probes moves from relatively simple assays with recombinant enzymes toward more complex environments. In order to introduce fluorescent kinase sensors into cells and obtain relevant data, much work needs to be done to resolve issues surrounding probe cross-reactivity and sensitivity.

The goal of the work presented in this dissertation is to create sensors with high selectivity toward kinases and to utilize the CHEF reporting platform previously developed in the laboratory.^{33, 35, 36} One way to develop sensors that are better able to discriminate between multiple kinases, whether in vitro, in vivo or in cell lysates, is by improving the kinetic parameters, for example, to lower the K_M while keeping the V_{max} high. This was accomplished by extending the consensus sequence to include additional amino acids that were absent in the original BTF probes, due to design requirements. The resulting recognition-domain focused (RDF) sensors displayed marked improvements in catalytic efficiency (k_{cat}/K_M) for multiple Ser/Thr and Tyr kinases (Chapter 2). Furthermore, to rapidly identify additional specificity determinants in short peptides, a high-throughput method was also developed that allowed us to screen individual positions in the consensus sequence with natural and unnatural elements. This approach yielded an improved peptide sensor for Aurora A kinase (Chapter 3) and should be generally applicable in substrate searches for any Ser/Thr or Tyr kinase of interest.

In addition, for some kinases, such as ERK1/2, short peptides, based on consensus sequences do not impart much selectivity. In the development of a sensor for ERK1/2, we took advantage of important docking interactions that MAPK kinases, such as ERK1/2, often utilize to differentiate their substrates. A key native chemical ligation (NCL) was employed to build a chimeric sensor that included the CHEF-sensing moiety and a docking domain specific for ERK1/2 (Chapter 4). Moreover, the same strategy was applied in the semisynthesis of a membrane-targeted sensor that will be used to specifically examine the role of ERK1/2 in migration at the cell edge.

Lastly, in order to be able to monitor kinases in cellulo, we sought to develop new CHEF derivatives based on the oxine chromophore with improved photophysical properties. Chapter 5 presents the synthesis and characterization of several derivatives that display the required bathochromic shifts in excitation and emission wavelengths as well as useful quantum yields.

The variety of methods presented in this thesis were used to synthesize sensors for 13 kinases, from Ser/Thr as well as receptor and nonreceptor Tyr families (Figure 1-6). The high-throughput approaches used here to extend sensor selectivity and sensitivity toward the cognate kinase should prove to be useful and complementary tools in the quest for better understanding of the complex roles that these enzymes play in normal and diseased states.

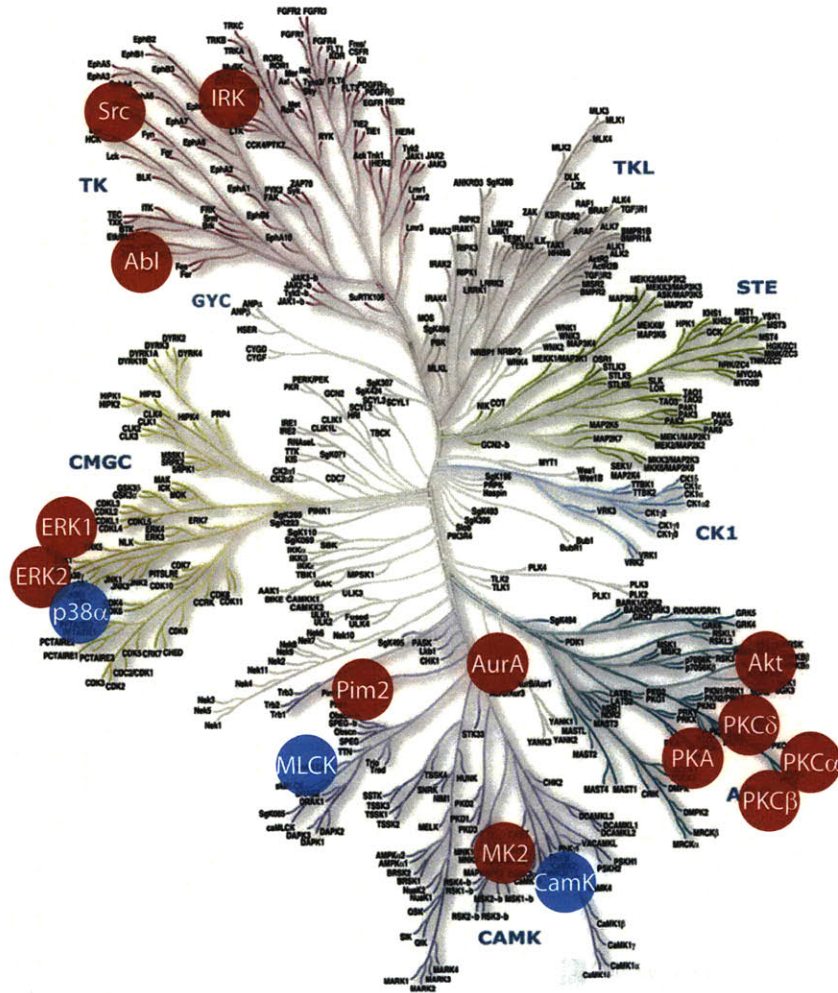


Figure 1-6. CHEF-based chemosensors. Thirteen kinases have been targeted with RDF sensors (red), while work is ongoing toward the synthesis and validation of several more reporters (blue). Dendrogram obtained from ref. 6 and www.cellsignal.com.

References

1. Hunter, T. Signaling—2000 and beyond. *Cell* **2000**, 100, 113-127.
2. Johnson, L. N.; Lewis, R. J. Structural basis for control by phosphorylation. *Chem. Rev.* **2001**, 101, 2209-2242.
3. Cohen, P. The origins of protein phosphorylation. *Nat. Cell Biol.* **2002**, 4, E127-130.
4. Adams, J. A. Kinetic and Catalytic Mechanisms of Protein Kinases. *Chem. Rev.* **2001**, 101, 2271-2290.
5. Hunter, T. Protein kinases and phosphatases: the yin and yang of protein phosphorylation and signaling. *Cell* **1995**, 80, 225-236.
6. Manning, G.; Whyte, D. B.; Martinez, R.; Hunter, T.; Sudarsanam, S. The Protein Kinase Complement of the Human Genome. *Science* **2002**, 298, 1912-1934.
7. Turk, B. E. Understanding and exploiting substrate recognition by protein kinases. *Curr. Opin. Chem. Biol.* **2008**, 12, 4-10.
8. Manning, G.; Plowman, G. D.; Hunter, T.; Sudarsanam, S. Evolution of protein kinase signaling from yeast to man. *Trends Biochem. Sci.* **2002**, 27, 514-520.
9. Zamir, E.; Geiger, B. Molecular complexity and dynamics of cell-matrix adhesions. *J. Cell Sci.* **2001**, 114, 3583-3590.
10. Cohen, P. Protein kinases--the major drug targets of the twenty-first century? *Nat. Rev. Drug Discov.* **2002**, 1, 309-315.
11. Dancey, J.; Sausville, E. A. Issues and progress with protein kinase inhibitors for cancer treatment. *Nat. Rev. Drug Discov.* **2003**, 2, 296-313.
12. Sawyers, C. Targeted cancer therapy. *Nature* **2004**, 432, 294-297.
13. Roskoski, R., Jr. STI-571: an anticancer protein-tyrosine kinase inhibitor. *Biochem. Biophys. Res. Commun.* **2003**, 309, 709-717.
14. Shah, N. P.; Nicoll, J. M.; Nagar, B.; Gorre, M. E.; Paquette, R. L.; Kuriyan, J.; Sawyers, C. L. Multiple BCR-ABL kinase domain mutations confer polyclonal resistance to the tyrosine kinase inhibitor imatinib (STI571) in chronic phase and blast crisis chronic myeloid leukemia. *Cancer Cell* **2002**, 2, 117-125.
15. Gorre, M. E.; Mohammed, M.; Ellwood, K.; Hsu, N.; Paquette, R.; Rao, P. N.; Sawyers, C. L. Clinical Resistance to STI-571 Cancer Therapy Caused by BCR-ABL Gene Mutation or Amplification. *Science* **2001**, 293, 876-880.
16. Shah, N. P.; Tran, C.; Lee, F. Y.; Chen, P.; Norris, D.; Sawyers, C. L. Overriding Imatinib Resistance with a Novel ABL Kinase Inhibitor. *Science* **2004**, 305, 399-401.
17. Rothman, D. M.; Shults, M. D.; Imperiali, B. Chemical approaches for investigating phosphorylation in signal transduction networks. *Trends Cell Biol.* **2005**, 15, 502-510.
18. Shanna, V.; Wang, Q.; Lawrence, D. S. Peptide-based fluorescent sensors of protein kinase activity: Design and applications. *Biochim. Biophys. Acta, Proteins Proteomics* **2008**, 1784, 94-99.
19. Li, Y.; Xie, W.; Fang, G. Fluorescence detection techniques for protein kinase assay. *Anal. Bioanal. Chem.* **2008**, 390, 2049-2057.
20. Zhang, J.; Allen, M. D. FRET-based biosensors for protein kinases: illuminating the kinome. *Mol. Biosyst.* **2007**, 3, 759-765.
21. Wang, Y.; Botvinick, E. L.; Zhao, Y.; Berns, M. W.; Usami, S.; Tsien, R. Y.; Chien, S. Visualizing the mechanical activation of Src. *Nature* **2005**, 434, 1040-1045.

22. Harvey, C. D.; Ehrhardt, A. G.; Cellurale, C.; Zhong, H.; Yasuda, R.; Davis, R. J.; Svoboda, K. A genetically encoded fluorescent sensor of ERK activity. *Proc. Natl. Acad. Sci. U.S.A.* **2008**, 105, 19264-19269.
23. Zhang, J.; Ma, Y.; Taylor, S. S.; Tsien, R. Y. Genetically encoded reporters of protein kinase A activity reveal impact of substrate tethering. *Proc. Natl. Acad. Sci. U.S.A.* **2001**, 98, 14997-5002.
24. Lawrence, D. S.; Wang, Q. Seeing is believing: peptide-based fluorescent sensors of protein tyrosine kinase activity. *ChemBioChem* **2007**, 8, 373-378.
25. Yeh, R. H.; Yan, X. W.; Cammer, M.; Bresnick, A. R.; Lawrence, D. S. Real time visualization of protein kinase activity in living cells. *J. Biol. Chem.* **2002**, 277, 11527-11532.
26. Sharma, V.; Wang, Q.; Lawrence, D. S. Peptide-based fluorescent sensors of protein kinase activity: design and applications. *Biochim. Biophys. Acta* **2008**, 1784, 94-99.
27. Wang, Q.; Cahill, S. M.; Blumenstein, M.; Lawrence, D. S. Self-reporting fluorescent substrates of protein tyrosine kinases. *J. Am. Chem. Soc.* **2006**, 128, 1808-1809.
28. Sharma, V.; Agnes, R. S.; Lawrence, D. S. Deep quench: An expanded dynamic range for protein kinase sensors. *J. Am. Chem. Soc.* **2007**, 129, 2742-2743.
29. Balakrishnan, S.; Zondlo, N. J. Design of a protein kinase-inducible domain. *J. Am. Chem. Soc.* **2006**, 128, 5590-5591.
30. Tremblay, M. S.; Lee, M.; Sames, D. A luminescent sensor for tyrosine phosphorylation. *Org. Lett.* **2008**, 10, 5-8.
31. Chen, C. A.; Yeh, R. H.; Lawrence, D. S. Design and synthesis of a fluorescent reporter of protein kinase activity. *J. Am. Chem. Soc.* **2002**, 124, 3840-3841.
32. Shults, M. D.; Pearce, D. A.; Imperiali, B. Modular and Tunable Chemosensor Scaffold for Divalent Zinc. *J. Am. Chem. Soc.* **2003**, 125, 10591-10597.
33. Shults, M. D.; Carrico-Moniz, D.; Imperiali, B. Optimal Sox-based fluorescent chemosensor design for serine/threonine protein kinases. *Anal. Biochem.* **2006**, 352, 198-207.
34. Haugland, R. P.; Spence, M. T. Z.; Johnson, I. D.; Basey, A. *The handbook: a guide to fluorescent probes and labeling technologies*. 10th ed.; Molecular Probes: [Eugene, OR], 2005; p iv, 1126 p.
35. Shults, M. D.; Imperiali, B. Versatile Fluorescence Probes of Protein Kinase Activity. *J. Am. Chem. Soc.* **2003**, 125, 14248-14249.
36. Shults, M. D.; Janes, K. A.; Lauffenburger, D. A.; Imperiali, B. A multiplexed homogeneous fluorescence-based assay for protein kinase activity in cell lysates. *Nat. Methods* **2005**, 2, 277-283.
37. Pinna, L. A.; Ruzzene, M. How do protein kinases recognize their substrates? *Biochim. Biophys. Acta.* **1996**, 1314, 191-225.
38. Cohen, P. The regulation of protein function by multisite phosphorylation--a 25 year update. *Trends Biochem. Sci.* **2000**, 25, 596-601.
39. Ubersax, J. A.; Ferrell, J. E. Mechanisms of specificity in protein phosphorylation. *Nat. Rev. Mol. Cell Biol.* **2007**, 8, 530-541.
40. Hanks, S. K.; Hunter, T. Protein kinases 6. The eukaryotic protein kinase superfamily: kinase (catalytic) domain structure and classification. *FASEB J.* **1995**, 9, 576-596.

41. Songyang, Z.; Blechner, S.; Hoagland, N.; Hoekstra, M. F.; Piwnica-Worms, H.; Cantley, L. C. Use of an oriented peptide library to determine the optimal substrates of protein kinases. *Curr. Biol.* **1994**, *4*, 973-982.
42. Hutti, J. E.; Jarrell, E. T.; Chang, J. D.; Abbott, D. W.; Storz, P.; Toker, A.; Cantley, L. C.; Turk, B. E. A rapid method for determining protein kinase phosphorylation specificity. *Nat. Methods* **2004**, *1*, 27-29.
43. Olsen, J. V.; Blagoev, B.; Gnad, F.; Macek, B.; Kumar, C.; Mortensen, P.; Mann, M. Global, in vivo, and site-specific phosphorylation dynamics in signaling networks. *Cell* **2006**, *127*, 635-648.
44. Biondi, R. M.; Nebreda, A. R. Signalling specificity of Ser/Thr protein kinases through docking-site-mediated interactions. *Biochem. J.* **2003**, *372*, 1-13.
45. Hubbard, S. R.; Till, J. H. Protein tyrosine kinase structure and function. *Annu. Rev. Biochem.* **2000**, *69*, 373-398.
46. Remenyi, A.; Good, M. C.; Lim, W. A. Docking interactions in protein kinase and phosphatase networks. *Curr. Op. Struct. Biol.* **2006**, *16*, 676-685.
47. Deshaies, R. J.; Ferrell, J. E., Jr. Multisite phosphorylation and the countdown to S phase. *Cell* **2001**, *107*, 819-822.
48. Pawson, T.; Scott, J. D. Signaling through scaffold, anchoring, and adaptor proteins. *Science* **1997**, *278*, 2075-2080.

Chapter 2. Improving the Kinetics of Peptide-Based Kinase Substrates through Recognition-Domain Focused Design

A significant portion of the work described in this chapter has been published in:
Luković, E.; González-Vera, J. A.; Imperiali, B. Recognition-Domain Focused Chemosensors: Versatile and Efficient Reporters of Protein Kinase Activity. *J. Am. Chem. Soc.* **2008**, *130*, 12821-12827.

Introduction

With more than 500 different kinases encoded in the human genome,¹ closely related enzymes will inevitably phosphorylate some of the same substrates. This is particularly true of peptide-based probes, which lack several of the characteristics of protein substrates in living systems, as discussed in Chapter 1. Briefly, in cells, kinases gain specificity through not only proximal recognition sequences, but also through the spatial and temporal control that the cell exercises over an enzyme and its protein substrate (i.e. by providing both in the same location at the same time). Furthermore, protein substrates can be involved in docking or scaffolding interactions that occur distal to the phosphorylation site and may derive specificity based primarily on those protein-protein contacts, rather than the short sequence surrounding the phosphorylatable residue. One way to develop more specific sensors is to improve the kinetic parameters; this can be accomplished either by employing unnatural recognition elements² or by extending the kinase recognition domain.

Previously, our laboratory has reported guidelines for the design of chemosensors that exhibit large fluorescence increases (4- to 12-fold) upon phosphorylation.³ The approach, termed the β -turn focused (BTF) design, exploits the chelation-enhanced fluorescence (CHEF) of the sulfonamido-oxine amino acid Sox.⁴ When incorporated into a modular peptide chemosensor design that also includes part of the kinase recognition motif (either C- or N-terminal to the phosphorylation site) and a constrained β -turn motif, the affinity for Mg^{2+} is low in the absence of the phosphoryl group. In contrast, upon phosphorylation, the Mg^{2+} affinity dramatically increases due to an advantageous chelate effect (Figure 2-1). The BTF design has been successfully applied for the development of chemosensors that monitor kinases both *in vitro*⁵ and in unfractionated cell extracts.⁶ However, although versatile, the BTF design does not allow for

exploitation of the full peptide recognition sequence due to the limitations imposed by the requirement for a conformationally-constrained β -turn motif.

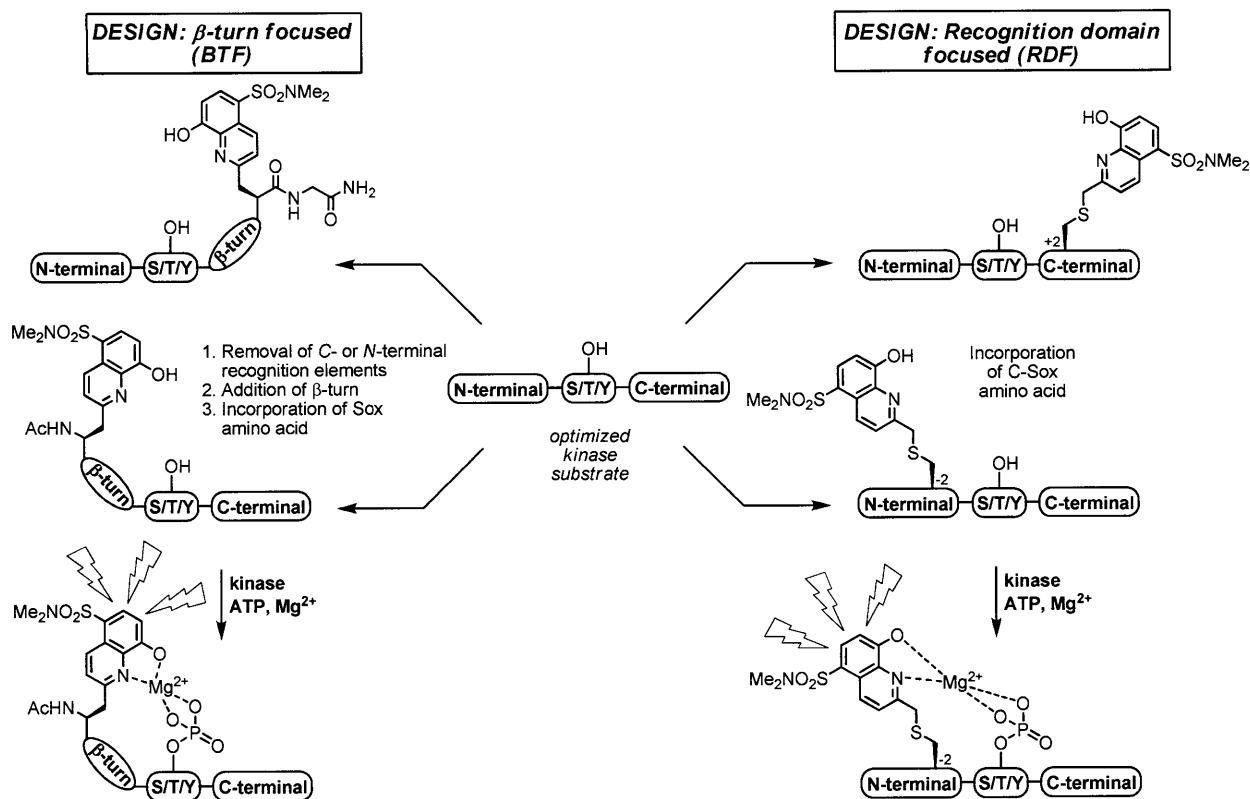


Figure 2-1. Schematic representations of the BTF and RDF designs from optimized non-fluorescent substrates. Highlighted is the fact that the recognition elements are fully conserved in the RDF design and only partially so in the BTF design due to the required β -turn. Upon kinase-catalyzed phosphorylation, the sensors become fluorescent ($\lambda_{\text{ex}} = 360$ nm, $\lambda_{\text{em}} = 485$ nm). The Sox chromophore can be positioned N- or C-terminal to the Ser/Thr/Tyr residue in both designs.

To address the issue of probe specificity, this chapter presents a more versatile and powerful chemosensor design that also exploits CHEF and is recognition-domain focused (RDF). The advantages of the new strategy are exemplified by the development of probes with greatly improved kinetic parameters for a variety of representative Ser/Thr and Tyr (non-receptor and receptor) kinases: protein kinase C (PKC) isozymes (α , β I and δ),⁷ protein kinase A (PKA),^{8, 9} protein kinase B/Akt1,^{10, 11} mitogen-activated protein kinase-activated protein kinase-2 (MK2),^{12, 13} Pim2,¹⁴ Abelson kinase (Abl),¹⁵ sarcoma kinase (Src),¹⁶⁻¹⁸ and insulin receptor kinase (IRK).^{19,}

²⁰ The RDF approach circumvents the constrained β -turn motif, which is required in the BTF design for optimal binding of Mg^{2+} by Sox and the phosphorylated residue; in RDF peptides alkylation of a nearby cysteine residue with a Sox chromophore derivative affords an amino acid termed C-Sox (Figure 2-2). The C-Sox containing peptides are flexible enough to effectively coordinate Mg^{2+} even without the pre-organizing β -turn. Thus, while the intrinsic nature of the BTF design necessitates removal of recognition elements from one terminus of an optimal peptide-based substrate, the RDF design allows for the inclusion of extended binding determinants to maximize recognition by the cognate kinase (Figure 2-1).

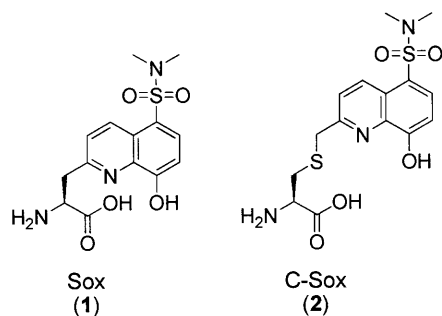


Figure 2-2. Structures of amino acids Sox (1) and C-Sox (2) that can be used to install the Sox chromophore, which in turn senses phosphoryl transfer.

Results and Discussion

Synthesis of RDF Sensors

The RDF chemosensor peptides can be constructed in two ways. In the first approach, Fmoc-based solid phase peptide synthesis (SPPS) is utilized to assemble the intact peptide that includes an appropriately placed cysteine protected with a hyper acid-labile thiol protecting group (Scheme 2-1). After selective on-resin sulfhydryl group deprotection, the free thiol is alkylated with Sox-Br.⁴ Standard TFA cleavage from the resin and concomitant removal of all side-chain protecting groups reveals the desired chemosensor with excellent conversion to the alkylated

product (>95%). The solid support-based alkylation is particularly valuable when utilizing automated SPPS or SPOT²¹ synthesis to generate libraries of peptides in a rapid parallel approach.

Alternatively, if larger amounts of a more limited range of chemosensor peptides are needed, a building block approach may be more appropriate. In this case, the synthesis of the building block, Fmoc-C(Sox[TBDPS])-OH (**5**), commences with the allylation of commercially available amino acid **3**, followed by removal of the *p*-methoxytrityl (Mmt) masking group to afford **2** (Scheme 2-1). The sulfhydryl of **4** is then alkylated with Sox-Br⁴ in excellent yield (95%). Lastly, Pd(II)-assisted deallylation produces the desired amino acid **5** that was subsequently used in standard Fmoc-based SPPS to produce RDF sensors in excellent yields. Peptide identities and purities were confirmed *via* matrix-assisted laser desorption ionization time-of-flight (MALDI TOF) or electrospray ionization (ESI) mass spectrometry together with high performance liquid chromatography (HPLC) analysis. The synthesis of C-Sox, and therefore of RDF peptides, is considerably more facile than BTF peptides, since the use of a chiral starting material **3** allowed us to completely circumvent the key asymmetric alkylation transformation required to install the stereogenic center in the Sox amino acid⁴—a key component of the BTF design.

Scheme 2-1. Synthesis of RDF Chemosensors a) on Solid Support and b) Using the Building Block Approach^a

a) On-resin alkylation

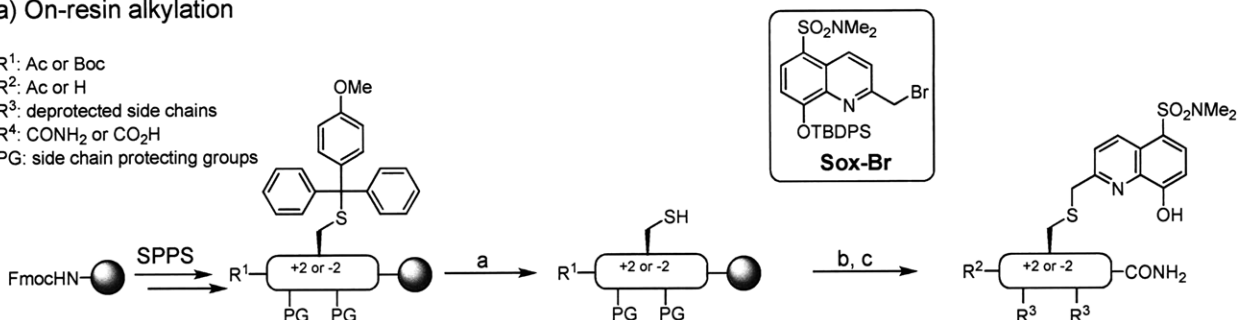
R¹: Ac or Boc

R²: Ac or H

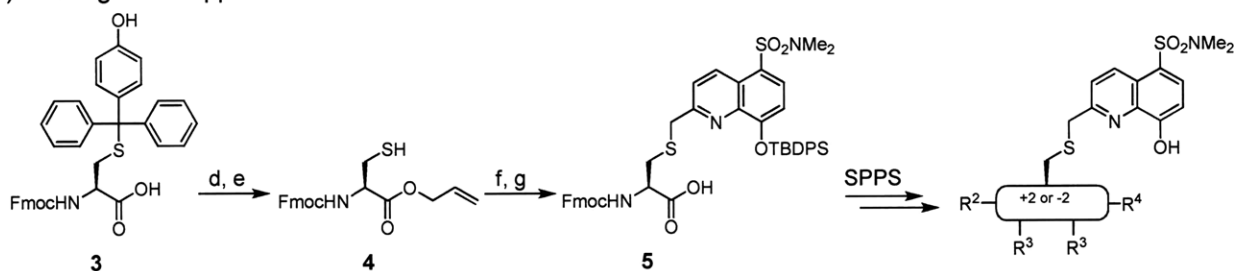
R³: deprotected side chains

R⁴: CONH₂ or CO₂H

PG: side chain protecting groups



b) Building Block Approach



^a Reagents and conditions: (a) 1% TFA, 5% TIS, CH₂Cl₂, 5 x 20 min; (b) Sox-Br, TMG, DMF, 12 h (95%); (c) 95% TFA, 2.5% TIS, 2.5% H₂O, 3 h; (d) Allyl-Br, Cs₂CO₃, MeOH/DMF; (e) 5% TFA, 5% TIS, CH₂Cl₂ (69% for two steps); (f) Sox-Br, *i*-Pr₂NEt, CH₂Cl₂ (95%); (g) Pd(PPh₃)₄, PhSiH₃, CH₂Cl₂ (77% crude).

Chromophore Positioning in the RDF Design

The first task with the RDF approach was to determine the optimal placement of the Sox chromophore within the probes. Several substrate and corresponding phosphopeptide sensors were synthesized in which C-Sox was positioned at various sites relative to the phosphorylatable residue (Table 2-1). The probes were evaluated based on the observed fluorescence increases because one of the main priorities was to obtain sensors with a robust signal for easy assay readout. The difference in fluorescence was determined by comparison of the fluorescence intensity at the maximum emission wavelength ($\lambda_{\text{ex}} = 485 \text{ nm}$) of synthetic phosphorylated and unphosphorylated peptides in the presence of Mg²⁺. We also calculated *Z'* factor values for each

RDF chemosensor pair (see Experimental Methods). Z' is a statistical quality parameter used to evaluate and validate performance of assays, particularly in high-throughput screening (HTS).²² Typically, in order for an HTS assay to be considered useful, Z' should be 0.5-1, as assays in this range exhibit large dynamic ranges and separation bands.

Table 2-1. Peptide Sequences Used to Determine Optimal Positioning of the Sox Chromophore in the RDF Design

Entry	Peptide Sequence ^a															
	-5	-4	-3	-2	-1	0	+1	+2	+3	+4	+5	+6	+7	+8		
1	Ac	R	R	R	K	C-Sox	S	F	R	R	K	A			CONH ₂	
2	Ac	R	R	R	C-Sox	G	S	F	R	R	K	A			CONH ₂	
3	Ac	R	R	R	C-Sox	A	S	F	R	R	K	A			CONH ₂	
4	Ac		V	P	L	L	T	P	C-Sox	G	R	R	G		COOH	
5	Ac		V	P	L	L	T	P	G	C-Sox	R	R	G		COOH	
6	Ac		V	P	C-Sox	L	T	P	G	G	R	R	G		COOH	
7	Ac			E	C-Sox	I	Y	A	A	P	F	A	K	K	K	CONH ₂
8	Ac			C-Sox	A	I	Y	A	A	P	F	A	K	K	K	CONH ₂
9	Ac		C-Sox	E	A	I	Y	A	A	P	F	A	K	K	K	CONH ₂
10	Ac			E	A	I	Y	A	A	C-Sox	F	A	K	K	K	CONH ₂

^a Phosphorylatable residue is bolded and set as the 0 position.

It is clear from high fluorescence enhancements that position +2 or -2 is favored over +1 or -1 in the case of sensors for Ser/Thr kinases (*e.g.* compare entry 1 with 2 and 3 in Table 2-2). Since the Tyr residue is significantly larger than Ser/Thr, placement of the Sox chromophore in position +3 or +4 or -3 or -4 was expected to yield the largest increase in fluorescence upon phosphorylation (*e.g.* entries 8-10). However, the peptide with C-Sox in the -2 (or +2) position (*e.g.* entry 7) is the preferred Tyr-containing probe in this series. In addition to having the largest fluorescence increases, peptide pairs with C-Sox in the optimal +2 or -2 position also have the highest Z' factor values (Table 2-2), making them particularly useful for high-throughput screens.

Table 2-2. Fluorescence Increase and Z' Factor Values for Ser/Thr and Tyr Kinase Substrates Described in Table 2-1

Entry	C-Sox Position ^a	Fold Fluorescence Increase ^b	Z' ^c
1	-1	1.6 ± 0.1	0.82
2	-2	2.9 ± 0.3	0.55
3	-2	3.7 ± 0.2	0.84
4	+2	5.4 ± 0.1	0.84
5	+3	6.3 ± 0.2	0.80
6	-2	6.9 ± 0.1	0.86
7	-2	4.6 ± 0.5	0.91
8	-3	3.2 ± 0.3	0.74
9	-4	2.1 ± 0.2	0.43
10	+3	2.2 ± 0.1	0.64

^a With reference to the phosphorylatable residue in Table 2-1. ^b Measured in triplicate as a quotient of fluorescence intensity at 485 nm of phosphopeptide and substrate in 20 mM HEPES (pH 7.4), 10 mM MgCl₂, and 10 μM peptide. ^c Z' factors were calculated using standard deviations and means (from triplicate measurements) of non-phosphorylated substrate (background) and synthetic phosphopeptide (signal) in the same conditions as reported for fluorescence increases.

Some kinases, such as ERK1/2, require Pro immediately next to the phosphorylatable residue (i.e. in position +1) for substrate recognition. As expected, the largest fluorescence enhancement is achieved when the chromophore is located on the side opposite of the Pro residue (relative to the phosphorylatable residue), in position -2 (e.g. entry 6). However, if the residues in that region are important in kinase recognition, C-Sox has to be placed on the same side as Pro. In such a case, a higher fluorescence increase is achieved when the fluorophore is placed in the +3 rather than the +2 position (e.g. compare entries 4 and 5). This flexibility is unique to the RDF design as the β-turn of the BTF design generally dictates and restricts the position of the fluorophore. Lastly, an additional improvement in fluorescence difference, and a further increase in Mg²⁺ affinity (see the section on the Origin of Fluorescence Increase, below), can be achieved by selecting an α-substituted amino acid rather than glycine at the -1 position between C-Sox and the Ser/Thr phosphorylation site (e.g. compare entries 2 and 3).

Fluorescence Properties of RDF Probes

After determination of the optimal chromophore position it was possible to examine a more comprehensive set of RDF probes by comparing their fluorescence differences to those of their BTF counterparts. Overall, the RDF reporters have robust fluorescence increases and high Z' values (Table 2-3). A range of 2- to 10-fold enhancement is observed due to the differing affinity for Mg^{2+} among the phosphopeptides. The RDF peptides also normally exhibit larger fluorescence increases than their BTF counterparts. More specifically, the RDF sensors for Src, Abl, IRK, PKC β I and ERK1/2 kinases have higher fluorescence differences than the corresponding BTF sensors. While this trend is reversed for PKC α , PKC δ , Akt1 and MK2 kinases, the fluorescence increases are still large enough for these to be useful probes in kinetic assays (*vide infra*). In the case of Pim2 and PKA, both designs afford probes with comparable fluorescence properties. Furthermore, the C-Sox moiety is tolerant of acidic (entries 2, 4 and 6), basic (entries 6, 8, 10, 16 and 18), aliphatic (entries 2, 4, 18, 20 and 22) and aromatic (entries 12 and 16) residues immediately flanking it. The chromophore can also be placed C- or N-terminal to the phosphorylatable residue, which gives great flexibility in the initial design stage. These results demonstrate that the RDF design is general enough to be applied to synthesis of sensors for a variety of important Ser and Thr (ERK1/2, entry 22) kinases (*e.g.* PKC, PKA, Pim2, MK2) as well as for non-receptor and receptor (IRK, entry 6) Tyr kinases (*e.g.* Src, Abl).

Table 2-3. Comparison of Substrate Sequences and Fluorescence Increases for BTF and RDF Chemosensors

Entry	Target Kinase	Design	Location of the Chromophore ^a	Substrate Sequence ^b	Fold Fluorescence Increase ^c	Z' ^d
1	Src	BTF	N	Ac-Sox-PEI <u>Y</u> * <u>GEFEAKKKK</u> -CONH ₂	1.6 ± 0.1	
2		RDF	N	Ac-AEE-CSox-I <u>Y</u> * <u>GEFEAKKKK</u> -CONH ₂	2.0 ± 0.1	0.85
3	Abl	BTF	N	Ac-Sox-PGI <u>Y</u> * <u>AAPFAKKK</u> -CONH ₂	3.6 ^e	
4		RDF	N	Ac-E-CSox-I <u>Y</u> * <u>AAPFAKKK</u> -CONH ₂	4.6 ± 0.5	0.91
5	IRK	BTF	N	Ac-Sox-PGD <u>Y</u> *-Nle-TMQIGKK-CONH ₂	2.0 ± 0.1	
6		RDF	N	Ac-R-CSox-D <u>Y</u> *-Nle-TMQIGKK-CONH ₂	4.2 ± 0.1	0.77
7	PKC α	BTF	N	Ac-Sox-PG <u>S</u> * <u>FRRR</u> -CONH ₂	6.7 ± 0.6	
8		RDF	N	Ac- <u>RRR</u> -CSox- <u>AS</u> * <u>FRRR</u> -CONH ₂	3.7 ± 0.2	0.84
9	PKC β I	BTF	N	Ac-Sox-PAS* <u>FKKFA</u> -CONH ₂	4.7 ± 0.2	
10		RDF	N	Ac- <u>LKR</u> -CSox- <u>AS</u> * <u>FKKFA</u> -CONH ₂	9.7 ± 0.5	0.87
11	PKC δ	BTF	C	Ac- <u>RKRKGS</u> *F-DPro-Sox-G-CONH ₂	12.1 ± 0.1	
12		RDF	C	Ac- <u>RKRKGS</u> *F-CSox- <u>YGG</u> -CONH ₂	7.3 ± 0.1	0.94
13	Pim2	BTF	C	Ac-ARKRRRHPS*G-DPro-Sox-G-CONH ₂	3.0 ± 0.4	
14		RDF	C	Ac-ARKRRRHPS*G-CSox-PTA-CONH ₂	3.2 ± 0.1	0.89
15	Akt1	BTF	C	Ac-ARK <u>RE</u> RAYS*F-DPro-Sox-G-CONH ₂	7.6 ± 0.6	
16		RDF	C	Ac-ARK <u>RE</u> RAYS*F-CSox-HHA-CONH ₂	3.9 ± 0.3	0.89
17	MK2	BTF	C	Ac-AH <u>LQRQLS</u> *I-DPro-Sox-G-CONH ₂	7.7 ± 0.9	
18		RDF	C	Ac-AH <u>LQRQLS</u> *I-CSox-HH-CONH ₂	4.4 ± 0.2	0.85
19	PKA	BTF	C	Ac-LRRAS*L-DPro-Sox-G-CONH ₂	5.3 ± 0.1	
20		RDF	C	Ac-ALRRAS*L-CSox-AA-CONH ₂	5.0 ± 0.2	0.95
21	ERK1/2	BTF	N	Ac-Sox-PLT* <u>PGGRRG</u> -COOH	2.9 ± 0.1	
22		RDF	N	Ac-VP-CSox-LT* <u>PGGRRG</u> -COOH	6.9 ± 0.1	0.86

^a In reference to the phosphorylatable residue. ^b Asterisk (*) denotes the residue that is phosphorylated. In cases where it has been determined, residues important in kinase recognition are underlined. Norleucine is designated as Nle. ^c Measured in triplicate as a quotient of fluorescence intensity at 485 nm of phosphopeptide and substrate in 20 mM HEPES (pH 7.4), 10 mM MgCl₂, and 10 μ M peptide ($\lambda_{\text{ex}} = 360$ nm, $\lambda_{\text{em}} = 485$ nm). ^d Z' factors were only calculated for RDF chemosensors using standard deviations and means (from triplicate measurements) of non-phosphorylated substrate (background) and synthetic phosphopeptide (signal) in the same conditions as reported for fluorescence increases. ^e Originally reported in ref. 23 as the mean of triplicate experiments without s.e.m.

Fluorescence Intensity Dependence on [ATP] and [Mg²⁺]

While the RDF sensors exhibited strong fluorescence increases under standard assay conditions, we also examined their properties in media that more closely resemble physiological ATP and Mg²⁺ concentrations (0.8-1 mM²⁴ and 0.5-5 mM,²⁵ respectively). As was the case without ATP (Table 2-3), the fluorescence enhancements in the presence of cellular concentrations of ATP for 11 of 13 chemosensors are quite robust (Table 2-4). In the remaining two samples, PKC α and Pim2 RDF sensors, at 1 mM ATP—the preferred concentration in our assay conditions—the fluorescence difference was minimal. To determine the cause, ATP was titrated into a solution containing PKC α RDF substrate (Figure 2-3). With higher concentrations of ATP an increase in substrate fluorescence was observed while the phosphopeptide fluorescence remained constant. Nevertheless, in the range of 100-250 μ M ATP, the fluorescence difference was optimal and similar to that without ATP. Because these kinases have surprisingly low ^{ATP} K_M values (ca. 5 μ M²⁶ and 0.2 μ M, respectively), enzymatic assays with PKC α and Pim2 contained 100 μ M ATP.

Table 2-4. Effects of ATP Concentration on Fold Fluorescence Increase of RDF Chemosensors

Entry	Target Kinase	Fold Fluorescence Increase ^a		
		0 mM ATP	0.1 mM ATP	1.1 mM ATP
1	Src	2.0 ± 0.1	2.0 ± 0.1	2.3 ± 0.1
2	Abl	4.6 ± 0.5	4.8 ± 0.1	5.6 ± 0.3
3	IRK	4.2 ± 0.1	4.2 ± 0.1	4.2 ± 0.2
4	PKC α	3.7 ± 0.2	3.0 ± 0.4	1.0 ± 0.2
5	PKC β I	9.7 ± 0.5	9.2 ± 0.9	4.7 ± 0.9
6	PKC δ	7.3 ± 0.1	7.5 ± 0.5	4.8 ± 0.3
7	Pim2	3.2 ± 0.1	3.1 ± 0.1	1.8 ± 0.1
8	Akt1	3.9 ± 0.3	3.9 ± 0.1	3.2 ± 0.1
9	MK2	4.4 ± 0.2	4.4 ± 0.1	4.2 ± 0.2
10	PKA	5.0 ± 0.2	5.2 ± 0.1	4.8 ± 0.3
11	ERK1/2	5.4 ± 0.1	ND ^b	5.1 ± 0.2
12	ERK1/2	6.3 ± 0.2	ND ^b	6.2 ± 0.2
13	ERK1/2	6.9 ± 0.1	ND ^b	8.1 ± 0.4

^a Measured in triplicate as a quotient of fluorescence intensity at 485 nm of phosphopeptide and substrate in 20 mM HEPES (pH 7.4), 10 mM MgCl₂, and 10 μ M peptide ($\lambda_{\text{ex}} = 360$ nm, $\lambda_{\text{em}} = 485$ nm). ^b ND: Not Determined.

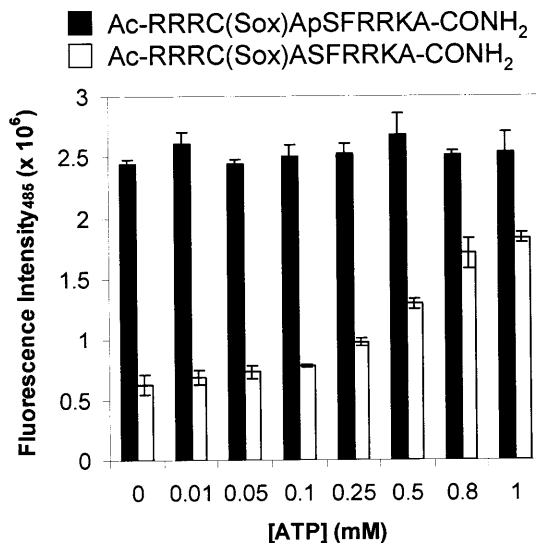


Figure 2-3. Higher concentrations of ATP increase the substrate fluorescence (open bars), while the phosphopeptide fluorescence remains constant (solid bars). However, in the range of 100-250 μ M ATP, the fluorescence increase is similar to that without ATP.

Additionally, fluorescence differences of RDF probes that contain acidic residues (such as many substrates for Tyr kinases) near the Sox chromophore tend to improve with lower Mg^{2+} concentrations. Acidic side chains may help to recruit Mg^{2+} ions, increasing the background fluorescence from the unphosphorylated substrate. As $[Mg^{2+}]$ is lowered, however, the substrate fluorescence becomes less intense while the phosphopeptide remains unchanged, resulting in an effective increase in fluorescence differences. Under more extreme conditions, such as with low $[Mg^{2+}]$ and high $[ATP]$, the fluorescence difference decreases somewhat, but even so, most of the Tyr-containing sensors exhibit useful fluorescence enhancements (Table 2-5). These promising results indicate that the RDF probes may also be translatable for use in cellular environments.

Table 2-5. Effects of $[Mg^{2+}]$ and $[ATP]$ on Fold Fluorescence Increase^a of RDF Tyr Kinase Chemosensors

Mg^{2+} (mM)	X =	Src Sensor + X mM ATP			Abl Sensor + X mM ATP			IRK Sensor + X mM ATP		
		0	0.1	1.1	0	0.1	1.1	0	0.1	1.1
10		2.0 ± 0.1	2.0 ± 0.1	2.3 ± 0.1	4.6 ± 0.5	4.8 ± 0.1	5.6 ± 0.3	4.2 ± 0.1	4.2 ± 0.1	4.2 ± 0.2
5		2.5 ± 0.1	2.6 ± 0.1	2.9 ± 0.1	6.6 ± 0.2	6.7 ± 0.3	6.7 ± 0.2	5.0 ± 0.1	5.1 ± 0.2	4.4 ± 0.3
2		3.3 ± 0.1	3.7 ± 0.4	3.5 ± 0.2	7.3 ± 0.1	8.0 ± 0.1	4.5 ± 0.2	5.3 ± 0.3	5.4 ± 0.3	2.5 ± 0.3
1		3.9 ± 0.2	3.9 ± 0.3	2.1 ± 0.1	7.9 ± 0.2	7.4 ± 0.1	2.4 ± 0.1	4.3 ± 0.3	4.2 ± 0.3	1.2 ± 0.1

^a Measured in triplicate as a quotient of fluorescence intensity at 485 nm of phosphopeptide and substrate.

Origin of Fluorescence Increase

Previously, with the BTF design large fluorescence increases were attributed to tighter binding of Mg^{2+} by the phosphopeptide.^{3, 5} Due to the differences between the BTF and RDF designs it was necessary to examine the origin of the fluorescence increase in RDF peptides. Specifically, a set of substrates and phosphopeptides pairs exhibiting a range of fluorescence differences were chosen from the PKC α and ERK1/2 chemosensors. In the PKC α set

fluorescence changes increased from 2 to 4 fold as the K_D of the corresponding phosphopeptides for Mg^{2+} decreased from 100 to 24 mM (Table 2-6, entries 1-3). The same trend was observed for ERK1/2 peptides (entries 4-6). Thus, we can conclude that greater fluorescence increases also generally indicate tighter binding of Mg^{2+} (Figure 2-4), which is in accordance with the trend described for the BTF chemosensors.^{3, 5}

Table 2-6. Peptide Sequences, Fluorescence Differences and Dissociation Constants for Mg^{2+}

Entry	Target Kinase	Peptide Sequence	Fold Fluorescence Increase ^a	Mg^{2+} K_D (mM) ^b
1	PKC α	Ac-RRRK-CSox-(p)S-FRRR-CONH ₂	1.6 \pm 0.1	98
2		Ac-RRR-CSox-G-(p)S-FRRR-CONH ₂	2.9 \pm 0.3	47
3		Ac-RRR-CSox-A-(p)S-FRRR-CONH ₂	3.7 \pm 0.2	24
4	ERK1/2	Ac-VPLL-(p)T-P-CSox-GRRG-COOH	5.4 \pm 0.1	8.7
5		Ac-VPLL-(p)T-P-G-CSox-RRG-COOH	6.3 \pm 0.2	6.3
6		Ac-VP-CSox-L-(p)T-PGGRRG-COOH	6.9 \pm 0.1	3.2

^a Measured in triplicate as a quotient of fluorescence intensity at 485 nm of phosphopeptide and substrate in 20 mM HEPES (pH 7.4), 10 mM $MgCl_2$, and 10 μ M peptide. ^b Mg^{2+} titrations were performed on phosphopeptides. The reported values are based on single measurements.

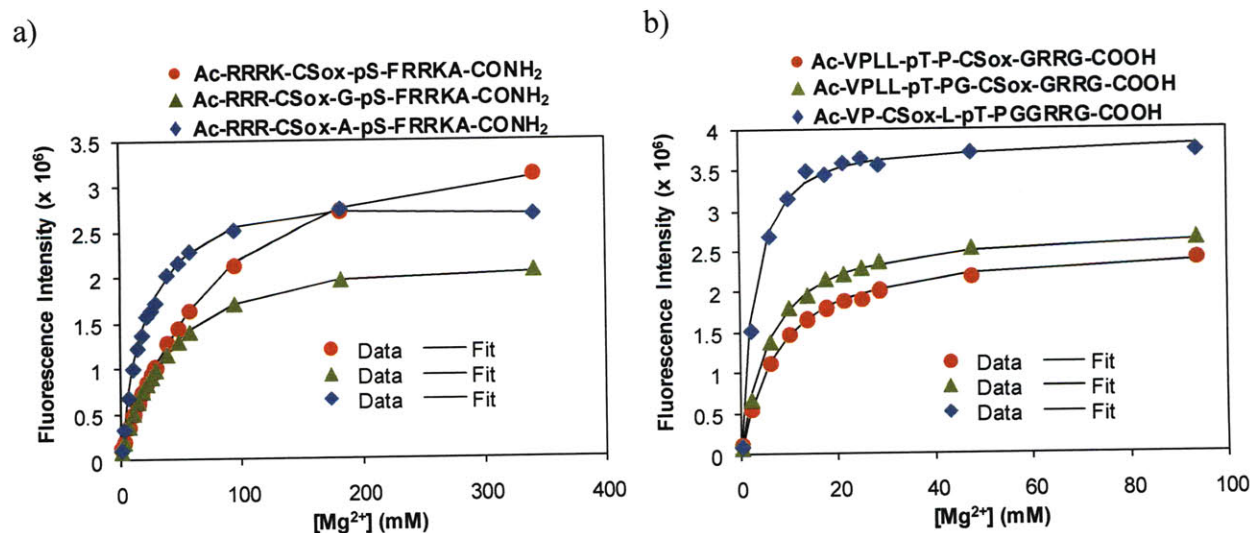


Figure 2-4. Mg^{2+} titration curves for a) PKC α (entries 1-3 in Table 2-6) and b) ERK1/2 (entries 4-6 in Table 2-6) sensors.

Fluorescence Difference under Biochemical Assay Conditions

Fluorescence increase under standard conditions (Table 2-3) is a necessary parameter to ensure consistency and easy comparison among various generations of probes for the same kinase, or among sensors for different kinases. However, optimal biochemical reaction conditions (which may include detergents, lipids, reducing agents, *et cetera*) can vary among kinases. Therefore, it is important to examine whether the fluorescence changes that were observed with standard conditions (Table 2-3) could be replicated under a variety of assay conditions.

Indeed, when fluorescence was measured under optimal assay conditions for each kinase, the RDF sensors retained robust fluorescence changes (Table 2-7). Moreover, fold fluorescence increases reported in Table 2-7 are similar in magnitude to the ones obtained under standard conditions (Table 2-3).

Table 2-7. Fold Fluorescence Increases of RDF Chemosensors Obtained from Substrate (f_S) and Phosphopeptide (f_P) Intensities under Appropriate Assay Conditions or Standard Conditions

Entry	Target Kinase	$f_{S, \text{avg}} (\times 10^3)$ (afu/ μM) ^b	$f_{P, \text{avg}} (\times 10^3)$ (afu/ μM) ^b	Fold Fluorescence Increase	
				Assay Conditions ^c	Standard Conditions ^d
1	Src	0.8 ± 0.01	2.8 ± 0.2	3.4 ± 0.3	2.0 ± 0.1
2	Abl	0.8 ± 0.01	3.8 ± 0.9	4.9 ± 0.1	4.6 ± 0.5
3	IRK	0.6 ± 0.01	2.9 ± 0.1	5.2 ± 0.1	4.2 ± 0.1
4	PKC α	257 ± 42	1048 ± 71	4.1 ± 0.1	3.7 ± 0.2
5	PKC β I	2.6 ± 0.3	13 ± 0.2	5.6 ± 1.2	9.7 ± 0.5
6	PKC δ	133 ± 85 ^e	735 ± 54 ^e	5.3 ± 0.5	7.3 ± 0.1
7	Pim2	3.3 ± 0.4	9 ± 0.2	2.8 ± 0.3	3.2 ± 0.1
8	Akt1	13 ± 0.4	43 ± 1.4	3.3 ± 0.2	3.9 ± 0.3
9	MK2	5.1 ± 0.2	25 ± 1.2	4.9 ± 0.1	4.4 ± 0.2
10	PKA	2.2 ± 0.1	12 ± 0.1	5.5 ± 0.3	5.0 ± 0.2

^a Residues that are phosphorylated are marked with an asterisk (*). ^b The values reported are the mean ± s.e.m. of triplicate experiments as calculated from a line fit to data for substrate (f_S) and phosphopeptide (f_P) in the absence of enzyme and under the appropriate assay conditions (see Experimental Methods), unless otherwise noted. ^c The values reported are the mean ± s.e.m. of triplicate experiments and are measured as f_P/f_S under the appropriate assay conditions. ^d Obtained from Table 2-3 and measured in triplicate as a quotient of fluorescence intensity at 485 nm of phosphopeptide and substrate in 20 mM HEPES (pH 7.4), 10 mM MgCl₂, and 10 μM peptide ($\lambda_{\text{ex}} = 360$ nm, $\lambda_{\text{em}} = 485$ nm). ^e Based on duplicate measurements.

Fluorescence Increase Corresponds to Product Formation

When BTF sensors were exposed to the cognate kinase, it was determined that the observed increase in fluorescence intensity during the reaction time corresponded to product formation.⁵ Furthermore, the amount of product formed during the reaction could be calculated from the fluorescence intensity at a specified time. Not surprisingly, the same equations and principles hold true for RDF sensors as demonstrated in the reaction with PKA and its RDF sensor (see Experimental Methods for details). Subjecting the reaction mixture to HPLC (Figure 2-5) separated the substrate and phospho-product, which were subsequently identified by mass spectrometry. The equations detailed in the Experimental Methods (particularly eq. (4)) were

used to calculate product formation from the fluorescent signal (Table 2-8). Indeed, the calculations confirmed that fluorescence increase during the course of the reaction is due to product formation and that product turnover can be quantified using fluorescence intensity at a specified time point.

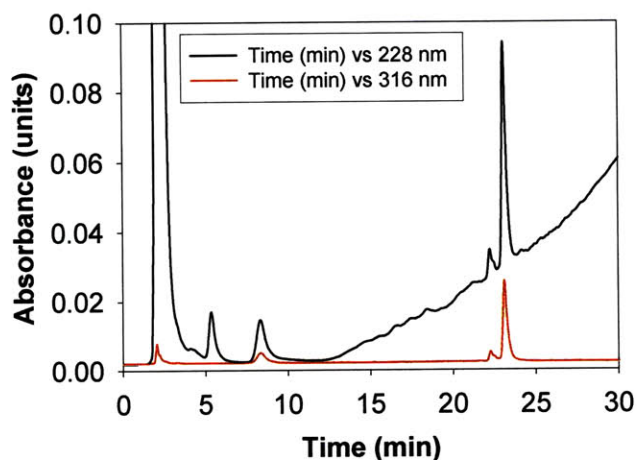


Figure 2-5. HPLC chromatogram of the PKA reaction with its RDF sensor after 616 sec of reaction time. Phospho-product ($t_R = 22.2$ min) and remaining substrate ($t_R = 23.1$ min) were characterized by MALDI-TOF MS.

Table 2-8. HPLC and ESI-MS Verification and Quantification of Product Formation Observed by Fluorescence

Kinase	Initial [S] (μM)	Reaction time	RDF Substrate			RDF Product			
			HPLC ^a		HPLC ^a		Concentration (μM)		
			t_R (min)	m/z	t_R (min)	m/z	Fluorescence ^b	HPLC ^c	
PKA	10	616 s	23.1	1336.69 1336.64	22.2	1416.62 1416.60	1.4	1.0	

^a HPLC gradient: 5% B (5 min) followed by linear gradient 5–95% B (30 min). ^b Calculated using equation (4). ^c Calculated from the integrated area on the HPLC trace where total area equals S_0 . Nearly identical numbers were obtained from traces at both 228 and 316 nm.

Comparison of Kinetic Parameters for BTF and RDF Chemosensors

In order to validate the advantages of the new RDF chemosensors over the corresponding BTF sensors in kinase assays, we compared their selectivities toward 11 different enzymes. Accommodation of the β -turn motif in the BTF design required elimination of several N- or C-

terminal residues that are either known to be involved in kinase recognition (underlined residues in Table 2-3) or that could be used to impart enzyme specificity through library screening. On the other hand, the RDF probes should benefit from inclusion of the entire kinase recognition motif.

In addition to demonstrating robust fluorescence increases under various enzyme reaction conditions (Table 2-7), for 8 of 11 kinases there were improvements in both the K_M and V_{max} parameters (Table 2-9). The results indicate that the RDF design is particularly useful in creating peptidyl sensors for kinases that require multiple residues both N- and C-terminal to the site of phosphorylation for adequate substrate recognition, as is the case for PKC α , PKC β I and PKC δ .²⁷ This is reflected in the catalytic efficiency (k_{cat}/K_M) of phosphoryl transfer by PKC α to its RDF chemosensor that is 27 times greater than that of the BTF chemosensor (Table 2-9, compare entries 7 to 8). A remarkable 66-fold improvement in the K_M value of the RDF probe was observed (entry 8), thereby underscoring the importance of the basic N-terminal sequence in the PKC α chemosensor selectivity. Even more strikingly, the BTF sensors for PKC β I and PKC δ (entries 9 and 11) show no appreciable turnover even under varying substrate concentrations or enzyme amounts (Figure 2-6). In contrast, the corresponding RDF probes (entries 10 and 12) are excellent substrates. Furthermore, they display kinetic parameters that are in close agreement with published values for their non-sensing (parent) peptides, once again demonstrating that the C-Sox sensing module does not negatively interfere with substrate-kinase binding.

Table 2-9. Comparison of Kinetic Parameters Obtained with BTF and RDF Substrate Sequences Presented in Table 2-3

Entry	Target Kinase	Design	K_M (μM) ^a	V_{max} ($\mu\text{mol mg}^{-1} \text{min}^{-1}$) ^a	Catalytic Efficiency ^b	Parent K_M (μM) ^c
1	Src	BTF	30.7 ± 5.8	0.54 ± 0.04	1	33^{28}
2		RDF	7.0 ± 1.0	3.4 ± 0.2	28	
3	Abl	BTF	26 ± 5^d	9.3 ± 0.5^d	1	4^{28}
4		RDF	10.5 ± 1.5	19.1 ± 1.0	5	
5	IRK	BTF	25.7 ± 0.7	7.3 ± 2.2	1	24^{29}
6		RDF	27.1 ± 3.9	6.3 ± 0.4	1	
7	PKC α	BTF	8.6 ± 2.9^e	5.9 ± 1.9^e	1	3.8^{27}
8		RDF	0.13 ± 0.02	2.4 ± 0.1	27	
9	PKC β I	BTF	NS ^f	NS ^f	NA ^g	2.8^{27}
10		RDF	0.81 ± 0.18	0.76 ± 0.06	NA ^g	
11	PKC δ	BTF	NS ^f	NS ^f	NA ^g	0.98^{27}
12		RDF	0.48 ± 0.07	0.39 ± 0.02	NA ^g	
13	Pim2	BTF	2.3 ± 0.2^h	0.52 ± 0.12^h	1	1.2^{30}
14		RDF	1.4 ± 0.1	0.67 ± 0.02	2	
15	Akt1	BTF	3.8 ± 0.2^h	0.59 ± 0.14^h	1	8.8^{31}
16		RDF	0.69 ± 0.11	2.5 ± 0.2	23	
17	MK2	BTF	21 ± 2^h	2.3 ± 0.2^h	1	31^{32}
18		RDF	1.2 ± 0.2	1.3 ± 0.1	10	
19	PKA	BTF	2.7 ± 0.4	26.5 ± 1.1	1	16^{33}
20		RDF	2.6 ± 0.3	17.9 ± 0.8	1	

^a Kinetic parameters (K_M and V_{max}) were obtained from initial slopes and corrected appropriately for substrate and product fluorescence as described in the Experimental Methods. The values reported are the mean \pm s.e.m. of triplicate experiments as calculated from a direct fit of v vs. $[S]$ plots using the Briggs-Haldane equation. ^b Catalytic efficiency of each substrate was calculated as k_{cat}/K_M ($\text{min}^{-1} \mu\text{M}^{-1}$). The values for BTF and RDF probes within each kinase subset were normalized to the number obtained with the BTF substrate. ^c The K_M values of the parent substrates from which the respective chemosensors were derived are obtained from the indicated literature references. ^d Results originally reported in reference 23. ^e Results originally reported in reference 6. ^f NS: Not a Substrate. ^g NA: Not Applicable. ^h Results originally reported in reference 4.

Two of the three kinases for which there was no improvement in kinetic parameters, IRK and PKA, showed no preference for either of the designs (Table 2-9, entries 5-6 and 19-20). This

result is not surprising since the consensus sequence for IRK is reported to be Y-Nle/M-X-M,²⁹ which is present in its entirety in both designs, and the PKA sensor is based on Kempptide³³ where the C-terminal Ala residues do not impart much additional specificity. Finally, despite a robust fluorescence increase of the peptidyl RDF sensor for ERK1/2,^{12, 34} it was not possible to derive kinetic parameters as this kinase requires an entire protein docking domain in addition to the short Thr-Pro consensus sequence for substrate recognition.³⁵

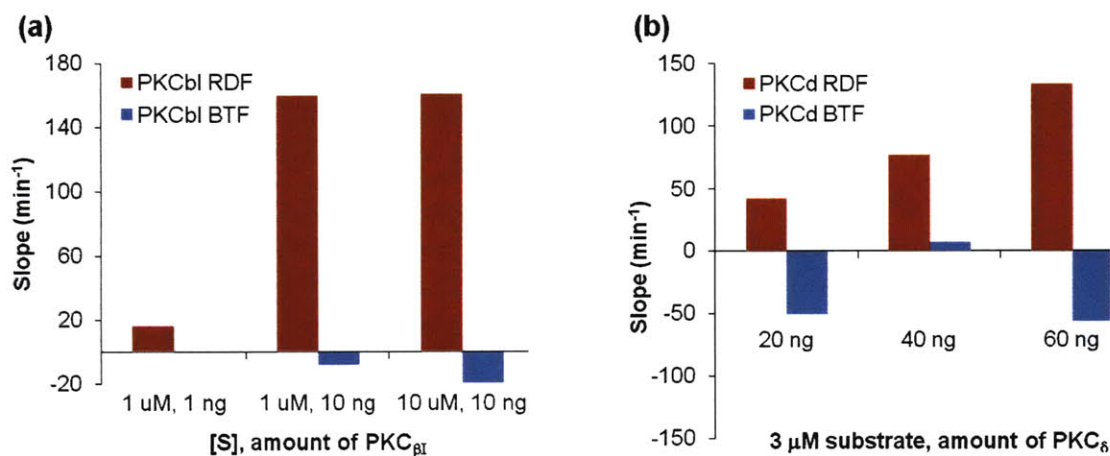


Figure 2-6. Assays of (a) PKCβI and (b) PKCδ enzymes with RDF (red bars) and BTF (blue bars) chemosensors under a variety of indicated conditions.

For substrates that have not been subjected to extensive specificity studies, comparison of the catalytic efficiencies of RDF and BTF sensors now allows easy identification of regions and/or residues that play a role in enzyme recognition. For example, we can make the generalization that the basic C-terminus is clearly important for Akt1 and MK2 kinases since their RDF chemosensors are 23- and 10-times, respectively, more efficient than the BTF probes (compare entries 15 to 16 and 17 to 18). Similarly, the acidic N-terminal sequence provides up to 28- and 5-fold improvement in catalytic efficiency toward Src and Abl, respectively (compare entries 1 to 2 and 3²³ to 4), which is in agreement with reported studies.²⁸ Lastly, while the 3-

residue N-terminal extension of the RDF substrate for Pim2 only modestly increases efficiency (compare entries 13 and 14), the RDF design now allows screens for further improvement in selectivity of this probe.

Finally, a major practical advantage of the assays with RDF chemosensors is that they are straightforward to apply. Kinetic assays were performed in either the fluorometer or fluorescence plate reader (FPR) by simple mixing of appropriate reaction components. Although the fluorometer is a much more sensitive instrument than FPR, most of the kinetic parameters for the aforementioned kinases were determined using a 96-well plate in the FPR. This was only possible because of the robust fluorescence enhancement that the sensors demonstrate upon phosphorylation under a wide range of kinase reaction conditions. Recently, the assay has also been further miniaturized to be viable in 384-well plates with a fraction of the volume required in the 96-well plates. Moreover, the use of multi-well plates in the FPR indicates not only the versatility of RDF chemosensors in obtaining kinetic parameters, but also the ease with which they could be adapted to high-throughput screens in search of potent inhibitors.

Conclusions

We have developed a general method for synthesis of versatile yet specific kinase chemosensors. The RDF design can incorporate both N- and C-terminal kinase recognition elements of Ser/Thr- and Tyr-containing substrates. The resulting chemosensors exhibit high and robust fluorescence enhancements under a variety of conditions. The RDF probes have also been used in the 96-well plate format to obtain complete kinetic parameters and recently adapted to the 384-well format, indicating that the assays can be easily tuned for use in high-throughput screening. More importantly, this approach allowed us to substantially improve substrate efficacy over the BTF-designed chemosensors and should be more easily amenable to screens for

additional specificity determinants. For example, the RDF approach now makes viable the construction of protein-based sensors where the C-Sox reporter can be placed anywhere in the protein (e.g., via native chemical ligation described in Chapter 4) in order to obtain probes that fully exploit protein-protein interactions in enzyme selection. The BTF reporters, on the other hand, can only be located at peptide (and protein) termini (due to the β -turn) and, thus, have a more restricted utility. Ongoing work is focused on modifying the Sox chromophore to increase the excitation and emission wavelengths (Chapter 5). The RDF chemosensors, along with their assaying ease, may provide a way to tackle a very important problem of enzyme specificity as fluorescent probes start to make their way into the arena of monitoring kinase activities *in vivo*.

Acknowledgements

First, I am grateful to Dr. Juan Antonio Gonzalez Vera for performing the synthesis, purification and characterization of some of the peptides presented here. I thank Dr. Anne Reynolds, Dr. Matthieu Sainlos, Dr. Melissa Shults and Angelyn Larkin for helpful discussions and Dr. Matthieu Sainlos for obtaining MALDI TOF MS. This research was supported by the NIH Cell Migration Consortium (GM064346) and the Invitrogen Corporation. The Biophysical Instrumentation Facility for the Study of Complex Macromolecular Systems (NSF-0070319) and the Department of Chemistry Instrumentation Facility (NIH-1S10RR013886-01) are also gratefully acknowledged.

Experimental Methods

General information

Unless otherwise noted, all solvents and reagents were obtained commercially and used without further purification. N^α-Fmoc-protected amino acids [Fmoc-Ala-OH, Fmoc-Arg(Pbf)-OH, Fmoc-Cyc(Mmt)-OH, Fmoc-Gly-OH, Fmoc-Leu-OH, Fmoc-Lys(Boc)-OH, Fmoc-Phe-OH, Fmoc-Pro-OH, Fmoc-Ser(tBu)-OH, Fmoc-Ser(PO(OBn)OH)-OH, Fmoc-Thr(tBu)-OH, Fmoc-Thr(PO(OBn)OH)-OH, Fmoc-Val-OH] were purchased from Novabiochem. Whenever anhydrous and/or degassed CH₂Cl₂ was necessary, it was distilled from calcium hydride and degassed by bubbling argon for at least 20 min. Analytical TLC was performed on silica gel 60 F₂₅₄ precoated plates (EMD Chemicals Inc.) and visualized by UV. Flash column chromatography was performed as previously described³⁶ using forced flow of the indicated solvent on AdTech Flash Silica Gel (32-60 μm packing, 60 Å pore diameter, Adedge Technologies). Organic solutions were concentrated in vacuo by rotary evaporation at ~10 Torr (house vacuum) at 25-40 °C, then at ~0.5 Torr (vacuum pump), unless otherwise indicated. Peptides were purified via preparative reverse-phase HPLC employing a gradient of solvents A (H₂O with 0.1% v/v TFA) and B (CH₃CN with 0.1% v/v TFA). Compounds were characterized by ¹H and ¹³C NMR and mass spectroscopy. Peptide purity was determined by analytical reverse-phase HPLC.

Instrumentation

NMR: ¹H and ¹³C NMR spectra were recorded on a Bruker 400 MHz Avance spectrometer. Chemical shifts (δ) are reported in parts per million (ppm) and referenced to CDCl₃ (7.26 ppm

for ^1H and 77.0 ppm for ^{13}C). Coupling constants (J) are reported in Hertz (Hz) and multiplicities are abbreviated as singlet (s), doublet (d), doublet of doublets (dd), triplet (t) and multiplet (m).

HPLC: HPLC was carried out on Waters Prep LC 4000 System or Waters Delta 600 System equipped with Waters 2487 dual wavelength absorbance detectors. Columns used: C_{18} analytical (flow rate = 1 mL/min), Beckman Ultrasphere ODS, 5 μm , 150 x 4.6 mm; C_{18} preparatory (flow rate = 15 mL/min), YMC-Pack Pro, 5 μm , 250 x 20 mm.

ESI-MS: Applied Biosystems Mariner mass spectrometer.

MALDI-TOF MS: PerSeptive Biosystems Voyager MALDI-TOF instrument.

HRMS: The Department of Chemistry Instrumentation Facility (DCIF), MIT.

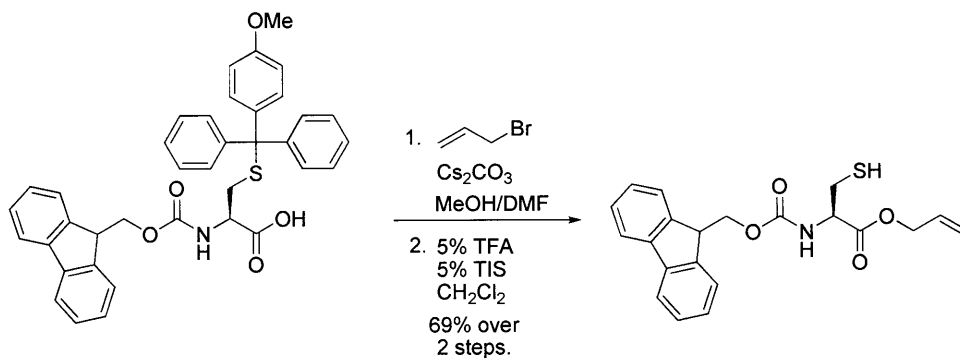
UV-Vis Spectrophotometer: Shimadzu UV-2401PC.

Fluorometer: Fluoromax 3 from Jobin Yvon. Cuvette: Starna Cells (16.100F-Q-10) 100 μL sub-micro cuvette, 1 cm path length.

Fluorescence Plate Reader: HTS 7000 Bio Assay Reader from Perkin Elmer. Plate: Corning (3992) assay plate, 96-well, half area, no lid, flat bottom, non-binding surface, non-sterile, white polystyrene.

Fmoc-C(Sox[TBDPS])-OH synthesis

a. Fmoc-Cys-OAllyl (3)



1. To an oven-dried, one-necked, 500 mL round-bottomed flask equipped with a stir bar and under positive N_2 pressure was added Fmoc-Cys(Mmt)-OH (**1**; 8.92 mmol, 5.49 g, 1 equiv. dissolved in 50 mL CH_2Cl_2) followed by MeOH (50 mL). The colorless solution was then allowed to stir for 3 min at room temperature. To this solution was added Cs_2CO_3 (4.46 mmol, 1.45 g, 0.5 equiv.) and mixture was allowed to stir at room temperature under N_2 for 45 min at which time the solvent was removed in vacuo. The resulting white, fluffy solid was dissolved in DMF (100 mL, anhydrous) and immediately following this, allyl bromide (26.75 mmol, 3.24 g, 3 equiv.) was added. The reaction mixture was stirred at room temperature under positive N_2 pressure for 5 hours. During this time, the reaction was monitored by TLC ($R_f = 0.23$, 20% EtOAc in hexanes). Upon completion, the reaction mixture was diluted with EtOAc (1 L), washed with 2% NaHCO_3 (200 mL), H_2O (250 mL x 3), brine (250 mL x 3), dried (Na_2SO_4), and concentrated in vacuo.
2. The crude product from the previous step was dissolved in degassed, anhydrous CH_2Cl_2 (90 mL). To the slightly yellow solution were added TIS (5 mL) and TFA (5 mL). The resulting red solution was allowed to react at room temperature under N_2 for 2.5 hrs and was monitored

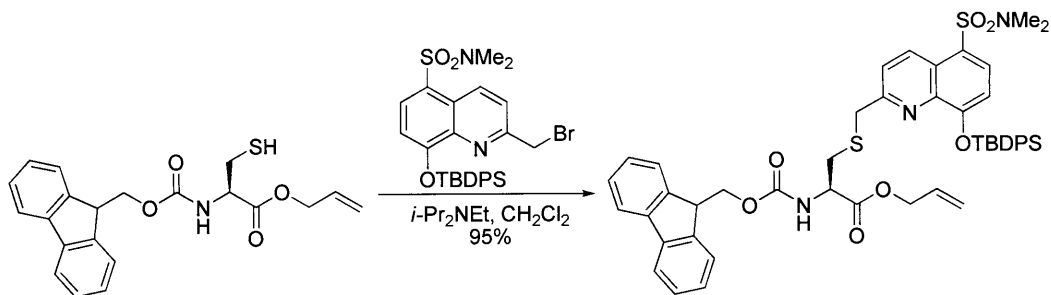
by TLC ($R_f = 0.28$, 20% EtOAc in hexanes). The reaction mixture turns a clear yellow color upon completion. The reaction was diluted in CH_2Cl_2 (300 mL), washed with 5% NaHCO_3 (250 mL x 2), H_2O (250 mL), brine (300 mL), dried (Na_2SO_4) and concentrated in vacuo. Flash column chromatography (SiO_2 ; diameter: 70 mm; length: 23 cm; packing: 20% EtOAc in hexanes; load crude product in CH_2Cl_2 ; eluent: 20% EtOAc in hexanes) was used to purify the product, which was isolated as a fluffy white solid. Yield: 69% (2.36 g).

^1H NMR (400 MHz, CDCl_3 , 20 °C) δ ppm: 1.38 (t, $J = 8.90$ Hz, 1H), 3.10-2.94 (m, 2H), 4.24 (t, $J = 6.83$ Hz, 1H), 4.49-4.38 (m, 2H), 4.78-4.62 (m, 3H), 5.29 (d, $J = 10.38$ Hz, 1H), 5.37 (d, $J = 17.15$ Hz, 1H), 5.72 (d, $J = 6.97$ Hz, 1H), 5.98-5.88 (m, 1H), 7.33 (t, $J = 7.45$ Hz, 2H), 7.41 (t, $J = 7.47$ Hz, 2H), 7.61 (d, $J = 7.25$ Hz, 2H), 7.77 (d, $J = 7.48$ Hz, 2H).

^{13}C NMR (100 MHz, CDCl_3 , 20 °C) δ ppm: 27.1, 47.1, 55.2, 66.5, 67.1, 119.4, 120.0, 125.0, 127.1, 127.7, 131.2, 141.3, 143.7, 155.6, 169.6.

HRMS (ESI): calcd for $\text{C}_{21}\text{H}_{21}\text{NNaO}_4\text{S}$ [$\text{M} + \text{Na}$] $^+$: 406.1089, found: 406.1098.

b. Fmoc-Cys(Sox[TBDPS])-OAllyl (6)



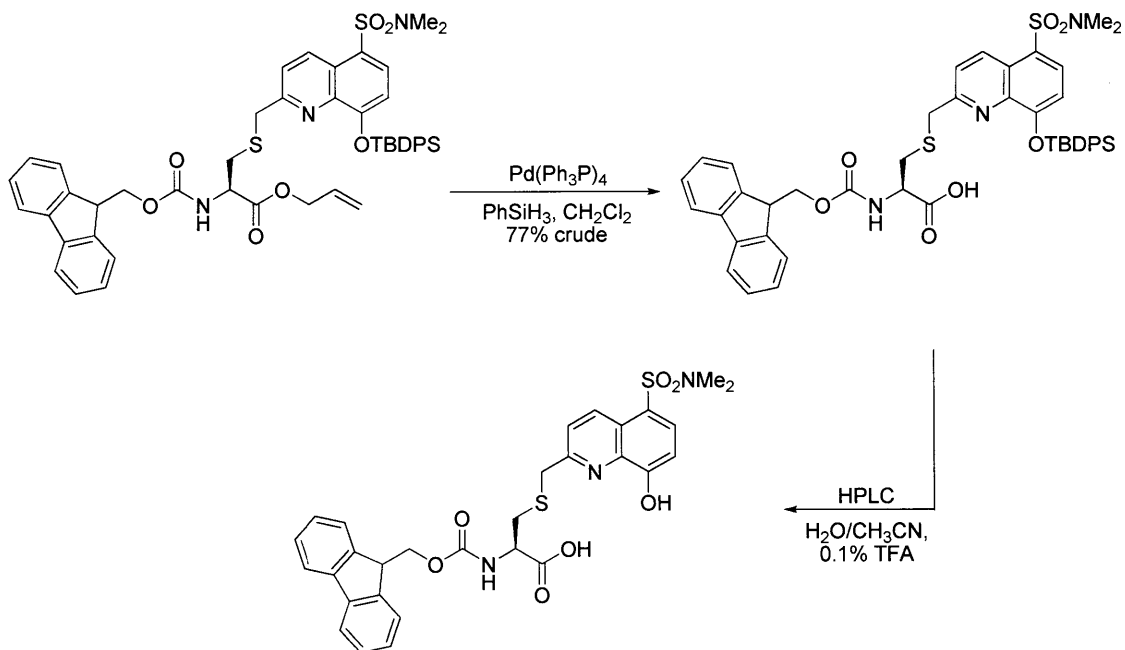
To an oven-dried, one-necked, 500 mL round-bottomed flask equipped with a stir bar and under positive N₂ pressure was added Fmoc-Cys-OAllyl (4.98 mmol, 1.91 g, 1 equiv.) dissolved in anhydrous CH₂Cl₂ (70 mL). To this colorless solution was added Sox-Br⁴ (4.98 mmol, 2.9 g, 1 equiv.) followed by freshly distilled DIEA (7.46 mmol, 1.3 mL, 1.5 equiv.). The reaction (pale yellow in color) was stirred at room temperature under the positive N₂ pressure overnight and was monitored by TLC (R_f = 0.36, 1:2 EtOAc in hexanes) until completion. The crude reaction was diluted with CH₂Cl₂ (400 mL), washed with sat'd. NH₄Cl (2 x 100 mL), H₂O (100 mL), brine (100 mL), dried (Na₂SO₄) and concentrated in vacuo. Flash column chromatography (SiO₂; diameter: 70 mm; length: 26 cm; packing: 10% EtOAc in hexanes; load crude product in CH₂Cl₂; eluent: 10, 20, 30% EtOAc in hexanes) was used to isolate the product as a white solid. Yield: 95% (3.43 g).

¹H NMR (400 MHz, CDCl₃, 20 °C) δ ppm: 1.18 (s, 9H), 2.82-2.67 (m, 2H), 2.72 (s, 6H), 3.57 (s, 2H), 4.24 (t, *J* = 7.04 Hz, 1H), 4.45-4.34 (m, 2H), 4.68-4.48 (m, 3H), 5.22 (dd, *J* = 10.42, 1.09 Hz, 1H), 5.28 (dd, *J* = 17.19, 1.23 Hz, 1H), 5.51 (d, *J* = 8.13 Hz, 1H), 5.89-5.78 (m, 1H), 7.11 (d, *J* = 8.32 Hz, 1H), 7.34-7.29 (m, 6H), 7.45-7.35 (m, 4H), 7.53 (d, *J* = 8.97 Hz, 1H), 7.61 (dd, *J* = 7.21, 2.86 Hz, 2H), 7.78-7.75 (m, 6H), 7.99 (d, *J* = 8.32 Hz, 1H), 8.95 (d, *J* = 8.96 Hz, 1H).

^{13}C NMR (100 MHz, CDCl_3 , 20 °C) δ ppm: 20.0, 26.4, 34.1, 37.2, 38.2, 46.9, 53.3, 66.2, 67.1, 115.3, 118.9, 119.9, 122.3, 123.7, 125.0, 125.1, 127.0, 127.6, 127.6, 129.6, 131.1, 131.6, 133.3, 133.3, 134.2, 134.8, 140.3, 141.1, 143.6, 143.6, 155.5, 156.8, 157.1, 170.1.

HRMS (ESI): calcd for $\text{C}_{49}\text{H}_{51}\text{N}_3\text{NaO}_7\text{S}_2\text{Si}$ $[\text{M} + \text{Na}]^+$: 908.2835, found: 908.2827.

c. *Fmoc-Cys(Sox[TBDPS])-OH (5)*



To an oven-dried, one-necked, 250 mL round-bottomed flask equipped with a stir bar and under positive N₂ pressure was added Fmoc-Cys(Sox[TBPDS])-Oallyl (3.62 mmol, 3.21 g, 1 equiv.) dissolved in anhydrous and degassed CH₂Cl₂ (100 mL). To the pale red solution was added PhSiH₃ (90.47 mmol, 11.2 mL, 25 equiv.) followed by Pd(PPh₃)₄ (0.145 mmol, 167.26 mg, 0.04 equiv.). After 10 min the reaction turned a deep red color. The resulting mixture was stirred at room temperature under the positive N₂ pressure for 3 hours and was monitored by TLC (R_f = 0.36, 10 % MeOH in CH₂Cl₂). Upon completion of the reaction, the solvent was removed in vacuo. The crude mixture was passed through a short flash column (SiO₂; diameter: 70 mm; length: 7 cm; packing: CH₂Cl₂; load crude product in CH₂Cl₂; eluent: 1, 2, 3, 4, 5, 10, 15% MeOH in CH₂Cl₂) to obtain 77% recovery of product. Analytical HPLC revealed one peak (t_R = 32.1 min; loading: dissolve 3 mg in DMSO; injection: 12 μL; method: 5% B (5 min) → 20% B (1 min) → 95% B (30 min), Abs: 280 nm and 316 nm) that was determined by ESI-MS to be Fmoc-C(Sox)-OH (calcd for C₃₀H₃₀N₃O₇S₂ [M + H]⁺: 608.15, found: 608.1) since the acidic

conditions of HPLC solvents remove the TBDPS protecting group. ^1H NMR, prior to HPLC analysis, shows that the TBDPS protecting group is still present in the crude material. The amino acid was used in SPPS without further purification.

^1H NMR (400 MHz, CDCl_3 , 20 °C) δ ppm 1.10 (s, 9H), 2.63 (s, 6H), 2.86-2.66 (m, 2H), 3.59-3.43 (m, 2H), 4.51-4.06 (m, 4H), 5.65-5.49 (m, 1H), 7.02 (d, $J = 7.94$ Hz, 1H), 7.33-7.27 (m, 2H), 7.46-7.39 (m, 4H), 7.57-7.48 (m, 4H), 7.76-7.59 (m, 9H), 7.91 (d, $J = 8.06$ Hz, 1H), 8.83 (d, $J = 8.77$ Hz, 1H)

HRMS (ESI) of Fmoc-C(Sox[TBDPS])-OH: calcd for $\text{C}_{46}\text{H}_{47}\text{N}_3\text{NaO}_7\text{S}_2\text{Si}$ $[\text{M} + \text{Na}]^+$: 868.2522, found: 868.2540.

Peptide synthesis

Coupling chemistry and conditions

All peptides were synthesized using the standard Fmoc-based amino acid protection chemistry. PKC peptides were synthesized on Fmoc-PAL-PEG-PS resin (Applied Biosystems, 0.19 mmol/g) using either the on-resin alkylation (vide infra) or the Fmoc-C(Sox[TBDPS])-OH building block. ERK1/2 peptides were synthesized on Fmoc-Gly-NovaSyn TGT resin (Novabiochem, 0.20 mmol/g) using the C-Sox building block. The resin was swelled in CH_2Cl_2 (5 min.) and then DMF (5 min) prior to synthesis. All the amino acids except for Fmoc-C(Sox[TBDPS])-OH were coupled according to the following procedure: Fmoc deprotection (20% 4-methylpiperidine in DMF, 3 x 5 min), rinsing step (DMF, 5 x), coupling step (amino acid/PyBOP/HOBt/DIEA, 6:6:6:6, 0.15 M in DMF, 30-45 min), rinsing step (DMF, 5 x; CH_2Cl_2 ,

5 x). Fmoc-C(Sox[TBDPS])-OH was coupled in the following manner: amino acid/PyAOP/HOAt/DIEA, 2:2:2:5, 0.15 M in DMF, 2-12 hr. The coupling was repeated if necessary (amino acid/PyAOP/HOAt/DIEA, 1:1:1:3, 0.15 M in DMF, 2-12 hr) as determined by the TNBS test for free amines. It is important to wash the resin rigorously (DMF followed by CH₂Cl₂) to remove excess amino acid before performing any tests for free amines. This is particularly necessary after coupling of Fmoc-C(Sox[TBDPS])-OH due to its deep red color, which does not affect its coupling efficiency. At the end of the synthesis, the Fmoc group was removed with 20% 4-methylpiperidine in DMF (3 x 5 min.) and the resin was rinsed with DMF (5 x). The resin-attached free amines were capped by exposure to Ac₂O (20 equiv.) and pyridine (20 equiv.) in DMF for 30 min. The resin was rinsed with DMF (5 x), CH₂Cl₂ (5 x) and subjected to 20% 4-methylpiperidine in DMF (3 x 5 min.) to remove any Sox aryl esters that might have formed during acetylation. The resin was finally washed with DMF, CH₂Cl₂, MeOH (5 x each) and dried under vacuum.

a. On-resin alkylation of peptides with Sox-Br

Resin-bound peptides (50 mg, 0.0095 mmol, 1 equiv.) incorporating Cys(Mmt) were swelled in CH₂Cl₂, then DMF (5 min each). The Mmt protecting group was removed from the resin-bound peptide by bubbling N₂ through a solution of 1% TFA, 5% TIS in CH₂Cl₂ (4 x 20 min or until most of the yellow color due to the Mmt cation has disappeared). The resin was then subjected to rigorous washing with CH₂Cl₂ (5 x) and DMF (5 x). Anhydrous DMF (200 μL) was added to the resin followed by freshly distilled tetramethylguanidine (5.96 μL, 0.0475 mmol, 5 equiv.). The mixture was incubated for 2-3 min. Sox-Br (17 mg, 0.0285 mmol, 3 equiv.) was dissolved in anhydrous DMF (150 μL) and added to the resin. After ca. 12 hours of reaction time, the excess reagents were drained and the resin washed with DMF, CH₂Cl₂, MeOH, CH₂Cl₂ (5 x each).

b. Side chain deprotection and cleavage from resin

The resin cleavage and protecting group removal was achieved by exposing the resin-bound peptides to TFA/EDT/H₂O/TIS (94:2.5:2.5:1% v/v) for sequences containing easily oxidized residues (e.g. Cys, Met, Trp) or TFA/H₂O/TIS (95:2.5:2.5% v/v) for sequences without such residues (C-Sox does not require EDT in the cleavage cocktail). The resulting solution was concentrated under a stream of N₂ and precipitated by addition of cold Et₂O. The pellet was triturated with cold Et₂O (3 x), redissolved in water, filtered and lyophilized. The peptides were purified by preparative reverse-phase HPLC using UV detection at either 228 nm (amide bond absorption) and 280 nm (Fmoc, Trp, and/or Tyr absorption) or 228 nm and 316 nm (Sox absorption). Only fractions showing a single peak of correct mass by analytical HPLC were used in further experiments.

c. Characterization data for peptides

Kinase	Peptide Sequence	Mol. Formula	HPLC <i>t_R</i> (min) ^a	[M+xH] ⁺⁺ Calcd.	[M+H] ⁺ found ^b
Src-2	Ac-Sox-PEIYGFEFAK ⁴ KKK-CONH ₂	C ₈₉ H ₁₃₃ N ₂₁ O ₂₅ S	27.4	1927.95	1928.93
	Ac-Sox-PEIpYGFEFAK ⁴ KKK-CONH ₂	C ₈₉ H ₁₃₄ N ₂₁ O ₂₈ PS	25.7	2007.92	2008.20
	Ac-AEE-CSox-IYGFEFAK ⁴ KKK-CONH ₂	C ₉₃ H ₁₄₀ N ₂₂ O ₂₈ S ₂	24.9	2077.96	2079.79
	Ac-AEE-CSox-IPYGFEFAK ⁴ KKK-CONH ₂	C ₉₃ H ₁₄₁ N ₂₂ O ₃₁ PS ₂	23.9	2157.93	2159.48
Abl	Ac-E-CSox-IYAAPFAK ⁴ KKK-CONH ₂	C ₇₈ H ₁₁₆ N ₁₈ O ₁₉ S ₂	22.9	1672.81	1674.01
	Ac-E-CSox-IPYAAPFAK ⁴ KKK-CONH ₂	C ₇₈ H ₁₁₇ N ₁₈ O ₂₂ PS ₂	22.3	1752.78	1753.30
	Ac-CSox-AIYAAPFAK ⁴ KKK-CONH ₂	C ₇₆ H ₁₁₄ N ₁₈ O ₁₇ S ₂	20.2	1614.81	1615.87
	Ac-CSox-ALPYAAPFAK ⁴ KKK-CONH ₂	C ₇₆ H ₁₁₅ N ₁₈ O ₂₀ PS ₂	19.2	1694.77	1695.67
	Ac-CSox-EAIYAAPFAK ⁴ KKK-CONH ₂	C ₈₁ H ₁₂₁ N ₁₉ O ₂₀ S ₂	23.8	1743.85	1744.82
	Ac-CSox-EALPYAAPFAK ⁴ KKK-CONH ₂	C ₈₁ H ₁₂₂ N ₁₉ O ₂₃ PS ₂	22.7	1823.81	1824.84
	Ac-EAIYAA-CSox-FAK ⁴ KKK-CONH ₂	C ₇₆ H ₁₁₄ N ₁₈ O ₁₉ S ₂	26.0	1646.79	1646.93
	Ac-EALPYAA-CSox-FAK ⁴ KKK-CONH ₂	C ₇₆ H ₁₁₅ N ₁₈ O ₂₂ PS ₂	24.4	1726.76	1727.09
IRK	Ac-Sox-PGDY-Nle-TMQIGKK-CONH ₂	C ₇₆ H ₁₁₆ N ₁₈ O ₂₃ S ₂	22.8	1712.79	1713.83
	Ac-Sox-PGDpY-Nle-TMQIGKK-CONH ₂	C ₇₆ H ₁₁₇ N ₁₈ O ₂₆ PS ₂	22.4	1792.76	1793.00
	Ac-R-CSox-DY-Nle-TMQIGKK-CONH ₂	C ₇₆ H ₁₂₁ N ₂₁ O ₂₁ S ₃	24.7	1847.90	1848.19
	Ac-R-CSox-DpY-Nle-TMQIGKK-CONH ₂	C ₇₆ H ₁₂₂ N ₂₁ O ₂₄ PS ₃	23.7	1927.90	1927.91
PKCα	Ac-RRRK-CSox-SFRRKA-NH ₂	C ₇₄ H ₁₂₅ N ₃₁ O ₁₆ S ₂	23.6	1767.94	1768.74
	Ac-RRRK-CSox-pSFRRKA-NH ₂	C ₇₄ H ₁₂₆ N ₃₁ O ₁₉ PS ₂	25.7	1847.90	1849.88

	Ac-RRR-CSox-GSFRRR-CONH ₂	C ₇₀ H ₁₁₆ N ₃₀ O ₁₆ S ₂	21.6 ^c	425.2 (+4)	425.8 ^e
	Ac-RRR-CSox-GpSFRRKA-CONH ₂	C ₇₀ H ₁₁₇ N ₃₀ O ₁₉ PS ₂	22.1 ^d	445.2 (+4)	445.0 ^e
	Ac-RRR-CSox-ASFRRR-CONH ₂	C ₇₁ H ₁₁₈ N ₃₀ O ₁₆ S ₂	21.3 ^c	428.7 (+4)	429.3 ^e
	Ac-RRR-Csox-ApSFRRKA-CONH ₂	C ₇₁ H ₁₁₉ N ₃₀ O ₁₉ PS ₂	23.7 ^c	448.7 (+4)	449.4 ^e
PKCδ	Ac-RKRKGSF-CSox-YGG-CONH ₂	C ₆₈ H ₁₀₂ N ₂₂ O ₁₇ S ₂	20.9	1562.72	1563.26
	Ac-RKRKGpSF-CSox-YGG-CONH ₂	C ₆₈ H ₁₀₃ N ₂₂ O ₂₀ PS ₂	20.5	1642.69	1643.34
	Ac-RKRKGSF-DPro-Sox-G-CONH ₂	C ₆₁ H ₉₅ N ₂₁ O ₁₅ S	21.8	1393.70	1394.77
	Ac-RKRKGpSF-DPro-Sox-G-CONH ₂	C ₆₁ H ₉₆ N ₂₁ O ₁₈ PS	19.6	1473.67	1474.65
PKCβI	Ac-LKR-CSox-ASFKKFA-CONH ₂	C ₇₄ H ₁₁₄ N ₂₀ O ₁₆ S ₂	24.9	1602.82	1603.58
	Ac-LKR-CSox-ApSFKKFA-CONH ₂	C ₇₄ H ₁₁₅ N ₂₀ O ₁₉ PS ₂	23.4	1682.78	1683.53
	Ac-Sox-PASFKKFA-CONH ₂	C ₆₁ H ₈₅ N ₁₃ O ₁₄ S	22.8	1256.61	1257.62
	Ac-Sox-PApSFKKFA-CONH ₂	C ₆₁ H ₈₆ N ₁₃ O ₁₇ PS	22.2	1335.57	1337.18
Pim2	Ac-ARKRRRHPSG-CSox-PTA-CONH ₂	C ₇₈ H ₁₂₈ N ₃₂ O ₂₀ S ₂	19.7	1896.94	1898.19
	Ac-ARKRRRHPpSG-CSox-PTA-CONH ₂	C ₇₈ H ₁₂₉ N ₃₂ O ₂₃ PS ₂	20.6	1976.91	1978.33
Akt1	Ac-ARKRERAYSF-CSox-HHA-CONH ₂	C ₈₈ H ₁₂₉ N ₃₁ O ₂₂ S ₂	20.5	2035.94	2036.60
	Ac-ARKRERAYpSF-CSox-HHA-CONH ₂	C ₈₈ H ₁₃₀ N ₃₁ O ₂₅ PS ₂	22.5	2115.90	2116.82
MK2	Ac-AHLQRQLSI-CSox-HH-CONH ₂	C ₇₆ H ₁₁₅ N ₂₅ O ₁₉ S ₂	21.6	1747.01	1748.25
	Ac-AHLQRQLpSI-CSox-HH-CONH ₂	C ₇₆ H ₁₁₆ N ₂₅ O ₂₂ PS ₂	23.6	1826.79	1830.02
PKA	Ac-LRRASL-DPro-Sox-G-CONH ₂	C ₅₆ H ₉₁ N ₁₉ O ₁₅ S	24.8	1230.63	1232.75
	Ac-LRRApSL-DPro-Sox-G-CONH ₂	C ₅₆ H ₉₂ N ₁₉ O ₁₈ PS	23.1	1310.60	1311.66
	Ac-ALRRASL-CSox-AA-CONH ₂	C ₅₆ H ₉₂ N ₁₈ O ₁₆ S ₂	25.8	1336.64	1336.70
	Ac-ALRRApSL-CSox-AA-CONH ₂	C ₅₆ H ₉₃ N ₁₈ O ₁₉ PS ₂	24.6	1416.60	1417.81
ERK1/2	Ac-VPLLTP-CSox-GRRG-COOH	C ₆₄ H ₁₀₃ N ₁₉ O ₁₇ S ₂	26.8	1474.70	1475.43
	Ac-VPLLpTP-CSox-GRRG-COOH	C ₆₄ H ₁₀₄ N ₁₉ O ₂₀ PS ₂	25.7	1554.70	1554.60
	Ac-VPLLTP-G-CSox-RRG-COOH	C ₆₄ H ₁₀₃ N ₁₉ O ₁₇ S ₂	26.4	1474.70	1474.81
	Ac-VPLLpTP-G-CSox-RRG-COOH	C ₆₄ H ₁₀₄ N ₁₉ O ₂₀ PS ₂	25.5	1554.70	1554.59
	Ac-VP-CSox-LTPGGRRG-COOH	C ₆₀ H ₉₅ N ₁₉ O ₁₇ S ₂	25.7	1418.60	1418.56
	Ac-VP-CSox-LpTPGGRRG-COOH	C ₆₀ H ₉₆ N ₁₉ O ₂₀ PS ₂	24.4	1498.60	1498.71
	Ac-Sox-PLTPGGRRG-COOH	C ₅₄ H ₈₄ N ₁₈ O ₁₆ S	22.9	1272.60	1273.47
	Ac-Sox-PLpTPGGRRG-COOH	C ₅₄ H ₈₅ N ₁₈ O ₁₉ PS	23.1	1352.57	1353.40

^a Reported retention times (t_R) and HPLC conditions are from analytical runs. Method: 5% B (5 min) followed by linear gradient 5–95% B (30 min) unless otherwise noted. ^b The data was collected on MALDI TOF mass spectrometer unless otherwise indicated. ^c Method: 5% B (5 min) followed by an increase to 15% B (1 min) and a linear gradient 15–30% B (30 min). ^d Method: 5% B (5 min) followed by linear gradient 5–50% B (30 min). ^e The data was collected on ESI mass spectrometer.

Stock solutions

Due to the affinity of the phosphorylated peptides for selected transition metal ions (including Zn²⁺),⁵ only reagents of the highest purity and lowest metal content were used to avoid the need to remove metal ion impurities after preparation.

1. Stock solutions of the peptides were prepared in doubly deionized water and concentrations were determined by UV-Vis (based on the determined extinction coefficient of the

fluorophore unit, 5-(*N,N*-dimethylsulfonamido)-8-hydroxy-2-methylquinoline, $\epsilon_{355} = 8247 \text{ M}^{-1} \text{ cm}^{-1}$ at 355 nm in 0.1 M NaOH with 1 mM Na_2EDTA).³ An average of the values from three separate solutions, each prepared using a different volume of the stock solution, was read on UV-Vis spectrophotometer. Purified peptide stock solutions could be stored at 4 °C for at least 6 months or -20 °C for longer periods.

2. A magnesium chloride stock solution of 2.66 M and a calcium chloride stock solution of 354 mM were prepared using Puratronic grade salts from Alfa Aesar. Most commercially available salts contain Zn^{2+} as significant impurities and should not be used due to the high affinity of the phosphorylated peptides for Zn^{2+} . The Mg^{2+} and Ca^{2+} concentrations were determined by titration with a standardized solution of EDTA (Aldrich) in the presence of an Eriochrome Black T (Aldrich) as described previously.⁵
3. 500 mM HEPES (SigmaUltra) was prepared and adjusted to pH 7.4 with NaOH (99.998+%, Aldrich) solution.
4. 10 mM DTT (Biotechnology grade, Mallinckrodt) was prepared in degassed ultrapure water and stored in aliquots at -80 °C.
5. 20 mg/mL BSA (Heat Shock Fraction V, Roche) was prepared in ultrapure water, filtered through a 0.45 micron syringe filter to remove particulates and stored at 4 °C.
6. 0.1% Brij-35 P (Fluka) solution was prepared by dissolving an appropriate amount in doubly deionized water and was stored at room temperature.
7. 100 mM ATP (Disodium salt, Low Metals Grade, Calbiochem) was prepared in ultrapure water. The solution was stored in aliquots at -80 °C.
8. 500 mM EGTA (SigmaUltra) was prepared in 2 M NaOH and stored at 4 °C.

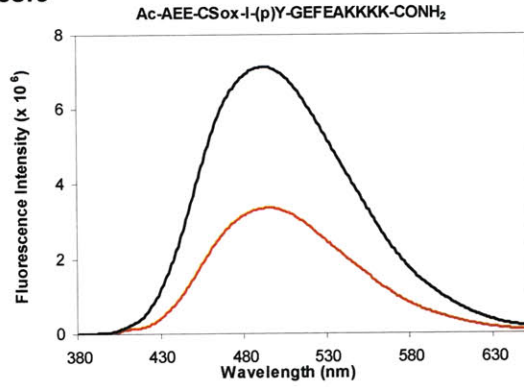
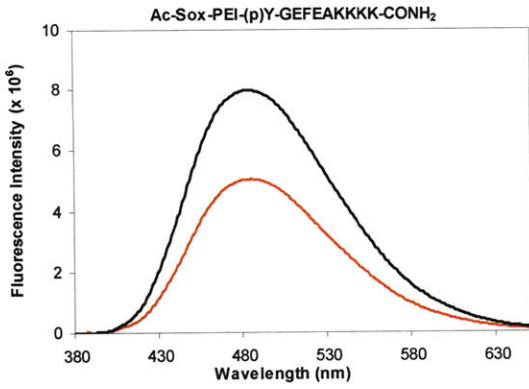
9. 10 $\mu\text{g}/\text{mL}$ phosphatidylserine and 2 $\mu\text{g}/\text{mL}$ diacylglycerol in 20 mM HEPES (pH 7.4) were prepared by combination of appropriate volumes of chloroform solutions of 10 mg/mL porcine brain phosphatidylserine (Avanti Polar Lipids, Inc.) and 2 mg/mL 1,2-dioleoyl-*sn*-glycerol (Avanti Polar Lipids, Inc.). The chloroform was evaporated and an appropriate amount of solution 3 was added. The solution was alternated between vortexing for 3 min intervals and incubating in warm water bath for 1 min for a total time of 12 min. The solution was stored in aliquots at $-20\text{ }^{\circ}\text{C}$. Samples were sonicated for 10 min before use in enzyme assays.

Fluorescence experiments

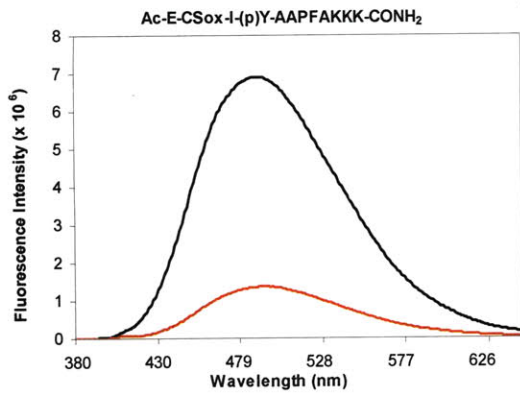
Spectral comparison of phosphorylated and unphosphorylated peptides

The fluorescence spectra of 10 μM phosphorylated (black) and unphosphorylated (red) peptides in 20 mM HEPES (pH 7.4) and 10 mM MgCl_2 were recorded in the fluorometer (slit widths: $E_m = 5\text{ nm}$, $E_x = 5\text{ nm}$; $\lambda_{ex} = 360\text{ nm}$, $\lambda_{em} = 380\text{-}650\text{ nm}$) in a quartz microcuvette (120 μL). The reported spectra are averages of three separate experiments.

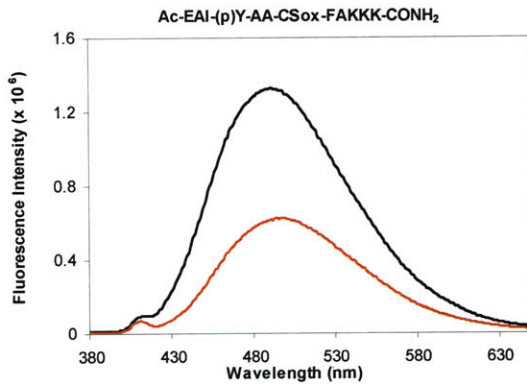
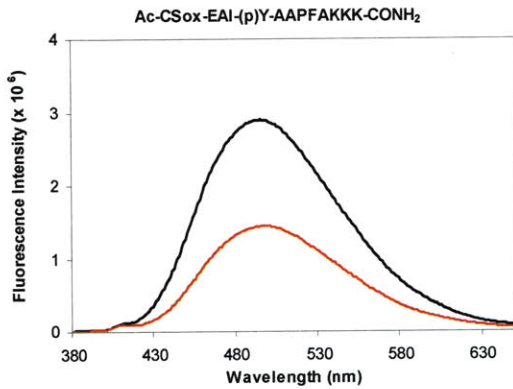
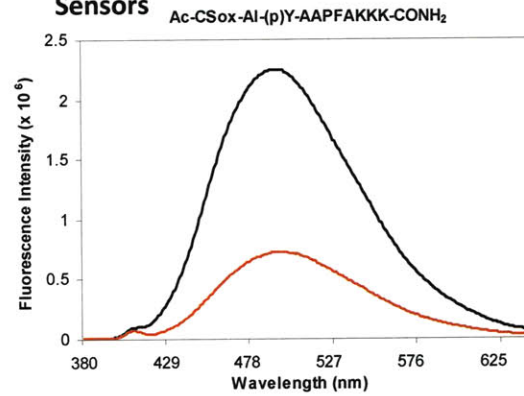
Src Sensors



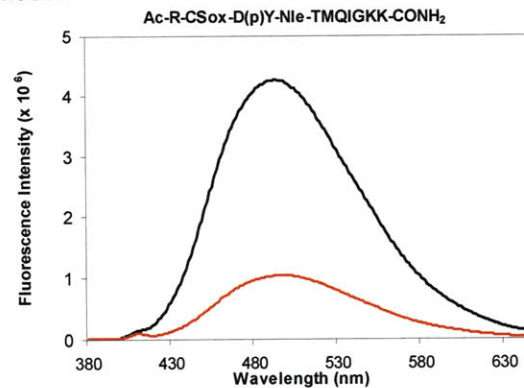
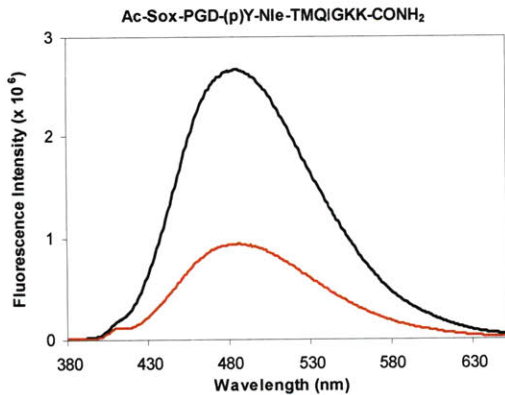
Abl



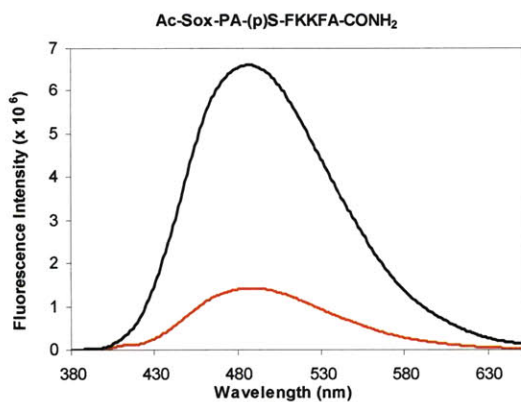
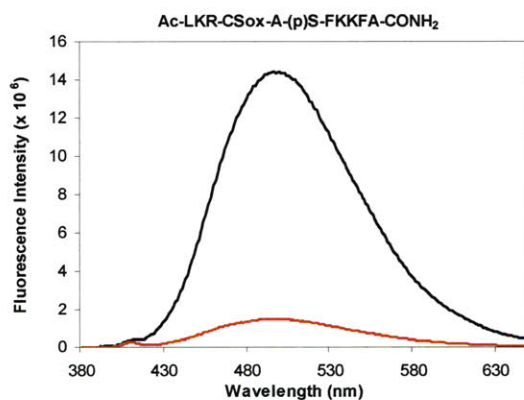
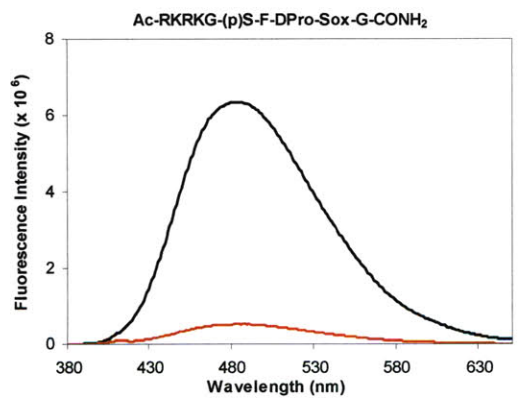
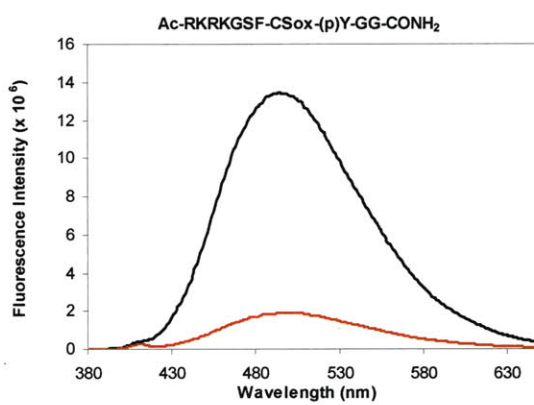
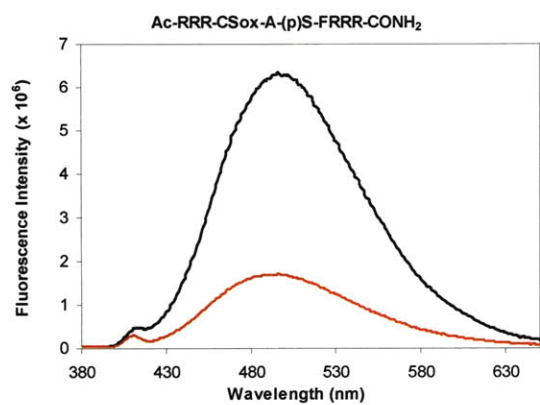
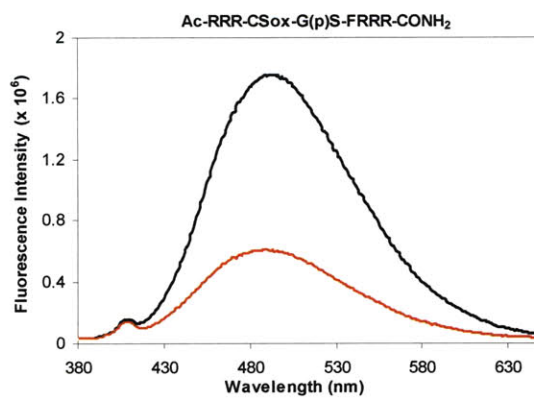
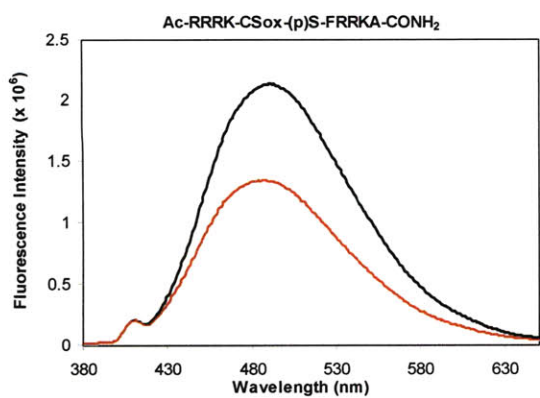
Sensors



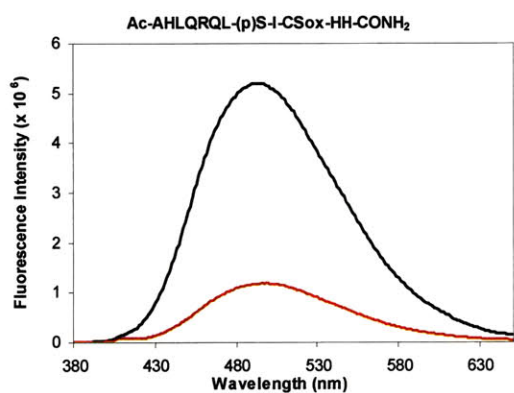
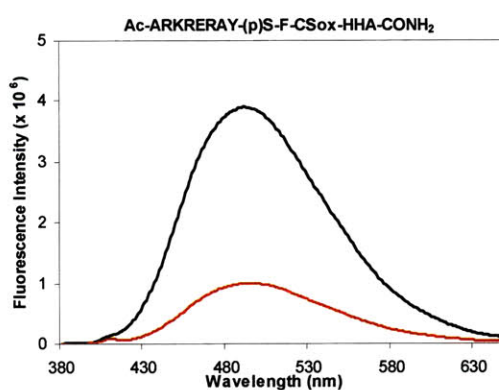
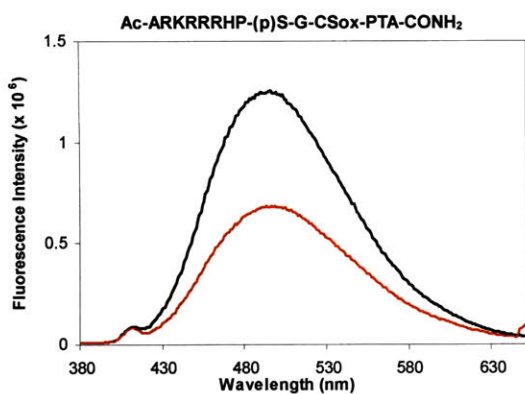
IRK Sensors



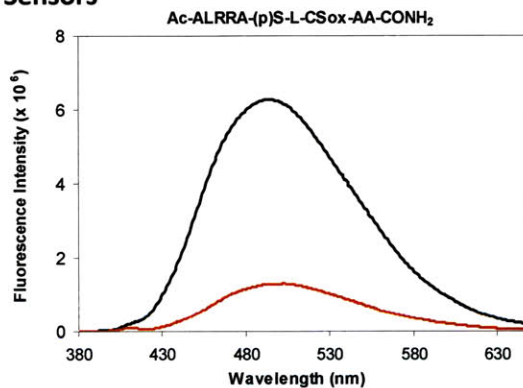
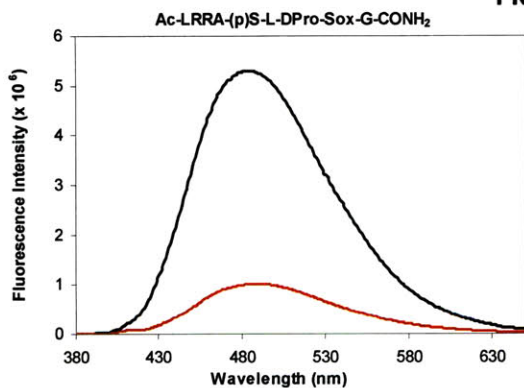
PKC Sensors



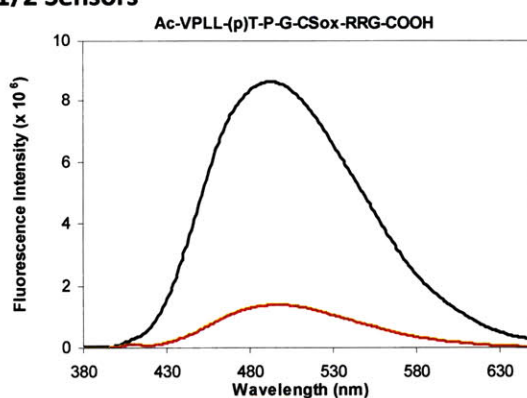
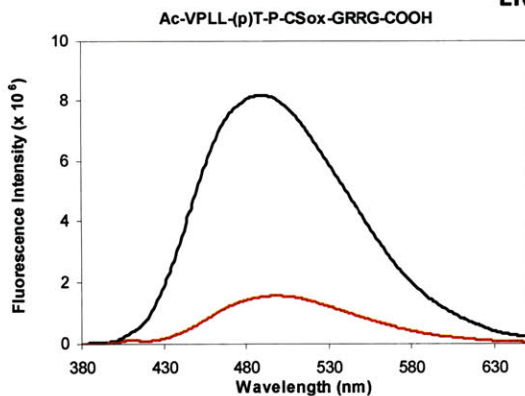
Pim2, Akt1 and MK2 Sensors

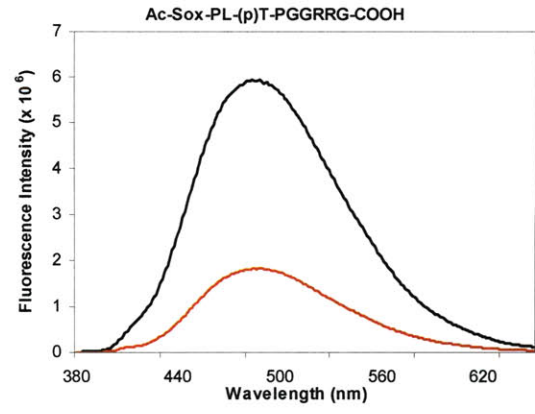
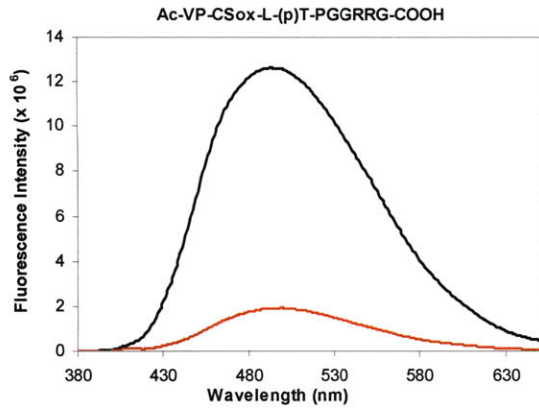


PKA Sensors



ERK1/2 Sensors





a. Calculation of Z' factors

The Z' factors are statistical quality parameters used in high-throughput screens to evaluate performance of such assays.²² Typically, assays are considered excellent if Z' is 0.5-1. The Z' values were calculated from data obtained for fluorescence increases using equation (1)

$$Z' = 1 - \frac{(3 \times \sigma_P) + (3 \times \sigma_S)}{|\mu_P - \mu_S|} \quad (1)$$

where μ_P and μ_S are the means of three measurements of fluorescence emission at 485 nm for phosphopeptide and substrate, respectively, and σ_P and σ_S are the standard deviations of those measurements for phosphopeptide and substrate, respectively.

b. Determination of Mg^{2+} dissociation constants (K_D)

Mg^{2+} titrations were performed in a buffer containing 20 mM HEPES (pH 7.4), 150 mM NaCl, 1 μ M of the appropriate phosphopeptide in a quartz cuvette for a total volume of 500 μ L. Aliquots of $MgCl_2$ stock solutions were added (for the final $MgCl_2$ concentration in the cuvette to be in the range of approximately 2-350 μ M) and the data was recorded in the fluorometer (slit widths: $E_m = 5$ nm, $E_x = 5$ nm; $\lambda_{ex} = 360$ nm, $\lambda_{em} = 380$ -650 nm). Data was fit with the program Specfit/32.³⁷ The reported values are from single experiments. Both Table 2-6 and Figure 2-4 indicate that higher affinity for Mg^{2+} generally results in larger fluorescence increase.

c. Fluorescence intensity dependence on [ATP] and [Mg^{2+}]

1. In the titrations reported in Figure 2-3, the concentration of the substrate was held constant while the concentration of ATP was varied. No enzyme was present. A solution of the substrate (or phosphopeptide) was prepared (20 mM HEPES [pH 7.4], 10 mM $MgCl_2$, 0.3 mM $CaCl_2$, 0.1 mM EGTA, 1 mM DTT, 0.5 μ g/mL phosphatidylserine, 0.1 μ g/mL

diacylglycerol, 10 μM peptide) and fluorometer readings were obtained without any ATP present. Then ATP (dilutions from stock solution 7) was added to final concentrations of 0.01, 0.05, 0.1, 0.25, 0.5, 0.8 or 1 mM. At each ATP concentration a fluorescence emission spectrum was recorded (slit widths: $E_m = 5 \text{ nm}$, $E_x = 5 \text{ nm}$; $\lambda_{\text{ex}} = 360 \text{ nm}$, $\lambda_{\text{em}} = 380\text{-}650 \text{ nm}$). Each measurement was repeated 3 times and the average fluorescence intensity \pm s.e.m. at 485 nm was plotted in bar graphs below.

2. In the measurements reported in Table 2-4 the concentration of the substrate was held constant while the concentration of ATP was varied. No enzyme was present. A solution of the substrate (or phosphopeptide) was prepared (20 mM HEPES [pH 7.4], 10 mM MgCl_2 , 10 μM peptide) and fluorometer readings were obtained without any ATP present. ATP (dilutions from stock solution 7) was then added to a final concentration of 0.1 or 1 mM. At each ATP concentration a fluorescence emission spectrum was recorded (slit widths: $E_m = 5 \text{ nm}$, $E_x = 5 \text{ nm}$; $\lambda_{\text{ex}} = 360 \text{ nm}$, $\lambda_{\text{em}} = 380\text{-}650 \text{ nm}$). Fluorescence increase was obtained by dividing the fluorescence of the phosphopeptide by the fluorescence of the substrate at 485 nm. The values reported are averages of at least three separate measurements.
3. In the measurements reported in Table 2-5 the concentration of the substrate was held constant while $[\text{ATP}]$ and $[\text{Mg}^{2+}]$ were varied. No enzyme was present. A solution of the substrate (or phosphopeptide) was prepared (20 mM HEPES [pH 7.4] and 10 μM peptide) and fluorometer readings were obtained without any ATP present. Then ATP (dilutions from stock solution 7) was added to a final concentration of 0.1 or 1 mM. At each ATP concentration, the appropriate volume of Mg^{2+} (dilutions of solution 2) was added to obtain fluorescence intensity at 1, 2, 5 or 10 mM. With every combination of $[\text{ATP}]$ and $[\text{Mg}^{2+}]$ the fluorescence emission spectra were recorded (slit widths: $E_m = 5 \text{ nm}$, $E_x = 5 \text{ nm}$; $\lambda_{\text{ex}} = 360 \text{ nm}$, $\lambda_{\text{em}} = 380\text{-}$

650 nm). Fluorescence increase was obtained by dividing the fluorescence of the phosphopeptide by the fluorescence of the substrate at 485 nm. The values reported are averages of at least three separate experiments

d. Recombinant enzyme assay protocols

Recombinant enzyme was added to initiate each reaction unless otherwise noted. Most of the kinetic assays were performed in the FPR ($\lambda_{\text{ex}} = 360$ nm, $\lambda_{\text{em}} = 485$ nm). The noted few were conducted in the fluorometer (same λ_{ex} and λ_{em} as in the FPR except for the BTF Src sensor: $\lambda_{\text{ex}} = 410$ nm). The reactions were carried out using either a fluorescence microcuvette (fluorometer) or a 96-well plate (FPR) (120 μL per reaction) containing varying chemosensor concentrations (generally 0.2–5 K_M) at 30 °C. Fluorescence slopes were determined by a least-squares fit using Microsoft Excel. Slopes were then either converted to a rate (see section VI.e.) or compared directly. The plots of v vs. $[S]$ were fit using SigmaPlot 9.01³⁸ in order to obtain K_M and V_{max} values. Standard assay conditions were as follows:

Src: 20 mM HEPES (pH 7.4), 10 mM MgCl_2 , 1 mM ATP, 1 mM DTT, 0.1 mM EGTA, 0.001% Brij-35 P, 60 ng Src with the BTF sensor and 4 ng Src with the RDF sensor (Upstate, appropriately diluted with 20 mM HEPES [pH 7.4], 0.1 mM EGTA, 1 mM DTT, 0.01% Brij-35 P, 5% glycerol and 1 mg/mL BSA). The BTF sensor kinetics were measured in the fluorometer.

Abl: 20 mM HEPES (pH 7.4), 10 mM MgCl_2 , 1 mM ATP, 1 mM DTT, 0.01 % Brij-35P, 4 ng Abl (New England Biolabs, appropriately diluted with 20 mM Tris pH 7.5, 10 mM MgCl_2 , 0.1 mM EGTA, 0.01% Brij-35 P and 1.0 mg/mL BSA).

IRK: 25 mM Tris (pH 7.3), 10 mM MgCl₂, 1 mM ATP, 2.5 mM DTT, 0.5 mM EGTA, 5 mM β -glycerophosphate, 0.01% Triton X-100, 0.2 mg/mL BSA, 4.3 ng IRK with the RDF sensor and 8.6 ng IRK with BTF sensor (Invitrogen, appropriately diluted with 20 mM Tris (pH 7.3), 10% Glycerol, 0.02% Triton X-100, 0.2 mg/mL BSA, and 2 mM DTT).

PKC α : 20 mM Hepes (pH 7.4), 10 mM MgCl₂, 0.3 mM CaCl₂, 0.1 mM EGTA, 0.1 mM ATP, 1 mM DTT, 0.5 μ g/mL phosphatidylserine, 0.1 μ g/mL diacylglycerol, 1 ng of PKC α (Calbiochem, appropriately diluted with 20 mM Hepes [pH 7.4], 10 mM MgCl₂, 0.3 mM CaCl₂, 1 mM DTT, 10 mg/mL BSA and 0.01% Brij-35 P). Substrate peptide was added to begin the reaction. The RDF sensor kinetics were measured in the fluorometer.

PKC β I: Same conditions as for PKC α using 10 ng of PKC β I with the RDF sensor and up to 100 ng PKC β I with the BTF sensor (Human, Recombinant, BioSource, same enzyme dilution conditions as for PKC α).

PKC δ : Same conditions as for PKC α using 10 ng of PKC δ with the RDF sensor and up to 60 ng with the BTF sensor (Human, Recombinant, BioSource, appropriately diluted with 20 mM HEPES [pH 7.4], 10 mM MgCl₂, 0.3 mM CaCl₂, 1 mM DTT, 10 mg/ml BSA, 0.1 M NaCl, and 0.01% Brij-35P). Substrate peptide was added to begin the reaction. The RDF sensor kinetics were measured in the fluorometer.

Pim2: 20 mM HEPES (pH 7.4), 10 mM MgCl₂, 0.1 mM ATP, 10 mM DTT, 0.5 mg/mL BSA, 0.1 mM EGTA, 11 ng Pim2 (Upstate, appropriately diluted with 20 mM Hepes [pH 7.4], 10 mM MgCl₂, 0.1 mM EGTA, 15 mM DTT, and 1 mg/mL BSA).

Akt1: 20 mM HEPES (pH 7.4), 10 mM MgCl₂, 1 mM ATP, 1 mM DTT, 0.1 mM EGTA, 1 ng Akt1 (Upstate, appropriately diluted with 20 mM HEPES [pH 7.4], 1 mM DTT, 0.1% Brij-35, and 1 mg/mL BSA).

MK2: 20 mM HEPES (pH 7.4), 10 mM MgCl₂, 1 mM ATP, 1 mM DTT, 0.1 mM EGTA, 0.01% Brij-35, 0.1 mg/mL BSA, 1 ng MK2 (Upstate, appropriately diluted with 20 mM HEPES [pH 7.4], 1 mM DTT, 0.1% Brij-35, and 1 mg/mL BSA).

PKA: 20 mM HEPES (pH 7.4), 10 mM MgCl₂, 1 mM ATP, 1 mM DTT, 0.1 mM EGTA, 0.5 ng PKA catalytic subunit (catalytic subunit, Calbiochem, appropriately diluted with 50 mM Tris [pH 7.3], 10 mM MgCl₂, 1 mM DTT, and 0.15 mg/mL BSA).

e. Determination of kinetic constants from fluorescence data

To solve for K_M and V_{max} for this reaction, determination of the initial rate of product formation from the increase in fluorescence intensity is necessary.⁵ With these sensors, a correction for the decrease in fluorescence intensity due to the starting material being consumed is needed to determine the rate of product formation from the initial slope. The fluorescence intensity at any given point can be determined from the following equation:

$$I(t) = f_s S(t) + f_p P(t) \tag{2}$$

where $I(t)$ is the fluorescence intensity, $S(t)$ is the amount of substrate in μM , $P(t)$ is the amount of product in μM , f_S is the fluorescence intensity per μM of substrate, and f_P is fluorescence intensity per μM of product. The amount of substrate and product at any given point are related by:

$$S(t) + P(t) = S_0 \quad (3)$$

where S_0 is the initial amount of substrate. Substitution of eq. (3) into eq. (2) followed by rearrangement yields:

$$P(t) = \frac{I(t) - f_S S_0}{f_P - f_S} \quad (4)$$

The initial velocity of the reaction is the change in the amount of product over time, so taking the derivative of eq. (4) with respect to time gives:

$$v = \frac{dP(t)}{dt} = \frac{\frac{dI(t)}{dt}}{f_P - f_S} \quad (5)$$

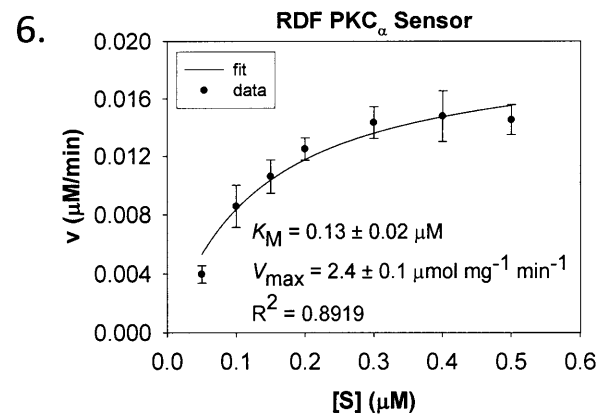
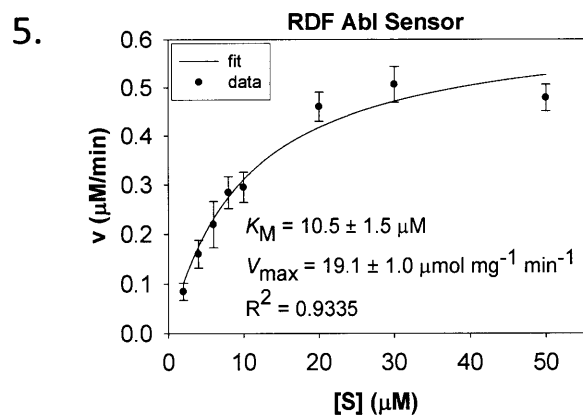
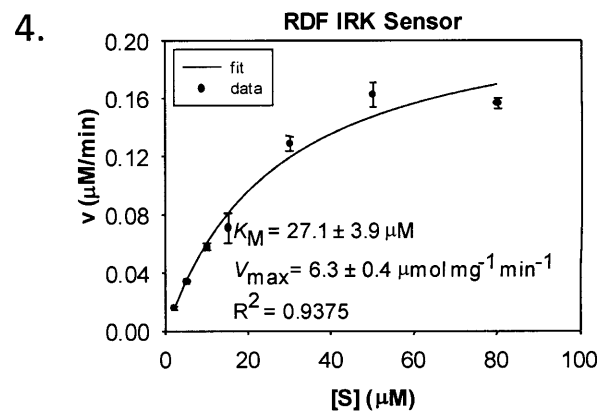
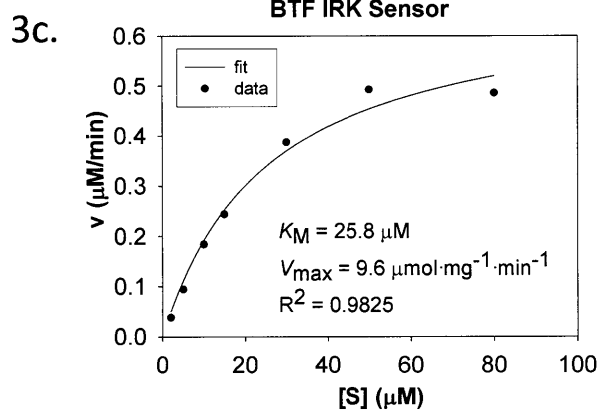
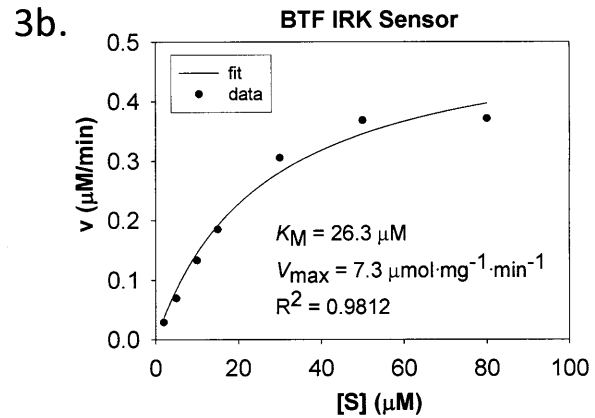
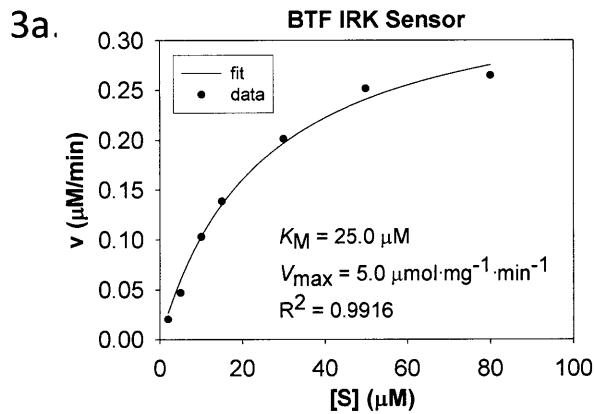
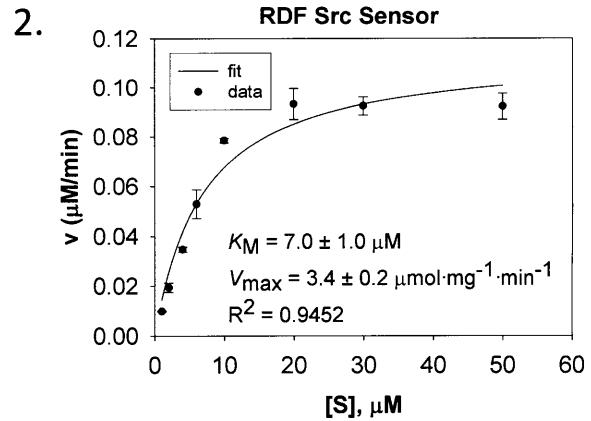
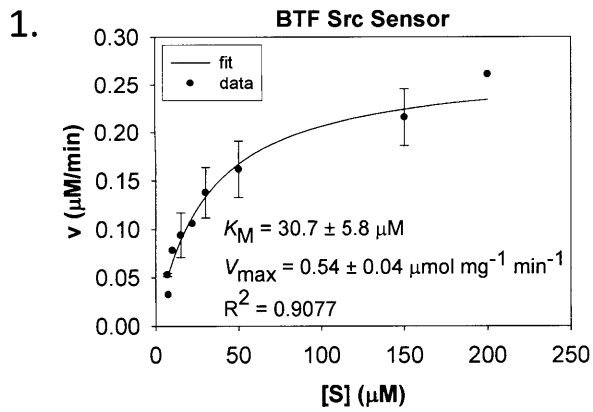
The initial slope of the reaction, $dI(t)/dt$, was measured within the first 10% of substrate turnover. The constants f_P and f_S were calculated from the slope of a line of fluorescence intensity versus concentration of P and S, respectively. These values depend on the concentration of Mg^{2+} and

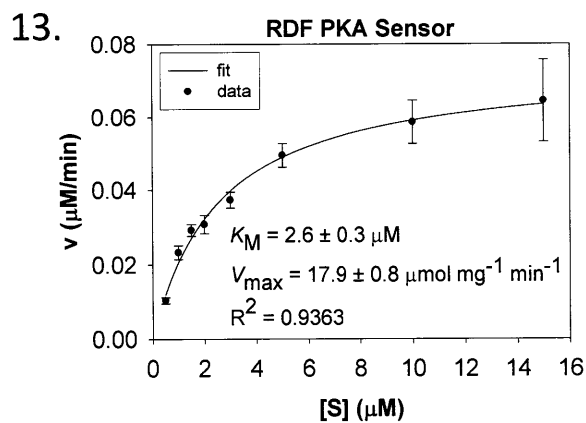
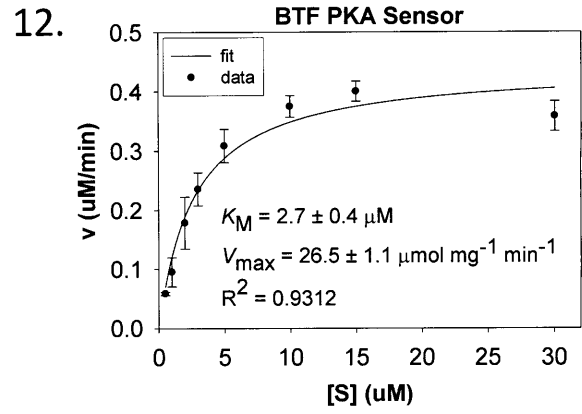
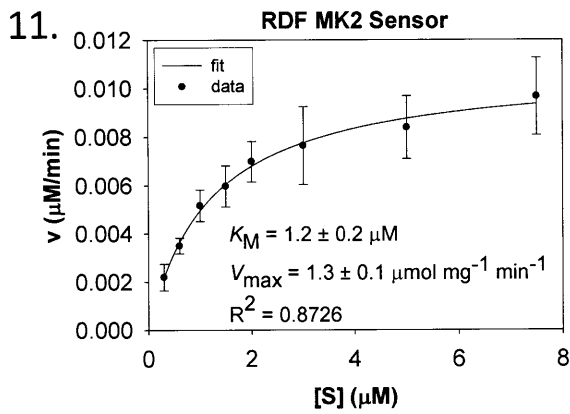
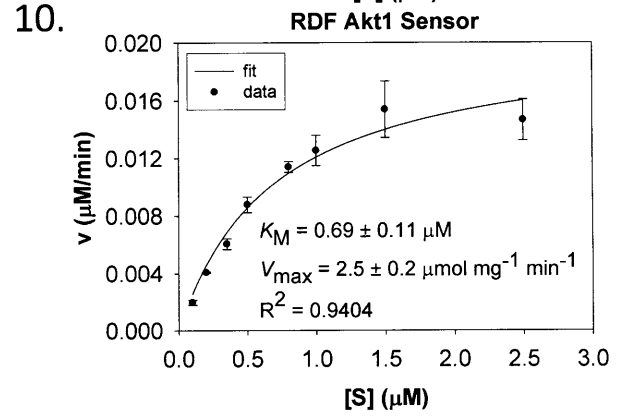
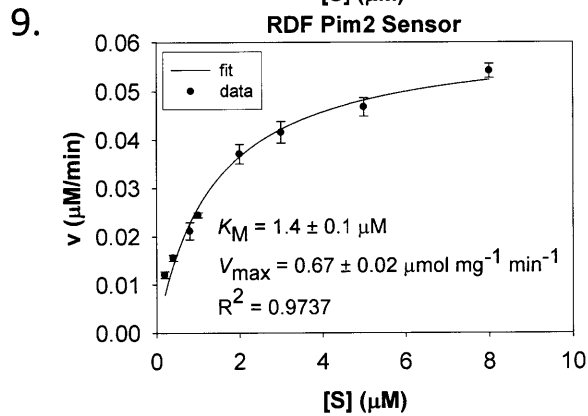
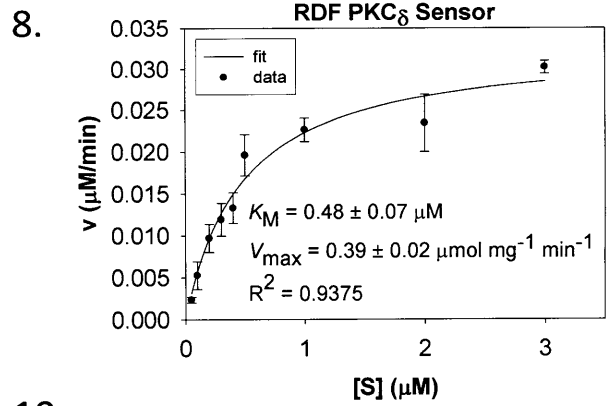
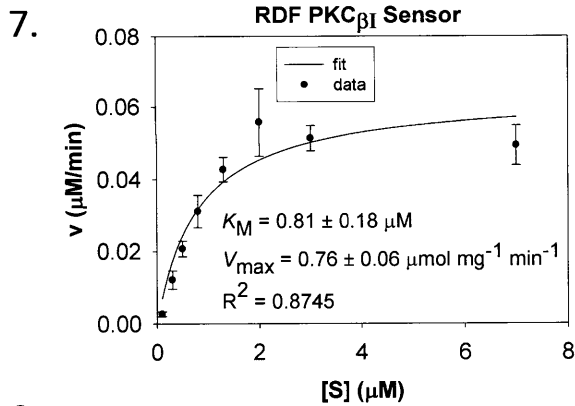
the Mg^{2+} dissociation constant of each peptide and are determined empirically under the desired assay conditions. A direct, non-linear fit of v vs. $[S]$ plots using the Briggs-Haldane equation (6) was used to find K_M and V_{\max} .

$$v = \frac{V_{\max} [S]}{K_M + [S]} \quad (6)$$

f. v vs. $[S]$ plots

Results of fluorescence increases reported in Table 2-7 were acquired by dividing the slope that was obtained for different concentrations of phosphopeptide (f_P) by the slope for the corresponding substrate (f_S) (Experimental Methods, section VI.f.). The f_P and f_S values were measured under appropriate assay conditions without the presence of kinases.





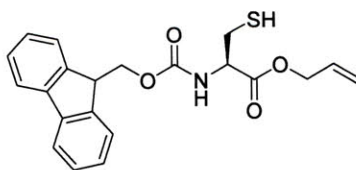
g. Assays with BTF probes for PKC β I and PKC δ

Assays with BTF and RDF chemosensors for PKC β I and PKC δ were performed with varying substrate and enzyme amounts (Figure 2-5) as described in Section VI.d. To ensure that the enzymes are active, they were first tested with RDF chemosensors (red bars). When next tested with the BTF substrates (blue bars), no detectable conversion to product is observed.

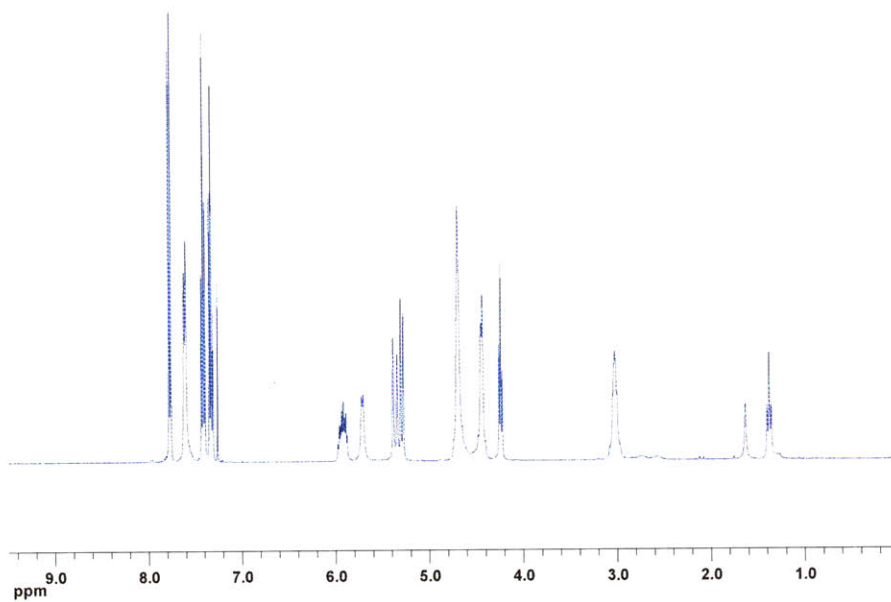
h. HPLC and MS data for kinase reactions

The PKA reaction with its RDF sensor (as detailed in Section VI.d.) was monitored by fluorescence for 616 sec, quenched with 40 μ L of a 0.1 M Na₂EDTA stock solution, stored on ice and lyophilized. The dry material was dissolved in Solvent A (50 μ L) and injected onto the analytical C₁₈ HPLC column.

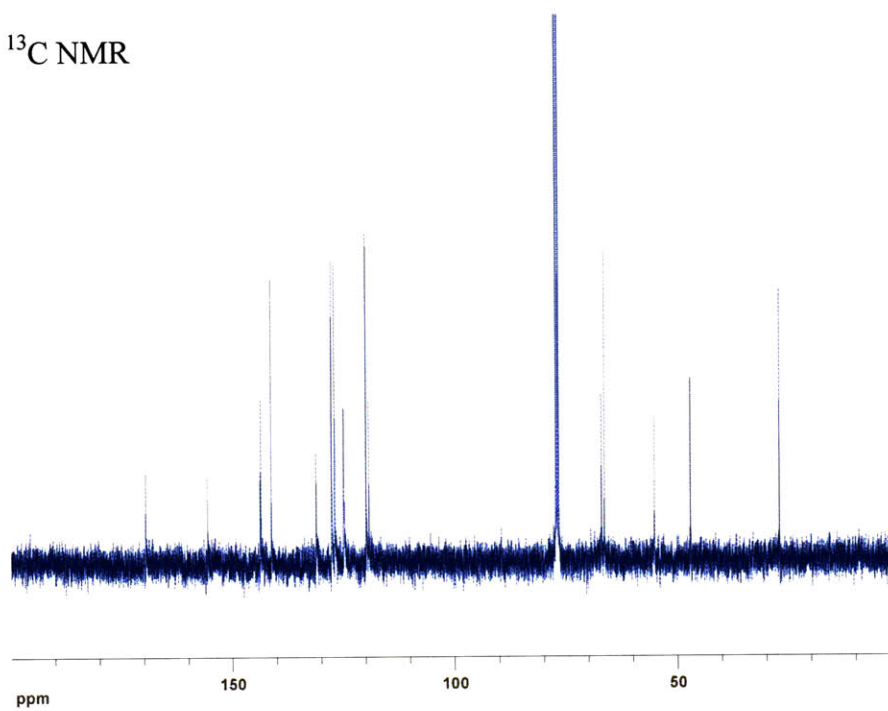
NMR spectra

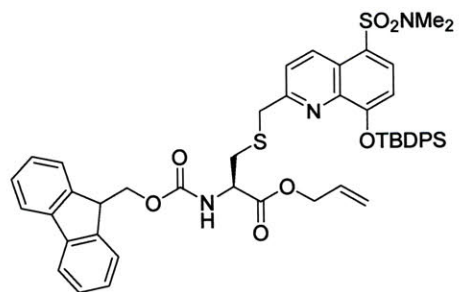


^1H NMR

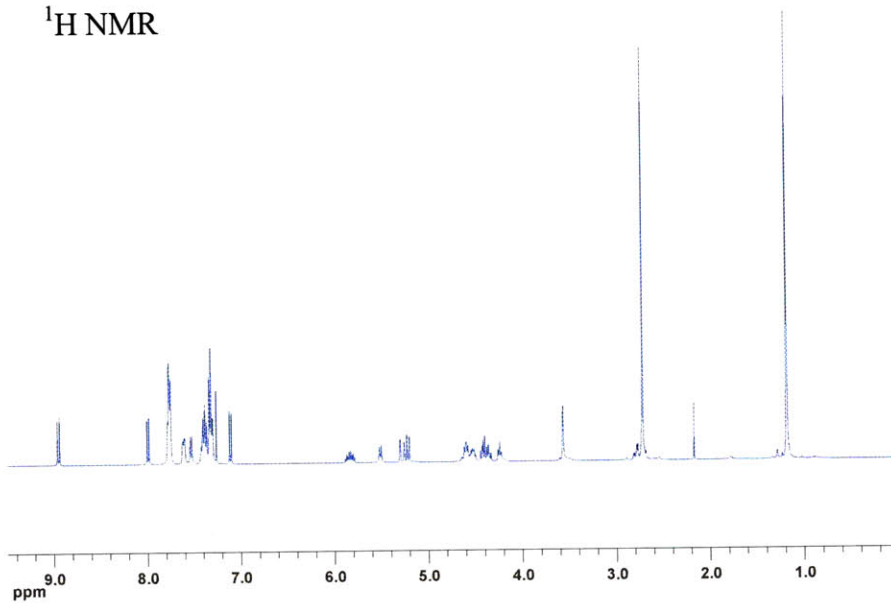


^{13}C NMR

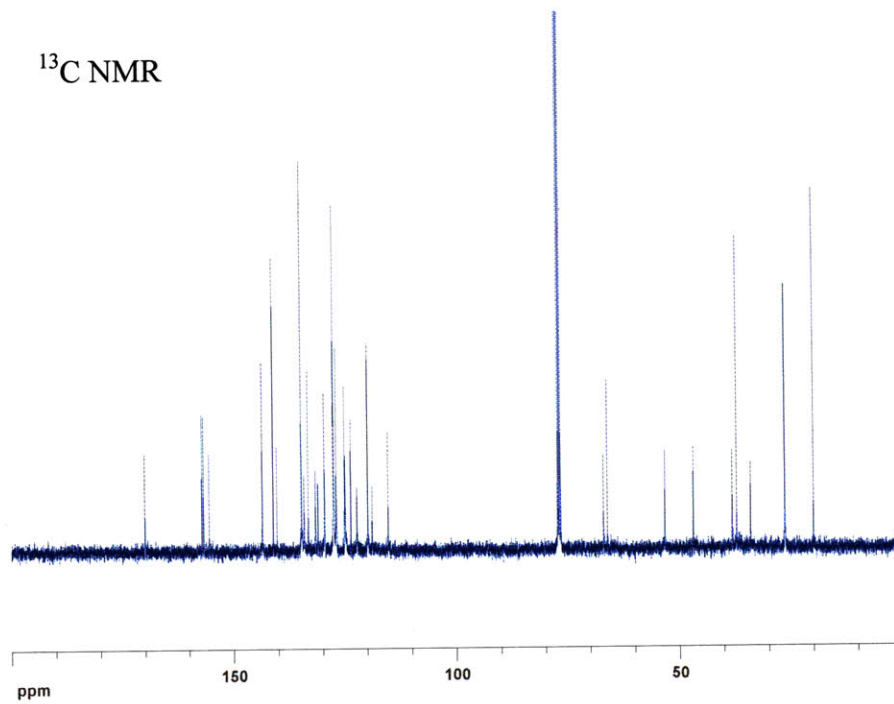


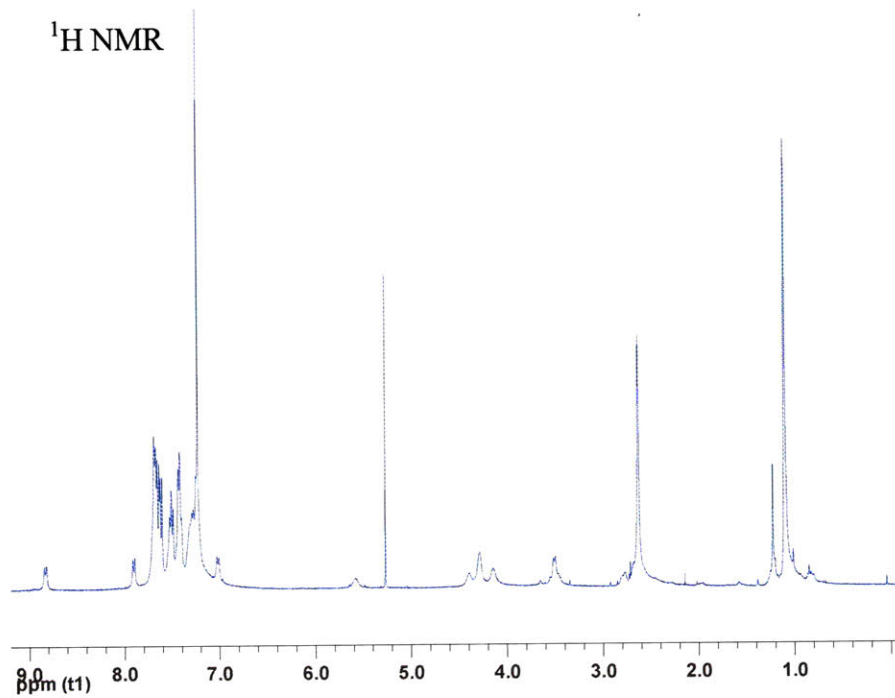
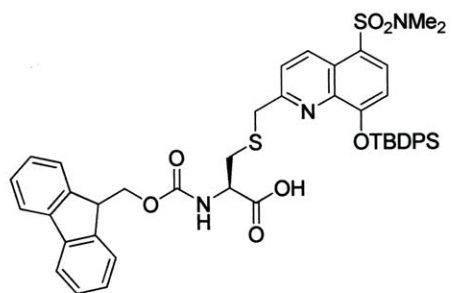


^1H NMR

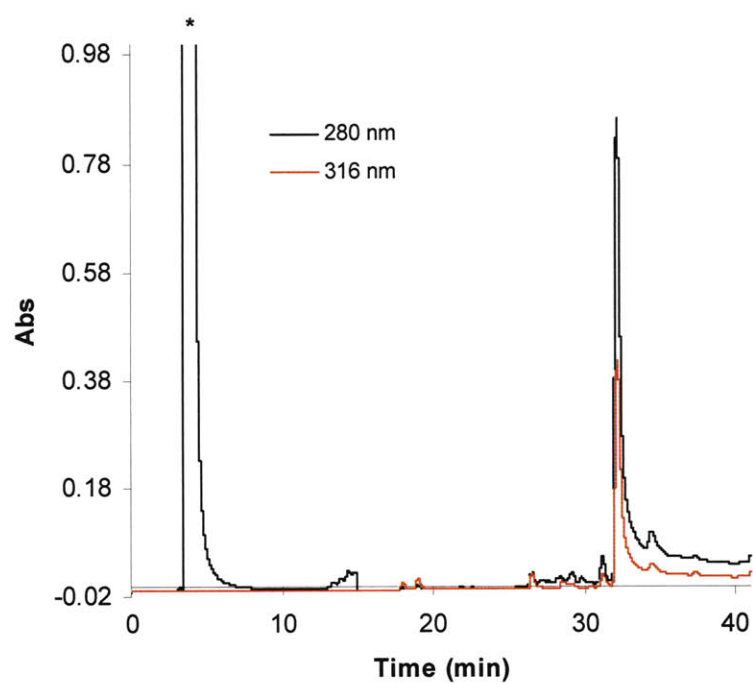
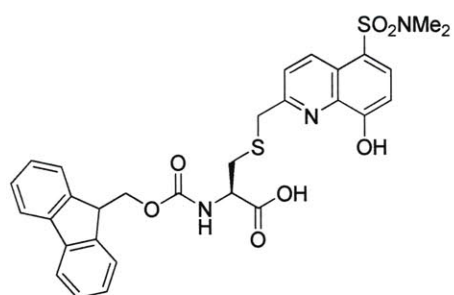


^{13}C NMR





HPLC chromatograms



* Absorbance due to the solvent in which the amino acid was dissolved (DMSO)

References

1. Manning, G.; Whyte, D. B.; Martinez, R.; Hunter, T.; Sudarsanam, S. The Protein Kinase Complement of the Human Genome. *Science* **2002**, 298, 1912-1934.
2. Lawrence, D. S. Signaling protein inhibitors via the combinatorial modification of peptide scaffolds. *Biochim. Biophys. Acta* **2005**, 1754, 50-57.
3. Shults, M. D.; Carrico-Moniz, D.; Imperiali, B. Optimal Sox-based fluorescent chemosensor design for serine/threonine protein kinases. *Anal. Biochem.* **2006**, 352, 198-207.
4. Shults, M. D.; Pearce, D. A.; Imperiali, B. Modular and Tunable Chemosensor Scaffold for Divalent Zinc. *J. Am. Chem. Soc.* **2003**, 125, 10591-10597.
5. Shults, M. D.; Imperiali, B. Versatile Fluorescence Probes of Protein Kinase Activity. *J. Am. Chem. Soc.* **2003**, 125, 14248-14249.
6. Shults, M. D.; Janes, K. A.; Lauffenburger, D. A.; Imperiali, B. A multiplexed homogeneous fluorescence-based assay for protein kinase activity in cell lysates. *Nat. Methods* **2005**, 2, 277-283.
7. Newton, A. C. Protein kinase C: structural and spatial regulation by phosphorylation, cofactors, and macromolecular interactions. *Chem. Rev.* **2001**, 101, 2353-2364.
8. Shabb, J. B. Physiological substrates of cAMP-dependent protein kinase. *Chem. Rev.* **2001**, 101, 2381-2411.
9. Taylor, S. S.; Yang, J.; Wu, J.; Haste, N. M.; Radzio-Andzelm, E.; Anand, G. PKA: a portrait of protein kinase dynamics. *Biochim. Biophys. Acta* **2004**, 1697, 259-269.
10. Brazil, D. P.; Hemmings, B. A. Ten years of protein kinase B signalling: a hard Akt to follow. *Trends Biochem. Sci.* **2001**, 26, 657-664.
11. Downward, J. PI 3-kinase, Akt and cell survival. *Semin. Cell Dev. Biol.* **2004**, 15, 177-182.
12. Roux, P. P.; Blenis, J. ERK and p38 MAPK-activated protein kinases: a family of protein kinases with diverse biological functions. *Microbiol. Mol. Biol. Rev.* **2004**, 68, 320-344.
13. Kotlyarov, A.; Yannoni, Y.; Fritz, S.; Laass, K.; Telliez, J. B.; Pitman, D.; Lin, L. L.; Gaestel, M. Distinct cellular functions of MK2. *Mol. Cell. Biol.* **2002**, 22, 4827-4835.
14. White, E. The pims and outs of survival signaling: role for the Pim-2 protein kinase in the suppression of apoptosis by cytokines. *Genes Dev.* **2003**, 17, 1813-1836.
15. Songyang, Z.; Cantley, L. C. Recognition and specificity in protein tyrosine kinase-mediated signalling. *Trends Biochem. Sci.* **1995**, 20, 470-475.
16. Martin, G. S. The hunting of the Src. *Nat. Rev. Mol. Cell Biol.* **2001**, 2, 467-475.
17. Frame, M. C. Src in cancer: deregulation and consequences for cell behaviour. *Biochim. Biophys. Acta* **2002**, 1602, 114-130.
18. Schlessinger, J. New roles for Src kinases in control of cell survival and angiogenesis. *Cell* **2000**, 100, 293-296.
19. Porter, A. C.; Vaillancourt, R. R. Tyrosine kinase receptor-activated signal transduction pathways which lead to oncogenesis. *Oncogene* **1998**, 17, 1343-1352.
20. Garcia, P.; Shoelson, S. E.; George, S. T.; Hinds, D. A.; Goldberg, A. R.; Miller, W. T. Phosphorylation of synthetic peptides containing Tyr-Met-X-Met motifs by nonreceptor tyrosine kinases in vitro. *J. Biol. Chem.* **1993**, 268, 25146-25151.
21. Frank, R. The SPOT-synthesis technique: Synthetic peptide arrays on membrane supports--principles and applications. *J. Immunol. Methods* **2002**, 267, 13-26.

22. Zhang, J. H.; Chung, T. D.; Oldenburg, K. R. A Simple Statistical Parameter for Use in Evaluation and Validation of High Throughput Screening Assays. *J. Biomol. Screen.* **1999**, *4*, 67-73.
23. Shults, M. D. Chemosensing strategies: utilizing the novel sulfonamidohydroxyquinoline amino acid Sox. Ph.D. Thesis, Massachusetts Institute of Technology, Cambridge, 2005.
24. Gribble, F. M.; Loussouarn, G.; Tucker, S. J.; Zhao, C.; Nichols, C. G.; Ashcroft, F. M. A Novel Method for Measurement of Submembrane ATP Concentration. *J. Biol. Chem.* **2000**, *275*, 30046-30049.
25. Haugland, R. P.; Spence, M. T. Z.; Johnson, I. D.; Basey, A. *The handbook: a guide to fluorescent probes and labeling technologies*. 10th ed.; Molecular Probes: [Eugene, OR], 2005; p iv, 1126 p.
26. Hannun, Y. A.; Bell, R. M. Rat Brain Protein Kinase C: Kinetic Analysis of Substrate Dependence, Allosteric Regulation, and Autophosphorylation. *J. Biol. Chem.* **1990**, *265*, 2962-2972.
27. Nishikawa, K.; Toker, A.; Johannes, F. J.; Songyang, Z.; Cantley, L. C. Determination of the specific substrate sequence motifs of protein kinase C isozymes. *J. Biol. Chem.* **1997**, *272*, 952-960.
28. Songyang, Z.; Carraway, K. L., 3rd; Eck, M. J.; Harrison, S. C.; Feldman, R. A.; Mohammadi, M.; Schlessinger, J.; Hubbard, S. R.; Smith, D. P.; Eng, C.; et al. Catalytic specificity of protein-tyrosine kinases is critical for selective signalling. *Nature* **1995**, *373*, 536-539.
29. Shoelson, S. E.; Chatterjee, S.; Chaudhuri, M.; White, M. F. YMXM motifs of IRS-1 define substrate specificity of the insulin receptor kinase. *Proc. Natl. Acad. Sci. U.S.A.* **1992**, *89*, 2027-2031.
30. Hutti, J. E.; Jarrell, E. T.; Chang, J. D.; Abbott, D. W.; Storz, P.; Toker, A.; Cantley, L. C.; Turk, B. E. A rapid method for determining protein kinase phosphorylation specificity. *Nat. Methods* **2004**, *1*, 27-29.
31. Obata, T.; Yaffe, M. B.; Leparc, G. G.; Piro, E. T.; Maegawa, H.; Kashiwagi, A.; Kikkawa, R.; Cantley, L. C. Peptide and protein library screening defines optimal substrate motifs for AKT/PKB. *J. Biol. Chem.* **2000**, *275*, 36108-36115.
32. Manke, I. A.; Nguyen, A.; Lim, D.; Stewart, M. Q.; Elia, A. E.; Yaffe, M. B. MAPKAP kinase-2 is a cell cycle checkpoint kinase that regulates the G2/M transition and S phase progression in response to UV irradiation. *Mol. Cell* **2005**, *17*, 37-48.
33. Kemp, B. E.; Graves, D. J.; Benjamini, E.; Krebs, E. G. Role of multiple basic residues in determining the substrate specificity of cyclic AMP-dependent protein kinase. *J. Biol. Chem.* **1977**, *252*, 4888-4894.
34. Kyriakis, J. M.; Avruch, J. Mammalian mitogen-activated protein kinase signal transduction pathways activated by stress and inflammation. *Physiol. Rev.* **2001**, *81*, 807-869.
35. Rainey, M. A.; Callaway, K.; Barnes, R.; Wilson, B.; Dalby, K. N. Proximity-induced catalysis by the protein kinase ERK2. *J. Am. Chem. Soc.* **2005**, *127*, 10494-10495.
36. Still, W. C.; Kahn, M.; Mitra, A. Rapid Chromatographic Technique for Preparative Separations with Moderate Resolution. *J. Org. Chem.* **1978**, *43*, 2923-2925.
37. SPECFIT/32 for Windows, v. 3.0; Spectrum Software Associates: Marlborough, MA., SPECFIT/32 for Windows, v. 3.0; Spectrum Software Associates: Marlborough, MA.

38. SigmaPlot 2004 for Windows, v. 9.01; Systat Software, Inc.: San Jose, CA., SigmaPlot 2004 for Windows, v. 9.01; Systat Software, Inc.: San Jose, CA.

Chapter 3. Development of a Mass Spectrometry-Based Method for Rapid Discovery of Selective Recognition-Domain Focused Sensors

A portion of the work described in this chapter has been published in:
González-Vera, J. A.; Luković, E.; Imperiali, B. A Rapid Method for Generation of Selective Sox-based Chemosensors of Ser/Thr Kinases Using Combinatorial Peptide Libraries. *Bioorg. Med. Chem. Lett.* **2009**, *19*, 1258-1260.

Introduction

In recent years, much effort has been devoted to identification of substrates for kinases, such as protein kinase C (PKC). Still, with hundreds of kinases in the human genome,¹ the specificity of substrates of many enzymes, like AurA, which plays a central role in cell cycle progression, remains poorly understood. Since the RDF method, described in Chapter 2, was able to provide sensors with greatly improved kinetic parameters for a number of kinases, we want to further extend the approach toward constructing probes that can distinguish closely related kinases (i.e., PKCs) or by developing new screening techniques that can rapidly and easily identify specific substrates for kinases where such information is scarce (i.e., AurA).

PKCs have a ubiquitous cellular presence, as they play important roles in phospholipid hydrolysis² and are found to be dysregulated in human cancers.³ The mammalian family is composed of 12 isozymes grouped into three classes: *conventional* PKCs (cPKCs) comprise α , γ , and the alternatively spliced β I and β II, *novel* PKCs (nPKCs) include δ , ϵ , η , and θ , and *atypical* PKCs (aPKCs) contain ζ and ι . Lastly, PKC μ and ν are considered by some as a fourth class, while others group them into a distinct family, protein kinase D (PKD).^{4, 5} While all PKCs share a conserved C-terminal kinase core, their activities are differentially stimulated due to variations in the N-terminal regulatory region.⁶ Specifically, cPKCs require diacylglycerol (DAG), Ca²⁺ and phosphatidylserine (PS) for function, nPKCs depend on DAG and PS, and aPKCs need only PS.

Despite the similarities in structure, PKCs act on a broad range of *in vivo* substrates, including growth factor receptors, ion channels, ion pumps, transcription factors, and translation factors.^{7, 8} The kinases are also involved in signal transduction of a variety of extracellular stimuli, such as hormones and growth factors.⁷ Therefore, much work has been devoted to

understanding specificity determinants, particularly among closely related PKCs. Based on the sequences of documented *in vivo* substrates, a consensus phosphorylation motif for PKC was determined to be Arg-Xaa-Xaa-Ser/Thr-Xaa-Arg-Xaa, where Xaa indicates any amino acid and Arg in position -3 is necessary for activity.⁸ Moreover, a long-time benchmark study conducted in the late 1990s containing 2.5 billion peptides found that each PKC isozyme had a unique optimal substrate sequence.⁹ The study indicated that generally PKCs preferentially phosphorylated peptides with hydrophobic amino acids at position +1 and basic residues at position -3. All isozymes, except for PKC μ , selected basic residues in positions -6, -4, and -2 and each had additional parameters that differed among classes of PKCs. Additionally, certain peptides were shown to have a high affinity and selectivity for their cognate PKC isoform (Table 3-1).

Table 3-1. Substrate Preferences of 9 PKC Isozymes^a

PKC Isozyme	Position ^b												
	-7	-6	-5	-4	-3	-2	-1	0	+1	+2	+3	+4	+5
PKC α	R	R	R	R	R	K	G	S	F	R	R	K	A
PKC β I	R	K	L	K	R	K	G	S	F	K	K	F	A
PKC β II	Y	K	L	K	R	K	G	S	F	K	K	K	A
PKC γ	R	R	R	R	R	K	G	S	F	K	R	K	A
PKC δ	A	A	R	K	R	K	G	S	F	F	Y	G	G
PKC ϵ	Y	Y	X	K	R	K	M	S	F	F	E	F	D
PKC η	A	R	L	R	R	R	R	S	F	R	R	X	R
PKC ζ	R	R	F	K	R	Q	G	S	F	F	Y	F	F
PKC μ	A	A	L	V	R	Q	M	S	V	A	F	F	F

^a Adapted from ref. 9. ^b Residues in bold were fixed in the screen.

Unlike the case of PKCs, much less is known about recognition requirements for the Aurora kinases. Aurora kinases (AurA, -B and -C) belong to the Ser/Thr protein kinase family and are involved in various aspects of mitosis.¹⁰ Specifically, AurA functions in centrosome maturation, mitotic spindle assembly, and plays a central role in cell cycle progression.¹¹⁻¹³

Additionally, the gene coding for AurA maps to a region that is frequently amplified in tumors and its overexpression has been detected in various cancers.¹⁴ Even with the clear importance in cell division, little is known about the substrate requirements of AurA. Only one study has been conducted to determine the preferred residues in the recognition domain surrounding the phosphorylation site.¹⁵ The resulting consensus sequence was proposed to be Arg-Arg-Xaa-Ser-Zaa (where Zaa denotes any hydrophobic residue except for Pro and Xaa is a small hydrophobic amino acid). This 5-residue motif was based on peptides derived from an extended version of the Kemptide sequence (Ala-Leu-Arg-Arg-Ala-Ser-Leu-Gly-Ala-Ala). However, the best peptide from this library exhibited a high K_M (ca. 300 μM) that renders the substrate of low utility in high-throughput screens (HTS) or studies where it would be readily phosphorylated a multitude of kinases, such as inside cells or in crude lysates.

Due to the greatly enhanced catalytic efficiency of RDF probes with a variety of kinases (including PKC) described in Chapter 2, we wanted to utilize the extended recognition region, which is the key feature of the RDF design, toward building sensors that can discriminate among closely related kinases (e.g. PKC isozymes) or that have more practical kinetic parameters (e.g. AurA). In this section, we first present the results of the PKC RDF peptide screen that was unable to reveal significant selectivity for one particular PKC isozyme, although highly improved kinetic parameters were obtained for selected family members. We then sought to apply the advantages of the RDF design toward expanding recognition elements for AurA substrates. To that end, the synthesis of a rationally-designed library of AurA peptides is described. Upon exposure to AurA, a sensor with a 3-fold improvement in catalytic efficiency was identified. However, attempts to extend recognition parameters beyond the reported AurA consensus sequence were unsuccessful. In order to take advantage of multiple additional binding

residues that can be present in the RDF design, we developed a new, moderate-throughput method for identification of Sox-based probes with enhanced specificity for target Ser/Thr kinases. This chapter culminates with the description of our work toward that goal. Specifically, a combinatorial peptide library from split and pool resin-based synthesis was first exposed to the desired kinase. Upon chemical modification of the phosphopeptides in the peptide mixture, Matrix-Assisted Laser Desorption Ionization Time-of-Flight mass spectrometry (MALDI TOF MS) was employed to identify the products. When applied to AurA, a peptide sequence was identified that exhibited an additional 4-fold improvement in catalytic efficiency ($k_{\text{cat}}/K_{\text{M}}$) over the substrate obtained from the rationally-designed library and a total of 7-fold enhancement in $k_{\text{cat}}/K_{\text{M}}$ compared to the best literature substrate (Kemptide).

Results and Discussion

Sensors for Protein Kinase C Isozymes

Synthesis of RDF chemosensors for PKC α , PKC β I, PKC δ , based on previously published substrates,⁹ is detailed in Chapter 2. Because there are 12 PKC isoforms present in human cells (α , β I, β II, γ , δ , ϵ , ζ , η , θ , ι , μ and ν), differentiation between them can be challenging, particularly for probes comprised of relatively short peptide sequences. With the highly improved kinetics parameters (i.e., $k_{\text{cat}}/K_{\text{M}}$) of the RDF probes compared to the BTF sensors (Table 3-2), we wanted to examine if the additional recognition residues would also improve the selectivity of those probes for their cognate isozymes.

Table 3-2. Kinetic Parameters of PKC RDF Chemosensors and the Parent Peptides

Entry	Target Kinase	Peptide	Sequence ^a	K_M (μM) ^b	V_{max} ($\mu\text{mol mg}^{-1} \text{min}^{-1}$) ^b	Catalytic Efficiency ^c
1	PKC α	BTF	Ac-Sox-PGS* <u>FRRR</u> -CONH ₂	8.6 ± 2.9^d	5.9 ± 1.9^d	1
2		RDF	Ac- <u>RRR</u> -CSox- <u>AS</u> * <u>FRRR</u> -CONH ₂	0.13 ± 0.02	2.4 ± 0.1	27
3	PKC β I	BTF	Ac-Sox-PAS* <u>FKKFA</u> -CONH ₂	NS ^e	NS ^e	NA ^f
4		RDF	Ac- <u>LKR</u> -CSox- <u>AS</u> * <u>FKKFA</u> -CONH ₂	0.81 ± 0.18	0.76 ± 0.06	NA ^f
5	PKC δ	BTF	Ac- <u>RKRKGS</u> *F-DPro-Sox-G-CONH ₂	NS ^e	NS ^e	NA ^f
6		RDF	Ac- <u>RKRKGS</u> *F-CSox- <u>YGG</u> -CONH ₂	0.48 ± 0.07	0.39 ± 0.02	NA ^f

^a Asterisk (*) denotes the residue that is phosphorylated. Residues important in kinase recognition are underlined. ^b Kinetic parameters (K_M and V_{max}) were obtained from initial slopes and corrected appropriately for substrate and product fluorescence as described in the Experimental Methods in Chapter 2. The values reported are the mean \pm s.e.m. of triplicate experiments as calculated from a direct fit of v vs. $[S]$ plots using the Briggs-Haldane equation. ^c Catalytic efficiency of each substrate was calculated as k_{cat}/K_M ($\text{min}^{-1} \mu\text{M}^{-1}$). The values for BTF and RDF probes within each kinase subset were normalized to the number obtained with the BTF substrate. ^d The results have been previously reported.¹⁶ ^e NS: Not a Substrate. ^f NA: Not Applicable.

After exposure of the RDF probes against a panel containing the 12 PKC isozymes, a preference for a set of isoforms emerged. However, none were able to further discriminate among the PKCs with high activity (conventional: α , β I, β II, and γ , and novel: θ) (Figure 3-1). Surprisingly, specificity was also not observed for the PKC δ RDF sensor, which was modeled after a peptide that was reported be specific for PKC δ —an enzyme that belongs to the novel subfamily.⁹ Instead, the PKC δ RDF probe was also a superior sensor for the conventional PKCs and PKC θ over other novel (δ , ϵ , and η) or atypical (ζ , ι , μ , and ν) kinases (Figure 3-1c). Further assays with peptide concentrations below the K_M (as measured with their cognate kinases) displayed the same trends that were observed at higher concentrations. For comparison, the BTF sensor for PKC α was also exposed to the panel of PKCs. As expected, the BTF substrate showed similar reactivity profile as the remaining RDF sensors (Figure 3-1d).

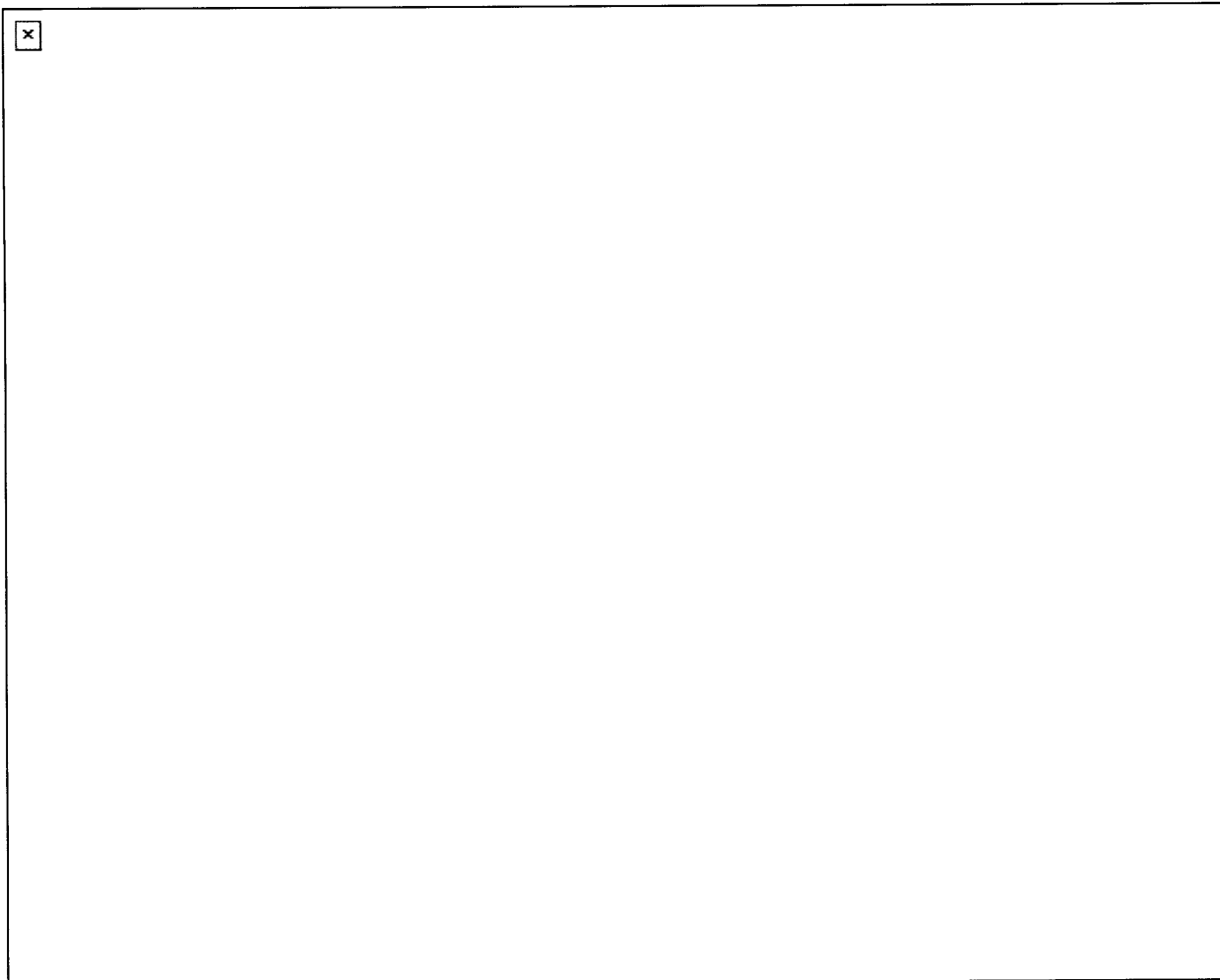


Figure 3-1. Reaction rates (slopes) of a) PKC α RDF substrate (0.2 μ M), b) PKC β I RDF substrate (1 μ M), c) PKC δ RDF substrate (1 μ M), and d) PKC α BTF substrate (8 μ M) with PKC isozymes. Reactions were done in 20 mM HEPES (pH 7.4), 10 mM MgCl₂, 0.3 mM CaCl₂, 0.1 mM EGTA, 100 μ M ATP, 1 mM DTT, 0.5 μ g/mL phosphatidylserine, 0.1 μ g/mL diacylglycerol with a) 1 ng, b) 2 ng, c) 10 ng, and d) 1 ng PKC isozyme.

Upon further examination, it was not surprising that the PKC α RDF sensor was unable to selectively monitor one kinase. The K_M values with PKC β I and PKC θ , enzymes that displayed high reaction rates in the isozyme screen (Figure 3-1), were nearly identical to the value obtained with PKC α (Table 3-3). Therefore, while we had successfully synthesized substrates with highly improved kinetics for PKCs, we were unable to secure a significant amount of discrimination among isozymes because the kinetic parameters were generally improved across the family.

Similarly, this trend has also been observed with the peptides that served as our literature starting points.⁹ For example, the K_M values for a peptide designed to be a selective substrate for PKC α indicate that the peptide is accepted almost equally by all isozyms except for PKC μ (Table 3-4). Our results underscore the difficulty in achieving specificity among these isozyms with simple peptide substrates.

Table 3-3. The Kinetic Parameters for PKC α RDF Substrate with PKC α , PKC β I and PKC θ Isozymes

Enzyme	K_M (μ M) ^a	V_{max} (μ mol min ⁻¹ mg ⁻¹) ^a
PKC α	0.13 \pm 0.02	2.4 \pm 0.1
PKC β I	0.085 \pm 0.007	3.7 \pm 0.7
PKC θ	0.14	2.4

^a The reported values are the mean \pm s.e.m. of triplicate experiments, except for PKC θ , as calculated from Hanes Plots. The values for PKC θ are from a single measurement.

Table 3-4. Kinetic Parameters of PKC α Substrate with PKC α , PKC β I and PKC δ ^a

Enzyme	K_M (μ M) ^b	V_{max} (nmol min ⁻¹ U ⁻¹) ^{b, c}	V_{max}/K_M (min ⁻¹ U ⁻¹) ^{b, c}
PKC α	3.8	1.6	14
PKC β I	8.2	1.2	5
PKC δ	3.9	2.5	21

^a Table adapted from ref. 9. ^b Previously reported kinetic parameters were obtained with a PKC α substrate (H₂N-RRRRRKGSFRRKK-COOH).⁹ ^c A unit (U) is defined as an amount of enzyme required to transfer 1 nmol of phosphate to ϵ -pseudosubstrate peptide per min.

In conclusion, we aimed to examine whether the extended recognition region in RDF probes would be enough to render our sensors specific for PKC α , PKC β I, and PKC δ . As shown, the additional residues greatly improved kinetic parameters compared to the parent and BTF-based probes. However, better kinetics did not intrinsically enhance selectivity toward one recombinant enzyme over another. Inevitably, due to their homology, PKC isozyms share

similar substrate recognition requirements and must rely on complex cellular regulation and activation to drive specificity.¹⁷ While in cellulo these enzymes might have specific targets, in biochemical assays the spatial and temporal control over both the enzyme and the substrate is lost. The in vivo intrinsic function of PKCs seems to be regulated in part by interaction with targeting proteins that position it near the corresponding regulators and substrates.^{4, 18} Furthermore, the expression, availability and activation state of these kinases are tightly regulated in the cell.^{19, 20} Therefore, although there is redundancy, not all 12 of the isozymes would necessarily compete for the same substrates in living systems. Additionally, there may be elements of protein-protein interactions between the enzyme and its substrate that aid in recognition, which are difficult to explore with short peptides. When these factors are considered together, it is not surprising that we have been unable to achieve selectivity with our sensors. Thus, without a high-throughput screening method it would be difficult and time-consuming to search for substrates that can discriminate among closely related kinases.

Sensors for Aurora A

a. Synthesis of Aurora A Substrates

While a high level of specificity was not achieved with PKCs, a marked improvement in the kinetic parameters was obtained with the RDF probes compared to both the BTF sensors and parent substrates. Since the studies of substrate specificity determinants for AurA are sparse, our next focus was to design peptidyl sensors with enhanced specificity for AurA. The best peptide-based substrate for AurA reported in the literature possessed a high K_M (300 μ M), especially unusual for a Ser/Thr kinase.¹⁵ With the success of RDF sensors in gaining specificity through the extended recognition area, development of a more selective substrate for AurA was

attempted. Toward that goal, a rationally-designed library of RDF peptides was synthesized (Table 3-5). The probes were based on Kemptide¹⁵ (AurA-S1, S2 and S6-23), PKItide (AurA-S5), or various proteins that are in vivo substrates for AurA and AurB, such as Histone H3^{15, 21} (AurA-S3-S4 and S24-S25), CPEB²¹ (AurA-S26) and CENP-A²¹ (AurA-S27-S28). Solid-Phase Peptide Synthesis (SPPS) was employed to generate the probes following previously described methods (Chapter 2, Scheme 2-1).

Table 3-5. Sequences of RDF Chemosensors for AurA

Entry	Substrate	Sequence ^a															
		-7	-6	-5	-4	-3	-2	-1	0	+1	+2	+3	+4	+5	+6		
1	Kemptide	H ₂ N			A	L	R	R	A	S	L	G	A	A			CONH ₂
2	AurA-S1	Ac			A	L	K	R	A	S	L	C-Sox	A	A			CONH ₂
3	AurA-S2	Ac			A	L	R	R	A	S	L	C-Sox	A	A			CONH ₂
4	AurA-S3	Ac		K	Q	T	A	R	K	S	T	C-Sox	G	K			CONH ₂
5	AurA-S4	Ac		K	Q	T	A	R	K	S	L	C-Sox	G	K			CONH ₂
6	AurA-S5	Ac	G	R	T	G	R	R	N	S	I	C-Sox	A	A			CONH ₂
7	AurA-S6	Ac			A	L	R	R	F	S	L	C-Sox	A	A			CONH ₂
8	AurA-S7	Ac			A	L	R	R	F	S	L	C-Sox	K	A			CONH ₂
9	AurA-S8	Ac			A	L	R	R	F	S	L	C-Sox	A	K			CONH ₂
10	AurA-S9	Ac			A	L	R	R	F	S	L	C-Sox	F	A			CONH ₂
11	AurA-S10	Ac			A	L	R	R	F	S	L	C-Sox	A	F			CONH ₂
12	AurA-S11	Ac			A	L	R	R	F	S	L	C-Sox	L	A			CONH ₂
13	AurA-S12	Ac			A	L	R	R	F	S	L	C-Sox	A	L			CONH ₂
14	AurA-S13	Ac			A	L	R	R	F	S	L	C-Sox	E	A			CONH ₂
15	AurA-S14	Ac			A	L	R	R	F	S	L	C-Sox	A	E			CONH ₂
16	AurA-S15	H ₂ N		A	A	L	R	R	F	S	L	C-Sox	A	A	R		CONH ₂
17	AurA-S16	H ₂ N		A	A	L	R	R	F	S	L	C-Sox	A	A	G	R	CONH ₂
18	AurA-S17	H ₂ N		A	A	L	R	R	F	S	L	C-Sox	L	F	R		CONH ₂
19	AurA-S18	H ₂ N		A	A	L	R	R	F	S	L	C-Sox	L	F	G	R	CONH ₂
20	AurA-S19	H ₂ N			A	L	R	R	F	S	L	C-Sox	L	A			CONH ₂
21	AurA-S20	H ₂ N			A	L	R	R	R	S	L	C-Sox	A	A			CONH ₂
22	AurA-S21	H ₂ N			A	L	R	R	R	S	L	C-Sox	L	A			CONH ₂
23	AurA-S22	H ₂ N			A	L	R	R	F	S	D	C-Sox	I	L			CONH ₂
24	AurA-S23	H ₂ N					R	R	F	S	L	C-Sox					CONH ₂
25	AurA-S24	H ₂ N		K	Q	T	R	R	F	S	L	C-Sox	G	A	P	R	CONH ₂
26	AurA-S25	H ₂ N		K	Q	T	R	R	F	S	L	C-Sox	G	A	P	E	CONH ₂
27	AurA-S26	H ₂ N				S	R	L	D	S	R	C-Sox	I	L	P		CONH ₂
28	AurA-S27	H ₂ N				P	R	R	R	S	R	C-Sox	P	E			CONH ₂
29	AurA-S28	H ₂ N			P	R	R	R	F	S	R	C-Sox	P	E			CONH ₂

^a Residue that is phosphorylated is set in the 0 position and the remaining residues are numbered accordingly. Residues that are added to the Kemptide core are shown in bold.

b. Fluorescence Increase

AurA-S1-S14

Fluorescence increases for peptides S1-S14 was robust (4-9 fold) (Table 3-6). It was observed that the more acidic probes (AurA-S13 and S14) had slightly lower fluorescence changes (4-5 fold). As observed previously with tyrosine kinase sensors, acidic residues in the vicinity of the Sox chromophore tend to increase the fluorescence intensity of the substrate presumably by sequestering Mg^{2+} ions that can coordinate with the chromophore and, thus display an enhancement in fluorescence (Chapter 2, Table 2-5). High ATP concentration (1 mM) did not appreciably affect the fluorescence difference in these cases.

Table 3-6. Fold Fluorescence Increase for Selected AurA Chemosensors

Entry	Substrate	Fold Fluorescence Increase ^a	
		0 mM ATP	1 mM ATP
1	AurA-S1	5	5
2	AurA-S2	5	4.8
3	AurA-S3	6.6	4.2
4	AurA-S4	7	4.8
5	AurA-S5	5.8	4.8
6	AurA-S6	7.5	7.5
7	AurA-S7	7.7	6.2
8	AurA-S8	8.2	6.4
9	AurA-S9	7.8	8.6
10	AurA-S10	8.1	8.9
11	AurA-S11	6.6	7.2
12	AurA-S12	7.6	7.6
13	AurA-S13	4.4	4.9
14	AurA-S14	4.4	5.1
15	AurA-S15	6.9	4.1
16	AurA-S16	7	4.5
17	AurA-S17	7.2	2.9
18	AurA-S18	7.8	2.4
19	AurA-S19	7.1	7.4
20	AurA-S20	6.1	3.9
21	AurA-S21	6	4.1

^a Measured in triplicate as a quotient of fluorescence intensity at 485 nm of phosphopeptide and substrate in 20 mM HEPES (pH 7.4), 10 mM MgCl₂, and 10 μM peptide.

AurA-S15-S28

On the other hand, the fluorescence increase for AurA-S15-S21 exhibited more variation (2-8 fold). In the absence of ATP, the fluorescence change was high (6-8 fold), while at 1 mM ATP it decreased among the more hydrophobic peptides such as AurA-S17 and S18 (Table 3-5, entries 17 and 18) and to a smaller degree among AurA-S20 and S21 (entries 20 and 21). Similar to PKC α and Pim2 RDF sensors reported in Chapter 2, at 100 μM ATP the fluorescence differences were similar to the ones obtained without ATP (Figure 3-2).

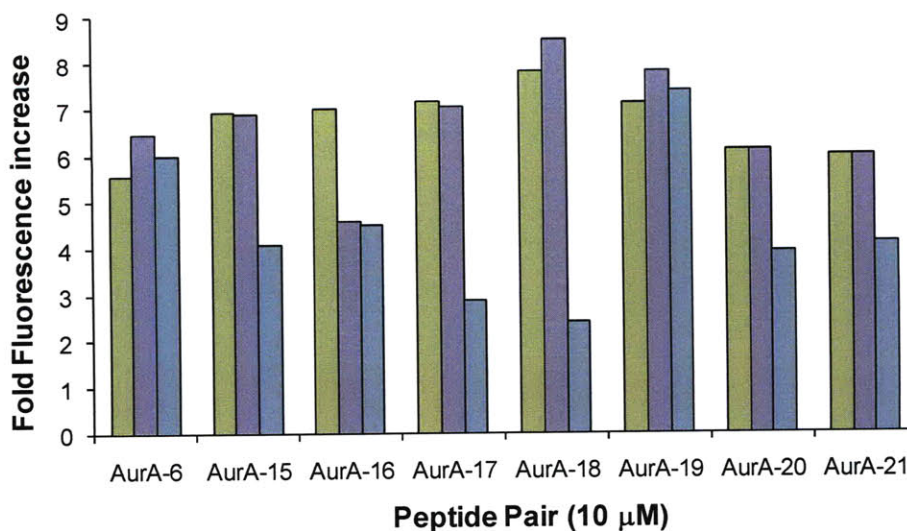


Figure 3-2. Fold fluorescence difference at 0 (green), 0.1 (purple) and 1.1 (blue) mM ATP for AurA-S15-S21. The increase was compared to AurA-S6. The reported values are based on a single measurement. Conditions: 20 mM HEPES (pH 7.5), 10 μM peptide, and 10 mM Mg²⁺. The differences were obtained by as a ratio of the fluorescence of the phosphopeptide to that of the substrate at 485 nm.

Fluorescence differences were not obtained with AurA-S22-S28 because these probes were directly screened with AurA and the corresponding phosphopeptides were not synthesized.

In conclusion, the fluorescence increases obtained with AurA-S1-S21 agree with the results presented with RDF probes in Chapter 2. Under variety of local chemical environments (with acidic, basic, aromatic, aliphatic, or strained amino acids), the C-Sox residue still exhibits quite robust fluorescence increases that are largely unaffected by ATP concentration.

c. Optimization of AurA Activity

Recombinant Aurora A and B generally exhibit lower activity compared to many other Ser/Thr kinases. Since the activity of AurA is instrumental in subsequent substrate screening, it was necessary to gain access to the most active form of the enzyme. Phosphorylation of Thr288 in the activation segment of AurA is crucial for activity.¹⁴ Furthermore, the interaction of AurA

with a partner protein, TPX2, leads to a strong activation of the kinase.²² Recently, the structures of both AurA and the AurA-TPX2(1-43) complex have been solved by X-ray crystallography.²³ Examination of the crystal structures illustrate that the binding of TPX2 to AurA causes a small, but important, conformational change that shields the pThr288 from phosphatases and locks the enzyme in the active conformation of the substrate binding site, transforming it into a better platform for substrates to dock (Figure 3-3a). This behavior has been observed for other kinases such as cyclin-dependent kinases (CDKs) that require not only phosphorylation of the equivalent threonine (Thr160), but also the binding by a partner protein, cyclin A, to be fully active.²⁴ Due to these reports, TPX2(2-43) was chemically synthesized employing pseudo-proline residues where appropriate (Figure 3-3b) to aid solubilization and to break up secondary structure formation during peptide elongation.^{25, 26} The first residue, methionine, was excluded due to complications with the handling and storage of Met-containing peptides, which are susceptible to facile oxidation.

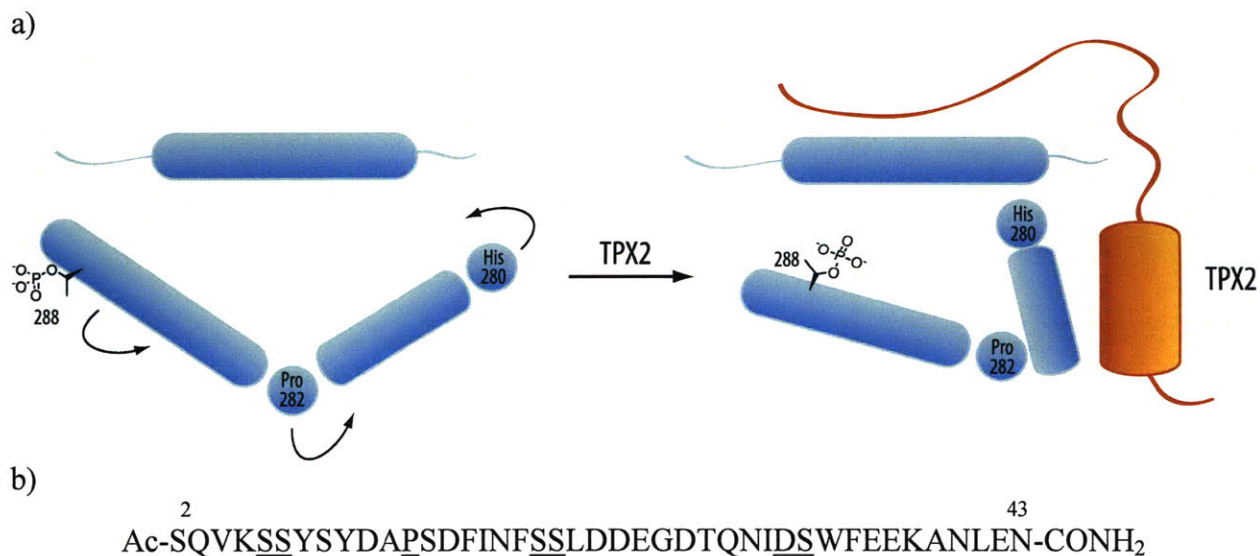


Figure 3-3. Activation of AurA by TPX2. a) Schematic representation of the molecular mechanism of TPX2-mediated activation of AurA. The activation segment moves with the help of TPX2 (orange). b) The primary sequence of TPX2(2-43). Naturally occurring proline and sites of pseudo-proline residue incorporation are underlined. Adapted from ref. 23.

Assays with TPX(2-43) showed slight increase in activity compared to assays conducted in the absence of TPX(2-43) (Figure 3-4). Albeit a modest increase in rate, the TPX(2-43) was included in the assays that screened reaction rates of AurA peptides previously discussed.

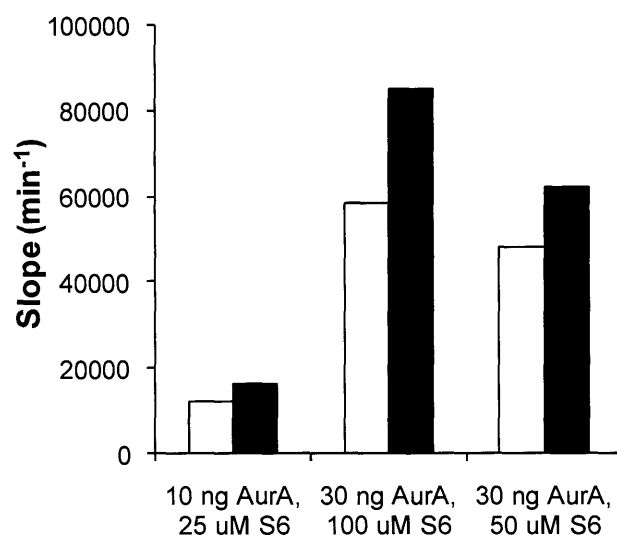


Figure 3-4. The activity of AurA measured with AurA-S6 in the presence (black bars) or absence (white bars) of TPX(2-43). Assay conditions: 20 mM HEPES (pH 7.4), 10 mM MgCl₂, 1 mM ATP, 0.1 mM EGTA, 0.1% BME, 0.01% Brij, 0.1 mg/mL BSA, 10 or 30 ng AurA, 25, 50 or 100 μ M of sensor, 30 °C, $\lambda_{\text{ex}} = 410$ nm, $\lambda_{\text{em}} = 485$ nm, slit widths 5 nm, monitored in a fluorometer over 10 min.

d. Rate Comparisons

The S1-S28 substrates were individually subjected to kinetic analysis with AurA to qualitatively compare the efficiency of phosphoryl transfer (Figure 3-5). The best substrate from the screen, AurA-S6, was used in all cases as an internal standard and all slopes were normalized to the S6 rate.

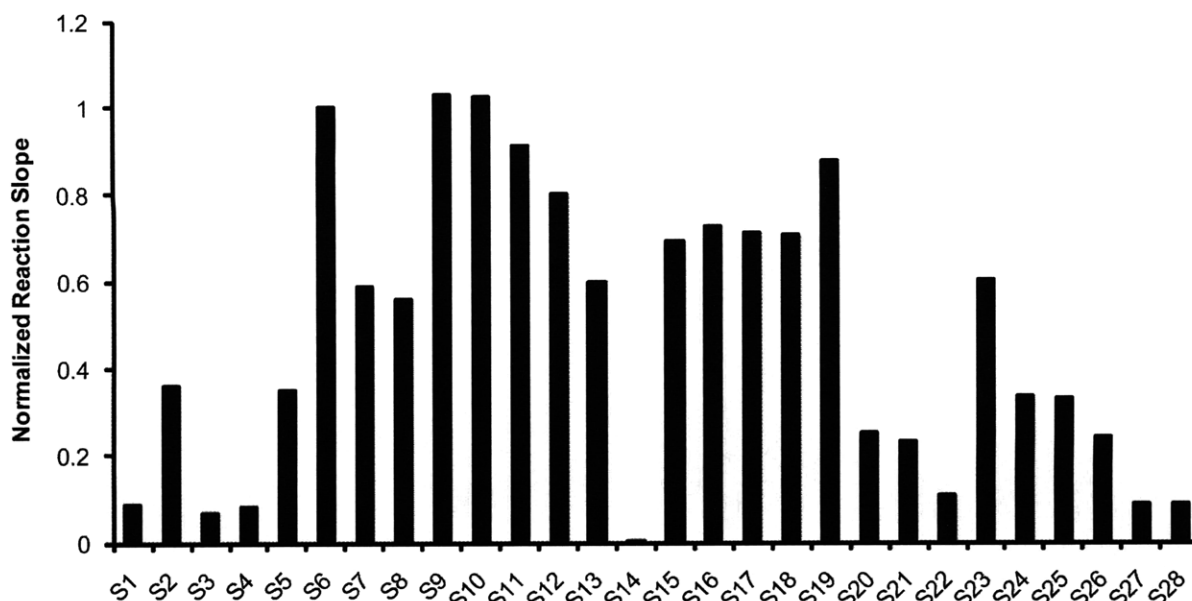


Figure 3-5. Qualitative comparison of reaction rates of chemosensors with AurA. All rates were normalized to the rate obtained with AurA-S6. Standard assay conditions included 20 mM HEPES (pH 7.4), 10 mM MgCl₂, 0.1 mM EGTA, 0.1% BME, 0.01% Brij, 0.1 mg/mL BSA, 4 μM TPX(2-43), and 30 ng AurA at 30 °C. The following concentrations differed among sensors: AurA-S1-S4 (50 μM substrate, 1 mM ATP), AurA-S5 (100 μM substrate, 1 mM ATP), AurA-S6-S14 (10 μM substrate, 1 mM ATP), AurA-S15-S16 (10 μM substrate, 1 mM ATP), AurA-S17-S28 (10 μM substrate, 0.1 mM ATP). The reactions were monitored in a fluorometer over 10 min ($\lambda_{\text{ex}} = 410 \text{ nm}$, $\lambda_{\text{em}} = 485 \text{ nm}$, slit widths 5 nm).

AurA-S1-S6

The initial set of sensors was built around known peptide or protein substrates of AurA (Table 3-5, entries 2-5 and 7) or PKA (entry 6), a kinase that has similar substrate preferences. When subjected to AurA, S2 and S5 showed some activity, which was not nearly as high as that obtained with S6. It is noteworthy that the only sequence difference between S2 and S6 is the residue in position -1. The other sensors, S3 and S4, were very poor substrates.

AurA-S7-S14

AurA-S7-S14 peptides were synthesized in order to explore the possibility of expanding the C-terminal end to include additional recognition elements. This was achieved by substitution of both of the C-terminal alanines, one at a time, with basic (Lys), aromatic (Phe), aliphatic (Leu), or acidic (Glu) residues (Table 3-5, entries 8-15).

Basic and acidic substitution (S9-S10 and S13-S14, respectively) afforded sensors with lower reaction rates when compared to S6 and in the instance of S14, containing Glu in position +4, there was no detectable turnover. On the other hand, chemosensors with aromatic and aliphatic substitution (S9-S12) had comparable reaction rates with S6, but much poorer solubility.

AurA-S15-S18

This series of peptides was synthesized with the free N-terminus and included a C-terminal Arg in position +5 or +6. Residues +3 and +4 were either both Ala (Table 3-5, entries 16-17) or Leu and Phe, respectively (entries 18-19). These probes were screened with 0.1 mM ATP to avoid the low fluorescence differences that were observed with S17 and S18 in the presence of 1 mM ATP (Table 3-6). The rates for all four substrates were similar to one another and showed no improvement over S6.

AurA-S19-S21

Upon closer examination of the crystal structure of the active form of AurA²⁷ (PDB 1MQ4) to which a short model substrate (H₂N-RFSLC(Npl)A-CO₂H) was docked (Figure 3-6), several more peptides were considered in order to test additional parameters. Peptide S19 was identical to AurA-S11 with the exception of the free N-terminus, which may be able to take

advantage of the acidic patch on the protein where the substrate is believed to bind (Figure 3-6a). However, it did not display improved reaction rates compared to S11.

Similarly, AurA-S20 and S21 were designed to examine whether replacement of Phe in the -1 position by Arg would improve reaction rates by providing an additional basic residue to form contact with the acidic patch in the substrate binding pocket (Figure 3-6b). Due to the greatly reduced reaction rates that were observed with S20 and S21, Phe in position -1 seems to form more favorable contacts than Arg.

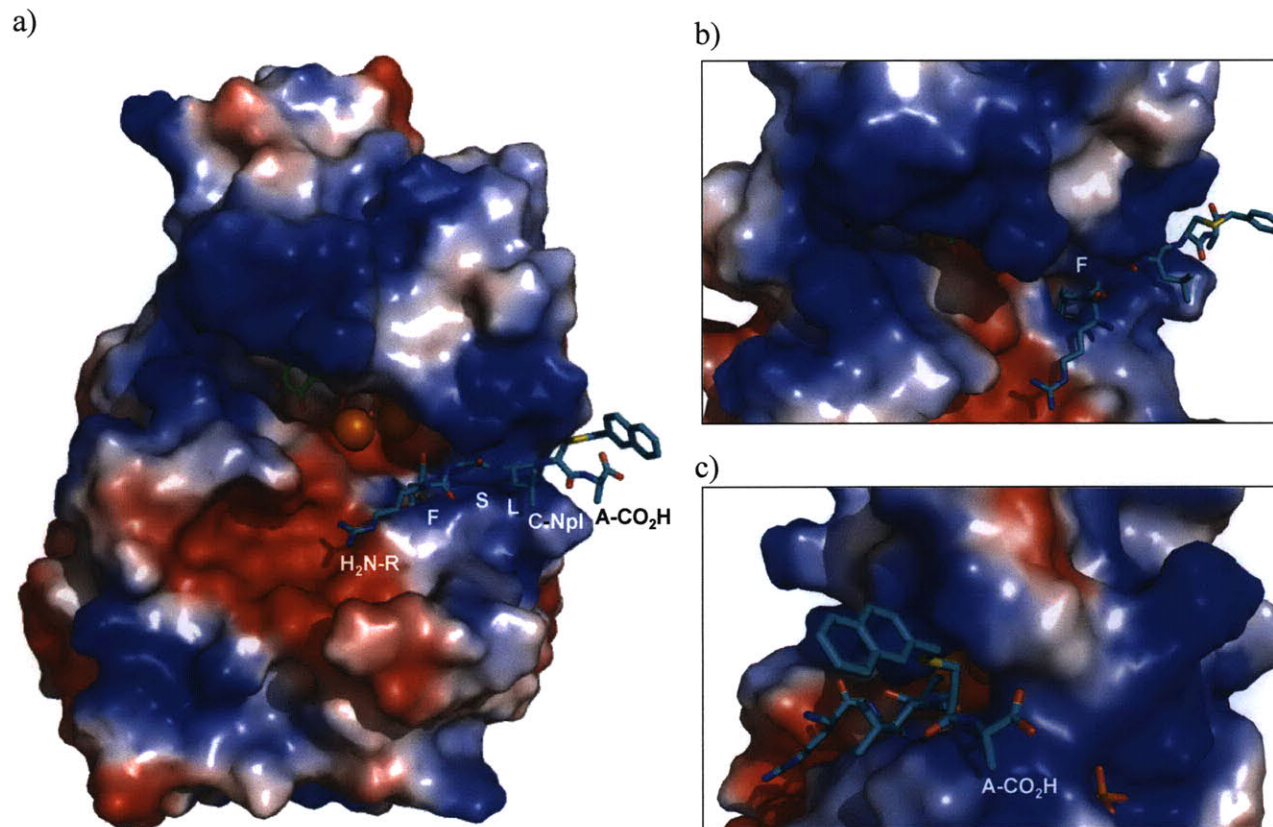


Figure 3-6. AurA (PDB 1MQ4) docking models with test peptide (H₂N-RFSLC(Npl)A-CO₂H). a) AurA with the test peptide docked in the orientation in which it is predicted to bind based on the favorable interactions between the crucial Arg in the -2 and -3 positions with the acidic patch on the protein (acidic = red, basic = blue). b) Closer look at the pocket into which Phe at the -1 position could enter. The pocket contains acidic and basic residues. c) The docked complex was rotated approximately 90° around the vertical axis to show the basic patch in the lower right hand corner and an acidic area in the upper center of the picture.

AurA-S22-S28

AurA-S22 was synthesized with Asp replacing Leu in the +1 position based on the observation that it might form contact with basic residues that line the peptide binding groove as predicted substrate-enzyme docking model (Figure 3-6). However, the reaction rate was drastically diminished, indicating that acidic residues are highly disfavored in the +1 position.

When the substrate sequence was truncated to only include the core five residues from Kemptide (AurA-S23) a somewhat reduced the reaction rate was detected compared to the full Kemptide-based sensor AurA-S6. This observation demonstrated that Ala and Leu residues in -5, -4, +3 and +4 contribute favorably to substrate turnover. AurA-S24 and 25 included charged residues at the *C*-terminus and were designed to combine the Histone H3 and Kemptide sequences. Peptide AurA-S26 was based on the sequence of CPEB protein, while S27 and S28 were modeled after the sequence from CENP-A, which is a substrate of AurB *in vivo*. All four peptides showed greatly diminished reaction rates compared to AurA-S6, particularly the proline-rich S27 and S28.

In conclusion, from the screen of 28 different probes, AurA-S6 emerged as the most promising chemosensor for AurA. Nonetheless, attempts to extend the recognition domain beyond the *C*- and *N*-termini of the parent peptide, Kemptide, were unsuccessful.

e. Cross-reactivity with Aurora B

Having screened 28 different substrates for improved activity with AurA, we also examined the cross-reactivity of a subset of those sensors with a closely related kinase, AurB. The six probes (AurA-S1-S6) that we examined display a range of reaction rates with AurA, yet none are phosphorylated by AurB (Table 3-7). While AurA and AurB have structural and

sequence homology, the lack of cross-reactivity indicates that they have different substrate requirements and that it may be possible to construct sensors that differentiate between them.

Table 3-7. Select Chemosensors were Tested for Reactivity with AurA and AurB

Entry	Substrate	Turnover ^a by:	
		AurA	AurB
1	AurA-S1	L	×
2	AurA-S2	M	×
3	AurA-S3	L	×
4	AurA-S4	L	×
5	AurA-S5	M	×
6	AurA-S6	H	×

^a × = no activity, L = low, M = medium, H = high reaction rates when exposed to enzyme.

f. Kinetic Parameters of AurA-S2 and S6 with AurA

The AurA-S6 probe was further examined by quantifying the kinetic parameters with AurA. For comparison purposes, kinetics of AurA-S2, the sensor that was entirely based on the best literature peptide substrate, Kemptide, were also measured (Table 3-8). Indeed, the kinetic parameters agreed with initial rate observations (Figure 3-5). Both kinetic parameters, the K_M and V_{max} , were improved slightly for AurA-S6 leading to a 3-fold higher catalytic efficiency compared to AurA-S2, although the only difference among the primary sequences of the probes was the residue in the -1 position—Ala for AurA-S2 and Phe for AurA-S6. It is likely that the differences in substrate kinetics are due to favorable interactions that may form between the hydrophobic pocket in the substrate binding region of the enzyme and the Phe residue of AurA-S6. However, at this point there are no co-crystal structures of this enzyme-peptide complex that would unequivocally support this hypothesis.

Table 3-8. Kinetic Parameters of Selected Chemosensors with AurA

Entry	Substrate	K_M (μM) ^{a,b}	V_{max} ($\mu\text{mol mg}^{-1} \text{min}^{-1}$) ^a
1	Kemptide	263	
2	AurA-S2	297.8 \pm 3.9	1.7 \pm 0.3
3	AurA-S6	152.3 \pm 2.7	2.6 \pm 0.21

^a Kinetic parameters (K_M and V_{max}) were obtained from initial slopes and corrected appropriately for substrate and product fluorescence as described in the Experimental Methods. The values reported are the mean \pm s.e.m. of triplicate experiments as calculated from Hanes Plots. ^b The K_M value for Kemptide has been previously reported.¹⁵ ^c Catalytic efficiency of each substrate was calculated as k_{cat}/K_M ($\text{min}^{-1} \mu\text{M}^{-1}$). The values were normalized to the number obtained with AurA-S6.

In conclusion, through a series of rationally-designed sequences, a sensor with improved kinetics emerged. This substrate, AurA-S6, can now be further expanded upon utilizing a higher throughput method to develop a sensor with even better preference for AurA.

Development and Validation of the MS-based Screening Method

While a chemosensor with enhanced AurA kinetics was obtained through rational design, the K_M value was still too high to be of practical use in more complex assays where competing kinases might be present. Due to time-consuming nature of individual peptide screens described above, we sought to develop a higher-throughput method for identifying promising kinase substrates. Ideally, this approach would allow a facile access to degenerate peptide libraries with natural and unnatural chemical moieties that can be subjected to the kinase of interest and rapidly decoded to identify substrates that exhibit preference for the enzyme. Traditional methods to elucidate specificity of kinases include solid-phase phosphorylation screening of either phage display libraries²⁸⁻³⁰ or synthetic peptides³¹⁻³⁶ and the use of degenerate libraries of peptides oriented around the residue to be phosphorylated.^{8, 37} However, these techniques depend on laborious substrate peptide decoding procedures.^{30, 31} Furthermore, the detection of phosphate is

based on the transfer of ^{32}P from $[\gamma\text{-}^{32}\text{P}]\text{ATP}$ to target peptides or proteins,³⁸ a risk to human health and the environment, or on antibodies directed against phosphorylated residues,³⁹ which in some cases is problematic due to their low specificity.

In this section we describe a new method for identification of Sox-based probes with improved specificity for Ser/Thr kinases (Figure 3-7). First, a library containing amino acid variations at the site of investigation was generated by Fmoc-based solid-phase peptide synthesis (SPPS). 2-Naphthyl alanine (2-Nal) was incorporated in place of C-Sox (generally placed in the +2 position) due to the tendency of the Sox chromophore to be partially eliminated under the MALDI conditions. The peptides were then released from resin, and the equimolar mixture was incubated with the desired kinase for varying times. The direct detection of the phosphopeptide product by MALDI TOF is usually poor due to the inefficient ionization of the negatively charged phosphate group and the propensity for the phosphate to eliminate under such conditions. Thus, to enhance signal intensities in the MALDI analysis, a previously reported method was employed.⁴⁰ Briefly, the kinase reaction products were subjected to base $[\text{Ba}(\text{OH})_2]$ to promote β -elimination of the serine phosphate moiety, followed by Michael addition of 4-mercaptoethylpyridine (4-MEP). New peaks appearing in the MALDI spectrum (121 g/mol greater than the parent peptide) were interpreted as evidence of phosphorylation. The change in mass after the reaction was due to the loss of phosphate (98 g/mol) during the β -elimination and addition of 4-MEP (139 g/mol). This strategy enabled us to follow the progress of the reaction and to evaluate the kinase activity semiquantitatively by comparing intensities of derivatized peaks with those of the parent peptides in the same spectrum (Figure 3-7). Once the best residue was found for a particular position, it was fixed in that place and the method was applied to a different position in an iterative fashion until the best substrate was obtained. Finally, the

optimized sequence was synthesized with C-Sox⁴¹ instead of 2-Nal, effectively turning the best substrate into a selective kinase reporter and simultaneously enabling determination of the kinetic parameters.

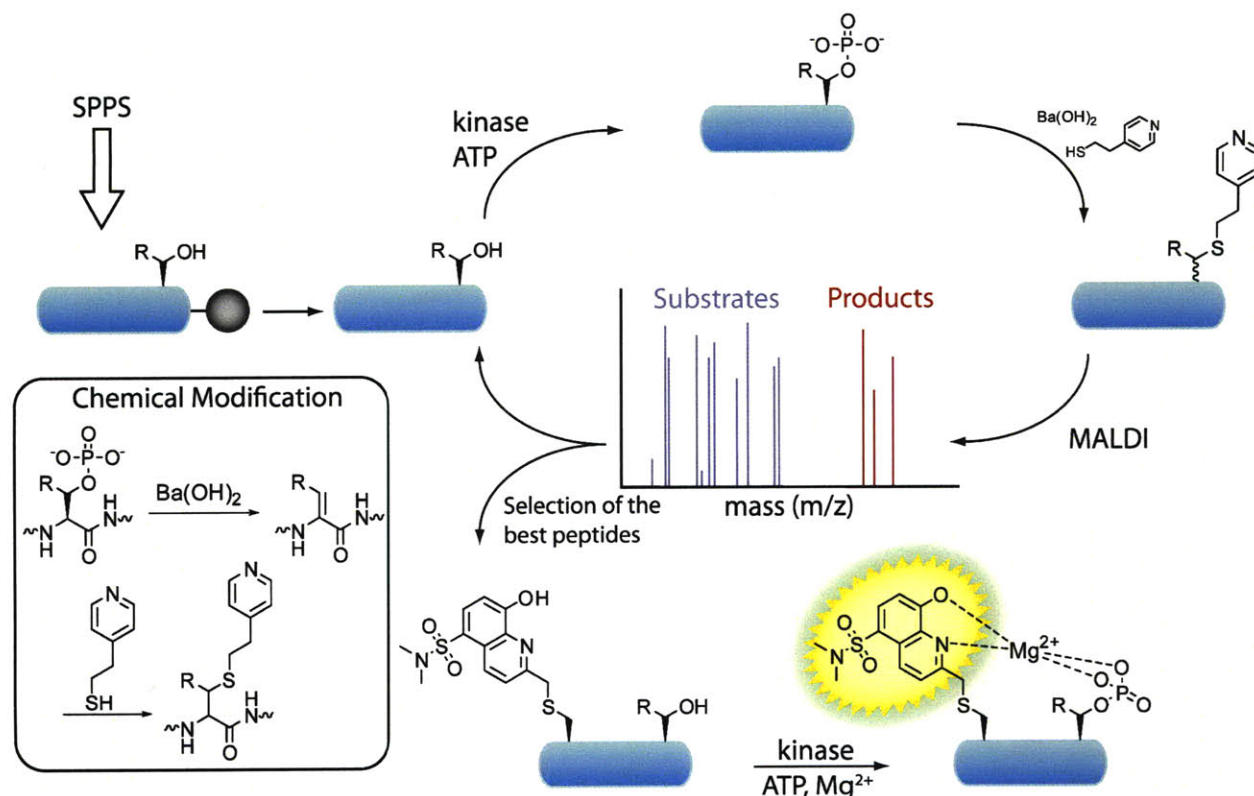


Figure 3-7. MS-based screening method to design selective substrates for Ser/Thr kinases. Chemical modification of phosphorylated peptides prior to MS analysis is also shown (inset).

In order to optimize and validate the screening method, we initially focused our efforts on PKA and its well studied and selective substrate, Kemptide (Ac-LRRASLG-CONH₂).⁴² Two peptide libraries based on Kemptide were used to assess the preference of PKA for residues at the -1 and -3 positions (Table 3-9). In all screens, Ser, Thr, Cys and Met were excluded to avoid side reactions, such as oxidations. Additionally, since there are three groups of amino acids with similar masses (Asp, Leu, Ile, Asn = 131-133 g/mol; Lys, Glu, Gln = 146-147 g/mol; and Val, Pro = 115-117 g/mol), only one from each group was chosen in order to simplify the MALDI

analysis. However, if necessary, it is also possible to use all amino acids in the screen by utilizing a peptide capping step during synthesis, effectively producing a nondegenerate mass ladder for each peptide.^{43, 44} A mixture of the following amino acids was selected: Asp, Lys, Val, Ala, Arg, Gly, His, Phe, Trp and Tyr. Libraries were synthesized on Fmoc-PAL-PEG-PS resin. For positions that were varied, an isokinetic mixture of 10 amino acids was created by using a ratio of amino acid equivalents based on their reported coupling rates.⁴⁵ The MALDI spectra of the peptide libraries before and after incubation with PKA for varying time periods (10 min, 30 min, 1 h, 2 h and 24 h) followed by chemical derivatization with 4-MEP showed that there is a preference for Arg at the -3 position (Figure 3-8) and for small hydrophobic residues at the -1 position (Table 3-9). This result is in full agreement with the consensus sequence described for PKA.^{15, 42}

Table 3-9. Peptide Libraries for PKA

Entry	Substrate Sequences ^a										
	-4	-3	-2	-1	0	+1	+2	+3	+4		
1	Ac	L	X	R	F	S	L	2-Nal	A	A	CONH ₂
2	Ac	L	R	R	X	S	L	2-Nal	A	A	CONH ₂
Result		L	R	R	G/A	S	L	2-Nal	A	A	

^a X = Asp, Lys, Val, Ala, Arg, Gly, His, Phe, Trp and Tyr.

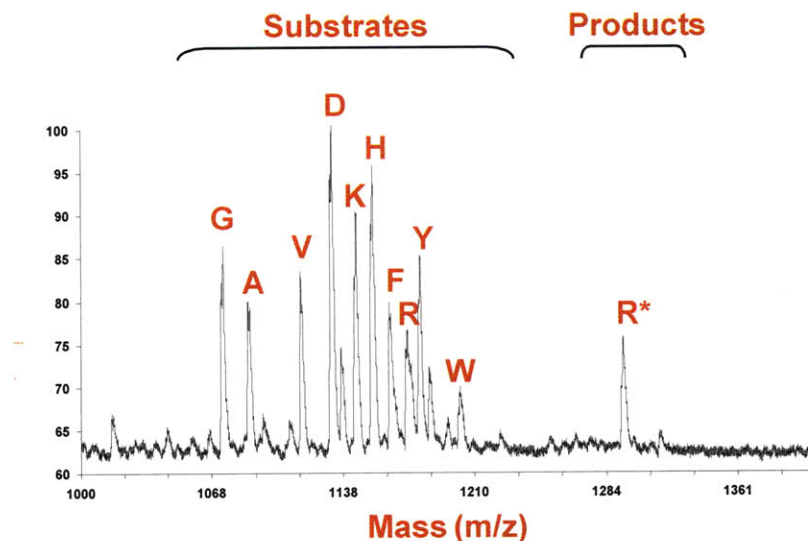


Figure 3-8. MALDI-TOF spectrum of the peptide library at the -3 position after its incubation with PKA for 1 h and chemical derivatization with $\text{Ba}(\text{OH})_2/4\text{-MEP}$.

Next, to demonstrate the generality and applicability of the method, substrates for AurA were generated. We made six peptide libraries using equimolar mixtures of amino acids at the -1 , -3 , -4 , $+1$, $+3$ and $+4$ positions based on the sequence of Kemptide (Table 3-10). The results of these libraries after incubation with AurA for varying time periods (10 min, 30 min, 1 h, 2 h and 24 h) followed by chemical derivatization with 4-MEP showed that first, there was an enhanced preference for an aromatic residue, Tyr or Phe, in the -1 position (Table 3-10, entry 3). For the remaining libraries, Phe was fixed in this position. Second, there was a high preference for Arg in the -3 position, which is in agreement with the consensus sequence described for AurA¹⁵ (entry 2). Third, in the $+1$ position, aromatic residues, such as Phe, were favored (entry 4). This result coincides with our earlier observations (Figure 3-5) and previous work done by Pinna *et al.*¹⁵ that identified Phe, Leu, and Ile in the $+1$ position (Leu and Ile were excluded from our screen). Fourth, small hydrophobic residues, mainly Gly, were selected for positions -4 , $+3$ and $+4$ (entries 1, 5 and 6). Lastly, due to the preference for Gly at -4 and $+3$ positions, we made two additional peptide libraries using D-amino acids (entries 1 and 5). As in the case of the L-

peptide libraries, AurA selected Gly in both positions and, interestingly, DAla in +3 position.

Table 3-10. Peptide Libraries for AurA

Entry	Substrate Sequences ^a										
	-4	-3	-2	-1	0	+1	+2	+3	+4		
1	Ac	X/Y	R	R	F	S	L	2-Nal	A	A	CONH ₂
2	Ac	L	X	R	F	S	L	2-Nal	A	A	CONH ₂
3	Ac	L	R	R	X	S	L	2-Nal	A	A	CONH ₂
4	Ac	L	R	R	F	S	X	2-Nal	A	A	CONH ₂
5	Ac	L	R	R	F	S	L	2-Nal	X/Y	A	CONH ₂
6	Ac	L	R	R	F	S	L	2-Nal	A	X	CONH ₂
Result	G/A	R	R	F	S	F	2-Nal	G/dA	G		

^a X = Asp, Lys, Val, Ala, Arg, Gly, His, Phe, Trp and Tyr; Y = DAsp, DLys, DVal, DAla, DArg, DGly, DHis, DPhe, DTrp and DTyr.

Several sequences selected by our screen were then individually synthesized with C-Sox in place of 2-Nal and evaluated as probes for AurA. Table 3-11 summarizes the sequences and the kinetics parameters of the best peptides. As seen previously with the rationally designed probes, a 2-fold improved K_M and a 3-fold improved catalytic efficiency were obtained by incorporating a Phe residue at the -1 position (Table 3-8, entry 2). However, a 6-fold enhanced K_M and a 5- to 7-fold rise in catalytic efficiency compared to Kemptide was obtained with Gly (entry 3) or DAla (entry 4) at position +3. These peptides are the best substrates described so far for AurA and should be able to be used in studies to dissect the role that AurA plays in mitosis and other cellular processes.

Table 3-11. Sequences and Kinetics of Sox-substrates for AurA

Entry	Substrate	Sequences											K_M (μM) ^a	V_{max} ($\mu\text{mol mg}^{-1} \text{min}^{-1}$) ^a	Catalytic Efficiency ^b	
		-5	-4	-3	-2	-1	0	+1	+2	+3	+4					
1	AurA-S2	Ac	A	L	R	R	A	S	L	C-Sox	A	A	CONH ₂	297.8 ± 3.9	1.7 ± 0.3	1
2	AurA-S6	Ac	A	L	R	R	F	S	L	C-Sox	A	A	CONH ₂	152.3 ± 2.7	2.6 ± 0.2	3
3	AurA-S29	Ac	A	L	R	R	F	S	L	C-Sox	G	A	CONH ₂	57.0 ± 8.2	2.2 ± 0.1	7
4	AurA-S30	Ac	A	G	R	R	Y	S	L	C-Sox	DA	A	CONH ₂	65.0 ± 7.0	1.8 ± 0.1	5

^a Kinetic parameters (K_M and V_{max}) were obtained from initial slopes and corrected appropriately for substrate and product fluorescence as described in Experimental Methods. The values reported are the mean ± s.e.m. of duplicate experiments as calculated from a direct fit of Hanes ($[\text{S}]/v$ vs. $[\text{S}]$) plots. ^c Catalytic efficiency of each substrate was calculated as k_{cat}/K_M ($\text{min}^{-1} \mu\text{M}^{-1}$) and normalized to the value obtained in entry 1.

Conclusions

Here we have presented screens for selective and improved probes for PKCs and Aurora kinases. However, due to the low throughput of such processes, we also developed a new mass spectrometry-based screening method. Although chemical methods to detect phosphorylated products using mass spectrometry and fluorescence have been reported, none were able to obtain substrates with improved selectivity for the desired kinase.⁴⁶ Our screen allows identification of substrates for serine/threonine kinases using a chemically modified combinatorial peptide library and MALDI TOF MS. The strategy was first validated by obtaining Kemptide as the most selective PKA peptide, which fully agrees with current literature. Moreover, the screen was applied to AurA resulting in a substrate with a 6-fold enhancement in K_M and a 7-fold rise in catalytic efficiency with respect to the best sequence described so far in the literature. Compared with the conventional approaches, this strategy is simple, easy to perform and it does not require complex instrumentation, the use of radioisotopes, or antibodies. The iterative nature of the method and its ability to incorporate unnatural elements (such as D-amino acids) should make searches for substrates of virtually any kinase possible. The conversion of the most selective peptides into fluorescent Sox-containing probes should give a specific reporter for any kinase of

choice.

Future Directions

Recently a new substrate demonstrating selectivity for PKC α in cell lysates has been reported (H₂N-FKKQGSFAKKK-CONH₂).⁴⁷ With our MS-based high throughput method there is now an opportunity to revisit PKCs and build truly isozyme-specific sensors, giving researchers a tool to differentiate cellular roles of individual isozymes in normal and diseased states.

Acknowledgments

I am grateful to Dr. Juan Antonio Gonzalez Vera for developing and validating the mass spectrometry-based screen for AurA substrates. This work was supported by the NIH Cell Migration Consortium (GM064346) and the Invitrogen Corporation. I also thank the Biophysical Instrumentation Facility for the Study of Complex Macromolecular Systems (NSF-0070319).

Experimental Methods

General Information

Unless otherwise noted, all solvents and reagents were obtained commercially and used without further purification. N^α-Fmoc-protected amino acids were purchased from Novabiochem. Whenever anhydrous and/or degassed CH₂Cl₂ was necessary it was distilled from calcium hydride and degassed by bubbling argon for at least 20 min. Peptides were purified *via* preparative reverse-phase HPLC employing a gradient of solvents A (H₂O with 0.1% v/v TFA) and B (CH₃CN with 0.1% v/v TFA) and characterized using mass spectrometry. Peptide purity was determined by analytical reverse-phase HPLC.

Instrumentation

HPLC: HPLC was carried out on Waters Prep LC 4000 System or Waters Delta 600 System equipped with Waters 2487 dual wavelength absorbance detectors. Columns used: C₁₈ analytical (flow rate = 1 mL/min), Beckman Ultrasphere ODS, 5 μm, 150 x 4.6 mm; C₁₈ preparatory (flow rate = 15 mL/min), YMC-Pack Pro, 5 μm, 250 x 20 mm.

MALDI-TOF MS: PerSeptive Biosystems Voyager MALDI-TOF instrument.

UV-Vis Spectrophotometer: Shimadzu UV-2401PC.

Fluorometer: Fluoromax 3 from Jobin Yvon. Cuvette: Starna Cells (16.100F-Q-10) 100 μL sub-micro cuvette, 1 cm path length.

Peptide Synthesis

a. Coupling chemistry and conditions

All peptides were synthesized using the standard Fmoc-based amino acid protection chemistry on Fmoc-PAL-PEG-PS resin (Applied Biosystems, 0.19 mmol g⁻¹) using either the on-resin alkylation (vide infra) or the Fmoc-C(Sox[TBDPS])-OH building block. The resin was swelled in CH₂Cl₂ (5 min.) and then DMF (5 min) prior to synthesis. All the amino acids except for Fmoc-C(Sox[TBDPS])-OH were coupled according to the following procedure: Fmoc deprotection (20% 4-methylpiperidine in DMF, 3 x 5 min), rinsing step (DMF, 5 x), coupling step (amino acid/PyBOP/HOBt/DIEA, 6:6:6:6, 0.15 M in DMF, 30-45 min), rinsing step (DMF, 5 x; CH₂Cl₂, 5 x). Fmoc-C(Sox[TBDPS])-OH was coupled in the following manner: amino acid/PyAOP/HOAt/DIEA, 2:2:2:5, 0.15 M in DMF, 2-12 hr. The coupling was repeated if necessary (amino acid/PyAOP/HOAt/DIEA, 1:1:1:3, 0.15 M in DMF, 2-12 hr) as determined by the TNBS test for free amines. It is important to wash the resin rigorously (DMF followed by CH₂Cl₂) to remove excess amino acid before performing any tests for free amines. This is particularly necessary after coupling of Fmoc-C(Sox[TBDPS])-OH due to its deep red color, which does not affect its coupling efficiency. At the end of the synthesis, the Fmoc group was removed with 20% 4-methylpiperidine in DMF (3 x 5 min.) and the resin was rinsed with DMF (5 x). The resin-attached free amines were capped by exposure to Ac₂O (20 equiv.) and pyridine (20 equiv.) in DMF for 30 min. The resin was rinsed with DMF (5 x), CH₂Cl₂ (5 x) and subjected to 20% 4-methylpiperidine in DMF (3 x 5 min.) to remove any Sox aryl esters that might have formed during acetylation. The resin was finally washed with DMF, CH₂Cl₂, MeOH (5 x each) and dried under vacuum.

a. On-resin alkylation of peptides with Sox-Br

Resin-bound peptides (50 mg, 0.0095 mmol, 1 equiv.) incorporating Cys(Mmt) were swelled in CH₂Cl₂, then DMF (5 min each). The Mmt protecting group was removed from the resin-bound peptide by bubbling N₂ through a solution of 1% TFA, 5% TIS in CH₂Cl₂ (4 x 20 min or until most of the yellow color due to the Mmt cation has disappeared). The resin was then subjected to rigorous washing with CH₂Cl₂ (5 x) and DMF (5 x). Anhydrous DMF (200 μL) was added to the resin followed by freshly distilled tetramethylguanidine (5.96 μL, 0.0475 mmol, 5 equiv.). The mixture was incubated for 2-3 min. Sox-Br (17 mg, 0.0285 mmol, 3 equiv.) was dissolved in anhydrous DMF (150 μL) and added to the resin. After ca. 12 hours of reaction time, the excess reagents were drained and the resin washed with DMF, CH₂Cl₂, MeOH, CH₂Cl₂ (5 x each).

b. Peptide library synthesis

Solid-phase peptide synthesis was performed manually by using Fmoc chemistry on Fmoc-PAL-PEG-PS resin (0.19 mmol g⁻¹). The resin was swelled in CH₂Cl₂ (5 min) and then DMF (5 min) prior to synthesis. Fixed positions were introduced by treating the amino acid (3 equiv./equiv. resin) with PyBOP (3 equiv./equiv. resin) and DIEA (8 equiv./equiv. resin) in DMF for one hour at room temperature. To install the randomized position, 10 equivalents of an isokinetic mixture of Fmoc-amino acids (Fmoc-amino acid, mole%: Fmoc-Ala-OH, 7.1; Fmoc-Arg(Pbf)-OH, 13.6; Fmoc-Asp(O-*t*Bu)-OH, 7.3; Fmoc-Gly-OH, 6.1; Fmoc-His(Boc)-OH, 7.3; Fmoc-Lys(Boc)-OH, 13.0; Fmoc-Phe-OH, 5.2; Fmoc-Trp(Boc)-OH, 8.0; Fmoc-Tyr(O-*t*Bu)-OH, 8.6; Fmoc-Val-OH, 23.7) were preactivated with DICl (10 equiv), and HOBT (10 equiv) in DMF (3 mL). The coupling was repeated after introducing the randomized position. Standard deprotection conditions were employed (20% 4-methylpiperidine in DMF for 10 min at RT). At the end of the synthesis the Fmoc group was removed with 20% 4-methylpiperidine in DMF, the resin was

rinsed with DMF and exposed to Ac₂O (20 equiv) and pyridine (20 equiv) for 30 min. The resin was finally washed with DMF, CH₂Cl₂, MeOH (5 x each) and dried under vacuum.

c. Side chain deprotection and cleavage from resin

The resin cleavage and protecting group removal was achieved by exposing the resin-bound peptides for 3 h to TFA/EDT/H₂O/TIS (94:2.5:2.5:1% v/v) for sequences containing easily oxidized residues (e.g. Cys, Met, Trp) or TFA/H₂O/TIS (95:2.5:2.5% v/v) for sequences without such residues (C-Sox does not require EDT in the cleavage cocktail). The resulting solution was concentrated under a stream of N₂ and precipitated by addition of cold Et₂O. The pellet was triturated with cold Et₂O (3 x), redissolved in water, filtered and lyophilized. The peptides were purified by preparative reverse-phase HPLC using UV detection at either 228 nm (amide bond absorption) and 280 nm (Fmoc, Trp, and/or Tyr absorption) or 228 nm and 316 nm (Sox absorption). Only fractions showing a single peak of correct mass by analytical HPLC were used in further experiments.

d. Characterization Data for AurA-S1-S30 Peptides

Name	Peptide Sequence	Mol. Formula	HPLC t _R (min.) ^a	[M] Calc.	[M+H] ⁺ found ^b
AurA-S1	Ac-ALKRASL-CSox-AA-CONH ₂	C ₅₆ H ₉₃ N ₁₇ O ₁₅ S ₂	25.2 ^c	1308.6	1307.3
AurA-P1	Ac-ALKRApSL-CSox-AA-CONH ₂	C ₅₆ H ₉₄ N ₁₇ O ₁₈ PS ₂	24.2 ^c	1388.5	1388.1
AurA-S2	Ac-ALRRASL-CSox-AA-CONH ₂	C ₅₆ H ₉₃ N ₁₉ O ₁₅ S ₂	25.8 ^c	1336.6	1336.5
AurA-P2	Ac-ALRRApSL-CSox-AA-CONH ₂	C ₅₆ H ₉₄ N ₁₉ O ₁₈ PS ₂	24.6 ^c	1416.6	1416.5
AurA-S3	Ac-KQTARKST-CSox-GK-CONH ₂	C ₆₂ H ₁₀₅ N ₂₁ O ₁₉ S ₂	21.2 ^c	1512.7	1513.5
AurA-P3	Ac-KQTARKpST-CSox-GK-CONH ₂	C ₆₂ H ₁₀₆ N ₂₁ O ₂₂ PS ₂	20.9 ^c	1592.7	1593.8
AurA-S4	Ac-KQTARKSL-CSox-GK-CONH ₂	C ₆₄ H ₁₀₉ N ₂₁ O ₁₈ S ₂	22.6 ^c	1524.8	1524.9
AurA-P4	Ac-KQTARKpSL-CSox-GK-CONH ₂	C ₆₄ H ₁₁₀ N ₂₁ O ₂₁ PS ₂	21.9 ^c	1604.8	1604.8
AurA-S5	Ac-GRTGRRNSI-CSox-AA-CONH ₂	C ₆₂ H ₁₀₃ N ₂₅ O ₁₉ S ₂	22.6 ^c	1566.8	1567.1
AurA-P5	Ac-GRTGRRNpSI-CSox-AA-CONH ₂	C ₆₂ H ₁₀₄ N ₂₅ O ₂₂ PS ₂	21.6 ^c	1646.7	1646.4
AurA-S6	Ac-ALRRFSL-CSox-AA-CONH ₂	C ₆₂ H ₉₇ N ₁₉ O ₁₅ S ₂	25.9 ^c	1412.7	1412.7
AurA-P6	Ac-ALRRFpSL-CSox-AA-CONH ₂	C ₆₂ H ₉₈ N ₁₉ O ₁₈ PS ₂	25.0 ^c	1492.7	1493.5
AurA-S7	Ac-ALRRFSL-CSox-KA-CONH ₂	C ₆₅ H ₁₀₄ N ₂₀ O ₁₅ S ₂	20.6 ^d	1469.8	1470.8
AurA-P7	Ac-ALRRFpSL-CSox-KA-CONH ₂	C ₆₅ H ₁₀₅ N ₂₀ O ₁₈ PS ₂	20.2 ^d	1549.7	1550.7
AurA-S8	Ac-ALRRFSL-CSox-AK-CONH ₂	C ₆₅ H ₁₀₄ N ₂₀ O ₁₅ S ₂	20.6 ^d	1469.8	1470.8
AurA-P8	Ac-ALRRFpSL-CSox-AK-CONH ₂	C ₆₅ H ₁₀₅ N ₂₀ O ₁₈ PS ₂	20.2 ^d	1549.7	1550.7
AurA-S9	Ac-ALRRFSL-CSox-FA-CONH ₂	C ₆₈ H ₁₀₁ N ₁₉ O ₁₅ S ₂	22.9 ^d	1488.8	1489.8
AurA-P9	Ac-ALRRFpSL-CSox-FA-CONH ₂	C ₆₈ H ₁₀₂ N ₁₉ O ₁₈ PS ₂	22.3 ^d	1568.7	1569.7
AurA-S10	Ac-ALRRFSL-CSox-AF-CONH ₂	C ₆₈ H ₁₀₁ N ₁₉ O ₁₅ S ₂	23.0 ^d	1488.8	1489.8
AurA-P10	Ac-ALRRFpSL-CSox-AF-CONH ₂	C ₆₈ H ₁₀₂ N ₁₉ O ₁₈ PS ₂	22.4 ^d	1568.7	1569.7
AurA-S11	Ac-ALRRFSL-CSox-LA-CONH ₂	C ₆₅ H ₁₀₃ N ₁₉ O ₁₅ S ₂	22.7 ^d	1454.8	1455.8
AurA-P11	Ac-ALRRFpSL-CSox-LA-CONH ₂	C ₆₅ H ₁₀₄ N ₁₉ O ₁₈ PS ₂	22.5 ^d	1534.7	1535.7
AurA-S12	Ac-ALRRFSL-CSox-AL-CONH ₂	C ₆₅ H ₁₀₃ N ₁₉ O ₁₅ S ₂	22.7 ^d	1454.8	1455.8
AurA-P12	Ac-ALRRFpSL-CSox-AL-CONH ₂	C ₆₅ H ₁₀₄ N ₁₉ O ₁₈ PS ₂	22.1 ^d	1534.7	1535.7
AurA-S13	Ac-ALRRFSL-CSox-EA-CONH ₂	C ₆₄ H ₉₉ N ₁₉ O ₁₇ S ₂	21.3 ^d	1470.7	1471.7
AurA-P13	Ac-ALRRFpSL-CSox-EA-CONH ₂	C ₆₄ H ₁₀₀ N ₁₉ O ₂₀ PS ₂	20.7 ^d	1550.7	1551.7
AurA-S14	Ac-ALRRFSL-CSox-AE-CONH ₂	C ₆₄ H ₉₉ N ₁₉ O ₁₇ S ₂	21.4 ^d	1470.7	1471.7
AurA-P14	Ac-ALRRFpSL-CSox-AE-CONH ₂	C ₆₄ H ₁₀₀ N ₁₉ O ₂₀ PS ₂	20.7 ^d	1550.7	1550.7
AurA-S15	H ₂ N-AALRRFSL-CSox-AAR-CONH ₂	C ₆₉ H ₁₁₂ N ₂₄ O ₁₆ S ₂	19.2	1596.8	1596.6
AurA-P15	H ₂ N-AALRRFpSL-CSox-AAR-CONH ₂	C ₆₉ H ₁₁₃ N ₂₄ O ₁₉ PS ₂	18.9	1676.8	1677.3
AurA-S16	H ₂ N-AALRRFSL-CSox-AAGR-CONH ₂	C ₇₁ H ₁₁₅ N ₂₅ O ₁₇ S ₂	19.4	1653.8	1654.2
AurA-P16	H ₂ N-AALRRFpSL-CSox-AAGR-CONH ₂	C ₇₁ H ₁₁₆ N ₂₅ O ₂₀ PS ₂	19.1	1733.8	1734.6
AurA-S17	H ₂ N-AALRRFSL-CSox-LFR-CONH ₂	C ₇₈ H ₁₂₂ N ₂₄ O ₁₆ S ₂	20.9	1714.9	1715.5
AurA-P17	H ₂ N-AALRRFpSL-CSox-LFR-CONH ₂	C ₇₈ H ₁₂₃ N ₂₄ O ₁₉ PS ₂	20.8	1794.8	1795.6
AurA-S18	H ₂ N-AALRRFSL-CSox-LFGR-CONH ₂	C ₈₀ H ₁₂₅ N ₂₅ O ₁₇ PS ₂	21.2	1771.9	1771.4
AurA-P18	H ₂ N-AALRRFpSL-CSox-LFGR-CONH ₂	C ₈₀ H ₁₂₆ N ₂₅ O ₂₀ PS ₂	20.8	1851.9	1852.4
AurA-S19	H ₂ N-ALRRFSL-CSox-LA-CONH ₂	C ₆₃ H ₁₀₁ N ₁₉ O ₁₄ S ₂	21.2	1411.7	1412.5

AurA-P19	H ₂ N-ALRRFpSL-CSox-LA-CONH ₂	C ₆₃ H ₁₀₂ N ₁₉ O ₁₇ PS ₂	20.7	1491.7	1492.5
AurA-S20	H ₂ N-AALRRRSL-CSox-AA-CONH ₂	C ₅₇ H ₉₈ N ₂₂ O ₁₄ S ₂	18.6	1378.7	1379.6
AurA-P20	H ₂ N-AALRRRpSL-CSox-AA-CONH ₂	C ₅₇ H ₉₉ N ₂₂ O ₁₇ PS ₂	18.0	1458.7	1459.6
AurA-S21	H ₂ N-AALRRRSL-CSox-LA-CONH ₂	C ₆₀ H ₁₀₄ N ₂₂ O ₁₄ S ₂	19.4	1420.7	1421.7
AurA-P21	H ₂ N-AALRRRpSL-CSox-LA-CONH ₂	C ₆₀ H ₁₀₅ N ₂₂ O ₁₇ PS ₂	18.9	1500.7	1501.6
AurA-S22	H ₂ N-ALRRFSD-CSox-AA-CONH ₂	C ₅₈ H ₈₉ N ₁₉ O ₁₆ S ₂	18.6	1371.6	1373.8
AurA-S23	H ₂ N-RRFSLC-CSox-CONH ₂	C ₄₅ H ₆₉ N ₁₅ O ₁₀ S ₂	19.9	1043.5	1045.4
AurA-S24	H ₂ N-KQTRRFSL-CSox-GAPR-CONH ₂	C ₇₄ H ₁₁₉ N ₂₇ O ₂₀ S ₂	19.9	1769.9	1773.0
AurA-S25	H ₂ N-KQTRRFSL-CSox-GAPE-CONH ₂	C ₇₃ H ₁₁₄ N ₂₄ O ₂₂ S ₂	18.9	1742.8	1744.9
AurA-S26	H ₂ N-SRLDSRC-CSox-IL-CONH ₂	C ₅₅ H ₉₂ N ₁₈ O ₁₆ S ₂	20.1	1324.6	1326.5
AurA-S27	H ₂ N-PRRRSRC-CSox-PE-CONH ₂	C ₅₇ H ₉₄ N ₂₄ O ₁₅ S ₂	21.2	1418.7	1421.5
AurA-S28	H ₂ N-PRRRFSR-CSox-PE-CONH ₂	C ₆₆ H ₁₀₂ N ₂₅ O ₁₆ S ₂	17.6	1565.7	1568.8
AurA-S29	Ac-ALRRFSL-CSox-GA-CONH ₂	C ₆₁ H ₉₅ N ₁₉ O ₁₅ S ₂	24.4 ^e	1398.6	1398.8
AurA-P29	Ac-ALRRFpSL-CSox-GA-CONH ₂	C ₆₁ H ₉₆ N ₁₉ O ₁₈ PS ₂	23.7 ^e	1478.6	1478.9
AurA-S30	Ac-AGRRYSL-CSox-DAA-CONH ₂	C ₅₈ H ₈₉ N ₁₉ O ₁₆ S ₂	26.7 ^e	1372.6	1374.1
AurA-S30	Ac-AGRRYpSL-CSox-DAA-CONH ₂	C ₅₈ H ₉₀ N ₁₉ O ₁₉ PS ₂	24.8 ^e	1452.5	1453.2

^a Peptides were purified using the following method: 5 % B (5 min) followed by a linear gradient 5–95% B (over 30 min) unless otherwise specified. All peptides, except AurA-S1, S3 and S4, prior to purification were dissolved in 20% AcOH in H₂O. AurA-S1, S3 and S4 were dissolved in H₂O. ^b MS data was collected on a MALDI TOF mass spectrometer. ^c Retention times are reported from runs on a reverse-phase analytical C₁₈ column. Method: 5% B (5 min) followed by a linear gradient 5–95% B (30 min). ^d Retention times are reported from run on a reverse-phase preparatory C₁₈ column. Method: 5% B (5 min) followed by a linear gradient 5–95% B (30 min). ^e Reported HPLC retention times and conditions are from analytical runs. Method: 5% B (5 min) then increased to 15% B (1 min) and followed by a linear gradient to 45% B (30 min).

Phosphorylation of peptide libraries

AurA: 200 μM of the corresponding peptide from the AurA library was added to a solution of 25 mM Tris, 10 mM MgCl₂, 5 mM β-glycerophosphate, 0.01 % TritonX-100, 1 mM ATP, 2.5 mM DTT, 0.5 mM EGTA and 200 ng AurA (Biosource, diluted with 20 mM Tris, 0.05 mM TritonX-100, 2 mM DTT, 0.1 mg/mL BSA, 10% glycerol) in a total volume of 100 μL.

PKA: 200 μM of the corresponding peptide from the PKA library was added to a solution of 20 mM HEPES (pH 7.4), 10 mM MgCl₂, 1 mM ATP, 1 mM DTT, 0.1 mM EGTA and 100 ng PKA

catalytic subunit (catalytic subunit, Calbiochem, diluted with 50 mM Tris–HCl [pH 7.5], 10 mM MgCl₂, 1 mM DTT, and 0.15 mg/mL BSA) in a total volume of 100 μL.

Five incubation reactions for each peptide library were performed and were stopped at five different times (10 min, 30 min, 1 h, 2 h and 24 h), followed by the derivatization reaction.

Chemical derivatization of phosphorylated peptide libraries

A 400 μL aliquot of a saturated solution of Ba(OH)₂ and 20 μL of 4-MEP (Toronto Research) were added to the corresponding phosphorylation reactions. The reaction was carried out for 2 h at 37 °C and the solution was acidified with 20 μL of formic acid, desalted and concentrated using Zip-Tip_{C18}. The samples were dissolved in 100 μL of 0.1% TFA in water and one aliquot (5 μL) of each sample was taken to be desalted using a Zip-Tip_{C18} and analyzed by MALDI.

Stock solutions

Due to the affinity of the phosphorylated peptides for Zn²⁺, by analogy with a previously reported peptide, the reagents with the highest purity and lowest metal content were used to avoid the necessity of removing metal ion impurities after preparations.

1. Stock solutions of the peptides were prepared in doubly deionized water and their concentrations were determined by UV-VIS (based on the determined extinction coefficient of the fluorophore unit, 5-(*N,N*-dimethylsulfonamido)-8-hydroxy-2-methylquinoline, $\epsilon_{355} = 8247 \text{ M}^{-1} \text{ cm}^{-1}$ at 355 nm in 0.1 M NaOH with 1 mM Na₂EDTA). An average of the values from three separate solutions, each prepared using a different volume of the stock solution, was read on a UV-Vis Spectrophotometer. Peptide stock solutions were stored at 4 °C.

2. Magnesium chloride stock solution of 2.66 M was prepared from Alfa Aesar's Puratronic grade salt. Most commercially available salts contain Zn^{2+} as significant impurities and should not be used due to the high affinity of the phosphorylated peptides for Zn^{2+} . The Mg^{2+} concentration was determined by titration with a standardized solution of EDTA (Aldrich) in the presence of an Eriochrome Black T (Aldrich).
3. 500 mM HEPES (SigmaUltra) was prepared and adjusted to pH 7.4 with sodium hydroxide (99.998+%, Aldrich) solution.
4. 10 mM DTT (Biotechnology grade, Mallinckrodt) was prepared in degassed ultrapure water and stored at $-80\text{ }^{\circ}\text{C}$.
5. 1% BME (Aldrich) was prepared in degassed ultrapure water and stored at $-80\text{ }^{\circ}\text{C}$.
6. 10 mg/mL BSA was prepared by dissolving bovine serum albumin (Heat Shock Fraction V, Roche) in ultrapure water and then filtered through a 0.45 micron syringe filter to remove particulates.
7. 0.1% Brij-35 P solution was prepared by dissolving an appropriate amount of Brij-35 P (Fluka) in doubly deionized water. The solution was stored at room temperature.
8. 100 mM ATP solution was prepared by dissolving 1.1024 g of ATP in 20 ml of doubly deionized water. The solution was then divided into 50 μl aliquots and stored at $-80\text{ }^{\circ}\text{C}$ until use.
9. 500 mM EGTA was prepared from ethylene glycol-bis(2-aminoethyl ether)-*N,N,N',N'*-tetraacetic acid (SigmaUltra) dissolved in 2 M NaOH and stored at $4\text{ }^{\circ}\text{C}$.
10. 10 $\mu\text{g/mL}$ phosphatidylserine and 2 $\mu\text{g/mL}$ diacylglycerol in 20 mM HEPES (pH 7.4) were prepared by combination of appropriate volumes of chloroform solutions of 10 mg/mL porcine brain phosphatidylserine (Avanti Polar Lipids, Inc.) and 2 mg/mL 1,2-dioleoyl-*sn*-

glycerol (Avanti Polar Lipids, Inc.). The chloroform was evaporated and an appropriate amount of solution 3 was added. The solution was alternated between vortexing for 3 min intervals and incubating in warm water bath for 1 min for a total time of 12 min. The solution was stored in aliquots at -20 °C. Samples were sonicated for 10 min before use in enzyme assays.

Fluorescence Experiments

The 5 nm emission and excitation slits were used for measurements of fluorescence increase in the fluorometer. For fluorescence spectra an excitation wavelength of 360 nm was used with emission 380-650 nm. Enzyme assays were performed by exciting at 410 nm and monitoring the emission at 485 nm with slit widths of 5 nm for emission and 5 nm for excitation. Readings were obtained every 3 second for 10 min with 1 sec integration time.

a. Fluorescence Intensity Dependence on [ATP]

ATP titrations were performed where concentration of the substrate was held constant and the concentration of ATP was varied. No enzyme was present in these experiments. A solution of the substrate (or phosphopeptide) was prepared in 20 mM HEPES (pH 7.4), 10 mM MgCl₂, and 10 μM peptide.

b. Assay Protocols

Screening for Enhanced Reaction Rates

PKCs: Reactions were done in 20 mM HEPES (pH 7.4), 10 mM MgCl₂, 0.3 mM CaCl₂, 0.1 mM EGTA, 100 μM ATP, 1 mM DTT, 0.5 μg/mL phosphatidylserine, 0.1 μg/mL diacylglycerol at 30 °C with appropriate amounts of PKC isozyme (Biosource, diluted with 20 mM HEPES [pH

7.4], 10 mM MgCl₂, 0.3 mM CaCl₂, 1 mM DTT, 10 mg/mL BSA and 0.01% Brij-35 P). Substrate peptide was added to begin the reaction. The assays were performed in the fluorometer ($\lambda_{\text{ex}} = 360$ nm, $\lambda_{\text{em}} = 485$ nm, slit widths = 5 nm).

AurA: Reactions were done in 20 mM HEPES (pH 7.4), 10 mM MgCl₂, 0.1 mM EGTA, 0.1% BME, 0.01% Brij, 0.1 mg/mL BSA, 4 μ M TPX(2-43) at 30 °C. The reactions were started by addition of 30 ng AurA (Biosource, diluted with 20 mM Tris, 0.05 mM TritonX-100, 2 mM DTT, 0.1 mg/mL BSA, 10% glycerol). The assays were performed in the fluorometer ($\lambda_{\text{ex}} = 360$ nm, $\lambda_{\text{em}} = 485$ nm, slit widths = 5 nm).

Determination of Kinetic Constants from Fluorescence Data

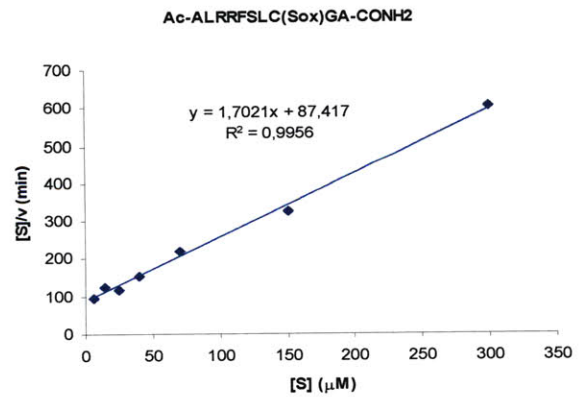
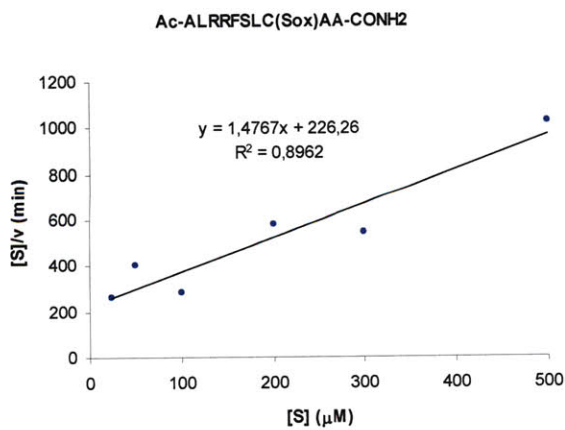
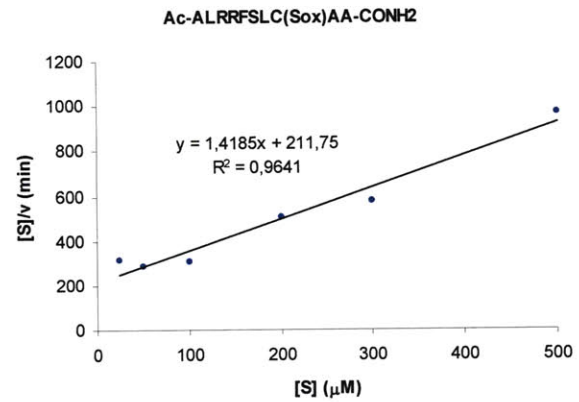
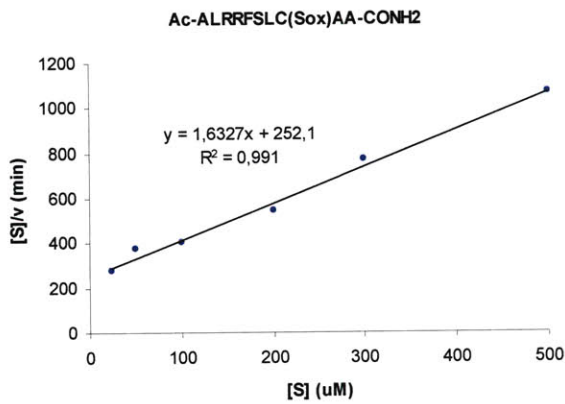
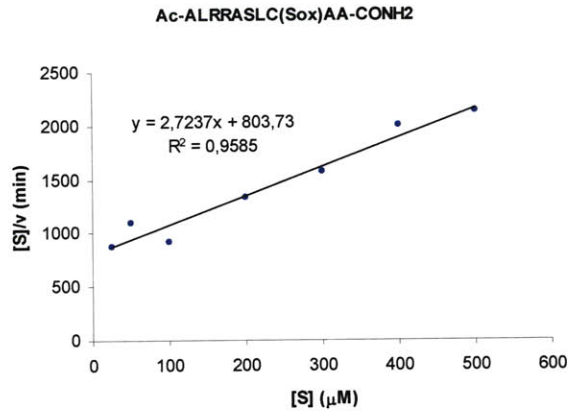
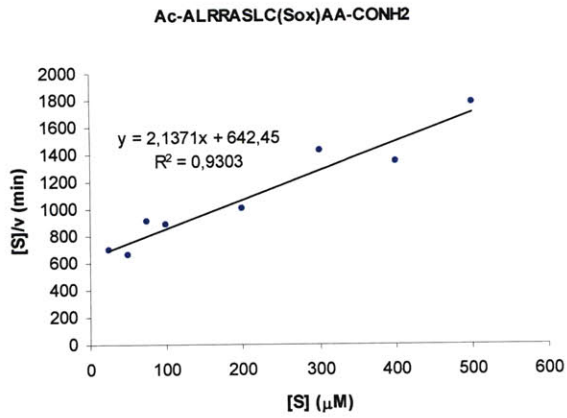
The reactions were initiated by addition of recombinant enzyme (AurA) or substrate (PKCs). The kinetic assays were performed in the fluorometer (PKCs: $\lambda_{\text{ex}} = 360$ nm, $\lambda_{\text{em}} = 485$; AurA: $\lambda_{\text{ex}} = 410$ nm, $\lambda_{\text{em}} = 485$; slit widths = 5 nm). The reactions were carried in a fluorescence microcuvette (120 μ L per reaction) containing varying chemosensor concentrations (generally $0.2\text{--}5 \times K_M$, unless otherwise noted) at 30 °C. Fluorescence slopes were determined by a least-squares fit using Microsoft Excel. Slopes were then either converted to a rate (see Chapter 2, Experimental Methods, section VI.e.). The kinetic parameters were obtained from Hanes plots ($[S]/v$ vs. $[S]$). Standard assay conditions were as follows:

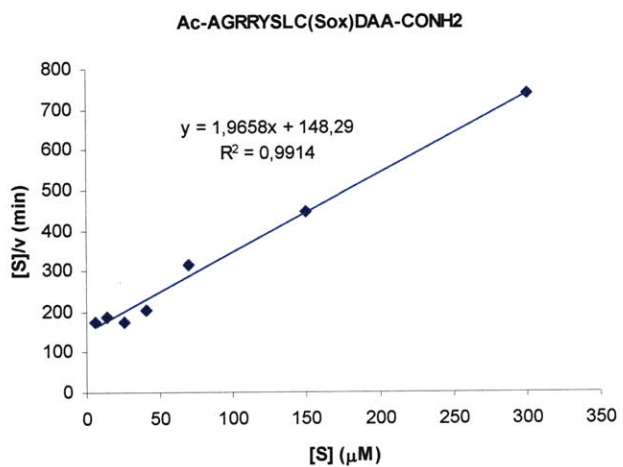
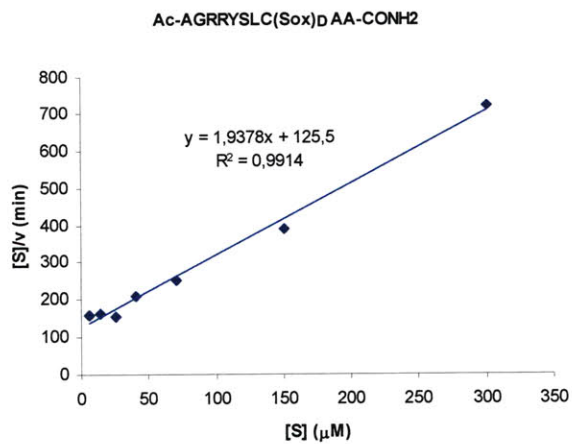
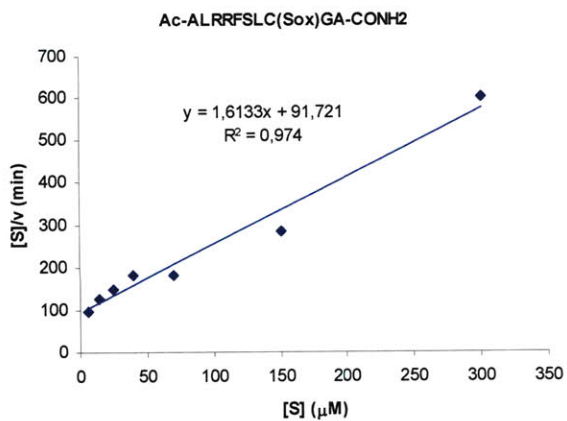
PKCs: Reactions were done in 20 mM HEPES (pH 7.4), 10 mM MgCl₂, 0.3 mM CaCl₂, 0.1 mM EGTA, 100 μ M ATP, 1 mM DTT, 0.5 μ g/mL phosphatidylserine, 0.1 μ g/mL diacylglycerol at 30 °C with appropriate amounts of PKC isozyme (Biosource, diluted with 20 mM HEPES [pH

7.4], 10 mM MgCl₂, 0.3 mM CaCl₂, 1 mM DTT, 10 mg/mL BSA and 0.01% Brij-35 P). Substrate peptide was added to begin the reaction. The assays were performed in the fluorometer ($\lambda_{\text{ex}} = 360 \text{ nm}$, $\lambda_{\text{em}} = 485 \text{ nm}$, slit widths = 5 nm).

AurA: Reactions were done in 25 mM Tris, 10 mM MgCl₂, 5 mM β -glycerophosphate, 0.01 % TritonX-100, 1 mM ATP, 2.5 mM DTT, 0.5 mM EGTA at 30 °C. The reactions were started by addition of 30 ng AurA (Biosource, diluted with 20 mM Tris, 0.05 mM TritonX-100, 2 mM DTT, 0.1 mg/mL BSA, 10% glycerol). Kinetic parameters are normally determined using concentrations of the substrate in the $0.2\text{-}5 \times K_M$ range. However, the K_M values of AurA substrates can be high, requiring very concentrated samples of substrate for the higher kinetic points. At high sensor concentrations most of the excitation light is absorbed by the Sox chromophore before it can reach all the molecules evenly along the cuvette's path length, giving slightly false results. Therefore, the substrate concentration was never greater than 500 μM . The assays were performed in the fluorometer ($\lambda_{\text{ex}} = 360 \text{ nm}$, $\lambda_{\text{em}} = 485 \text{ nm}$, slit widths = 5 nm).

Hanes Plots





References

1. Manning, G.; Whyte, D. B.; Martinez, R.; Hunter, T.; Sudarsanam, S. The Protein Kinase Complement of the Human Genome. *Science* **2002**, *298*, 1912-1934.
2. Nishizuka, Y. Protein kinase C and lipid signaling for sustained cellular responses. *FASEB J.* **1995**, *9*, 484-496.
3. Griner, E. M.; Kazanietz, M. G. Protein kinase C and other diacylglycerol effectors in cancer. *Nat. Rev. Cancer* **2007**, *7*, 281-294.
4. Newton, A. C. Protein kinase C: structural and spatial regulation by phosphorylation, cofactors, and macromolecular interactions. *Chem. Rev.* **2001**, *101*, 2353-2364.
5. Rykx, A.; De Kimpe, L.; Mikhalap, S.; Vantus, T.; Seufferlein, T.; Vandenheede, J. R.; Van Lint, J. Protein kinase D: a family affair. *FEBS Lett.* **2003**, *546*, 81-86.
6. Steinberg, S. F. Structural basis of protein kinase C isoform function. *Physiol. Rev.* **2008**, *88*, 1341-1378.
7. Hug, H.; Sarre, T. F. Protein kinase C isoenzymes: divergence in signal transduction? *Biochem. J.* **1993**, *291* (Pt 2), 329-343.
8. Pearson, R. B.; Kemp, B. E. Protein kinase phosphorylation site sequences and consensus specificity motifs: tabulations. *Methods Enzymol.* **1991**, *200*, 62-81.
9. Nishikawa, K.; Toker, A.; Johannes, F. J.; Songyang, Z.; Cantley, L. C. Determination of the specific substrate sequence motifs of protein kinase C isozymes. *J. Biol. Chem.* **1997**, *272*, 952-960.
10. Nigg, E. A. Mitotic kinases as regulators of cell division and its checkpoints. *Nat. Rev. Mol. Cell Biol.* **2001**, *2*, 21-32.
11. Glover, D. M.; Leibowitz, M. H.; McLean, D. A.; Parry, H. Mutations in aurora prevent centrosome separation leading to the formation of monopolar spindles. *Cell* **1995**, *81*, 95-105.
12. Hannak, E.; Kirkham, M.; Hyman, A. A.; Oegema, K. Aurora-A kinase is required for centrosome maturation in *Caenorhabditis elegans*. *J. Cell. Biol.* **2001**, *155*, 1109-1116.
13. Mendez, R.; Hake, L. E.; Andresson, T.; Littlepage, L. E.; Ruderman, J. V.; Richter, J. D. Phosphorylation of CPE binding factor by Eg2 regulates translation of c-mos mRNA. *Nature* **2000**, *404*, 302-307.
14. Bischoff, J. R.; Anderson, L.; Zhu, Y.; Mossie, K.; Ng, L.; Souza, B.; Schryver, B.; Flanagan, P.; Clairvoyant, F.; Ginther, C.; Chan, C. S.; Novotny, M.; Slamon, D. J.; Plowman, G. D. A homologue of *Drosophila* aurora kinase is oncogenic and amplified in human colorectal cancers. *EMBO J* **1998**, *17*, 3052-3065.
15. Ferrari, S.; Marin, O.; Pagano, M. A.; Meggio, F.; Hess, D.; El-Shemerly, M.; Krystyniak, A.; Pinna, L. A. Aurora-A site specificity: a study with synthetic peptide substrates. *Biochem. J.* **2005**, *390*, 293-302.
16. Shults, M. D.; Imperiali, B. Versatile Fluorescence Probes of Protein Kinase Activity. *J. Am. Chem. Soc.* **2003**, *125*, 14248-14249.
17. Michie, A. M.; Nakagawa, R. The link between PKC α regulation and cellular transformation. *Immunol. Lett.* **2005**, *96*, 155-162.
18. Dekker, L. V.; Parker, P. J. Protein kinase C--a question of specificity. *Trends Biochem. Sci.* **1994**, *19*, 73-77.

19. Mochly-Rosen, D. Localization of protein kinases by anchoring proteins: a theme in signal transduction. *Science* **1995**, 268, 247-251.
20. Nakashima, S. Protein kinase C α (PKC α): regulation and biological function. *J. Biochem.* **2002**, 132, 669-675.
21. Meraldi, P.; Honda, R.; Nigg, E. A. Aurora kinases link chromosome segregation and cell division to cancer susceptibility. *Curr. Opin. Genet. Dev.* **2004**, 14, 29-36.
22. Eyers, P. A.; Erikson, E.; Chen, L. G.; Maller, J. L. A novel mechanism for activation of the protein kinase Aurora A. *Curr. Biol.* **2003**, 13, 691-697.
23. Bayliss, R.; Sardon, T.; Vernos, I.; Conti, E. Structural basis of Aurora-A activation by TPX2 at the mitotic spindle. *Mol. Cell* **2003**, 12, 851-62.
24. Pavletich, N. P. Mechanisms of cyclin-dependent kinase regulation: structures of Cdks, their cyclin activators, and Cip and INK4 inhibitors. *J. Mol. Biol.* **1999**, 287, 821-8.
25. Wohr, T.; Wahl, F.; Nefzi, A.; Rohwedder, B.; Sato, T.; Sun, X. C.; Mutter, M. Pseudo-prolines as a solubilizing, structure-disrupting protection technique in peptide synthesis. *J. Am. Chem. Soc.* **1996**, 118, 9218-9227.
26. Dumy, P.; Keller, M.; Ryan, D. E.; Rohwedder, B.; Wohr, T.; Mutter, M. Pseudo-prolines as a molecular hinge: Reversible induction of cis amide bonds into peptide backbones. *J. Am. Chem. Soc.* **1997**, 119, 918-925.
27. Nowakowski, J.; Cronin, C. N.; McRee, D. E.; Knuth, M. W.; Nelson, C. G.; Pavletich, N. P.; Rogers, J.; Sang, B. C.; Scheibe, D. N.; Swanson, R. V.; Thompson, D. A. Structures of the cancer-related Aurora-A, FAK, and EphA2 protein kinases from nanovolume crystallography. *Structure* **2002**, 10, 1659-1667.
28. Obata, T.; Yaffe, M. B.; Leparo, G. G.; Piro, E. T.; Maegawa, H.; Kashiwagi, A.; Kikkawa, R.; Cantley, L. C. Peptide and protein library screening defines optimal substrate motifs for AKT/PKB. *J. Biol. Chem.* **2000**, 275, 36108-36115.
29. Fukunaga, R.; Hunter, T. MNK1, a new MAP kinase-activated protein kinase, isolated by a novel expression screening method for identifying protein kinase substrates. *EMBO J.* **1997**, 16, 1921-1933.
30. Jiang, W.; Jimenez, G.; Wells, N. J.; Hope, T. J.; Wahl, G. M.; Hunter, T.; Fukunaga, R. PRC1: a human mitotic spindle-associated CDK substrate protein required for cytokinesis. *Mol Cell* **1998**, 2, 877-885.
31. Hutti, J. E.; Jarrell, E. T.; Chang, J. D.; Abbott, D. W.; Storz, P.; Toker, A.; Cantley, L. C.; Turk, B. E. A rapid method for determining protein kinase phosphorylation specificity. *Nat. Methods* **2004**, 1, 27-29.
32. Uttamchandani, M.; Chan, E. W.; Chen, G. Y.; Yao, S. Q. Combinatorial peptide microarrays for the rapid determination of kinase specificity. *Bioorg. Med. Chem. Lett.* **2003**, 13, 2997-3000.
33. Wu, J.; Ma, Q. N.; Lam, K. S. Identifying substrate motifs of protein kinases by a random library approach. *Biochemistry* **1994**, 33, 14825-33.
34. Akita, S.; Umezawa, N.; Higuchi, T. On-bead fluorescence assay for serine/threonine kinases. *Org. Lett.* **2005**, 7, 5565-5568.
35. Slon-Usakiewicz, J. J.; Dai, J. R.; Ng, W.; Foster, J. E.; Deretey, E.; Toledo-Sherman, L.; Redden, P. R.; Pasternak, A.; Reid, N. Global kinase screening. Applications of frontal affinity chromatography coupled to mass spectrometry in drug discovery. *Anal. Chem.* **2005**, 77, 1268-1274.

36. von Ahsen, O.; Bomer, U. High-throughput screening for kinase inhibitors. *Chembiochem* **2005**, *6*, 481-490.
37. Songyang, Z.; Blechner, S.; Hoagland, N.; Hoekstra, M. F.; Piwnica-Worms, H.; Cantley, L. C. Use of an oriented peptide library to determine the optimal substrates of protein kinases. *Curr. Biol.* **1994**, *4*, 973-982.
38. MacBeath, G.; Schreiber, S. L. Printing proteins as microarrays for high-throughput function determination. *Science* **2000**, *289*, 1760-1763.
39. Kim, Y. G.; Shin, D. S.; Kim, E. M.; Park, H. Y.; Lee, C. S.; Kim, J. H.; Lee, B. S.; Lee, Y. S.; Kim, B. G. High-throughput identification of substrate specificity for protein kinase by using an improved one-bead-one-compound library approach. *Angew. Chem. Int. Ed. Engl.* **2007**, *46*, 5408-5411.
40. Arrigoni, G.; Resjo, S.; Levander, F.; Nilsson, R.; Degerman, E.; Quadroni, M.; Pinna, L. A.; James, P. Chemical derivatization of phosphoserine and phosphothreonine containing peptides to increase sensitivity for MALDI-based analysis and for selectivity of MS/MS analysis. *Proteomics* **2006**, *6*, 757-766.
41. Lukovic, E.; Gonzalez-Vera, J. A.; Imperiali, B. Recognition-domain focused chemosensors: Versatile and efficient reporters of protein kinase activity. *J. Am. Chem. Soc.* **2008**, *130*, 12821-12827.
42. Moore, M. J.; Adams, J. A.; Taylor, S. S. Structural basis for peptide binding in protein kinase A. Role of glutamic acid 203 and tyrosine 204 in the peptide-positioning loop. *J. Biol. Chem.* **2003**, *278*, 10613-10618.
43. Hoffmann, C.; Blechschmidt, D.; Kruger, R.; Karas, M.; Griesinger, C. Mass spectrometric sequencing of individual peptides from combinatorial libraries via specific generation of chain-terminated sequences. *J Comb Chem* **2002**, *4*, 79-86.
44. Nitz, M.; Franz, K. J.; Maglathlin, R. L.; Imperiali, B. A powerful combinatorial screen to identify high-affinity terbium(III)-binding peptides. *Chembiochem* **2003**, *4*, 272-276.
45. Backes, B. J.; Harris, J. L.; Leonetti, F.; Craik, C. S.; Ellman, J. A. Synthesis of positional-scanning libraries of fluorogenic peptide substrates to define the extended substrate specificity of plasmin and thrombin. *Nat. Biotechnol.* **2000**, *18*, 187-193.
46. Akita, S.; Umezawa, N.; Kato, N.; Higuchi, T. Array-based fluorescence assay for serine/threonine kinases using specific chemical reaction. *Bioorg. Med. Chem.* **2008**, *16*, 7788-7794.
47. Kang, J. H.; Asai, D.; Yamada, S.; Toita, R.; Oishi, J.; Mori, T.; Niidome, T.; Katayama, Y. A short peptide is a protein kinase C (PKC) alpha-specific substrate. *Proteomics* **2008**, *8*, 2006-2011.

Chapter 4. Highly Selective Chimeric Reporters for ERK1/2 in Cellular Media

A portion of the work described in this chapter has been published in:
Luković, E.; Vogel Taylor, E.; Imperiali, B. Monitoring Protein Kinases in Cellular Media with Highly Selective Chimeric Reporters. *Angew. Chem. Int. Ed. Engl.* **2009**, in press.

Introduction

Mitogen-activated protein kinases (MAPKs) are important regulators of cellular function, and the dynamics of their activities are critical indicators of the health or pathology of living systems.^{1, 2} Since their discovery 20 years ago, abnormal regulation of MAPKs has been implicated in multiple illnesses including many cancers,³ obesity,⁴ diabetes,⁴ polycystic kidney diseases,⁵ cardiovascular problems,^{6, 7} Alzheimer's⁸ and pulmonary diseases.⁹⁻¹¹ The MAPK family comprises at least 4 members, including extracellular-signal-regulated kinase 1/2 (ERK1/2), c-Jun-*N*-terminal kinase (JNK), p38 and ERK5. These enzymes are all activated through a similar mechanism. First, extracellular stimuli (e.g. growth factors, cytokines, mitogens, hormones and oxidative or heat stress) activate receptor tyrosine kinases (RTKs) and G protein-coupled receptors (GPCRs). Through a series of cascade reactions the receptors turn on Raf, a MAPK kinase kinase (MAPKKK), which can then phosphorylate MEK, a MAPK kinase (MAPKK) that finally phosphorylates MAPKs, such as ERK (Figure 4-1).

In particular, ERK1/2 plays a pivotal role in the MAPK signaling pathway responsible for regulated cell survival and proliferation (Figure 4-1).¹² Bis-phosphorylation of ERK1/2 in the ThrGluTyr sequence by MEK1/2 results in the kinase translocation to the nucleus, where it acts to activate various transcription factors, such as Elk-1, Ets-1, Fos and Sap-1a.^{13, 14} Although ERK activation is normally associated with proliferation, evidence has emerged that, depending on the stimuli and cell types involved, activation of ERK can mediate cell death as well.¹⁵ Some proteins, including phosphoprotein enriched in astrocytes 15 (PEA-15) and death associated protein kinase (DAPK), can sequester ERK from the nucleus to the cytoplasm,^{16, 17} thereby disrupting the activation of survival-promoting transcription factors. Moreover, ERK is an

upstream activator of DAPK, which is crucial in mediating proapoptotic signals that eventually lead to death.

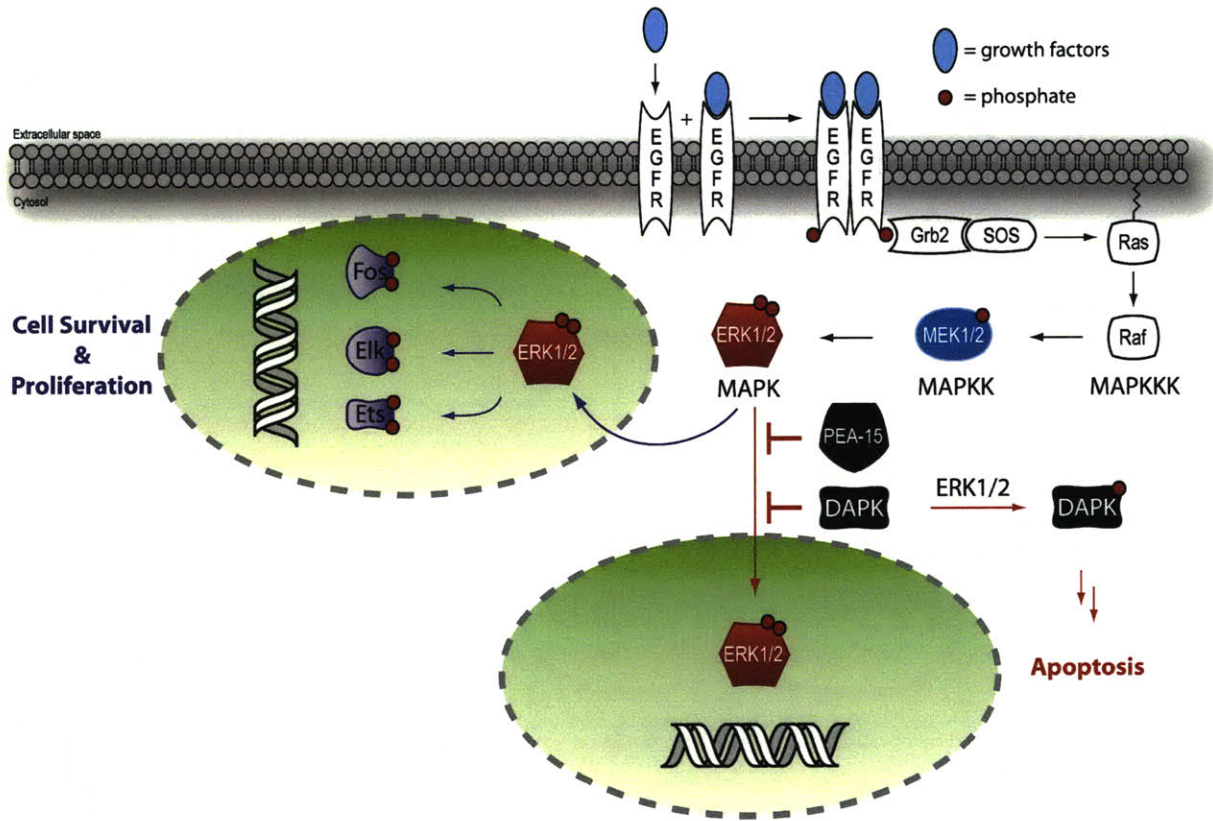


Figure 4-1. The mechanisms of ERK-mediated cell proliferation or apoptosis. Activation of RTKs or GPCRs by growth factors leads to a cascade of reactions and ultimate activation of ERK (black arrows). Phosphorylated ERK translocates to the nucleus where it activates multiple transcription factors, leading to cell survival and proliferation (purple arrows). Conversely, the cytoplasmic sequestration of ERK1/2 by PEA-15 or DAPK increases activation of DAPK, which results in proapoptotic signaling and eventual cell death (red arrows).

The centrality of these enzymes in normal and diseased cell states underscores the need for high throughput, selective, and sensitive methods that quantitatively and directly diagnose kinase activities both in vitro and in cells. For cellular imaging, genetically-encoded sensors that rely on phosphorylation-based changes in fluorescence resonance energy transfer (FRET) between fluorescent protein pairs^{18, 19} have been constructed for several kinases, including ERK1/2.²⁰⁻²³ These sensors are powerful because they can be expressed in cells; however, they

cannot be used for high throughput screening of recombinant enzymes and unfractionated cell lysates due to the very limited fluorescence changes that accompany phosphorylation. In addition, the GFP-based sensors are generally large and their size may disrupt the systems under study. As a complementary approach, probes based on small, organic fluorophores with direct readouts,²⁴ including the Sox-based probes,⁶ can give sensitive and robust signals under physiological conditions. These sensors are not only amenable to high throughput applications, but can also be adapted to cellular work through microinjection or via the use of conjugated cell penetrating peptides. Lastly, the synthesis of these sensors is generally modular so that additional selectivity determinants can be quickly incorporated. This is particularly important because more than 500 different kinases are encoded in the human genome, and sensor selectivity in complex assay environments becomes paramount.¹⁹

While many protein kinases exploit linear recognition motifs comprising 4-8 residues that are proximal to the phosphorylation site to drive specificity, a number of physiologically important kinases, including ERK1/2 and other MAPKs, phosphorylate substrates with short and ubiquitous consensus sequences. For these enzymes specificity is derived from extended recognition elements that include protein-protein interactions distal to the phosphorylation site.²⁵ For example, ERK1 and 2 phosphorylate the transcription factor Ets-1 at Thr38 within a short ThrPro (TP) consensus motif.²⁶ Since this short sequence alone would be the target of multiple kinases, ERK recognition of Ets-1 depends on an adjoining *N*-terminal pointed (PNT) domain²⁷ to dock the substrate specifically to ERK1/2, which engages the phosphorylation machinery (Figure 4-2).²⁸ With this docking-domain strategy, PNT-based substrates demonstrate good affinity for ERK1/2 ($K_M \sim 6-9 \mu\text{M}$),²⁷ in stark contrast to short peptide substrates derived only from the TP sequence ($K_M > 200 \mu\text{M}$).^{27, 29} Due to the size of the PNT domain (11 kDa) these

docking-domain interactions cannot be exploited with the types of synthetic peptide-based sensors that have been previously reported. However, in light of its importance in cellular homeostasis and the prominence of ERK dysregulation in cancer, we set out to construct a chimeric sensor for ERK1/2 that combines the advantageous reporting properties of the Sox fluorophore with the outstanding specificity provided by the native protein domain-based recognition (Figure 4-2). Most importantly, to ensure unambiguous analysis of ERK1/2 activity in high throughput assays and in cellulo applications, our ultimate requirement was that the probe be highly selective in lysates and cells where it would be exposed to hundreds of other active kinases.

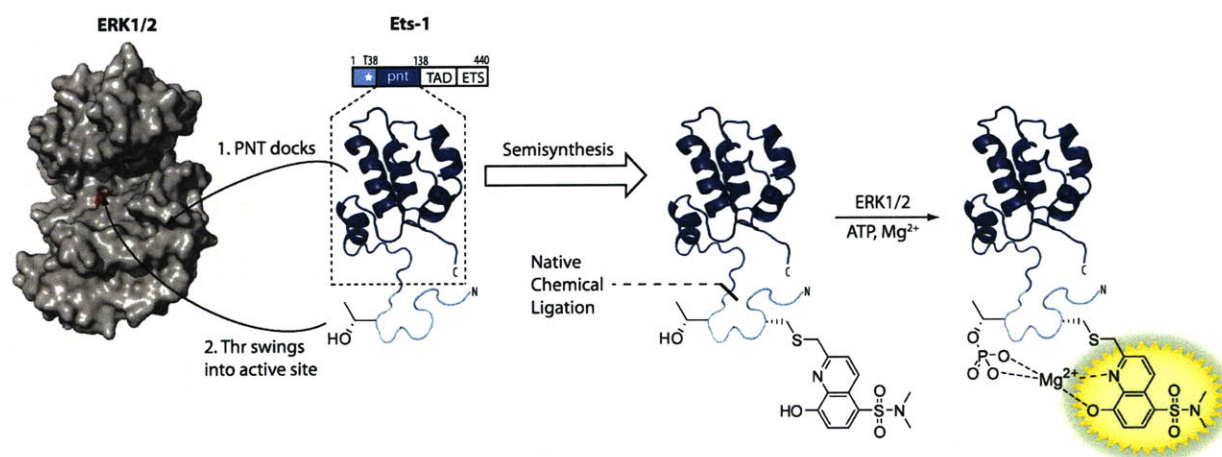


Figure 4-2. ERK utilizes the PNT domain of its substrate Ets-1 to drive specificity. The PNT domain (dark blue, PDB 1BQV) first docks to ERK (PDB 2ERK), followed by binding of the N-terminal portion in the active site. Conserved active site base, Asp147 (red), is also shown. The Sox-based chemosensor, assembled through NCL, utilizes the PNT domain to gain specificity for ERK1/2 and reports phosphorylation via CHEF ($\lambda_{\text{ex}} = 360 \text{ nm}$, $\lambda_{\text{em}} = 485 \text{ nm}$) in cell lysates and in cellulo.

In this chapter we describe the semisynthesis of a chimeric Sox-based ERK1/2 sensor through a key native chemical ligation (NCL) reaction that efficiently conjugates the recombinant PNT domain of Ets-1 to a synthetic ERK1/2 consensus sequence including the Sox

sensing module (Figure 4-2). The extended PNT recognition element confers the ERK1/2 sensor with excellent selectivity, as demonstrated by comparative quantitative analyses with a panel of related recombinant enzymes and in unfractionated lysates from four different cell lines. The biochemical assays have also been optimized for high-throughput applications in both 96- and 384-well plates.

Furthermore, due to its superb selectivity, we have also synthesized Sox-PNT derivatives that may facilitate uptake, and spatial and temporal control of the sensor during ERK1/2 imaging in live cells. Most importantly, the docking domain-based sensor design should be generally applicable to the development of selective sensors for other medically important kinases.

Results and Discussion

Semisynthesis of the Sox-PNT Sensor

The new sensor was assembled as illustrated in Figure 4-3, using NCL³⁰ to ligate the synthetic Sox-containing peptide thioester with the expressed PNT domain, comprising Ets-1 residues 46-138. An optimized phosphorylation motif based on the ERK2 phosphorylation sequence within the myelin basic protein (MBP)²⁹ (TPGGRR) was used in place of the phosphorylated region of Ets-1 (TPSSKE). When the Sox chromophore was incorporated into these short peptides, preliminary studies indicated that the MBP-based sequence had better fluorescent properties than the Ets-based sequence (Table 4-1). The distance between the TP recognition sequon and the PNT domain in the wild type protein was preserved in the sensor (Table 4-2). This design introduced residue replacements in the unstructured N-terminal region of Ets-1, thereby minimizing perturbations to the overall secondary structure. Additionally, the C-terminal residue, Met44, was changed to Gly to eliminate the possibility of epimerization during thioesterification and to increase ligation efficiency.³¹ The peptide thioester **9** was

synthesized using Fmoc-based solid phase peptide synthesis (SPPS) on highly acid-labile TGT resin, followed by an off-bead thioesterification of the protected peptide.³² The Sox chromophore was introduced as the amino acid C-Sox.³³ The C-terminal fragment of the sensor was expressed as a GST-fusion protein, GST-PNT (**7**), to improve yields of protein expression. GST-PNT was then proteolyzed by TEV protease to reveal Cys-PNT (**8**). After ligation of Cys-PNT to the peptide thioester under non-denaturing conditions, the ERK1/2 probe, Sox-PNT (**10**), was isolated in good yield (24%; the accurate mass of the isolated material was based on the ϵ_{\max} of the Sox chromophore) (see the Experimental Methods). The corresponding phosphoprotein (pThr38), pSox-PNT (**11**), was constructed using analogous methods.

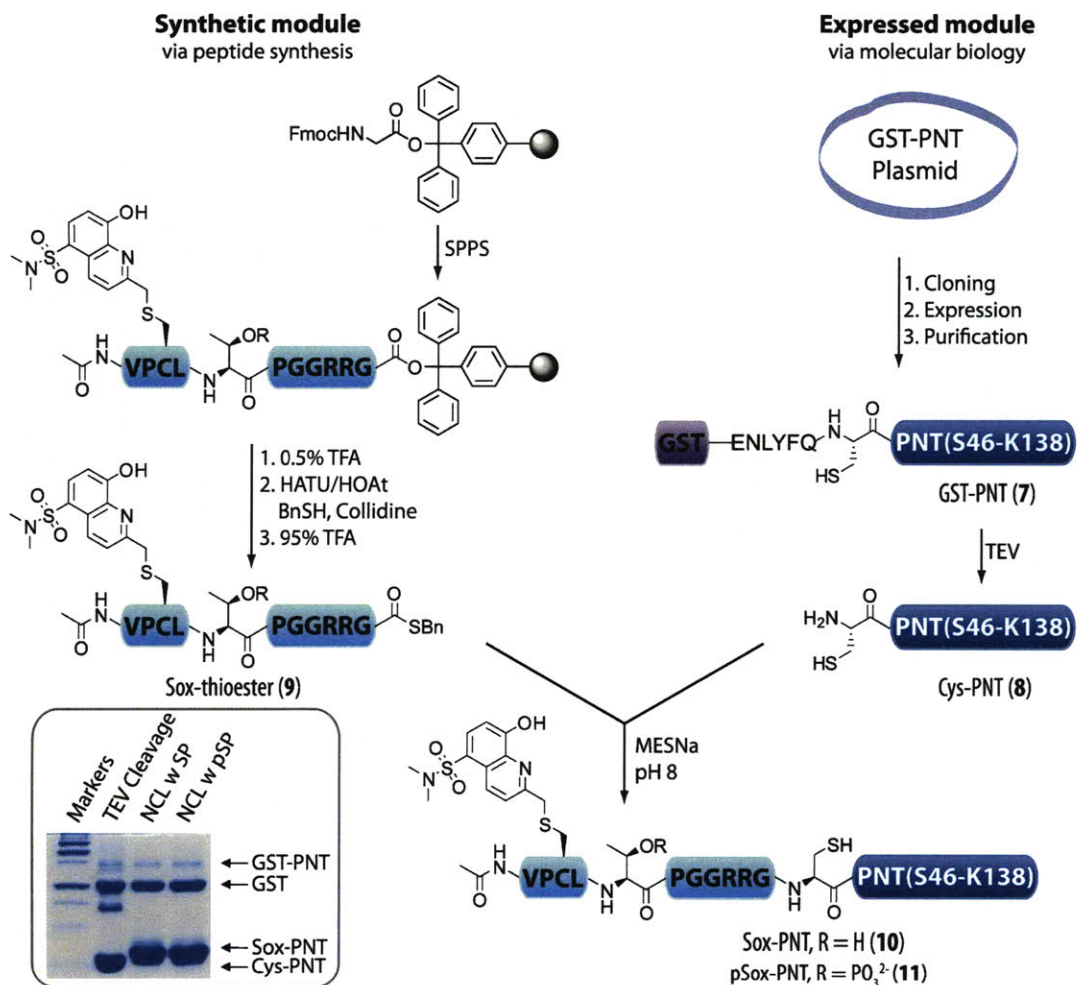


Figure 4-3. The semisynthesis of the Sox-PNT sensor via NCL. The thioester peptide containing C-Sox was synthesized via SPPS. The Cys-PNT domain was obtained through standard molecular biology methods. Inset: Comassie-stained gel of the ligation reactions indicated 80-90% conversion of the Cys-PNT expressed segment to the products, Sox-PNT and pSox-PNT. SP = Sox-Peptide thioester; pSP = pSox-Peptide thioester.

Table 4-1. Fold Fluorescence Increase of BTF and RDF Chemosensors in the Presence and Absence of ATP

Entry	Origin of Sequence	Peptide Sequence ^a	Fold fluorescence increase ^b	
			0 mM ATP	1 mM ATP
1	Ets-1	H ₂ N-DDK-Sox-PL-(p)T-P <u>SSKE</u> G-CO ₂ H	1.7	1.5
2	MBP	H ₂ N-DDK-Sox-PL-(p)T-P <u>GRRR</u> G-CO ₂ H	2.1	2.3
3	MBP	Ac-VPLL-(p)T-P-CSox- <u>GRRR</u> -CO ₂ H	5.4	5.1
4	MBP	Ac-VPLL-(p)T-P <u>G</u> -CSox- <u>RRR</u> -CO ₂ H	6.3	6.2
5	MBP	Ac-VP-CSox-L-(p)T-P <u>GRRR</u> G-CO ₂ H	6.9	8.1

^a Underlined residues are part of the phosphorylation sequence. ^b Measured in triplicate as a quotient of fluorescence intensity at 485 nm of phosphopeptide and substrate in 20 mM HEPES (pH 7.4), 10 mM MgCl₂, and 10 μM peptide.

Table 4-2. Sequences Surrounding the TP Recognition Region (Red Residues) of the Wild Type Ets-1, MBP and Sox-PNT

Substrate	Sequence ^a														
	38											46	138		
Ets-1(32-138)	V	P	L	L	T	P	S	S	K	E	<u>M</u>	<u>M</u>	S	...	K
MBPptide		A	P	R	T	P	G	G	R	R					
Sox-PNT	V	P	C-Sox	L	T	P	G	G	R	R	<u>G</u>	<u>C</u>	S	...	K

^a The Met44-Met45 site in Ets-1 was changed to Gly44-Cys45 (underlined residues) in Sox-PNT due to requirements for NCL.

Evaluation of the Sox-PNT Probe

Initial spectroscopic studies with Sox-PNT and pSox-PNT revealed a robust 3-fold enhancement in fluorescence upon phosphorylation under standard biochemical assay conditions (Figure 4-4b), which is somewhat lower than the changes observed with Sox-Peptide (Figure 4-4a). Furthermore, a similar change (3.7-fold) was obtained when Sox-PNT was enzymatically phosphorylated by ERK2 to afford pSox-PNT (Figure 4-4c) (see the Experimental Methods). Moreover, similar to Sox-based peptide sensors,³³ Sox-PNT was found to have an excellent Z' factor value (0.81), which is a statistical quality parameter used to evaluate and validate performance of assays, with useful ranges being 0.5-1.³⁴

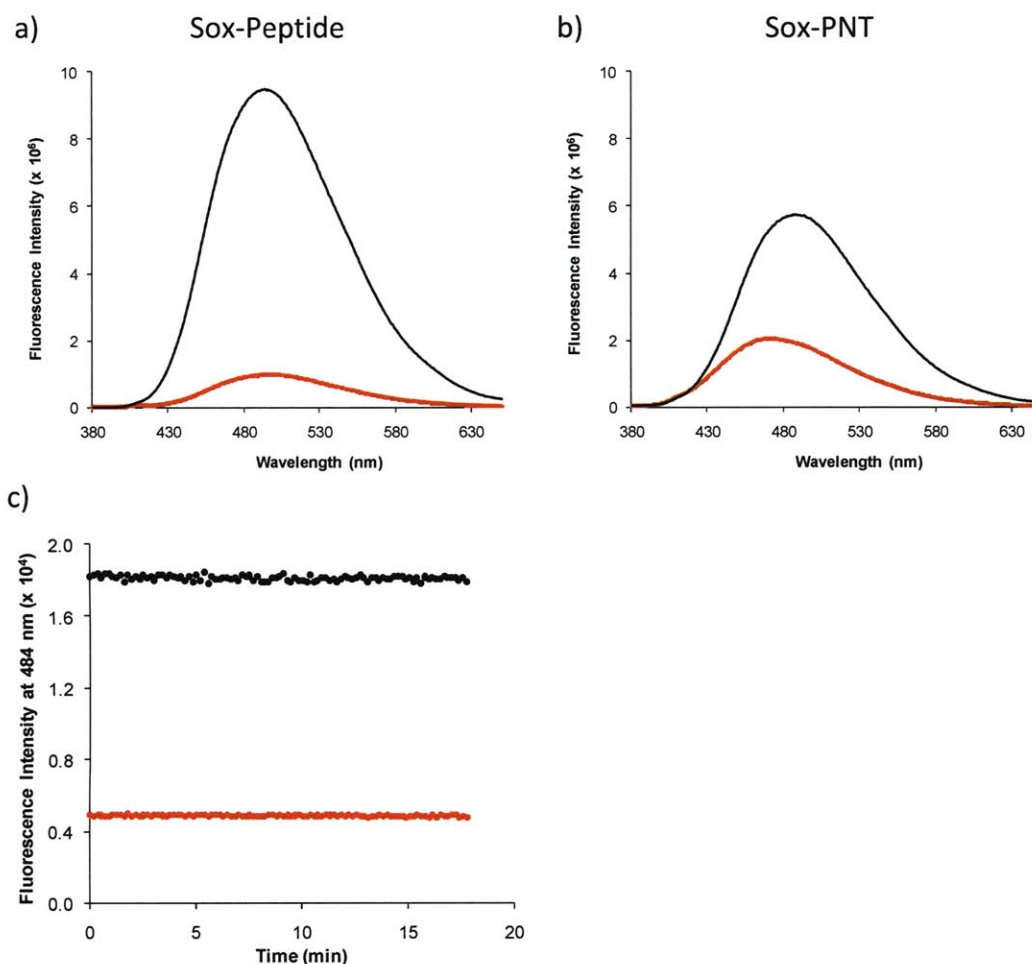


Figure 4-4. Fluorescence spectra of phosphorylated (black) and unphosphorylated (red) versions of a) Sox-Peptide and b) Sox-PNT sensors. Conditions: 10 μ M Sensor, 50 mM Tris (pH 7.5), 10 mM $MgCl_2$, 1 mM EGTA, 2 mM DTT and 0.01% Brij 35 P at 30 $^{\circ}C$. d) Fluorescence intensity of Sox-PNT at time 0 (red) and at 17 hours (black), after ERK2 completely turned over the substrate to pSox-PNT. Conditions: 10 μ M Sox-PNT, 50 mM Tris (pH 7.5 at 25 $^{\circ}C$), 10 mM $MgCl_2$, 1 mM EGTA, 2 mM DTT, 0.01% Brij 35 P, 1 mM ATP and 5 nM ERK at 30 $^{\circ}C$.

Subsequent *in vitro* assays were used to establish that Sox-PNT is an efficient substrate for ERK2 when compared with the corresponding Sox-peptide (Ac-VP-CSox-LTPGGRRG-OH) (Figure 4-5a and Figure 4-16 in the Experimental Methods). Furthermore, Sox-PNT

demonstrated a similar K_M (14.9 μM) value and a slightly lower catalytic efficiency ($k_{\text{cat}}/K_M = 47 \text{ min}^{-1} \mu\text{M}^{-1}$) compared to the wild type PNT ($K_M = 9 \mu\text{M}$, $k_{\text{cat}}/K_M = 132 \text{ min}^{-1} \mu\text{M}^{-1}$)³⁵ indicating that use of the MBP-derived TP sequence had a minimally disruptive effect relative to the native protein (Figure 4-5b). In contrast, the peptide MBPtide (APRTPGGRR), the basis of the Sox-PNT phosphorylation sequence, was reported to have substantially poorer kinetic parameters ($K_M = 2 \text{ mM}$, $k_{\text{cat}}/K_M = 0.11 \text{ min}^{-1} \mu\text{M}^{-1}$)²⁹ for ERK2, underscoring the importance of the PNT domain recognition in substrate kinetics. Finally, Sox-PNT exhibited high selectivity for ERK1/2 when compared to related kinases from the JNK, p38 and CDK families (Figure 4-5c).

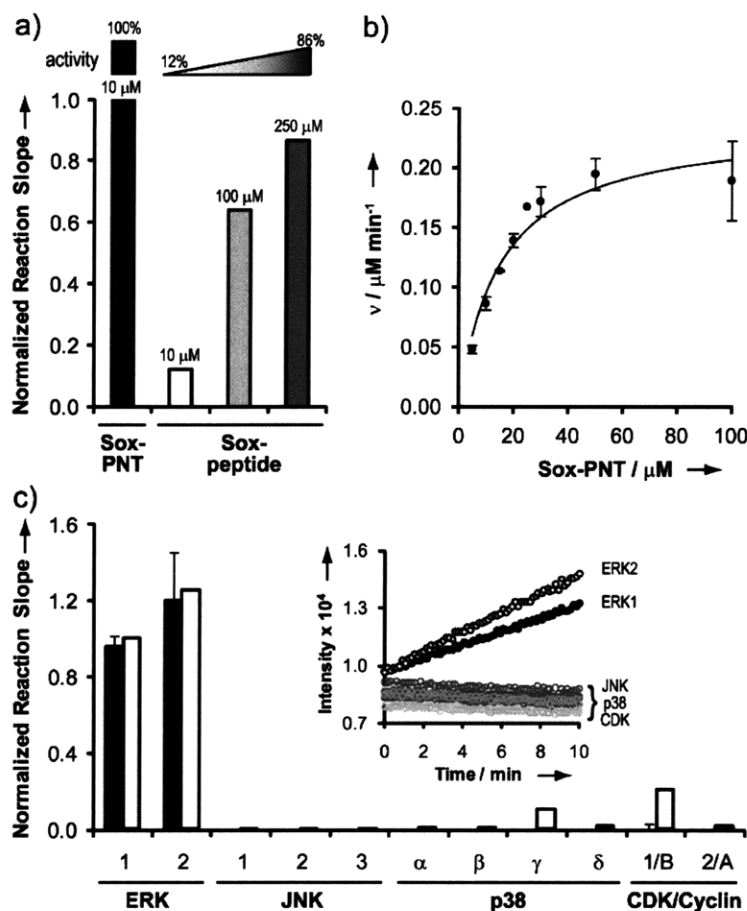


Figure 4-5. In vitro characterization of Sox-PNT. a) The efficiency of phosphorylation by recombinant ERK2 (11 ng) of the Sox-PNT probe was compared to that of the Sox-peptide under identical conditions. b) The kinetic parameters for Sox-PNT were obtained with ERK2 (10 ng) from a direct fit of v vs. $[S]$ plots using the Briggs-Haldane equation. Plotted values indicate the mean \pm s.e.m. for triplicate measurements. c) Promiscuity of Sox-PNT (5 μM) was tested with a panel of related kinases at 15 nM (black bars) and 150 nM (clear bars) of each enzyme. Inset: a representative plot of the change in the fluorescent signal over time obtained with 15 nM enzyme in the fluorescence plate reader. Plotted values for 15 nM of enzyme indicate the mean \pm s.e.m. for triplicate measurements.

Studies with Crude Cell Lysates

In order to demonstrate that the preference of Sox-PNT for ERK1/2 can translate to applications in complex media, the probe was exposed to a panel of unfractionated cell lysates that contained varying levels of active ERK1/2. As described in the introduction, the activity of cellular ERK1/2 is linked to its phosphorylation state, which can be modulated by the epidermal

growth factor (EGF) signaling pathway (Figure 4-6). Briefly, EGF interacts with EGF receptors (EGFRs), which leads to activation of MEK1/2 that in turn phosphorylates and activates ERK1/2. This event can be regulated either by the upstream MEK1/2 inhibitor, U0126, or by a direct ERK1/2 inhibitor, PEA-15.¹⁶

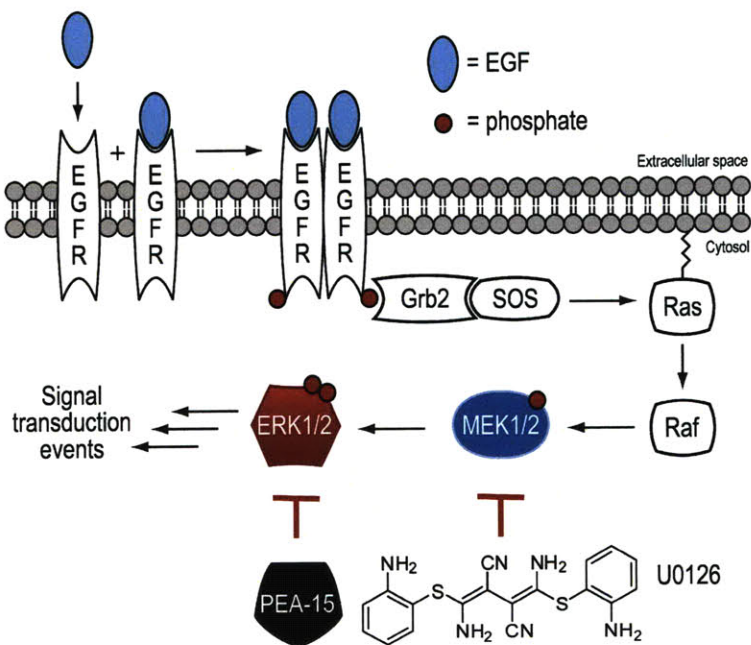


Figure 4-6. The EGF signaling pathway results in stimulation of ERK1/2 activity. U0126, an inhibitor of an upstream kinase, MEK1/2, and PEA-15, a direct inhibitor of ERK1/2 can regulate the activity of ERK1/2.

Summarized in Figure 4-7a are the results of ERK1/2 activity analyses on the crude lysates from four mammalian cell lines, which revealed the selectivity of the sensor in these complex media. In all cases, untreated lysates showed relatively low basal activity, while displaying slight variation among different cell lines, as expected. Upon EGF stimulation, activity increased 4- to 10-fold, similar to previous reports.³⁶ To demonstrate that Sox-PNT was specifically monitoring ERK1/2 activity, cells were exposed to the upstream MEK inhibitor U0126 and subsequently stimulated with EGF and lysed. Under these conditions, the ERK1/2 activity returned to nearly basal levels. Western blot analysis demonstrated that both stimulated

and U0126 inhibitor-treated cells expressed ERK1/2 (Figure 4-7a); however, only EGF-stimulated samples showed enhanced levels of activated ERK1/2 as evidenced by analysis with the phospho-ERK1/2-specific antibody. As expected DMSO, the solvent for U0126, did not have an effect on ERK activity (Figure 4-18). In contrast, the Sox-peptide, lacking the PNT docking domain, showed highly promiscuous activity and signaled phosphorylation that could not be correlated with ERK1/2 activity (Figure 4-7b).

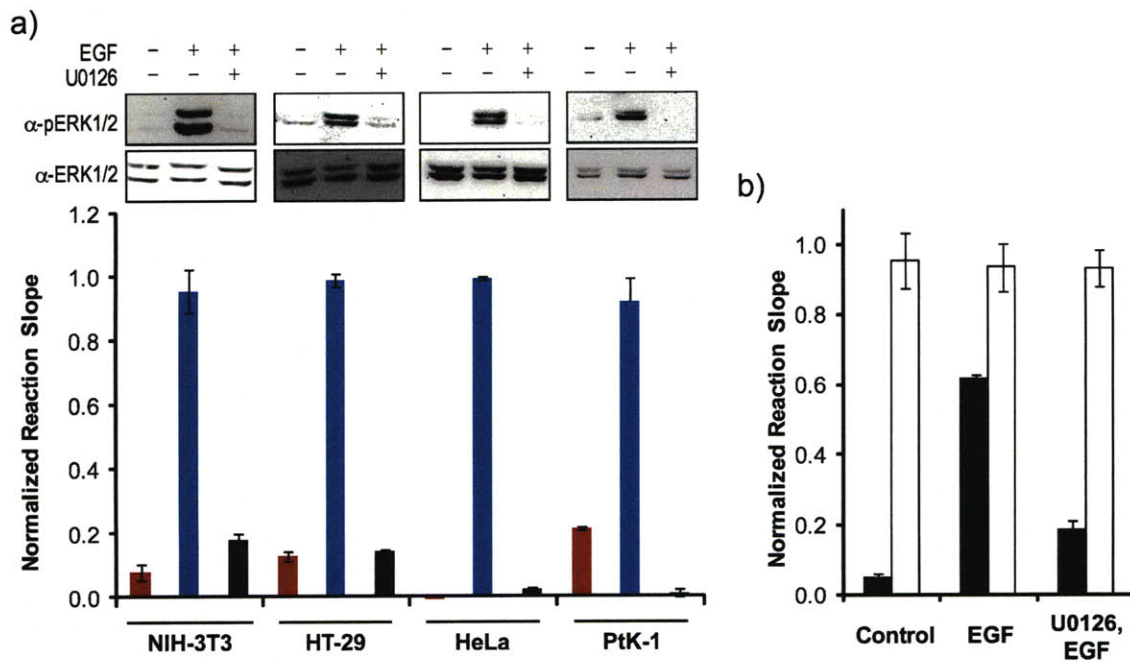


Figure 4-7. Specificity of the Sox-PNT sensor toward ERK1/2 in unfractionated cell lysates. a) Sox-PNT (5 μ M) was used to measure enzyme activity in 40 μ g of untreated lysates (red bars), EGF-stimulated lysates (blue bars), or U0126-treated and then EGF-stimulated lysates (black bars). Inset: Western blot for pERK1/2 (top) and ERK1/2 (bottom). b) The ability of Sox-PNT (black bars, 5 μ M) to report the different phosphorylation states of ERK1/2 in HeLa lysates (40 μ g) was directly compared to the Sox-peptide (white bars, 5 μ M). Plotted values indicate the mean \pm s.e.m. for triplicate measurements.

Direct Titrations of Inhibitor PEA-15 into EGF-stimulated Cell Lysates

Further evidence that Sox-PNT is selectively modified by ERK1/2 was obtained with PEA-15, which is a direct protein inhibitor of ERK1/2. Titration of PEA-15 into EGF-stimulated NIH-3T3 lysates created a dose-dependent response with a half inhibitory concentration of 40 nM and a K_i (30 nM) that reflected the reported K_i values (20 nM) (Figure 4-8 and the Experimental Methods).¹⁶

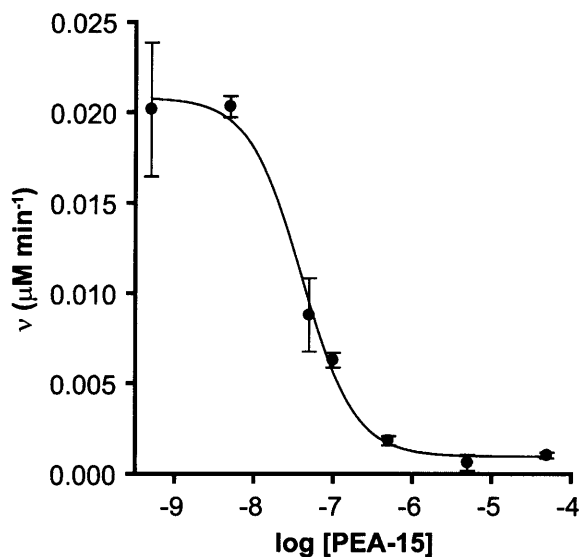


Figure 4-8. Half inhibitory concentration of PEA-15 with ERK1/2. To obtain the IC_{50} value for inhibition of ERK1/2 by PEA-15, EGF-stimulated NIH-3T3 lysates (40 µg) were treated with various concentrations of PEA-15 and enzyme activity was measured with Sox-PNT (5 µM). Plotted values indicate the mean \pm s.e.m. for triplicate measurements.

Immunodepletion of ERK1/2 from EGF-stimulated Lysates

To directly correlate the observed fluorescent signal to the presence of ERK, we exposed our probe to ERK1/2-depleted lysates. Indeed, immunodepletion of ERK1/2 from EGF-stimulated HeLa lysate reduced activity by 7-fold compared to the input lysate or the sample that had been depleted with naïve rabbit IgG (Figure 4-9a). This indicates that the Sox-PNT signal

was predominantly due to the ERK1/2-mediated phosphorylation. Slight residual activity in anti-ERK1/2 lysate can be attributed to incomplete removal of the kinase, which is highly dependent on the efficiency of antibody and kinase binding. Immunodepletion was confirmed by western blot analysis with the immunodepleting antibody (Figure 4-9a, inset). Having validated the selectivity of Sox-PNT for ERK1/2, we used the sensor to measure the amount of active ERK1/2 (13 ng) in EGF-stimulated lysate (40 μ g) (Figure 4-9b). Thus, the probe will be an important tool for quantifying ERK1/2 levels in tissue samples.

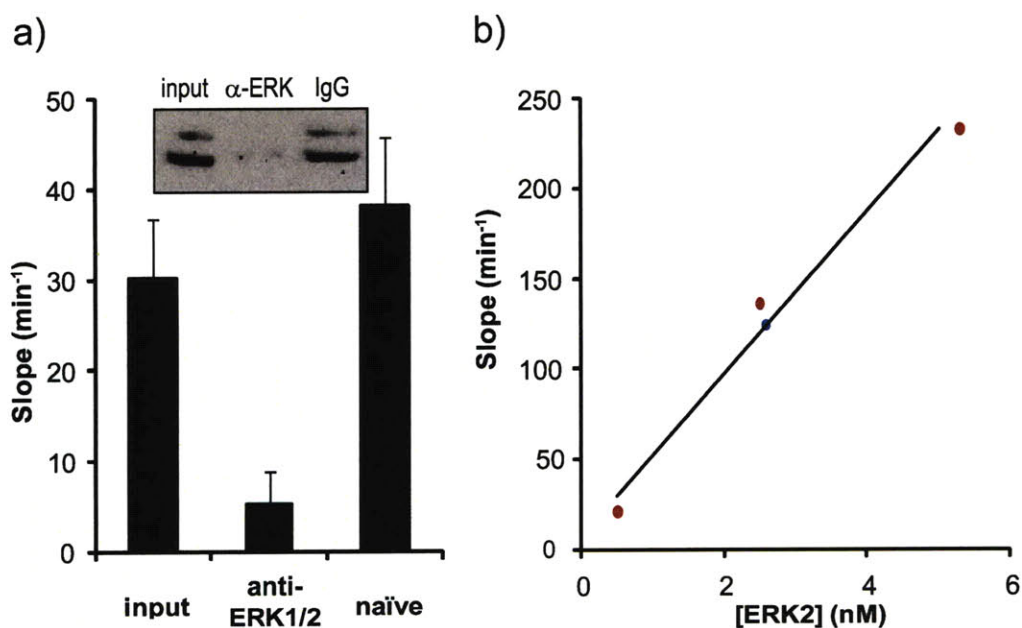


Figure 4-9. ERK1/2 activity in immunodepleted and EGF-stimulated lysates. a) The immunodepletion assays. Kinase activity was measured with Sox-PNT (5 μ M) from an EGF-stimulated HeLa lysate (40 μ g) before (input) and after immunodepletion of this lysate with anti-ERK1/2 or naïve rabbit IgG. Plotted values indicate the mean \pm s.e.m. for triplicate measurements. Inset: western blot for ERK1/2 in the measured samples. The top band in all western blots is ERK1 (44 kDa) and the bottom band ERK2 (42 kDa). b) Determination of [ERK1/2] in lysate. Standard curve with a range of ERK2 concentrations (red circles, 0.5-5 nM) was first obtained. The standard curve was then used to measure the concentration (blue circle, 2.6 nM) and amount (13 ng) of ERK1/2 in 40 μ g of EGF-stimulated NIH-3T3 lysates.

Mircoinjection of Sox-PNT into PtK-1 Cells

Having demonstrated the utility of Sox-PNT in unfractionated cell lysates and the selectivity for ERK1/2 in such complex environments, we wanted to examine if the sensor could report kinase activity in live cells. With collaborators in the Danuzer laboratory at the Scripps Research Institute, Sox-PNT was co-microinjected into live PtK-1 cells with a standard, Alexa Fluor 568-labeled dextran. The labeled dextran was used as a marker of microinjection as well as a control of dye diffusion within the cell.

The cells were serum starved overnight, microinjected and then stimulated with EGF during imaging. Among several dozen cells that were imaged (Figure 4-10), one showed promising preliminary results (Figure 4-10e). The raw overlaid image (Figure 4-11) displayed a band of fluorescence in the Sox filter ($\lambda_{\text{ex}} = 387 \text{ nm}$, $\lambda_{\text{em}} = 447 \text{ nm}$) that followed the perimeter of the cell. Conversely, the fluorescence observed with the Alexa filter ($\lambda_{\text{ex}} = 560 \text{ nm}$, $\lambda_{\text{em}} = 630 \text{ nm}$) indicated that the sensor and labeled dextran had evenly diffused throughout the cell and that the fluorescence from the Sox filter was not an artifact. Rather, the signal was most likely due to ERK1/2 activity at the cell edge. Since ERK1/2 is believed to be involved in lamellipodia formation³⁷⁻³⁹ our observation is in agreement with those reports. Studies with more appropriate filters and localized sensors are ongoing.

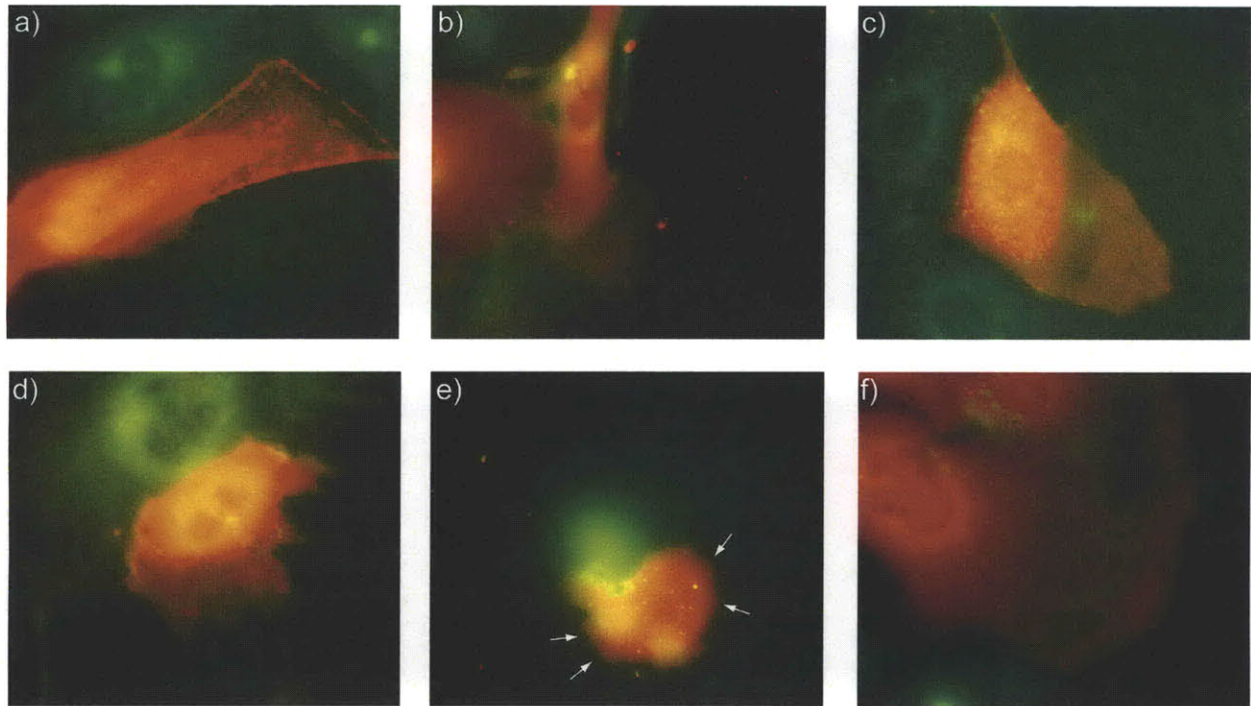


Figure 4-10. Overlaid, false-colored images of a panel of cells microinjected with Sox-PNT and Alexa Fluor 568-labeled dextran (a-f). The images were created by overlaying the fluorescence images obtained through the Sox filter ($\lambda_{\text{ex}} = 387 \text{ nm}$, $\lambda_{\text{em}} = 447 \text{ nm}$, false-colored green) and the Alexa Fluor 568 filter ($\lambda_{\text{ex}} = 560 \text{ nm}$, $\lambda_{\text{em}} = 630 \text{ nm}$, false-colored red).

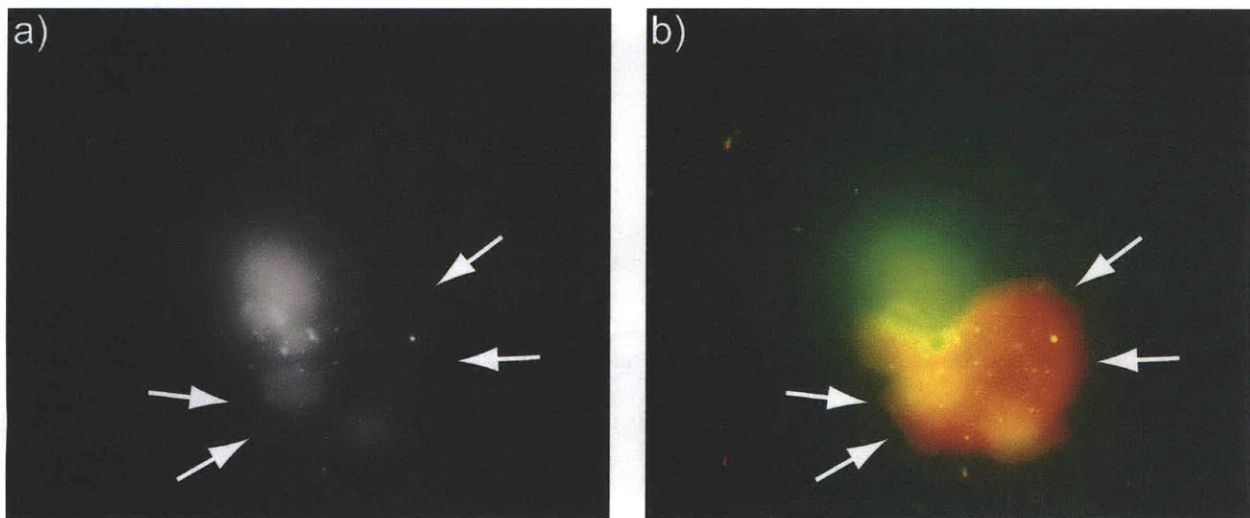


Figure 4-11. Overlaid a) raw and b) false-colored images of a cell microinjected with Sox-PNT and Alexa Fluor 568-labeled dextran. Fluorescence at the edge of the cell may be due to cellular ERK1/2 activity.

While the results obtained with microinjection were quite promising, we wanted to further explore two areas: 1. Alternative ways to deliver the substrate into cells because microinjection can be time-consuming and low-throughput, and 2. Localization of the fluorescent signal because the chemosensor can freely diffuse throughout the cell, therefore impeding the detection of enzyme activity.

Membrane-Permeable Sox-PNT-TAT ERK1/2 Sensor

As a complementary approach to microinjection, we also explored cellular delivery of the probe utilizing a protein transduction domain (PTD). Over the last two decades much work has been devoted to the development of PTDs, also known as cell-penetrating peptides (CPPs). These peptides have been used to successfully transport into cells various cargoes, from small molecules to large systems, such as DNA,⁴⁰ polymers,⁴¹ nanoparticles,^{42, 43} liposomes⁴⁴ and many proteins.^{45, 46} The initial discovery of PTDs in the late 1980s came from the observation that the transactivator of transcription (TAT) from HIV-1 could be taken up from the surrounding media by numerous cell types.^{47, 48} Since then many additional natural and artificial PTDs have been discovered. Although extensively studied,⁴⁹⁻⁵² even today the mechanism and efficiency of delivery are not well-parameterized and can vary, depending on the type of cargo and cell target. Due to its long and relatively successful history, the TAT sequence (YGKKRRQRRR) was chosen as the most appropriate PTD to transport Sox-PNT.

The same semisynthetic strategy that was described for the Sox-PNT assembly was employed in the construction of Sox-PNT-TAT (Figure 4-12). A gene encoding the C-terminal TAT sequence and the PNT domain was commercially synthesized. After standard molecular cloning into suitable plasmids, the product was expressed with an N-terminal GB1 tag. The GB1 protein has been used, similarly to GST, to improve protein expression^{53, 54} and was easily

removed with TEV protease to reveal Cys-PNT-TAT (**12**). The Cys-PNT-TAT module was ligated to the Sox-Peptide thioester (**9**) as previously described (vide supra), and the final product **13** was isolated in 5% yield.

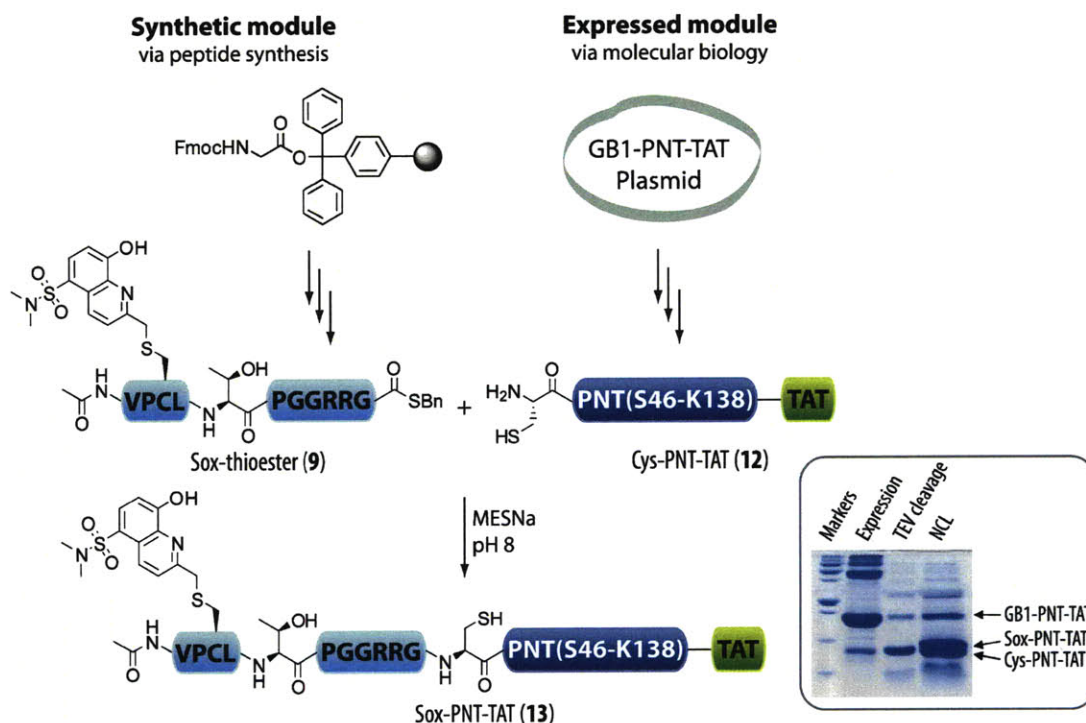


Figure 4-12. The semisynthesis of the Sox-PNT-TAT sensor via NCL. The thioester peptide containing C-Sox was synthesized via SPPS. The Cys-PNT-TAT domain was obtained through standard molecular biology methods. Inset: Coomassie-stained gel of the ligation reaction indicated 40-50% conversion of the Cys-PNT-TAT expressed segment to the product, Sox-PNT-TAT.

The next goal will be to determine the efficacy of internalization by exposing cells to the Sox-PNT-TAT derivative. Compared to microinjection, the cell-permeable reporter should easily enter a larger number of cells, and, thus, should simplify the subsequent fluorescence imaging and allow for studies of ERK activity upon stimulation or during specific cellular events.

Membrane-Targeted Sox-PNT-CAAX ERK1/2 Sensor

The second modification that we explored would facilitate membrane localization of the sensor to increase the fluorescence signal at the site of kinase activity. Diffusion of the fluorescent signal is a challenge when working at wavelengths where cells naturally display high background fluorescence. Thus, by anchoring the ERK1/2 sensor to the membrane through prenylation, we hope to increase the local concentration of the chromophore and, by extension, the fluorescence intensity. Prenylation is a post-translational modification involving covalent addition of either farnesyl (15-carbon) or geranylgeranyl (20-carbon) isoprenoids to Cys residues near the C-terminus of proteins.⁵⁵ The proteins farnesyltransferase (FTase) and geranylgeranyltransferase (GGTase) are responsible for Cys alkylation with a polyisoprene derivative within the CAAX box, where A denotes an aliphatic amino acid and X is an unspecified C-terminal residue.⁵⁶ After covalent modification of the acceptor protein in the cytoplasm, the AAX tripeptide is removed by proteases Ras and Ras-converting enzyme (Rce1), and the remaining prenylcysteine residue is methyl esterified by isoprenylcysteine carboxyl methyltransferase (ICMT).⁵⁷ For endogenous substrates of prenyltransferases, the attached lipid is required for proper functioning by mediating membrane associations and specific protein-protein interactions.⁵⁸ Furthermore, these endogenous prenylated proteins play crucial roles in vital cellular processes including signal transduction and intracellular trafficking pathways.⁵⁹ Because fully processed proteins exhibit high affinity for cellular membranes, the CAAX box has been used to tether cytosolic proteins to membranes in several studies where localization was of importance.^{60, 61} With such precedence, we sought to construct a membrane-targeted derivative ERK1/2 probe, Sox-PNT-CAAX (Figure 4-13).

A gene encoding a C-terminal CAAX sequence (KMSKDGGKKKKKSKTKCVIM)^{60, 61} and an N-terminal GST tag was commercially synthesized. After expression and purification of the GST-PNT-CAAX construct, TEV protease was utilized to remove GST and reveal Cys-PNT-CAAX. Following the aforementioned procedures, Cys-PNT-CAAX was ligated to the Sox-thioester. Upon FPLC purification, the isolated product was obtained in 5% yield.

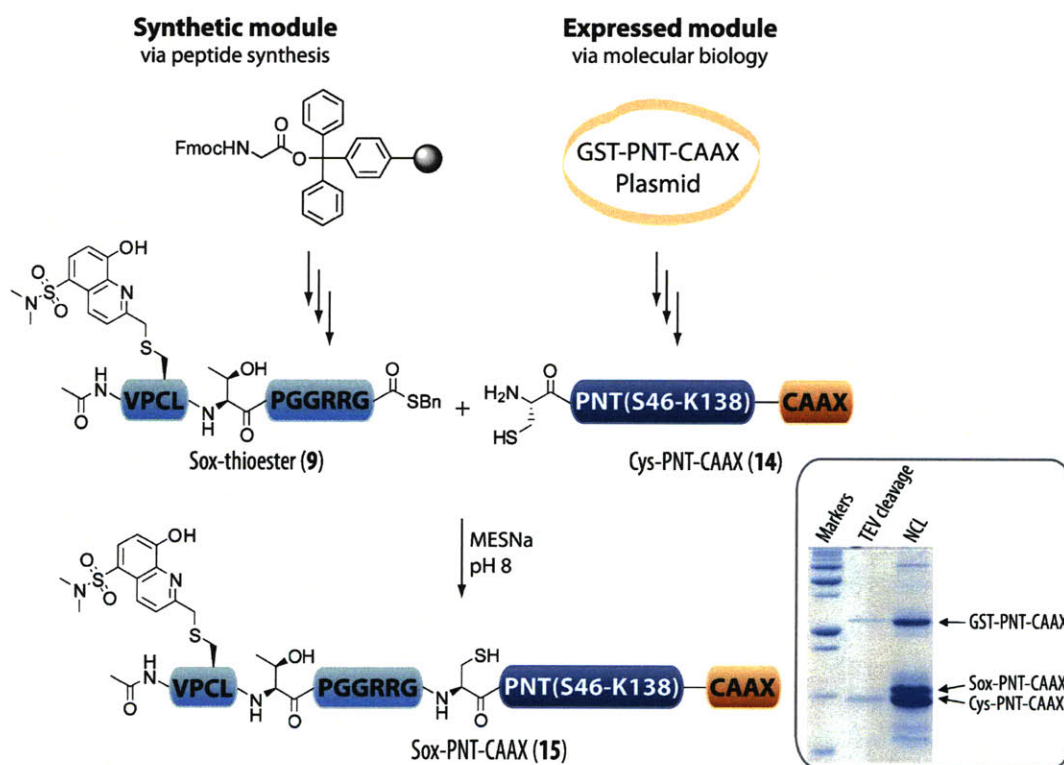


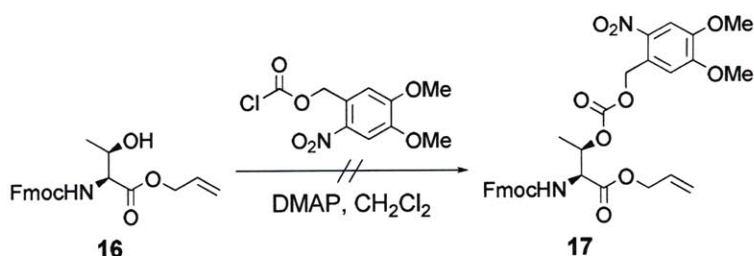
Figure 4-13. The semisynthesis of the Sox-PNT-CAAX sensor via NCL. The thioester peptide containing C-Sox was synthesized via SPPS. The Cys-PNT-CAAX domain was obtained through standard molecular biology methods. Inset: Commassie-stained gel of the ligation reaction indicated 30-40% conversion of the Cys-PNT-CAAX expressed segment to the product, Sox-PNT-CAAX.

The new membrane-targeted probe, Sox-PNT-CAAX, will be microinjected to study the role of ERK in cell migration at the cytosolic membrane surface in collaboration with Prof. Martin Schwartz's lab at the University of Virginia.

Caging the Thr Side Chain to Provide Temporal Control of Phosphorylation

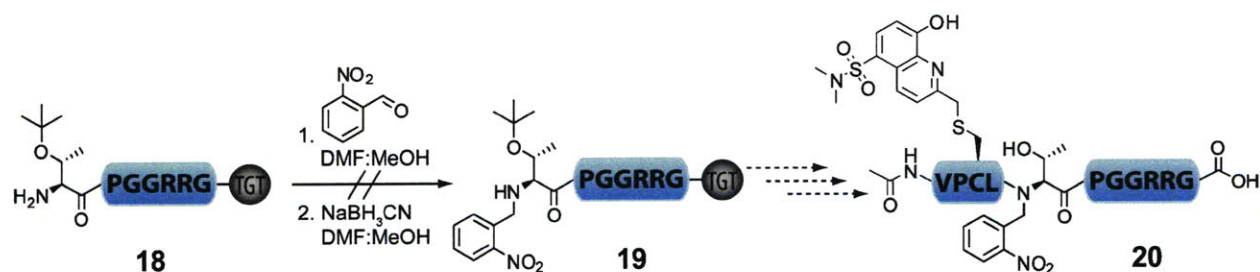
Since the probe will be introduced into cells either via microinjection or PTDs there will inevitably be some delay time between sensor delivery and imaging. During this period ERK1/2 may phosphorylate the probe, making the change in fluorescence more difficult to observe during imaging. To control the timing of phosphorylation, we envisioned a sensor with a protecting group that would temporarily mask the reactive functionality and that could be easily removed. To that end, the caging, or photolabile protection, of phosphorylatable Thr would enable the light-mediated release of the substrate. Caging of important biological small molecules and macromolecules has been used extensively to enable controlled release of activated species.^{62, 63} The most widely utilized caging groups are *o*-nitrobenzyl derivatives that can be photolyzed on a microsecond to millisecond time scale with long wavelength UV light (> 350 nm), causing minimal cellular damage in the process.⁶⁴ For example, the 2-nitrophenethyl (NPE) group has been extensively used in our laboratory to study downstream effects of phosphorylation.^{32, 65-69} In contrast, there are far fewer reports that study kinases by caging their substrates. While syntheses of photoprotected Ser and Tyr side chains with 4,5-dimethoxy-2-nitrobenzyl (DMNB) and their incorporation into kinase substrates have been reported,⁷⁰⁻⁷³ syntheses of caged Thr have not been found in the literature. This may be ascribed to the steric constraints that the 2° alcohol nucleophile experiences, as no product was obtained when we attempted the reaction with DMNB-choloroformate (Scheme 4-1).

Scheme 4-1. Synthesis of Caged Thr Amino Acid



Thus, two alternative caging strategies were further explored to generate a temporally-controlled ERK1/2 sensor. First, following the protocol reported by Lawrence *et al.*,⁷⁰ we attempted to cage the amide backbone of the Thr phosphoacceptor with *o*-nitrobenzyl group. We reasoned that the additional bulk of the caging moiety would disrupt enzyme-substrate contacts and in the process prevent kinase-catalyzed phosphorylation, as was observed with caged peptides for protein kinase A (PKA).⁷⁰ However, the method was not fruitful in our hands due to the instability of the TGT resin-bound peptide when exposed to conditions necessary for reductive alkylation (Scheme 4-2).

Scheme 4-2. Synthesis of Backbone-Caged Sox-Peptide^a



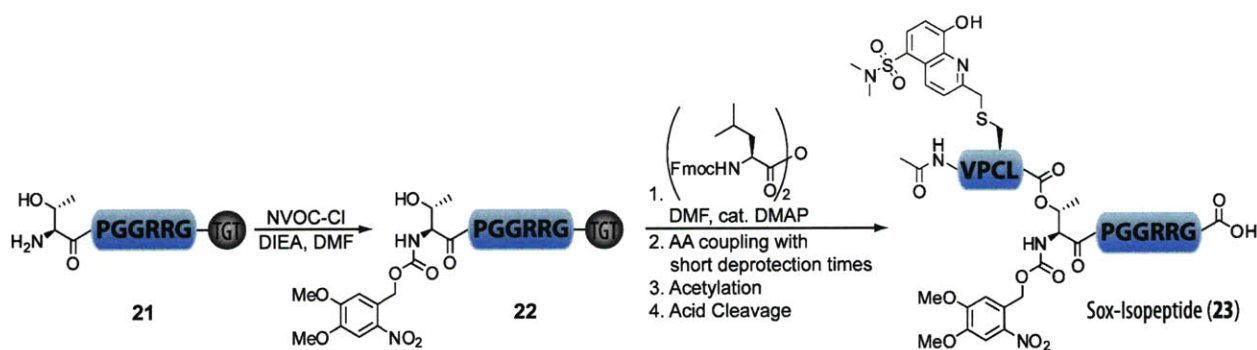
^a All residues bear the standard side chain protecting groups as dictated by Fmoc-based SPPS protocols.

The second approach took advantage of the well-characterized O to N intramolecular acyl migration,⁷⁴ which has recently been used in chemical biology to study protein splicing⁷⁵ and amyloid β aggregation.^{44, 76} Incorporation of an *O*-acyl isomer of a peptide bond at a Ser/Thr

residue in a peptide sequence (*O*-acyl isopeptide) introduces a kink in the main chain, and also masks the reactive side chain alcohol in our case. In the course of the synthesis, the N^α -group of the Ser/Thr residue is also transiently protected with the NVOC moiety. Finally, photolysis triggers the spontaneous O to N acyl shift, restoring the native amide bond, and in the process revealing the Ser/Thr alcohol. The strategy has only been reported with a building block NVOC-Ser-OH amino acid that was then incorporated into NVOC-Ser-*O*-acyl isopeptides through SPPS. The assembly of photocontrolled *O*-acyl Thr-containing peptides, to our knowledge, has not been attempted.

We decided to synthesize our peptide of interest, Sox-Isopeptide, entirely on-resin (Scheme 4-3). Employing standard Fmoc-based SPPS protocols, the peptide was assembled with a Thr residue that contained a free α -amine and β -alcohol (**21**). The α -amine was capped with the NVOC group first (**22**), followed by addition of the next amino acid onto the Thr side chain as an activated symmetric anhydride. The remaining residues were attached using short Fmoc deprotection times and base-free couplings to minimize diketopiperazine formation, as previously reported.^{75, 77} Standard acidic conditions were employed for concomitant release from the resin and protecting group removal. HPLC analysis coupled with mass spectrometry revealed that the major product was the desired material (**23**).

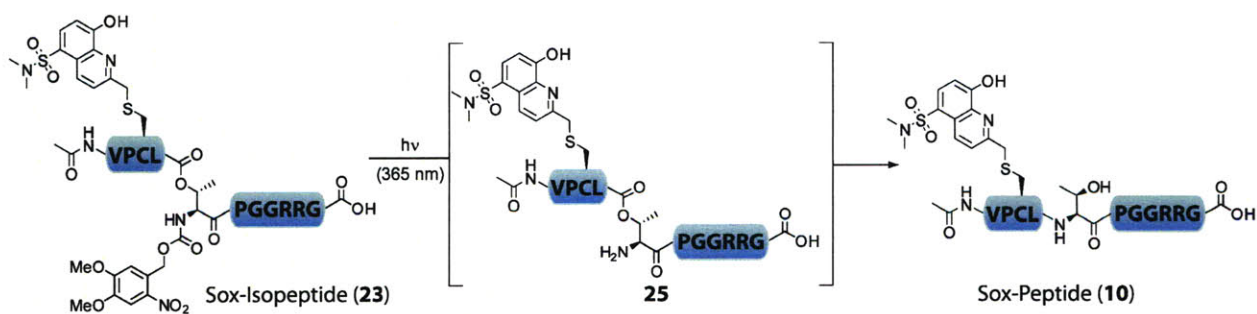
Scheme 4-3. Synthesis of Sox-Isopeptide^a



^a Details of reagents and reaction conditions are provided in the Experimental Methods. All residues bear the standard side chain protecting groups as dictated by Fmoc-based SPPS protocols.

Next, two important parameters in the future utility of Sox-Isopeptide (**23**) were characterized, namely, its uncaging properties and *O*-acyl bond stability over a range of relevant conditions. When photolyzed ($\lambda_{\text{ex}} = 365 \text{ nm}$) in a controlled environment (Scheme 4-4), a high percentage of uncaging was obtained within the first 3 min (Figure 4-14). The rate of product formation (Sox-Peptide (**10**)) was not determined because Sox-Isopeptide (**23**) and Sox-Peptide (**10**) have widely different extinction coefficients that cannot be directly compared. Having verified that NVOC photorelease and *O* to *N* rearrangement rates were suitable for cellular studies, we examined the *O*-acyl bond stability in a highly reducing environment that the bond will be exposed to during NCL and in the cell. Over 24 hours, however, Sox-Isopeptide remained mostly intact with only a small side product arising due to oxidation.

Scheme 4-4. Uncaging of Sox-Isopeptide and Spontaneous *O* to *N* acyl shift to form Sox-Peptide



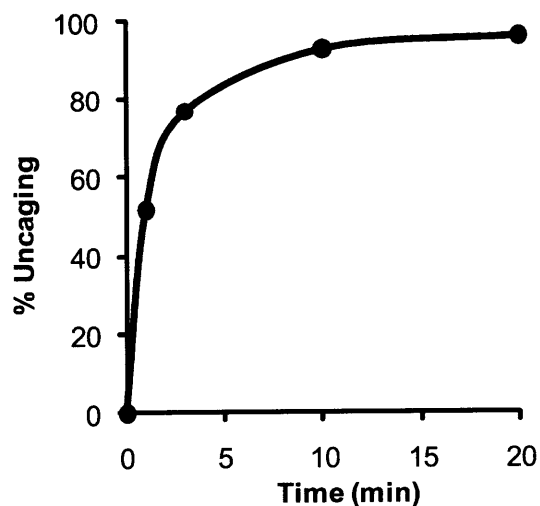


Figure 4-14. Rate of uncaging for Sox-Isopeptide. Sox-Isopeptide was illuminated ($\lambda_{\text{ex}} = 360$ nm) for 1, 3, 10 and 20 min and immediately subjected to HPLC. Isolated peaks were analyzed by mass spectrometry. Percent of uncaging was calculated with reference to inosine. Conditions: 100 μM Sox-Isopeptide, 10 mM HEPES (pH 7.4), 5 mM DTT, 1 mM inosine.

Our future goal is to convert Sox-Isopeptide into the corresponding thioester and perform NCL with the PNT-CAAX domain. This would furnish a sensor derivative that is both temporally and spatially controlled and will allow more detailed experiments to be carried out that could elucidate the role of ERK1/2 in numerous cellular processes.

Conclusions

The MAPK signaling pathways integrate the actions of numerous kinases that are exquisitely regulated by stress responses and extracellular signals. Deconvoluting the specific functions of individual enzymes has been challenging, partly due to the difficulty of creating probes that exclusively target a kinase of interest. Here we have presented a selective ERK1/2 activity chemosensor that comprises both a chemical sensing motif and recombinant enzyme docking domain. Thereby, the Sox-based kinase-sensing strategy has been extended beyond the realm of enzymes that recognize linear peptide substrates. Quantitative studies with the probe indicate that the PNT domain confers exquisite selectivity toward ERK1/2, which was

impossible to achieve with simple peptide probes. Moreover, the docking-domain approach now allows us to target a wider set of kinases (such as other members of the MAPK family, JNK and p38) that have thus far been elusive due to their complex substrate recognition mechanisms. Recently, Dr. Cliff Stains in our lab has been able to build a selective sensor for p38 α using an adaptation of this technique and p38-specific recognition peptides.⁷⁸

The Sox-PNT chimeric protein probe also offers distinct advantages for solution-based analyses that can be carried out with simple equipment. The reliable semisynthesis of multimilligram (6 mg) quantities of Sox-PNT allows at least 5000 assays to be performed in 384-well plates. Furthermore, Sox-based sensors exhibit large dynamic ranges with excellent Z' factor values.^{33, 34} Currently, in light of the efficient semisynthesis, excellent selectivity and robustness in high throughput analysis, the Sox-PNT sensor can be broadly applied for quantifying ERK1/2 activities in applications ranging from drug discovery to diagnostics.

Additionally, due to the excellent selectivity of the sensor, we successfully microinjected Sox-PNT into live PtK-1 cells and observed ERK1/2 activity at the periphery. This prompted the synthesis of two more derivatives that would aid cellular work, one conjugated to a membrane permeabilization peptide (Sox-PNT-TAT) and another with membrane-tethering capabilities (Sox-PNT-CAAX). Lastly, investigation was initiated into temporal control of phosphorylation of the PNT-based reporters through caging strategies. While further work is necessary to deliver the probe into cells and accurately detect ERK1/2 activity, the synthesis of the various derivatives and the selectivity that our chimeric reporters display should significantly help us in deconvoluting the complex and important role that ERK1/2 play in a multitude of pathways.

Acknowledgements

Dr. Beth Vogel Taylor has been instrumental in starting this project. She carried out the initial native chemical ligation and screened NCL reaction conditions. I thank Prof. K. A. Dalby for providing DNA of the PNT domain and the PEA-15 protein, and Prof. Kevin Janes for helpful discussions. I am also grateful to Prof. Gaudenz Danuser, James Lim and the entire Danuser lab for their invaluable help with microinjection and image analysis. This research was supported by the NIH Cell Migration Consortium (GM064346). The Biophysical Instrumentation Facility for the Study of Complex Macromolecular Systems (NSF-0070319) is also acknowledged.

Experimental Methods

General information

Unless otherwise noted, all solvents and reagents were obtained commercially and used without further purification. *N*^α-Fmoc-protected amino acids [Fmoc-Arg(Pbf)-OH, Fmoc-Gly-OH, Fmoc-Leu-OH, Fmoc-Pro-OH, Fmoc-Thr(tBu)-OH, Fmoc-Thr(PO(OBn)OH)-OH, Fmoc-Val-OH] were purchased from Novabiochem. Fmoc-C(Sox[TBDPS])-OH was synthesized according to published procedures.³³ Anhydrous CH₂Cl₂ was distilled from calcium hydride. Doubly deionized water was degassed by bubbling argon for 20 min at room temperature. Organic solutions were concentrated *in vacuo* by rotary evaporation at ~10 Torr (house vacuum) at 25-40 °C, then at ~0.5 Torr (vacuum pump), unless otherwise indicated. Peptides were purified via preparative reverse-phase HPLC employing a gradient of solvents A (H₂O with 0.1% v/v TFA) and B (CH₃CN with 0.1% v/v TFA). Peptide purity was determined by analytical reverse-phase HPLC. FPLC protein purification was done in 20 mM Tris (pH 8.0 at 25 °C) and 200 mM NaCl. Protein purity was confirmed by SDS-PAGE with Coomassie blue staining or by western blots visualized using appropriate antibodies.

Instrumentation

HPLC: HPLC was carried out on Waters Prep LC 4000 System or Waters Delta 600 System equipped with Waters 2487 dual wavelength absorbance detectors. Columns used: C₁₈ analytical (flow rate = 1 mL/min), Beckman Ultrasphere ODS, 5 μm, 150 x 4.6 mm; C₁₈ preparatory (flow rate = 15 mL/min), YMC-Pack Pro, 5 μm, 250 x 20 mm.

FPLC: FPLC was carried out on Pharmacia Biotech system equipped with Pharmacia Biotech UV-MII absorbance detector and Pump P-500. Columns used: Pharmacia Biotech Superdex™ 75 analytical; Pharmacia Biotech HiLoad™ 16/60 Superdex™ 75 prep grade. Flow rate = 1 mL/min for both.

ESI-MS: Applied Biosystems Mariner mass spectrometer.

MALDI-TOF MS: PerSeptive Biosystems Voyager MALDI-TOF instrument.

UV-Vis Spectrophotometer: Shimadzu UV-2401PC.

Fluorometer: Fluoromax 3 from Jobin Yvon. Cuvette: Starna Cells (16.100F-Q-10) 100 μ L sub-micro cuvette, 1 cm path length.

Fluorescence Plate Reader: HTS 7000 Bio Assay Reader from Perkin Elmer. Plate: Corning (3992) assay plate, 96-well, half area, no lid, flat bottom, non-binding surface, non-sterile, white polystyrene (120 μ L reaction volume) or MatriCal (MP101-1-PP) 384-well MatriPlate, 50 μ L, black polystyrene (20 μ L reaction volume).

Chemiluminescence Reader: Bio-Rad with Quantity One 1-D Analysis Software.

Stock solutions

Due to the affinity of the phosphorylated probes for Mg^{2+} ,^{33, 79} the reagents with the highest purity and lowest metal content were used where indicated to avoid the necessity of removing metal ion impurities after preparations.

1. Stock solutions of the Sox-containing peptides and proteins were prepared in doubly deionized water (Sox-peptides) or TBS (solution 7 for Sox-PNT), and concentrations were determined by UV-Vis (based on the determined extinction coefficient of the fluorophore unit, 5-(*N,N*-dimethylsulfonamido)-8-hydroxy-2-methylquinoline, $\epsilon_{355} = 8247 \text{ M}^{-1} \text{ cm}^{-1}$ at 355 nm in 0.1 M NaOH with 1 mM Na_2EDTA). An average of the UV absorbance values from three separate solutions, each prepared using a different volume of the stock solution, was taken. Purified peptide stock solutions can be stored at 4 °C for at least 6 months or -20 °C for longer periods. Protein stock solutions were flash-frozen and stored at -80 °C.
2. Magnesium chloride stock solution was prepared from Alfa Aesar's Puratronic grade salt and stored at room temperature. Most commercially available salts contain Zn^{2+} as significant impurities and should not be used due to the high affinity of the phosphorylated peptides for Zn^{2+} . The Mg^{2+} concentration was determined by titration with a standardized solution of EDTA (Aldrich) in the presence of an Eriochrome Black T (Aldrich) as described previously.⁷⁹
3. 500 mM HEPES (SigmaUltra) was prepared and adjusted to pH 7.4 with NaOH (99.998+%, Aldrich) solution and stored at 4 °C.
4. 1 M Tris (Calbiochem, ULTROL grade) was prepared and adjusted to pH 7.5 with NaOH (99.998+%, Aldrich) solution and stored at 4 °C.

5. 2 M NaCl (SigmaUltra) was prepared in doubly deionized water and stored at room temperature.
6. 500 mM and 10 mM dithiothreitol (DTT, Biotechnology grade, Mallinckrodt) solutions were prepared in degassed doubly deionized water and stored at -80 °C.
7. 10x TBS Buffer (200 mM Tris-HCl [pH 8 at 4 °C], 2 M NaCl) was prepared from Tris-HCl (Calbiochem, ULTROL grade, 15.76 g for 1 L solution) and NaCl (SigmaUltra, 58.453 g for 1 L solution) and adjusted to pH 8 at 4 °C with NaOH (99.998+%, Aldrich) solution.
8. 20 mg/mL BSA (Heat Shock Fraction V, Roche) was prepared in ultrapure water, filtered through a 0.45 micron syringe filter to remove particulates and stored at 4 °C.
9. 0.1% Brij-35 P (Fluka) was prepared in doubly deionized water and stored at room temperature.
10. 20% Triton X-100 (SigmaUltra) was prepared in doubly deionized water and stored at 4 °C.
11. 100 mM ATP (Disodium salt, Low Metals Grade, Calbiochem) was prepared in ultrapure water and stored in aliquots at -80 °C.
12. 500 mM EGTA was prepared from ethylene glycol-bis(2-aminoethyl ether)-*N,N,N',N'*-tetraacetic acid (SigmaUltra) dissolved in 2 M NaOH and stored at 4 °C.
13. 10x Assay Buffer I: 500 mM Tris-HCl (pH 7.5 at 25 °C), 100 mM MgCl₂, 10 mM EGTA, 20 mM DTT and 0.1% Triton X-100.
14. 10x Assay Buffer II: 500 mM Tris-HCl (pH 7.5 at 25 °C), 100 mM MgCl₂, 10 mM EGTA, 20 mM DTT and 0.1% Brij 35 P.
15. Lysis Buffer I: PBS, 1 mg/mL lysozyme, 1 mM DTT, 1% NP-40 Alternative and protease inhibitor cocktail III (Calbiochem: 100 μM AEBSF, 80 nM aprotinin, 5 μM bestatin, 1.5 μM E-64, 2 μM leupeptin, 1 μM pepstatin A).

16. Lysis Buffer II: 50 mM Tris (pH 7.5 at 25 °C), 150 mM NaCl, 50 mM β -glycerophosphate (pH 7.3), 10 mM sodium pyrophosphate, 30 mM NaF, 1% Triton X-100, 1 mM benzamidine, 2 mM EGTA, 100 μ M Na_3VO_4 , 1 mM DTT, protease inhibitor cocktail III (10 μ L/mL, Calbiochem: 10 mM AEBSF, 8 μ M aprotinin, 0.5 mM bestatin, 0.15 mM E-64, 0.2 mM leupeptin, 0.1 mM pepstatin A), and phosphatase inhibitor cocktail 1 (10 μ L/mL, Sigma, P2825). The buffer can be stored at -20 °C for up to 3 months; without protease and phosphatase inhibitors, it can be stored at -20 °C indefinitely.
17. HeLa Medium: DMEM (Gibco, 11995) supplemented with 10% (v/v) heat-deactivated FBS (fetal bovine serum, warmed to 56 °C for 30 min, inverted several times every 10 min), 100 U/mL penicillin (Gibco, 15140) and 100 μ g/mL streptomycin (Gibco, 15140). Serum-free medium: DMEM, 2 mM L-Gln (Gibco, 25030), 100 U/mL penicillin and 100 μ g/mL streptomycin. All cell media were filtered through a 1 L filter flask (0.22 μ m PES sterilizing low protein binding membrane, non-pyrogenic, polystyrene, Corning 431098).
18. NIH-3T3 Medium: DMEM (Gibco, 11995) supplemented with 10% (v/v) FBS, 100 U/mL penicillin and 100 μ g/mL streptomycin. Serum-free medium: DMEM, 2 mM L-Gln, 100 U/mL penicillin and 100 μ g/mL streptomycin.
19. HT-29 Medium: McCoy's 5A Medium (Gibco, 1660) supplemented with 10% (v/v) FBS, 2 mM L-Gln, 100 U/mL penicillin and 100 μ g/mL streptomycin. Serum-free medium: McCoy's 5A Media, 4 mM L-Gln, 100 U/mL penicillin and 100 μ g/mL streptomycin.
20. PtK-1 Medium: Ham's F-12 Medium (Sigma, N8641) supplemented with 10% (v/v) FBS, 2 mM L-Gln, 1 mM sodium pyruvate (Gibco, 11360), 100 U/mL penicillin and 100 μ g/mL streptomycin. Serum-free medium: Ham's F12 Medium, 4 mM L-Gln, 1 mM sodium pyruvate, 100 U/mL penicillin and 100 μ g/mL streptomycin.

Semisynthesis of (p)Sox-PNT Derivatives

a. Peptide synthesis

Peptides were synthesized using standard Fmoc amino acid protection chemistry on Fmoc-Gly-Novasyn-TGT resin (Novabiochem, 0.2 mmol/g). The resin was swelled in CH_2Cl_2 (5 min.) and then DMF (5 min.) prior to synthesis. All the amino acids except for Fmoc-C(Sox[TBDPS])-OH were attached according to the following procedure: Fmoc deprotection (20% 4-methylpiperidine in DMF, 3 x 5 min.), rinsing step (DMF, 5 x), coupling step (amino acid/PyBOP/HOBt/DIEA, 6:6:6:6, 0.15 M in DMF, 30-45 min.), rinsing step (DMF, 5 x; DCM, 5 x). Fmoc-C(Sox[TBDPS])-OH was coupled in the following manner: amino acid/PyAOP/HOAt/2,4,6-collidine, 2:2:2:5, 0.15 M in DMF, 2-12 hr. The coupling was repeated if necessary (amino acid/PyAOP/HOAt/2,4,6-collidine, 1:1:1:3, 0.15 M in DMF, 2-12 hr) as determined by the TNBS test for free amines. It is important to wash the resin rigorously (DMF followed by CH_2Cl_2) to remove excess amino acid before performing any tests for free amines. This is particularly necessary after coupling of Fmoc-C(Sox[TBDPS])-OH due to its deep red color, which does not affect its coupling efficiency. At the end of the synthesis, the Fmoc group was removed with 20% 4-methylpiperidine in DMF (3 x 5 min.) and the resin was rinsed with DMF (5 x). The resin-attached free amines were capped by exposure to Ac_2O (20 equiv.) and pyridine (20 equiv.) in DMF for 30 min. The resin was rinsed with DMF (5 x), CH_2Cl_2 (5 x) and subjected to 20% 4-methylpiperidine in DMF (3 x 5 min.) to remove any C-Sox aryl esters that might have formed during acetylation. The resin was finally washed with DMF, CH_2Cl_2 , MeOH (5 x each) and dried under vacuum.

b. Thioesterification of Sox-containing peptides

Following SPPS the peptide (10 μ mol from 50 mg of resin) was cleaved from the resin with side-chain protection intact by agitating with 0.5% TFA in CH_2Cl_2 for 1.5 h. The resin was removed by filtration and rinsed with CH_2Cl_2 . The solvent was mostly evaporated under a stream of nitrogen, and the peptide was triturated with cold hexanes. The hexanes were removed *in vacuo*, and the resulting white powder was dissolved in 16 mL of anhydrous CH_2Cl_2 and treated with HATU (30 mg, 80 μ mol) and HOAt (10.8 mg, 80 μ mol) dissolved in 0.5 mL dry DMF, followed by addition of 2,4,6-collidine (21 μ L, 160 μ mol) and benzylmercaptan (19 μ L, 160 μ mol). The reaction was stirred under N_2 overnight. The solvent was removed *in vacuo*, and the peptide was deprotected with TFA/ H_2O /TIS (95:2.5:2.5% v/v) for 3 h. The resulting solution was concentrated under a stream of N_2 and precipitated by addition of cold Et_2O . The pellet was triturated with cold Et_2O (3 x), redissolved in water, filtered and lyophilized. The peptides were purified by preparative reverse-phase HPLC using UV detection at 228 nm (amide bond absorption) and 316 nm (C-Sox absorption). Only fractions showing a single peak by analytical HPLC and with a correct mass were used in further experiments.

c. Characterization data for peptides

Name	Peptide Sequence	Mol. Formula	HPLC t_R (min.) ^a	[M] Calcd.	[M+H] ⁺ found ^b
Sox-Peptide	Ac-VP-CSox-LTPGGRRG-CO ₂ H	C ₆₇ H ₁₀₁ N ₁₉ O ₁₆ S ₃	25.7	1418.6	1419.3
Sox-Thioester	Ac-VP-CSox-LTPGGRRG-COSBn	C ₆₄ H ₉₆ N ₁₇ O ₁₆ PS	27.2	1523.7	1524.8
pSox-Peptide	Ac-VP-CSox-LpTPGGRRG-CO ₂ H	C ₆₀ H ₉₆ N ₁₉ O ₂₀ PS ₂	24.4	1498.6	1499.2
pSox-Thioester	Ac-VP-C-Sox-LpTPGGRRG-COSBn	C ₄₄ H ₈₂ N ₁₇ O ₁₅ PS	27.2	1603.7	1604.9

^a Peptides were purified according to the following method: 5% B (5 min) followed by a linear gradient 5–95% B (30 min.). ^b The data was collected on a MALDI-TOF mass spectrometer. ^c Data was collected on an ESI mass spectrometer.

d. Plasmid construction for GST-ENLYFQC-PNT(46-138)-His₆ (GST-PNT)

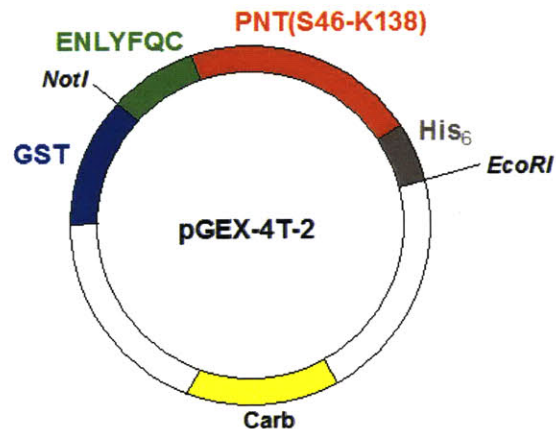
The gene fragment encoding residues 46-138 of Ets-1 (including the PNT domain) was amplified from an Ets-1 plasmid using primers to insert 5' EcoR1 and 3' Not1 restriction sites for incorporation into a pGEX-4T-2 vector. The primers also encoded an amino-terminal TEV protease cleavage site (ENLYFQ\timesC) and a carboxy-terminal hexahistidine tag. For this amplification the following PCR primers were used:

5'- GCC GGA ATT CGT GAA AAC CTG TAT TTT CAG TGC TCC CAA GCC TTG AAA
GCT -3'

3'- GCC CCC TTT TGC GGC CGC CTA GTG ATG GTG ATG GTG ATG ACC TTT CAC
ATC CTC TTT CTG -5'

The PCR-amplified fragments were digested with NotI and EcoRI and ligated to NotI/EcoRI-digested and CIP-treated pGEX-4T-2 (Figure 4-15). The ligation mixture was transformed into DH5 α cells and grown on carbenicillin-resistant plates. Plasmid DNA was isolated from selected colonies and confirmed by sequencing.

a)



b)

MSPILGYWKIKGLVQPTRLLEYLEEKYEEHL YERDEGDKWRNKKFELGLEFPNLPYYI
DGDVKLTQSMAIRYIADKHNMLGGCPKERAEISMLEGA VLDIRYGVSR IAYSKDFETLK
VDFLSKLPEMLKMFEDRLCHKTYLNGDHVTHPDFMLYDALDVVLYMDPMCLDAFPKL
VCFKKRIEAI PQIDKYLKSSKYIAWPLQG WQATFGGGDHPPKSDENLYFQCSQALKATF
SGFTKEQQRLGIPK DPRQWTETHVRD WVMWAVNEFSLKGVDFQKFCMSG AALCALGK
ECFLELAPDFVGDIL WEHLEILQKEDVKHHHHHHH

Figure 4-15. The GST-PNT-His₆ product. a) Map of the pGEX plasmid containing GST-PNT-His₆. b) Primary sequence of the gene product.

e. Expression of GST-PNT

The PNT domain plasmid was transformed into BL21(DE3) competent cells (Stratagene) and grown at 37 °C to midlog phase in 1 L of LB media with carbenicillin (50 mg/L). The culture was cooled to 30 °C, and the cells were induced with 0.2 mM IPTG and grown for an additional 4.5 h. Cells were harvested by centrifugation and frozen at -80 °C. For cell lysis, the pellet from a 1 L expression was thawed and resuspended in 40 mL of freshly prepared lysis buffer I and incubated for 20 min at 4 °C. The cells were then sonicated and subjected to centrifugation at 12,429 x g for 25 min, followed by filtration through a 0.2 micron filter.

f. Isolation of GST-PNT and on-resin TEV proteolysis to yield Cys-PNT(46-138)-His₆ (Cys-PNT)

The filtered supernatant was incubated with 5 mL of Glutathione Sepharose 4 Fast Flow resin (Amersham Biosciences) for 1.5 hours at 4 °C, following the manufacturer's protocol. After extensive washes with PBS (20 column volumes) the resin-bound GST-PNT was proteolyzed overnight with TEV (prepared in house) in 5 mL of PBS, 5 mM EDTA and 5 mM BME at 25 °C with slight agitation. Upon completion of the reaction (ca. 12 hours), the soluble fraction was filtered and the resin was washed with PBS (4 x 2 mL). The filtrate and PBS washes were combined and concentrated in a swinging bucket centrifuge using 3.5 kDa MWCO Amicon Ultra-15 centrifugal filters (Millipore) to give 24 mg of Cys-PNT (MW = 11,672.34 g/mol) as determined by Bio-Rad's Protein Assay. The protein was analyzed by SDS-PAGE and visualized with Coomassie blue dye and by western blot with a mouse anti-hexahistidine primary antibody. Purified protein was stored at 4 °C.

g. Native Chemical Ligation to obtain Sox-PNT

To a 2 mL centrifuge tube was added Cys-PNT (21.7 mg, 1.86 μmol, 1 equiv.), followed by MESNa and Tris (pH 8.0 at 25 °C) so that the final concentrations were: 1.4 mM Cys-PNT, 150 mM MESNa and 50 mM Tris in 1.3 mL total reaction volume. Lastly, Sox-thioester (4.2 mg, 2.79 μmol, 1.5 equiv.) dissolved in 40 μL of water was added and the reaction was gently mixed for 24-48 h at 25 °C. The progress of the reaction was analyzed by SDS-PAGE, and visualized with Coomassie blue dye (Figure 4-2, inset).

h. Purification of Sox-PNT

The crude mixture was immediately purified on the FPLC using the Superdex 75 prep column in 20 mM Tris (pH 8 at 25 °C) and 200 mM NaCl. The protein was analyzed by SDS-PAGE, and visualized with Coomassie blue dye. The fractions with the desired product were combined and concentrated in a swinging bucket centrifuge using 3.5 kDa MWCO Amicon Ultra-15 centrifugal filters. The final concentration of Sox-PNT was determined using the Sox chromophore absorbance in the UV-Vis. The overall yield of isolated product from NCL to final purification of Sox-PNT (6.2 mg, MW = 13,016.73 g/mol) was 24%. The protein was aliquoted, flash-frozen and stored at -80 °C where it is stable for at least 1 year.

In vitro evaluations of Sox-based probes

a. Ets-1- and MBP-derived peptide probes for ERK1/2

Early peptide probes were based on the β -Turn Focused (BTF) design developed in our lab using the Sox amino acid as the sensing moiety.⁷⁹ Two peptides, one derived from the Ets-1 phosphorylation sequence (entry 1 in Table 4-1) and one from the MBP phosphorylation sequence (entry 2), were synthesized and their fluorescence difference measured. The main differences lie in the underlined region in Table 4-1.

In fluorescence increase measurements the concentration of the substrate was held constant while the concentration of ATP was varied. No enzyme was present. A solution of the substrate (or phosphopeptide) was prepared (20 mM HEPES [pH 7.4], 10 mM MgCl₂, 10 μ M peptide at 30 °C), and fluorometer readings were obtained without any ATP present. ATP (stock solution 11) was then added to a final concentration of 1 mM. At each ATP concentration a fluorescence

emission spectrum was recorded (slit widths: $E_m = 5$ nm, $E_x = 5$ nm; $\lambda_{ex} = 360$ nm, $\lambda_{em} = 380$ -650 nm). Fluorescence increase was obtained by dividing the fluorescence of the phosphopeptide by the fluorescence of the substrate at 485 nm. The values reported are averages of at least three separate measurements.

a. Fluorescence increases of Sox-peptide and Sox-PNT chemosensors

The fluorescence increases of the Sox-peptide (Figure 4-S2a) and Sox-PNT (Figure 4-S2b) were measured in the fluorometer (slit widths: $E_m = 5$ nm, $E_x = 5$ nm; $\lambda_{ex} = 360$ nm, $\lambda_{em} = 380$ -650 nm) in a quartz microcuvette (total volume of 120 μ L) under the following conditions: 10 μ M unphosphorylated (red) or phosphorylated (black) sample, 50 mM Tris (pH 7.5), 10 mM $MgCl_2$, 1 mM EGTA, 2 mM DTT and 0.01% Brij 35 P at 30 $^{\circ}C$.

Nearly the same (3.7-fold) fluorescence increase was observed when Sox-PNT was enzymatically converted to its phosphorylated version, pSox-PNT, by ERK2 (Figure 4-S3). This ensured that the changes in fluorescence that were measured with synthetic Sox-PNT and pSox-PNT (3-fold, Figure S2) were also relevant under biochemical conditions. The assays were performed in the FPR ($\lambda_{ex} = 360$ nm, $\lambda_{em} = 485$ nm) in a 96-well plate (120 μ L per reaction) containing 10 μ M Sox-PNT at 30 $^{\circ}C$. Substrate (Sox-PNT) fluorescence at 485 nm was recorded over 17 min and then 5 nM ERK2 was added. After 17 hours at 30 $^{\circ}C$, during which time the wells were sealed to prevent evaporation, the reaction was finished and fluorescence of the phosphorylated product (pSox-PNT) was recorded for 17 min. The final assay conditions were as follows: 10 μ M Sox-PNT, 50 mM Tris (pH 7.5 at 25 $^{\circ}C$), 10 mM $MgCl_2$, 1 mM EGTA, 2 mM DTT, 0.01% Brij 35 P, 1 mM ATP and 5 nM ERK at 30 $^{\circ}C$.

b. Calculation of Z' factors

The Z' factors are statistical quality parameters used in high-throughput screens to evaluate performance of such assays.³⁴ Typically, assays are considered excellent if Z' is 0.5-1. The Z' values were calculated from data obtained for fluorescence increases under assay conditions with ERK2 as described above (V.b.) and using equation (1)

$$Z' = 1 - \frac{(3 \times \sigma_P) + (3 \times \sigma_S)}{|\mu_P - \mu_S|} \quad (1)$$

where μ_P and μ_S are the means of three measurements of fluorescence emission at 485 nm for phosphoprotein and starting substrate, respectively, and σ_P and σ_S are the standard deviations of those measurements for phosphoprotein and substrate, respectively.

c. Affinity of ERK2 for Sox-PNT and Sox-peptide

The activity of recombinant ERK2 (NEB) was measured over time with Sox-PNT and Sox-peptide in the fluorometer (slit widths: Em = 5 nm, Ex = 5 nm; λ_{ex} = 360 nm, λ_{em} = 485 nm) in a quartz microcuvette (total volume of 120 μ L) under the following conditions: 50 mM Tris (pH 7.5 at 25 °C), 10 mM MgCl₂, 1 mM EGTA, 2 mM DTT, 0.01% Brij 35 P, 10 μ M Sox-PNT or 10-250 μ M Sox-peptide and 11 ng ERK2 at 30 °C. The fluorescence slopes (m) of the reactions (Figure 4-16) were determined by a least-squares fit using Microsoft Excel, then normalized to the highest slope (obtained with 10 μ M Sox-PNT) and plotted in the bar graph form (Figure 4-5a in the Results and Discussion) for clearer visualization.

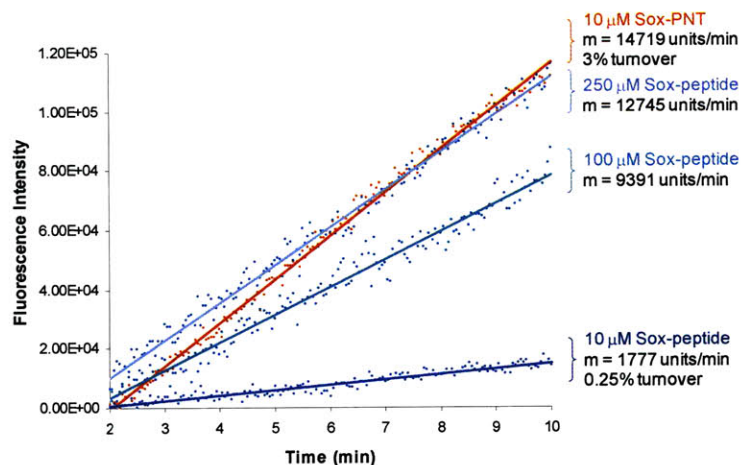


Figure 4-16. Comparison of Sox-PNT and Sox-peptide as substrates for ERK2. Reaction curves of 10 μM Sox-PNT (red) and 10-250 μM Sox-peptide (shades of blue) with 11 ng ERK2 showed that nearly 300 μM of Sox-peptide is required to reach the same slope that was obtained with 10 μM Sox-PNT.

d. Determination of kinetic constants for ERK2 with Sox-PNT

Recombinant ERK2 (Invitrogen, 5 nM, 42 ng, MW = 69,700 g/mol) was added to initiate each reaction. The kinetic assays were performed in the FPR ($\lambda_{\text{ex}} = 360 \text{ nm}$, $\lambda_{\text{em}} = 485 \text{ nm}$) in a 96-well plate (120 μL per reaction) containing varying chemosensor concentrations (0.2–5 K_M) at 30 $^{\circ}\text{C}$. Fluorescence slopes were determined by a least-squares fit using Microsoft Excel. Slopes were then converted to a rate using published procedures.³³ The plots of v vs. $[\text{S}]$ were fit using SigmaPlot 9.01⁸⁰ in order to obtain K_M and V_{max} values. The assay conditions were as follows: 50 mM Tris (pH 7.5 at 25 $^{\circ}\text{C}$), 10 mM MgCl_2 , 1 mM EGTA, 2 mM DTT, 0.01% Triton X-100, 1 mM ATP at 30 $^{\circ}\text{C}$. Alternatively, 384-well plates can be used (20 μL reaction volume) with, otherwise, the same conditions.

e. Selectivity of Sox-PNT in a panel of MAPKs

The assays were performed in the FPR ($\lambda_{\text{ex}} = 360 \text{ nm}$, $\lambda_{\text{em}} = 485 \text{ nm}$) in a 96-well plate (120 μL per reaction) containing 5 μM chemosensor at 30 $^{\circ}\text{C}$. Recombinant ERK1 and 2, JNK1, 2, and 3, p38 α , β , γ and δ and CDK1/Cyclin B and CDK2/Cyclin A (all enzymes were obtained from Invitrogen) were appropriately diluted with 50 mM Tris (pH 7.5 at 25 $^{\circ}\text{C}$), 10 mM MgCl_2 , 1 mM ATP, 1 mM EGTA, 2 mM DTT, 0.01% Triton X-100. Addition of 15 or 150 nM of enzyme initiated reactions. Fluorescence slopes were determined by a least-squares fit using Microsoft Excel. The slopes obtained with 15 and 150 nM of enzyme were normalized to the slope with ERK1 and plotted on the same graph for easy visualization (Fig. 2c in the main text). Due to the high 150 nM concentration of enzymes, these experiments could only be performed once. The assays with 15 nM enzyme are reported with s.e.m. for triplicate measurements. The final assay conditions were as follows: 5 μM Sox-PNT, 50 mM Tris (pH 7.5 at 25 $^{\circ}\text{C}$), 10 mM MgCl_2 , 1 mM EGTA, 2 mM DTT, 0.01% Triton X-100, 1 mM ATP and 15 or 150 nM enzyme at 30 $^{\circ}\text{C}$.

Experiments in crude cell lysates with Sox-PNT

a. Crude cell lysate preparation

Cell cultures were maintained according to manufacturer's recommendations using the appropriate media (FBS-containing solutions 17-20) that were stored at 4 $^{\circ}\text{C}$ in the dark and warmed to 37 $^{\circ}\text{C}$ for 30 min before use. Prior to lysis, cells were serum-starved on 150 mm tissue culture dishes for 15-18 h in serum-free media supplemented with an additional 2 mM L-Gln (Serum-free media solutions 17-20). Cells were either 1. untreated, 2. stimulated with EGF (100 ng/mL) for 5 min at 37 $^{\circ}\text{C}$, 3. preincubated with U0126 (5 μM delivered in 2.5 μL DMSO) for 1 h and then stimulated with EGF (100 ng/mL) for 5 min at 37 $^{\circ}\text{C}$, or 4. treated with DMSO (2.5

μL) for 1 h followed by stimulation with EGF (100 ng/mL) for 5 min at 37 °C. The media was aspirated and cells washed with cold PBS (2 x 20 mL). The cells were kept on ice and lysed by addition of Lysis Buffer II (~ 100 μL /dish) directly on the plate followed by scraping and passing the mixture through a 22-gauge needle attached to a 1 mL syringe. The lysed solution was clarified at 14,000 x g for 10 min at 4 °C. The supernatant was collected and stored in aliquots at -80 °C. Total protein concentration was determined using Bio-Rad's Protein Assay.

b. Western blot visualization of ERK1/2 by chemiluminescence

ERK1/2 expression was analyzed by western blots that were probed with anti-ERK1/2 antibody (Upstate) or anti-pERK1/2 antibody (Cell Signaling Tech.) according to the manufacturer's protocols. Incubation with secondary antibody (goat anti-rabbit antibody conjugated to HRP from Pierce) was followed by exposure of the blot to SuperSignal West Dura Extended Duration Substrate (Pierce) and visualized by enhanced sensitivity chemiluminescence (Bio-Rad, Quantity One 1-D Analysis Software).

c. Assays with crude cell lysates and Sox-PNT

The assays were performed either in the fluorometer (slit widths: $\lambda_{\text{em}} = 5 \text{ nm}$, $\lambda_{\text{ex}} = 5 \text{ nm}$; $\lambda_{\text{ex}} = 360 \text{ nm}$, $\lambda_{\text{em}} = 485 \text{ nm}$) in a quartz microcuvette (120 μL per reaction) or in the FPR ($\lambda_{\text{ex}} = 360 \text{ nm}$, $\lambda_{\text{em}} = 485 \text{ nm}$) in a 96-well plate (120 μL per reaction) containing 5 μM Sox-PNT at 30 °C. Untreated, EGF-stimulated, U0126-treated then EGF-stimulated or DMSO-treated then EGF-stimulated (Figure 4-18) lysates from NIH-3T3, HT-29, HeLa or PtK-1 cells were added to start the reactions. The reactions were monitored for 15 min. Fluorescence slopes were determined by a least-squares fit using Microsoft Excel then normalized to the highest slope and plotted in the bar graph form (Figure 4-7a in the Results and Discussion and Figure 4-17) for clearer

visualization. The final assay conditions were as follows: 5 μ M Sox-PNT, 50 mM Tris (pH 7.5 at 25 $^{\circ}$ C), 10 mM MgCl₂, 1 mM EGTA, 2 mM DTT, 0.01% Brij 35 P, 1 mM ATP and 40 μ g lysate at 30 $^{\circ}$ C.

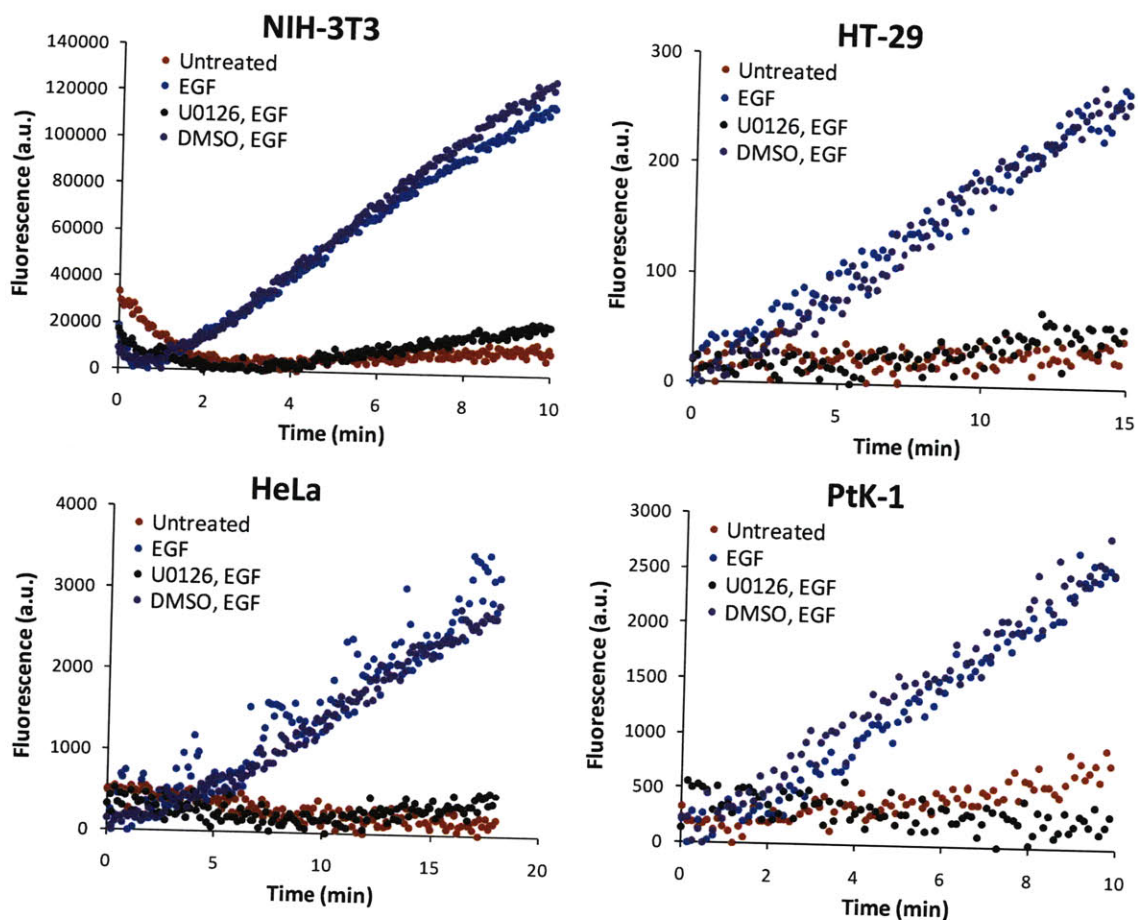


Figure 4-17. Detection of ERK1/2 activity by Sox-PNT (5 μ M) in lysates (40 μ g) from four cell lines. In all cases there is low basal ERK1/2 activity (red) compared to activity that is observed with lysates that have been stimulated with EGF (blue). However, treatment of cells with a MEK1/2 inhibitor, U0126, followed by EGF stimulation returned activity to basal levels (black). Lastly, cells were pre-treated with DMSO, the carrier solvent for U0126, and then EGF-stimulated to show that DMSO does not have an effect on observed activity (purple). Each experiment was performed in triplicate, but for clarity only one, representative reaction curve is shown per condition.

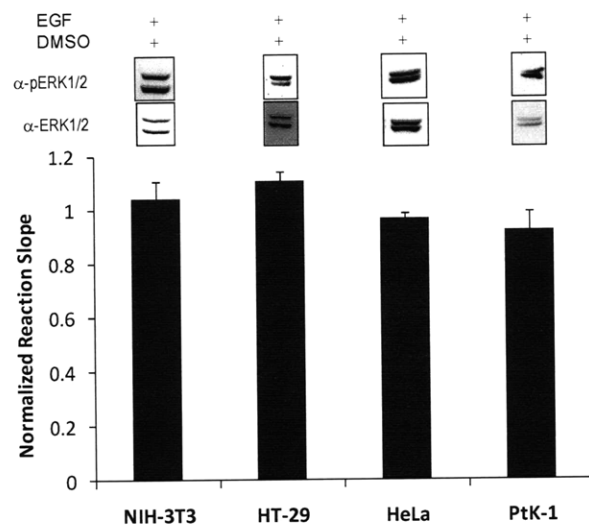


Figure 4-18. Effects of DMSO on ERK1/2 activation. DMSO-treated and then EGF-stimulated lysates were assayed with Sox-PNT to show that DMSO does not have an effect on ERK1/2 activity. Plotted values indicate the mean \pm s.e.m. for triplicate measurements. This was also confirmed by western blots (inset) probed with anti-pERK1/2 (top) and anti-ERK1/2 (bottom) antibodies.

To show that Sox-PNT can successfully report the different activity states of ERK1/2 it was compared directly to Sox-peptide (Figure 4-19 and Figure 4-7b). Each substrate was exposed to either untreated, EGF-stimulated or U0126 pre-treated and then EGF-stimulated HeLa lysates. The reactions were monitored in the fluorometer (slit widths: $E_m = 5$ nm, $E_x = 5$ nm; $\lambda_{ex} = 360$ nm, $\lambda_{em} = 485$ nm) in a quartz microcuvette (120 μ L per reaction) containing 5 μ M substrate at 30 $^{\circ}$ C. Fluorescence slopes were determined by a least-squares fit using Microsoft Excel then normalized to the highest slope and plotted in the bar graph form (Figure 4-5b in the Results and Discussion) for clearer visualization. The final assay conditions were as follows: 5 μ M substrate, 50 mM Tris (pH 7.5 at 25 $^{\circ}$ C), 10 mM $MgCl_2$, 1 mM EGTA, 2 mM DTT, 0.01% Brij 35 P, 1 mM ATP and 40 μ g lysate at 30 $^{\circ}$ C.

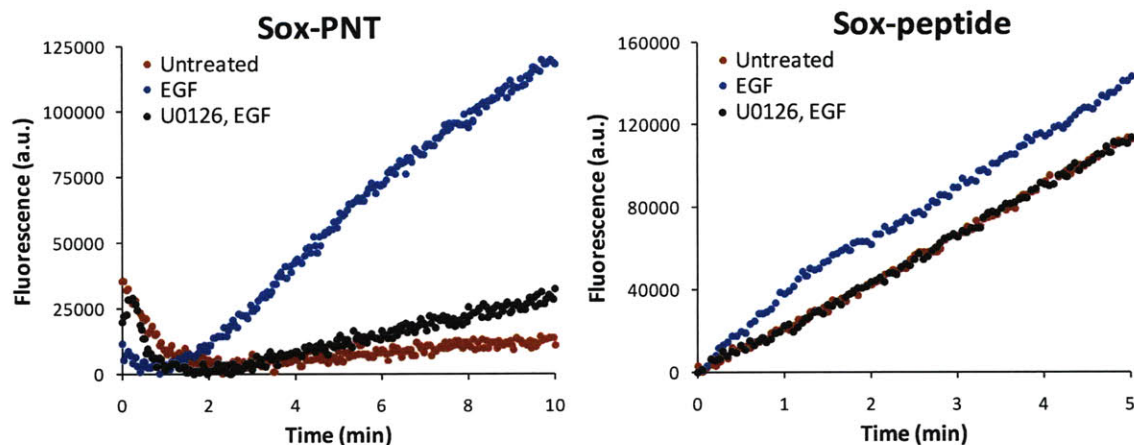


Figure 4-19. Specificity of substrates. Sox-PNT (5 μM) easily reported high ERK1/2 activity in EGF-stimulated lysates (blue) and low activity in untreated (red) and U0126 and EGF-stimulated (black) lysates, while Sox-peptide (5 μM) failed to do so and was phosphorylated regardless of presence or absence of active ERK1/2. Each experiment was performed in triplicate, but for clarity only one, representative reaction plot is shown per condition.

d. Determination of IC_{50} and K_i with PEA-15 in EGF-stimulated NIH-3T3 lysates

The assays were performed in the FPR ($\lambda_{\text{ex}} = 360 \text{ nm}$, $\lambda_{\text{em}} = 485 \text{ nm}$) in a 96-well plate (120 μL per reaction). Sox-PNT (5 μM) was preincubated for 5 min with PEA-15 (7 concentrations in the 0.0005-50 μM range) at 30 $^{\circ}\text{C}$. The reactions were started by addition of EGF-stimulated NIH-3T3 lysate and monitored for 15 min. Fluorescence slopes were determined by a least-squares fit using Microsoft Excel and converted to rates (v in $\mu\text{M}/\text{min}$) using published procedures.³³ The plots of v vs. $\log [\text{PEA-15}]$ were fit using SigmaPlot 9.01⁸⁰ in order to obtain the IC_{50} value (Figure 3d in the main text). The final assay conditions were as follows: 5 μM Sox-PNT, 50 mM Tris (pH 7.5 at 25 $^{\circ}\text{C}$), 10 mM MgCl_2 , 1 mM EGTA, 2 mM DTT, 0.01% Brij 35 P, 1 mM ATP and 40 μg lysate at 30 $^{\circ}\text{C}$.

The K_i value was derived from the above-determined IC_{50} using the following equation,⁸¹

$$IC_{50} = \left(1 + \frac{[S]}{K_M}\right) K_i \quad (2)$$

where S is the concentration of Sox-PNT in the assays. Upon rearranging, eq. (2) can be solved for K_i .

e. Immunodepletions of ERK1/2 from EGF-stimulated HeLa lysate

EGF-stimulated HeLa lysate (900 μ g) was precleared first by incubation with Protein A sepharose beads (50 μ L, Amersham) for 1 hr on a rotating shaker at 4 °C. The precleared EGF-stimulated HeLa lysate (300 μ g) was incubated with anti-ERK1/2 antibody (5 μ g, Upstate) or naïve rabbit IgG (5 μ g, Santa Cruz) for 1 hr on a rotating shaker at 4 °C. The immune complexes were precipitated with 50 μ L Protein A sepharose beads for 1 hr with mixing at 4 °C. In total, three rounds of immunodepletions were carried out to ensure removal of all ERK1/2. The immunodepletions were analyzed by western blots (probed with anti-ERK1/2 antibody from Upstate) that were visualized using chemiluminescence, as described above.

The immunodepleted lysates were then analyzed for ERK1/2 activity with Sox-PNT (Figure 4-20 and Figure 4-9a in the Results and Discussion) according to described protocols (vide supra) in the 96-well plate format in the FPR.

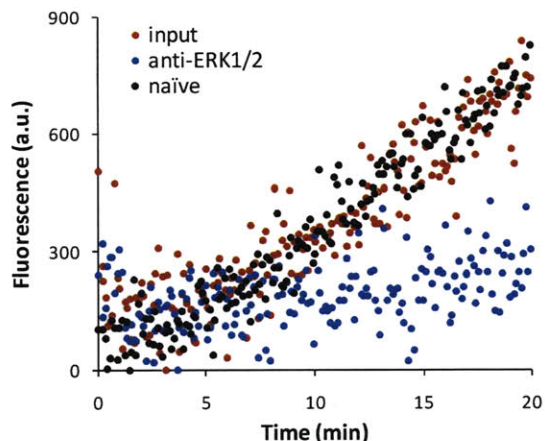


Figure 4-20. Immunodepletion of ERK1/2. Removal of ERK1/2 (blue) led to low turnover of Sox-PNT (5 μ M), while the input lysate (red) and lysate treated with a generic Rabbit IgG (naïve, black) retained active ERK1/2.

f. Estimation of active ERK1/2 in EGF-stimulated HeLa lysates

The assays were performed in the FPR ($\lambda_{\text{ex}} = 360 \text{ nm}$, $\lambda_{\text{em}} = 485 \text{ nm}$) in a 96-well plate (120 μ L per reaction) containing 5 μ M Sox-PNT at 30 $^{\circ}$ C. The standard curve was obtained by incubating Sox-PNT with 0.5, 2.5 or 5 nM recombinant ERK2 and then plotting the average slope of each reaction as a function of ERK2 concentration (Figure 4-9b). Using a least-squares fit in Microsoft Excel the following equation was obtained,

$$y = 45.07x + 7.47 \quad (2)$$

where y is the fluorescence intensity at a given concentration of ERK2 (x) in the 0.5-2.5 nM range. At the same time, Sox-PNT was incubated with EGF-stimulated NIH lysates and the reaction slope was determined (124 min^{-1}) by a least-squares fit using Microsoft Excel. When substituted in eq. (2) and solved for x , the concentration of ERK2 in EGF-stimulated NIH lysates is obtained (2.6 nM in 40 μ g of lysate) that can also be converted to amount of enzyme (13 ng)

because of the known reaction volume (120 μL) and ERK2 molecular weight (42,000 g/mol). However, since lysates contain both ERK1 and 2, the concentration (and amount) is representative of both enzymes. The final assay conditions were as follows: 5 μM Sox-PNT, 50 mM Tris (pH 7.5 at 25 $^{\circ}\text{C}$), 10 mM MgCl_2 , 1 mM EGTA, 2 mM DTT, 0.01% Brij 35 P, 1 mM ATP and 40 μg lysate, 0.5, 2.5 or 5 nM recombinant ERK2 at 30 $^{\circ}\text{C}$.

Microinjection and Microscopy

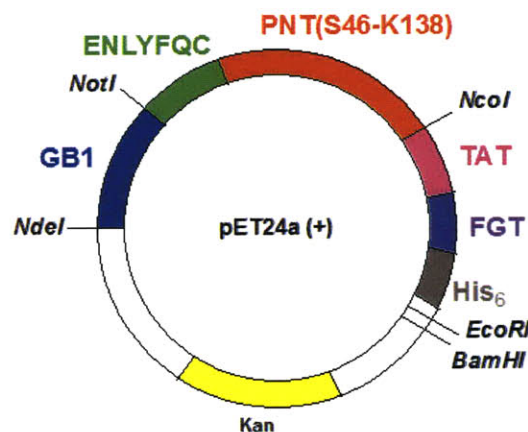
PtK-1 cells were plated on acid-washed glass coverslips for 20–24 h before experiments and were serum-starved overnight (ca. 12 h) at 37 $^{\circ}\text{C}$ and 5% CO_2 . To reduce the effects of photobleaching, Oxyrase (1.0 U, Oxyrase.) was added to 1 mL of culture medium. Cells were co-microinjected with Sox-PNT (149 μM), Alexa Fluor 568-conjugated dextran (0.5 mg mL^{-1}) and MgCl_2 (0.75 M) using an Eppendorf transjector 5246 (Eppendorf) into the cell cytoplasm at 0.5 mg mL^{-1} , as described previously.⁸² The microinjected cells were incubated at 37 $^{\circ}\text{C}$ and 5% CO_2 for 5 min and then stimulated with EGF (100 ng mL^{-1}).

Time-lapse image sequences were acquired by spinning disc confocal microscopy using a $\times 100/1.4$ NA Plan Apo phase objective lens (Nikon). Images were acquired with illumination at 387 nm (Sox) and 560 nm (Alexa Fluor 568) provided by a 2.5W KrAr laser (Coherent). Images were captured using a CoolSNAP-HQ2 camera from Photometrics at 447 nm (Sox) and 630 nm (Alexa Fluor 568). Raw images were viewed and false-colored using ImageJ software, which is freely available from the National Institutes of Health.

Semisynthesis of Sox-PNT-TAT

The gene incorporating GB1, the PNT(46-138) domain, the TEV cleavage site (ENLYFQ~~C~~), the TAT sequence (YGKKRRQRRR), the formylglycine tag (FGT) (LCTPSR) and the His₆ tag was commercially synthesized by BioBasic Inc in the pUC-57 plasmid. The gene fragment encoding for GB1-PNT-TAT-FGT-His₆ was amplified from pUC-57 and digested with NdeI and BamHI followed by ligation to NdeI/BamHI-digested and CIP-treated p24a (+) (Figure 4-21). The ligation mixture was transformed into DH5 α cells and grown on kanamycin-resistant plates. Plasmid DNA was isolated from selected colonies and confirmed by sequencing.

a)



b)

MQYKLILNGKTLKGETTTEAVDAATAEKVFKQYANDNGVDGEWTYDDATKTFTVTEG
GRENLYFQCSQALKATFSGFTKEQQLGIPKDPQWTETHVRDWVMWAVNEFSLKGV
DFQKFCMSGAAALCALGKECFLELAPDFVGDILWEHLEILQKEDVKPWYGKKRRQRRRL
CTPSRHHHHHH

Figure 4-21. The GB1-PNT-TAT-FGT-His₆ product. a) Map of the p24a (+) plasmid containing GB1-PNT-TAT-FGT-His₆. b) Primary sequence of the gene product.

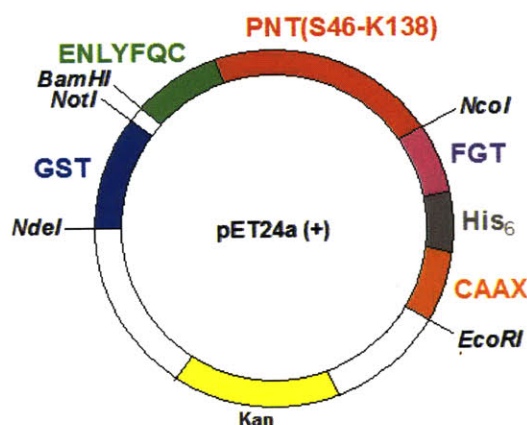
The GB1-PNT-TAT protein (MW = 21,212.1 g/mol) was expressed following the same protocol as described for GST-PNT-H₆ (vide supra), except that kanamycin (30 mg/mL) was used as the antibiotic instead of carbenicillin.

TEV removal of GB1 to give Cys-PNT-TAT (MW = 13,942.1 g/mol), NCL, purification and quantification of Sox-PNT-TAT (MW = 15,343.5 g/mol) were performed according to the protocols used for Sox-PNT (vide supra).

Semisynthesis of Sox-PNT-CAAX

The gene incorporating GST, the PNT(46-138) domain, the TEV cleavage site (ENLYFQ<C), the formylglycine tag (FGT) (LCTPSR), the His₆ tag, and the CAAX sequence (KMSKDGKKKKKSKTKCVIM), the formylglycine tag (LCTPSR) and the His₆ tag was commercially synthesized by BioBasic Inc in the pUC-57 plasmid. The gene fragment encoding for GST-PNT-FGT-His₆-CAAX was amplified from pUC-57 and digested with NdeI and BamHI followed by ligation to NdeI/BamHI-digested and CIP-treated p24a (+) (Figure 4-22). The ligation mixture was transformed into DH5 α cells and grown on kanamycin-resistant plates. Plasmid DNA was isolated from selected colonies and confirmed by sequencing.

a)



b)

MSPILGYWKIKGLVQPTRLLEYLEEKYEEHLYERDEGDKWRNKKFELGLEFPNLPYYI
DGDVKL TQSMAIRYIADKHNMLGGCPKERAEISMLEGAVLDIRYGVSR IAYSKDFETLK
VDFLSKLPEMLKMFEDRLCHKTYLNGDHVTHPDFMLYDALDVVLYMDPMCLDAFPKL
VCFKKRIEAI PQIDKYLKSSKYIAWPLQGWQATFGGGDHPPKSDLVPRENL YFQCSQAL
KATFSGFTKEQQRLGIPKDP RQWTETHVRDWVMWAVNEFSLKGVDFQKFCMSG AALC
ALGKECFLELAPDFVGDILWEHLEILQKEDVKGLCTPSRHHHHHHHKMSKD GKKKKKKS
KTKCVIM

Figure 4-22. The GST-PNT-FGT-His₆-CAAX product. a) Map of the p24a (+) plasmid containing GST-PNT-FGT-His₆-CAAX. b) Primary sequence of the gene product.

The GST-PNT-CAAX protein (MW = 41,580.5 g/mol) was expressed following the same protocol as described for GST-PNT-H₆ (vide supra), except that kanamycin (30 mg/mL) was used as the antibiotic instead of carbenicillin.

TEV removal of GST to give Cys-PNT-CAAX (MW = 14,637.1 g/mol), NCL, purification and quantification of Sox-PNT-CAAX (MW = 16,038.5 g/mol) were performed according to the protocols used for Sox-PNT (vide supra).

Synthesis and Characterization of Sox-Isopeptide

a. Synthesis

The first 6 residues (TPGGRR), including Fmoc-Thr-OH with the free side chain alcohol, were attached to Gly-preloaded TGT resin (0.0215 mmol, 1 equiv) following described protocols (vide supra). Upon Fmoc removal with 20% 4-methylpiperidine/DMF, the resin was washed ($5 \times$ DMF, $5 \times$ CH₂Cl₂) followed by addition DMF (500 μ L) DIEA (37.5 μ L, 0.215 mmol, 10 equiv) and NVOC-Cl (35.6 mg, 0.129 mmol, 6 equiv) dissolved in DMF (100 μ L). The reaction vessel was wrapped in aluminum foil; care was taken from this point onward to protect the peptide from light. After 2 h of shaking at RT the contents of the reaction were drained and the beads washed ($10 \times$ DMF). Next, Fmoc-Leu-OH was coupled using the symmetric anhydride method with DIC (18 μ L, 0.107 mmol, 5 equiv) and cat. DMAP (0.1 equiv) (2×2 h). Fmoc-C(Sox[TBDPS])-OH (2 equiv) was coupled using PyAOP/HOAt/2,4,6-collidine (2:2:5, 0.15 M in DMF) for 12 h. The last two amino acids (VP) were coupled using 6 equiv of amino acid and DIC:HOBt (5:5 equiv) (1×1 h) and deprotections were carried out with 20% 4-methylpiperidine/DMF (2×4 min, 1×2 min). After acetylation (20 equiv of Ac₂O and 20 equiv of pyridine, 45 min) the peptides were subjected to 20% 4-methylpiperidine/DMF (2×4 min, 1×2 min) to remove C-Sox aryl esters that might have formed during acetylation. The resin was finally washed with DMF, CH₂Cl₂, MeOH ($5 \times$ each) and dried under vacuum.

The Sox-Isopeptide was cleaved and fully deprotected with TFA/H₂O/TIS (95:2.5:2.5% v/v) for 3 h. The resulting solution was concentrated under a stream of N₂ and precipitated by addition of cold Et₂O. The pellet was triturated with cold Et₂O (3 x), redissolved in water, filtered and lyophilized. The peptides were purified by preparative reverse-phase HPLC using UV detection

at 228 nm (amide bond absorption) and 316 nm (C-Sox absorption) or 350 nm (NVOC absorption). Only fractions showing a single peak by analytical HPLC and with a correct mass were used in further experiments.

Name	Peptide Sequence	Mol. Formula	HPLC t_R (min.) ^a	[M+xH] ^{x+} Calcd.	[M+xH] ^{x+} found ^b
Sox-Isopeptide	Ac-VP-CSox-L-(N ^α -NVOC)T-PGGRRG-CO ₂ H	C ₇₀ H ₁₀₄ N ₂₀ O ₂₃ S ₂	28.4	829.3 (+3)	829.0 (+3) ^c

^a Purified according to the following method: 5% B (5 min) followed by a linear gradient 5–95% B (30 min). ^b Data was collected on an ESI mass spectrometer.

A stock solution of Sox-Isopeptide was prepared in doubly deionized water and its concentration was determined by UV-Vis (based on the determined extinction coefficient of the fluorophore unit, 5-(*N,N*-dimethylsulfonamido)-8-hydroxy-2-methylquinoline, $\epsilon_{355} = 8247 \text{ M}^{-1} \text{ cm}^{-1}$ at 355 nm in 0.1 M NaOH with 1 mM Na₂EDTA and NVOC, $\epsilon_{350} = 6336 \text{ M}^{-1} \text{ cm}^{-1}$ at 350 nm⁸³). An average of the values from three separate solutions, each prepared using a different volume of the stock solution, was read on UV-Vis spectrophotometer. Purified peptide stock solutions can be stored at 4 °C for at least 6 months or -20 °C for longer periods.

b. Rate of Uncaging

To determine the rate of uncaging, a solution of Sox-Isopeptide (100 μM) in 10 mM HEPES (pH 7.4) with 5 mM DTT and 1 mM inosine was prepared and exposed to light on the transilluminator ($\lambda_{\text{ex}} = 365 \text{ nm}$) for 1, 3, 10 or 20 min. Immediately after the allotted time, the mixture was injected and separated on the RP-HPLC (C₁₈ analytical column, method: 5%B (5 min) followed by a linear gradient to 95%B (30 min)). Isolated peaks were subjected to ESI MS to confirm their identity.

The percentage of uncaging (disappearance of Sox-Isopeptide peak) was calculated with inosine as an internal standard. At a first glance, formation of Sox-Peptide does not seem to correlate to Sox-Isopeptide uncaging, but the extinction coefficient for Sox-Peptide is substantially lower than that of Sox-Isopeptide. Thus, the two cannot be directly compared.

Time (min) ^a	Peak Area		Sox-Isopeptide:Inosine	Normalized to 0 min	% Sox-Isopeptide	% Uncaging
	Inosine	Sox-Isopeptide				
0	46.33	53.67	1.16	1	100	0
1	63.99	36.01	0.56	0.49	48.58	51.42
3	78.67	21.33	0.27	0.23	23.41	76.59
10	92.3	7.70	0.08	0.07	7.20	92.80
20	94.71	4.29	0.05	0.04	3.91	96.09

^a HPLC method: 5% B (5 min) followed by a linear gradient 5–95% B (30 min).

c. Stability in Reducing Conditions

To determine if the ester bond would survive future handling, Sox-Isopeptide (100 μ M) was also exposed to harshly reducing conditions (10 mM HEPES (pH 7.4), 150 mM DTT, 150 mM MESNa, 150 mM BME and 1 mM inosine) and was monitored periodically (0, 1, 24 and 48 h) via RT-HPLC (C₁₈ analytical column, method: 5%B (5 min) followed by a linear gradient to 95%B (30 min)). Sox-Isopeptide is quite robust over a period of 24 hours. Over 48 hours, however, a side product starts to grow more prominent. The mass of the side product corresponds to an oxidation product; no sign of ester hydrolysis is detected.

References

1. Manning, G.; Whyte, D. B.; Martinez, R.; Hunter, T.; Sudarsanam, S. The Protein Kinase Complement of the Human Genome. *Science* **2002**, *298*, 1912-1934.
2. Hunter, T. Signaling—2000 and beyond. *Cell* **2000**, *100*, 113-127.
3. Roberts, P. J.; Der, C. J. Targeting the Raf-MEK-ERK mitogen-activated protein kinase cascade for the treatment of cancer. *Oncogene* **2007**, *26*, 3291-3310.
4. Hirosumi, J.; Tuncman, G.; Chang, L.; Gorgun, C. Z.; Uysal, K. T.; Maeda, K.; Karin, M.; Hotamisligil, G. S. A central role for JNK in obesity and insulin resistance. *Nature* **2002**, *420*, 333-336.
5. Omori, S.; Hida, M.; Fujita, H.; Takahashi, H.; Tanimura, S.; Kohno, M.; Awazu, M. Extracellular signal-regulated kinase inhibition slows disease progression in mice with polycystic kidney disease. *J. Am. Soc. Nephrol.* **2006**, *17*, 1604-1614.
6. Muslin, A. J. MAPK signalling in cardiovascular health and disease: molecular mechanisms and therapeutic targets. *Clin. Sci. (Lond.)* **2008**, *115*, 203-218.
7. Ravingerova, T.; Barancik, M.; Strniskova, M. Mitogen-activated protein kinases: a new therapeutic target in cardiac pathology. *Mol. Cell. Biochem.* **2003**, *247*, 127-138.
8. Giovannini, M. G.; Cerbai, F.; Bellucci, A.; Melani, C.; Grossi, C.; Bartolozzi, C.; Nosi, D.; Casamenti, F. Differential activation of mitogen-activated protein kinase signalling pathways in the hippocampus of CRND8 transgenic mouse, a model of Alzheimer's disease. *Neuroscience* **2008**, *153*, 618-633.
9. Pelaia, G.; Cuda, G.; Vatrella, A.; Gallelli, L.; Caraglia, M.; Marra, M.; Abbruzzese, A.; Caputi, M.; Maselli, R.; Costanzo, F. S.; Marsico, S. A. Mitogen-activated protein kinases and asthma. *J. Cell. Physiol.* **2005**, *202*, 642-653.
10. Duan, W.; Chan, J. H.; Wong, C. H.; Leung, B. P.; Wong, W. S. Anti-inflammatory effects of mitogen-activated protein kinase kinase inhibitor U0126 in an asthma mouse model. *J. Immunol.* **2004**, *172*, 7053-7059.
11. Mercer, B. A.; Kolesnikova, N.; Sonett, J.; D'Armiento, J. Extracellular regulated kinase/mitogen activated protein kinase is up-regulated in pulmonary emphysema and mediates matrix metalloproteinase-1 induction by cigarette smoke. *J. Biol. Chem.* **2004**, *279*, 17690-17696.
12. Roux, P. P.; Blenis, J. ERK and p38 MAPK-activated protein kinases: a family of protein kinases with diverse biological functions. *Microbiol. Mol. Biol. Rev.* **2004**, *68*, 320-44.
13. Gille, H.; Sharrocks, A. D.; Shaw, P. E. Phosphorylation of transcription factor p62TCF by MAP kinase stimulates ternary complex formation at c-fos promoter. *Nature* **1992**, *358*, 414-417.
14. Chen, R. H.; Sarnecki, C.; Blenis, J. Nuclear localization and regulation of erk- and rsk-encoded protein kinases. *Mol. Cell. Biol.* **1992**, *12*, 915-927.
15. Mebratu, Y.; Tesfaigzi, Y. How ERK1/2 activation controls cell proliferation and cell death: Is subcellular localization the answer? *Cell Cycle* **2009**, *8*, 1168-1175.
16. Callaway, K.; Abramczyk, O.; Martin, L.; Dalby, K. N. The Anti-apoptotic Protein PEA-15 is a Tight Binding Inhibitor of ERK1 and ERK2, Which Blocks Docking Interactions at the D-Recruitment Site. *Biochemistry* **2007**, *46*, 9187-9198.
17. Chen, C. H.; Wang, W. J.; Kuo, J. C.; Tsai, H. C.; Lin, J. R.; Chang, Z. F.; Chen, R. H. Bidirectional signals transduced by DAPK-ERK interaction promote the apoptotic effect of DAPK. *EMBO J.* **2005**, *24*, 294-304.

18. Ni, Q.; Titov, D. V.; Zhang, J. Analyzing protein kinase dynamics in living cells with FRET reporters. *Methods* **2006**, 40, 279-86.
19. Rothman, D. M.; Shults, M. D.; Imperiali, B. Chemical approaches for investigating phosphorylation in signal transduction networks. *Trends Cell Biol.* **2005**, 15, 502-510.
20. Green, H. M.; Alberola-Ila, J. Development of ERK Activity Sensor, an in vitro, FRET-based sensor of Extracellular Regulated Kinase activity. *BMC Chem. Biol.* **2005**, 5, 1.
21. Fujioka, A.; Terai, K.; Itoh, R. E.; Aoki, K.; Nakamura, T.; Kuroda, S.; Nishida, E.; Matsuda, M. Dynamics of the Ras/ERK MAPK cascade as monitored by fluorescent probes. *J. Biol. Chem.* **2006**, 281, 8917-26.
22. Sato, M.; Kawai, Y.; Umezawa, Y. Genetically encoded fluorescent indicators to visualize protein phosphorylation by extracellular signal-regulated kinase in single living cells. *Anal. Chem.* **2007**, 79, 2570-5.
23. Harvey, C. D.; Ehrhardt, A. G.; Cellurale, C.; Zhong, H.; Yasuda, R.; Davis, R. J.; Svoboda, K. A genetically encoded fluorescent sensor of ERK activity. *Proc. Natl. Acad. Sci. U.S.A.* **2008**, 105, 19264-9.
24. Sharma, V.; Wang, Q.; Lawrence, D. S. Peptide-based fluorescent sensors of protein kinase activity: design and applications. *Biochim. Biophys. Acta* **2008**, 1784, 94-99.
25. Remenyi, A.; Good, M. C.; Lim, W. A. Docking interactions in protein kinase and phosphatase networks. *Curr. Opin. Struct. Biol.* **2006**, 16, 676-685.
26. Foulds, C. E.; Nelson, M. L.; Blaszcak, A. G.; Graves, B. J. Ras/mitogen-activated protein kinase signaling activates Ets-1 and Ets-2 by CBP/p300 recruitment. *Mol. Cell. Biol.* **2004**, 24, 10954-10964.
27. Seidel, J. J.; Graves, B. J. An ERK2 docking site in the Pointed domain distinguishes a subset of ETS transcription factors. *Genes Dev.* **2002**, 16, 127-137.
28. Rainey, M. A.; Callaway, K.; Barnes, R.; Wilson, B.; Dalby, K. N. Proximity-induced catalysis by the protein kinase ERK2. *J. Am. Chem. Soc.* **2005**, 127, 10494-10495.
29. Haycock, J. W. Peptide substrates for ERK1/2: structure-function studies of serine 31 in tyrosine hydroxylase. *J. Neurosci. Meth.* **2002**, 116, 29-34.
30. Dawson, P. E.; Muir, T. W.; Clark-Lewis, I.; Kent, S. B. H. Synthesis of proteins by native chemical ligation. *Science* **1994**, 266, 776-779.
31. Hackeng, T. M.; Griffin, J. H.; Dawson, P. E. Protein synthesis by native chemical ligation: Expanded scope by using straightforward methodology. *Proc. Natl. Acad. Sci. U.S.A.* **1999**, 96, 10068-10073.
32. Vogel, E. M.; Imperiali, B. Semisynthesis of unnatural amino acid mutants of paxillin: Protein probes for cell migration studies. *Protein Sci.* **2007**, 16, 550-556.
33. Lukovic, E.; Gonzalez-Vera, J. A.; Imperiali, B. Recognition-domain focused chemosensors: Versatile and efficient reporters of protein kinase activity. *J. Am. Chem. Soc.* **2008**, 130, 12821-12827.
34. Zhang, J. H.; Chung, T. D.; Oldenburg, K. R. A Simple Statistical Parameter for Use in Evaluation and Validation of High Throughput Screening Assays. *J. Biomol. Screen.* **1999**, 4, 67-73.
35. Abramczyk, O.; Rainey, M. A.; Barnes, R.; Martin, L.; Dalby, K. N. Expanding the repertoire of an ERK2 recruitment site: cysteine footprinting identifies the D-recruitment site as a mediator of Ets-1 binding. *Biochemistry* **2007**, 46, 9174-9186.

36. Asthagiri, A. R.; Horwitz, A. F.; Lauffenburger, D. A. A rapid and sensitive quantitative kinase activity assay using a convenient 96-well format. *Anal. Biochem.* **1999**, *269*, 342-347.
37. Webb, D. J.; Donais, K.; Whitmore, L. A.; Thomas, S. M.; Turner, C. E.; Parsons, J. T.; Horwitz, A. F. FAK-Src signalling through paxillin, ERK and MLCK regulates adhesion disassembly. *Nat. Cell Biol.* **2004**, *6*, 154-161.
38. Ishibe, S.; Joly, D.; Liu, Z. X.; Cantley, L. G. Paxillin serves as an ERK-regulated scaffold for coordinating FAK and Rac activation in epithelial morphogenesis. *Mol. Cell* **2004**, *16*, 257-267.
39. Cheng, C.; Kong, X.; Wang, H.; Gan, H.; Hao, Y.; Zou, W.; Wu, J.; Chi, Y.; Yang, J.; Hong, Y.; Chen, K.; Gu, J. Trihydrophobin 1 Interacts with PAK1 and Regulates ERK/MAPK Activation and Cell Migration. *J. Biol. Chem.* **2009**, *284*, 8786-8796.
40. Astriab-Fisher, A.; Sergueev, D.; Fisher, M.; Shaw, B. R.; Juliano, R. L. Conjugates of antisense oligonucleotides with the Tat and antennapedia cell-penetrating peptides: effects on cellular uptake, binding to target sequences, and biologic actions. *Pharm. Res.* **2002**, *19*, 744-754.
41. Nori, A.; Jensen, K. D.; Tijerina, M.; Kopeckova, P.; Kopecek, J. Tat-conjugated synthetic macromolecules facilitate cytoplasmic drug delivery to human ovarian carcinoma cells. *Bioconjugate Chem.* **2003**, *14*, 44-50.
42. Zhao, M.; Kircher, M. F.; Josephson, L.; Weissleder, R. Differential conjugation of tat peptide to superparamagnetic nanoparticles and its effect on cellular uptake. *Bioconjugate Chem.* **2002**, *13*, 840-844.
43. Lewin, M.; Carlesso, N.; Tung, C. H.; Tang, X. W.; Cory, D.; Scadden, D. T.; Weissleder, R. Tat peptide-derivatized magnetic nanoparticles allow in vivo tracking and recovery of progenitor cells. *Nat. Biotechnol.* **2000**, *18*, 410-414.
44. Torchilin, V. P.; Rammohan, R.; Weissig, V.; Levchenko, T. S. TAT peptide on the surface of liposomes affords their efficient intracellular delivery even at low temperature and in the presence of metabolic inhibitors. *Proc. Natl. Acad. Sci. U.S.A.* **2001**, *98*, 8786-8791.
45. Fawell, S.; Seery, J.; Daikh, Y.; Moore, C.; Chen, L. L.; Pepinsky, B.; Barsoum, J. Tat-mediated delivery of heterologous proteins into cells. *Proc. Natl. Acad. Sci. U.S.A.* **1994**, *91*, 664-668.
46. Schwarze, S. R.; Ho, A.; Vocero-Akbani, A.; Dowdy, S. F. In vivo protein transduction: Delivery of a biologically active protein into the mouse. *Science* **1999**, *285*, 1569-1572.
47. Green, M.; Loewenstein, P. M. Autonomous functional domains of chemically synthesized human immunodeficiency virus tat trans-activator protein. *Cell* **1988**, *55*, 1179-1188.
48. Frankel, A. D.; Pabo, C. O. Cellular uptake of the tat protein from human immunodeficiency virus. *Cell* **1988**, *55*, 1189-1193.
49. Joliot, A.; Prochiantz, A. Transduction peptides: from technology to physiology. *Nat. Cell Biol.* **2004**, *6*, 189-196.
50. Wagstaff, K. M.; Jans, D. A. Protein transduction: cell penetrating peptides and their therapeutic applications. *Curr. Med. Chem.* **2006**, *13*, 1371-1387.
51. Stewart, K. M.; Horton, K. L.; Kelley, S. O. Cell-penetrating peptides as delivery vehicles for biology and medicine. *Org. Biomol. Chem.* **2008**, *6*, 2242-2255.

52. Jones, S. W.; Christison, R.; Bundell, K.; Voyce, C. J.; Brockbank, S. M.; Newham, P.; Lindsay, M. A. Characterisation of cell-penetrating peptide-mediated peptide delivery. *Br. J. Pharmacol.* **2005**, *145*, 1093-1102.
53. Bao, W. J.; Gao, Y. G.; Chang, Y. G.; Zhang, T. Y.; Lin, X. J.; Yan, X. Z.; Hu, H. Y. Highly efficient expression and purification system of small-size protein domains in *Escherichia coli* for biochemical characterization. *Protein Expr. Purif.* **2006**, *47*, 599-606.
54. Hammarstrom, M.; Woestenenk, E. A.; Hellgren, N.; Hard, T.; Berglund, H. Effect of N-terminal solubility enhancing fusion proteins on yield of purified target protein. *J. Struct. Funct. Genomics* **2006**, *7*, 1-14.
55. Casey, P. J.; Seabra, M. C. Protein prenyltransferases. *J. Biol. Chem.* **1996**, *271*, 5289-5292.
56. Long, S. B.; Casey, P. J.; Beese, L. S. Reaction path of protein farnesyltransferase at atomic resolution. *Nature* **2002**, *419*, 645-650.
57. Lane, K. T.; Beese, L. S. Thematic review series: lipid posttranslational modifications. Structural biology of protein farnesyltransferase and geranylgeranyltransferase type I. *J. Lipid Res.* **2006**, *47*, 681-699.
58. Zhang, F. L.; Casey, P. J. Protein prenylation: molecular mechanisms and functional consequences. *Annu. Rev. Biochem.* **1996**, *65*, 241-269.
59. Casey, P. J. Protein lipidation in cell signaling. *Science* **1995**, *268*, 221-225.
60. Leever, S. J.; Paterson, H. F.; Marshall, C. J. Requirement for Ras in Raf activation is overcome by targeting Raf to the plasma membrane. *Nature* **1994**, *369*, 411-414.
61. Moissoglu, K.; Slepchenko, B. M.; Meller, N.; Horwitz, A. F.; Schwartz, M. A. In vivo dynamics of Rac-membrane interactions. *Mol. Biol. Cell* **2006**, *17*, 2770-2779.
62. Mayer, G.; Heckel, A. Biologically active molecules with a "light switch". *Angew. Chem. Int. Ed. Engl.* **2006**, *45*, 4900-4921.
63. Lawrence, D. S. The preparation and in vivo applications of caged peptides and proteins. *Curr. Opin. Chem. Biol.* **2005**, *9*, 570-575.
64. Bochet, C. G. Photolabile protecting groups and linkers. *J. Chem. Soc. Perkin Trans 1* **2002**, 125-142.
65. Rothman, D. M.; Petersson, E. J.; Vazquez, M. E.; Brandt, G. S.; Dougherty, D. A.; Imperiali, B. Caged phosphoproteins. *J. Am. Chem. Soc.* **2005**, *127*, 846-847.
66. Rothman, D. M.; Vazquez, E. M.; Vogel, E. M.; Imperiali, B. General method for the synthesis of caged phosphopeptides: Tools for the exploration of signal transduction pathways. *Org. Lett.* **2002**, *4*, 2865-2868.
67. Rothman, D. M.; Vazquez, M. E.; Vogel, E. M.; Imperiali, B. Caged phospho-amino acid building blocks for solid-phase peptide synthesis. *J. Org. Chem.* **2003**, *68*, 6795-6798.
68. Vazquez, M. E.; Nitz, M.; Stehn, J.; Yaffe, M. B.; Imperiali, B. Fluorescent caged phosphoserine peptides as probes to investigate phosphorylation-dependent protein associations. *J. Am. Chem. Soc.* **2003**, *125*, 10150-10151.
69. Nguyen, A.; Rothman, D. M.; Stehn, J.; Imperiali, B.; Yaffe, M. B. Caged phosphopeptides reveal a temporal role for 14-3-3 in G1 arrest and S-phase checkpoint function. *Nat. Biotechnol.* **2004**, *22*, 993-1000.
70. Nandy, S. K.; Agnes, R. S.; Lawrence, D. S. Photochemically-activated probes of protein-protein interactions. *Org. Lett.* **2007**, *9*, 2249-2252.
71. Veldhuyzen, W. F.; Nguyen, Q.; McMaster, G.; Lawrence, D. S. A light-activated probe of intracellular protein kinase activity. *J. Am. Chem. Soc.* **2003**, *125*, 13358-13359.

72. Wang, Q.; Dai, Z.; Cahill, S. M.; Blumenstein, M.; Lawrence, D. S. Light-regulated sampling of protein tyrosine kinase activity. *J. Am. Chem. Soc.* **2006**, 128, 14016-14017.
73. Lemke, E. A.; Summerer, D.; Geierstanger, B. H.; Brittain, S. M.; Schultz, P. G. Control of protein phosphorylation with a genetically encoded photocaged amino acid. *Nat. Chem. Biol.* **2007**, 3, 769-772.
74. Kemp, D. S.; Kerkman, D. J.; Leung, S. L.; Hanson, G. Intramolecular O,N-Acyl Transfer Via Cyclic Intermediates of 9 and 12 Members - Models for Extensions of the Amine Capture Strategy for Peptide-Synthesis. *J. Org. Chem.* **1981**, 46, 490-498.
75. Vila-Perello, M.; Hori, Y.; Ribo, M.; Muir, T. W. Activation of protein splicing by protease- or light-triggered O to N acyl migration. *Angew. Chem. Int. Ed. Engl.* **2008**, 47, 7764-7767.
76. Taniguchi, A.; Sohma, Y.; Kimura, M.; Okada, T.; Ikeda, K.; Hayashi, Y.; Kimura, T.; Hirota, S.; Matsuzaki, K.; Kiso, Y. "Click peptide" based on the "o-acyl isopeptide method": control of A beta1-42 production from a photo-triggered A beta1-42 analogue. *J. Am. Chem. Soc.* **2006**, 128, 696-697.
77. Coin, I.; Dolling, R.; Krause, E.; Bienert, M.; Beyermann, M.; Sferdean, C. D.; Carpino, L. A. Depsipeptide methodology for solid-phase peptide synthesis: circumventing side reactions and development of an automated technique via depsidipeptide units. *J. Org. Chem.* **2006**, 71, 6171-6177.
78. Fernandes, N.; Bailey, D. E.; Vanvraken, D. L.; Allbritton, N. L. Use of docking peptides to design modular substrates with high efficiency for mitogen-activated protein kinase extracellular signal-regulated kinase. *ACS Chem. Biol.* **2007**, 2, 665-673.
79. Shults, M. D.; Imperiali, B. Versatile Fluorescence Probes of Protein Kinase Activity. *J. Am. Chem. Soc.* **2003**, 125, 14248-14249.
80. SigmaPlot 2004 for Windows, v. 9.01; Systat Software, Inc.: San Jose, CA., SigmaPlot 2004 for Windows, v. 9.01; Systat Software, Inc.: San Jose, CA.
81. Segel, I. H. *Enzyme kinetics: behavior and analysis of rapid equilibrium and steady state enzyme systems*. Wiley: New York, 1975; p xxii, 957 p.
82. Ji, L.; Lim, J.; Danuser, G. Fluctuations of intracellular forces during cell protrusion. *Nat. Cell Biol.* **2008**, 10, 1393-1400.
83. Ellman, J.; Mendel, D.; Anthony-Cahill, S.; Noren, C. J.; Schultz, P. G. Biosynthetic method for introducing unnatural amino acids site-specifically into proteins. *Methods Enzymol* **1991**, 202, 301-336.

Chapter 5. Toward 8-Hydroxyquinoline Derivatives with Improved Photophysical Properties as Reporter Moieties for Phosphorylation

Prof. Dora Carrico-Moniz and Dr. Juan Antonio Gonzalez Vera made significant intellectual contributions to this work. Dora prepared many of the tricyclic compounds, while Juan Antonio synthesized most of the bicyclic derivatives.

A portion of the work described in this chapter has been submitted for publication: González-Vera, J. A.; Luković, E.; Imperiali, B. Synthesis of Red-Shifted 8-Hydroxyquinoline Derivatives Using Click Chemistry and Their Incorporation into Phosphorylation Chemosensors. **2009**, in press.

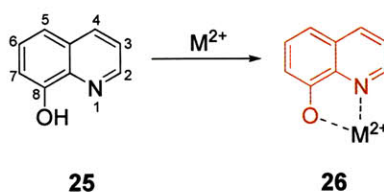
Introduction

The use of the 8-hydroxyquinoline (Oxn) derivative, 8-hydroxy-5-(*N,N*-dimethylsulfonamido)-2-methylquinoline (Sox), as a chelation-sensitive fluorophore to detect kinase activity has been quite fruitful in our laboratory. By exploiting the properties of the Sox chromophore, we have developed both sensitive and selective sensors that can report Ser/Thr and Tyr phosphorylation both *in vitro*¹⁻³ and in unfractionated cell lysates.^{4, 5} In addition, efforts toward introducing Sox-PNT, the sensor for ERK1/2 presented in Chapter 4, into cells have shown much promise. However, while the Sox chromophore has many advantageous properties for *in vitro* and cell lysate work, cellular imaging would benefit from improvement in brightness and a shift of wavelengths of excitation and emission to lower energy. Fluorophore brightness is a product of the extinction coefficient (ϵ), which measures the probability of the electronic transition, and the quantum yield (Φ), which is a measure of the efficiency with which absorbed photons are emitted. Enhanced fluorophore brightness would improve the sensitivity toward visualization of kinase activity, while red-shifted excitation and emission wavelengths would reduce photodamage to living cells and decrease background signal due to cellular autofluorescence.

In addition to phosphorylation sensing, Oxn (**25**) has also been used to signal metal ion binding^{6, 7} due to its small size and low susceptibility to photobleaching. Oxn is minimally fluorescent in aqueous solutions, but the presence of certain metal ions strongly increases its fluorescence (Scheme 5-1). Hence, this process is also known as chelation-enhanced fluorescence (CHEF). Currently, two theories explain the origin of the fluorescence change. In the first theory, the lowest electronic excited state of unbound Oxn (n to π^* transition) is non-fluorescent due to rapid intersystem crossing. Divalent metal binding alters the lowest energy

excited state to the π to π^* transition, which does not undergo intersystem crossing and is, therefore, fluorescent.⁷ However, intersystem crossing in unbound Oxn has been difficult to verify. The alternate theory proposes that photo-induced proton transfer from the phenolic hydroxyl to the quinoline nitrogen in the excited state of unbound Oxn results in fluorescence quenching.^{8, 9} Metal binding aids deprotonation of the phenolic hydroxyl (due to a significantly lowered pK_a), disrupting the quenching mechanism.¹⁰

Scheme 5-1. A General Representation of CHEF upon Divalent Metal Binding



Much work has been devoted in our laboratory to optimizing the fluorescent properties of Oxn and its derivatives. Initially, Oxn and 5-phenyl-substituted Oxn (5-PhOxn) amino acids were prepared and introduced into peptides as sensors for divalent zinc.^{11, 12} However, because of the poor photophysics of 2-methyl-8-hydroxyquinoline (2-MeOxn; $\epsilon_{\max} = 2290 \text{ M}^{-1} \text{ cm}^{-1}$ and $\Phi = 0.004$) several other electron-withdrawing substitutions at C5 and C7 were explored. Specifically, the photophysical properties of the Oxn core were dramatically altered by the addition of sulfonamide group in the 5 position giving rise to the Sox chromophore.¹³ The Sox- Zn^{2+} complex is 150 times brighter than that of the parent fluorophore, 2-MeOxn. Due to its useful photophysical properties in kinase sensing, the Sox chromophore was also transformed into a building block for Fmoc-based SPPS either as the Sox¹⁴ or C-Sox³ amino acid (Figure 5-1).

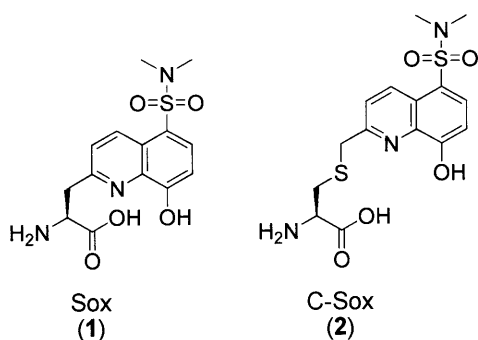


Figure 5-1. Derivatives of 8-hydroxyquinoline-based amino acids used to report kinase activity.

Additionally, the Anzenbacher laboratory has prepared numerous derivatives of Oxn with a range of excitation/emission wavelengths and quantum yields.^{15, 16} In particular, they have explored substitution in the C5 position with electron-donating or electron-withdrawing arylethynyl and aryl groups. These studies demonstrate that electron-withdrawing groups (EWGs) result in an overall hypsochromic shift and increased quantum yield. Conversely, electron-donating groups (EDGs) sometimes display large bathochromic shifts, which are always accompanied with reduced quantum yield. When complexed with Al^{3+} (Alq_3 , $q = \text{Oxn}$ derivative), the largest red-shift is observed with dimethylamino-substituted Oxn ($\lambda_{\text{ex}} = 422$ nm, $\lambda_{\text{em}} = 612$ nm) compared to Oxn ($\lambda_{\text{ex}} = 388$ nm, $\lambda_{\text{em}} = 526$ nm).¹⁷ However, a drastic decrease in quantum yield ($\Phi = 0.008$ and 0.171 for dimethylamino-Oxn and Oxn, respectively) is also observed. Derivatives with acetylene spacers follow the same trends.^{17, 18}

To expand the scope of these sensors toward visualizing kinase activities in living cells, the photophysical properties of the chemosensor should ideally be manipulated to shift the excitation and the emission wavelengths of the quinoline reporter to longer, lower energy wavelengths, while retaining high quantum yield. The irradiation of such fluorophores would cause less photodamage to biological systems, and the use of longer wavelengths would mitigate problems with high background signals that commonly complicate in cellulo studies. Finally, the

addition of another distinctly colored chromophore could potentially allow simultaneous visualization of activities among multiple kinases.

Toward that goal, herein we describe studies on the chemical modification of the 8-hydroxyquinoline (Oxn) moiety in order to develop it as a building block for the assembly of new phosphorylation sensors that employ CHEF. In the extended aromatic systems the π - π^* gap would be reduced,¹⁹ thereby resulting in longer excitation and emission wavelength maxima. We present a systematic modification of the quinoline moiety by expanding conjugation with additional aromatic rings or moieties with multiple bonds. Unfortunately, the majority of derivatives did not show improved wavelengths or quantum yields compared to Sox. On the other hand, incorporation of p-bromophenyl-substituted triazole into the 5 position of Oxn (Clk), via click chemistry,²⁰ resulted in a significant red shift in the excitation (15 nm) and emission (40 nm) maxima while retaining a useful quantum yield (0.111). When the Clk fluorophore was attached onto peptidyl kinase substrates through alkylation of the cysteine residue side chain (C-Clk (**27**)) (Figure 5-2), it was shown to be an efficient reporter of MK2 activity when compared to the existing C-Sox-based MK2 probe. Together, these results extend the utility range of kinase sensors that employ chelation-enhanced fluorescence (CHEF) and provide new chemical approaches for expanding the scope of these important reagents.

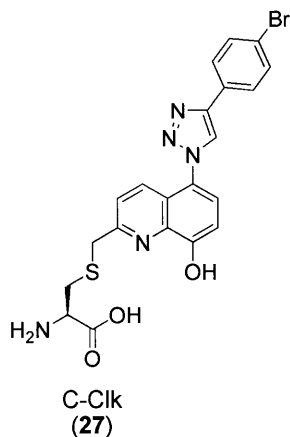
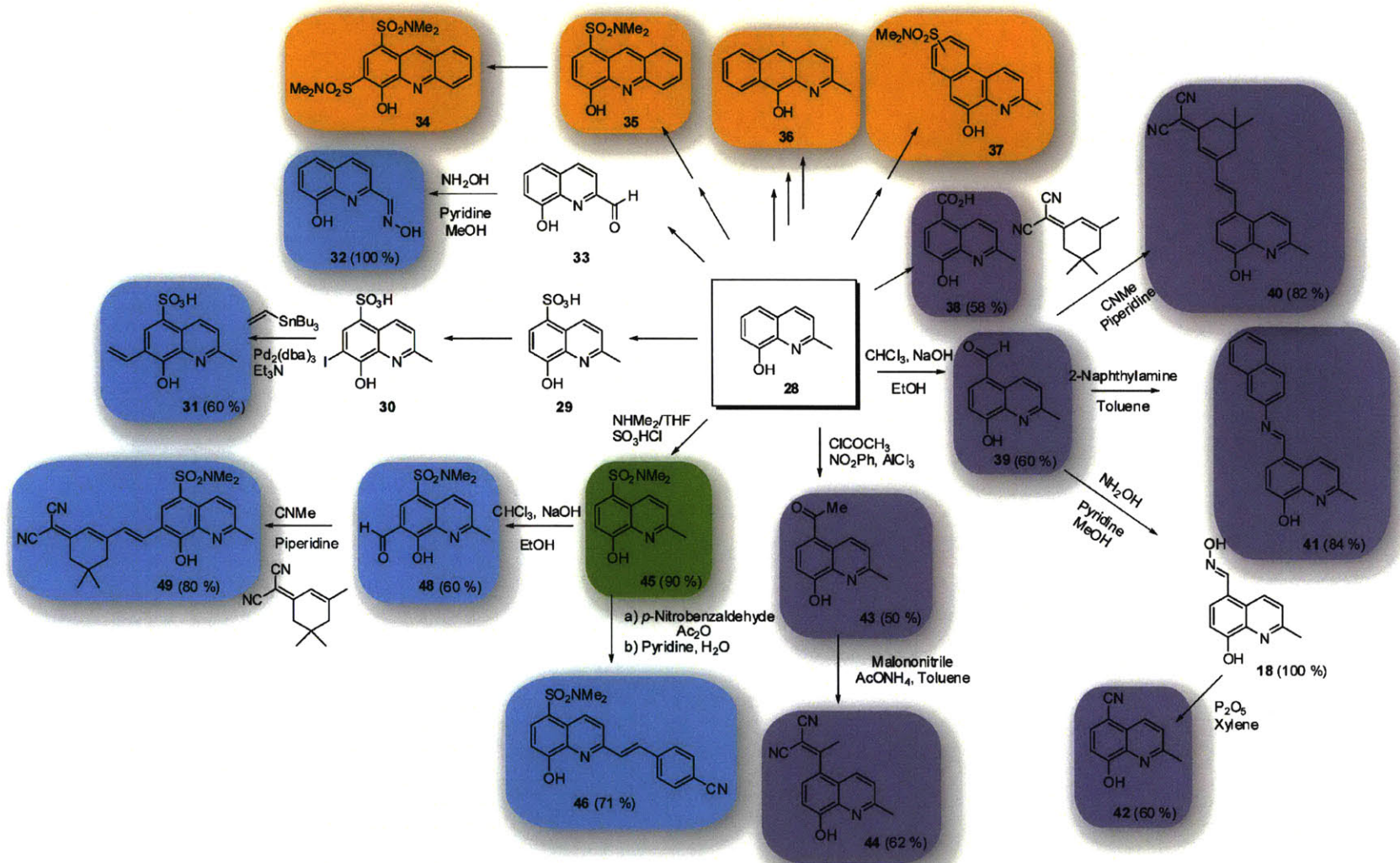


Figure 5-2. The novel C-Clk amino acid based on the Oxn core.

Results and Discussion

More than 20 compounds were synthesized (Scheme 5-2) and evaluated. They can be grouped into two general classes based on the quinoline core: 1. Fused tricyclic chromophores, and 2. 2-, 5- or 7-substituted bicyclics. The synthesis of these was largely performed by Drs. Dora Carrico-Moniz and Juan Antonio Gonzalez Vera, thus their synthetic characterization will not be provided in this document, as they are reported elsewhere. However, the general photophysical properties will be shown.

Scheme 5-2. Synthesis and Chemical Structures of Oxn Derivatives^a



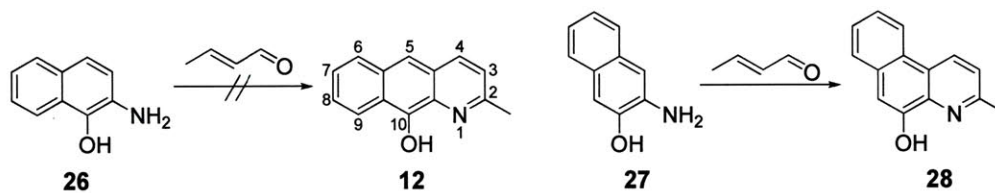
^a The chromophores are colored-coded: Sox (green), tricycles (orange), and 5-substituted (purple) and 2- and 7-substituted (blue) bicycles.

Fused Tricyclic Derivatives of Oxn

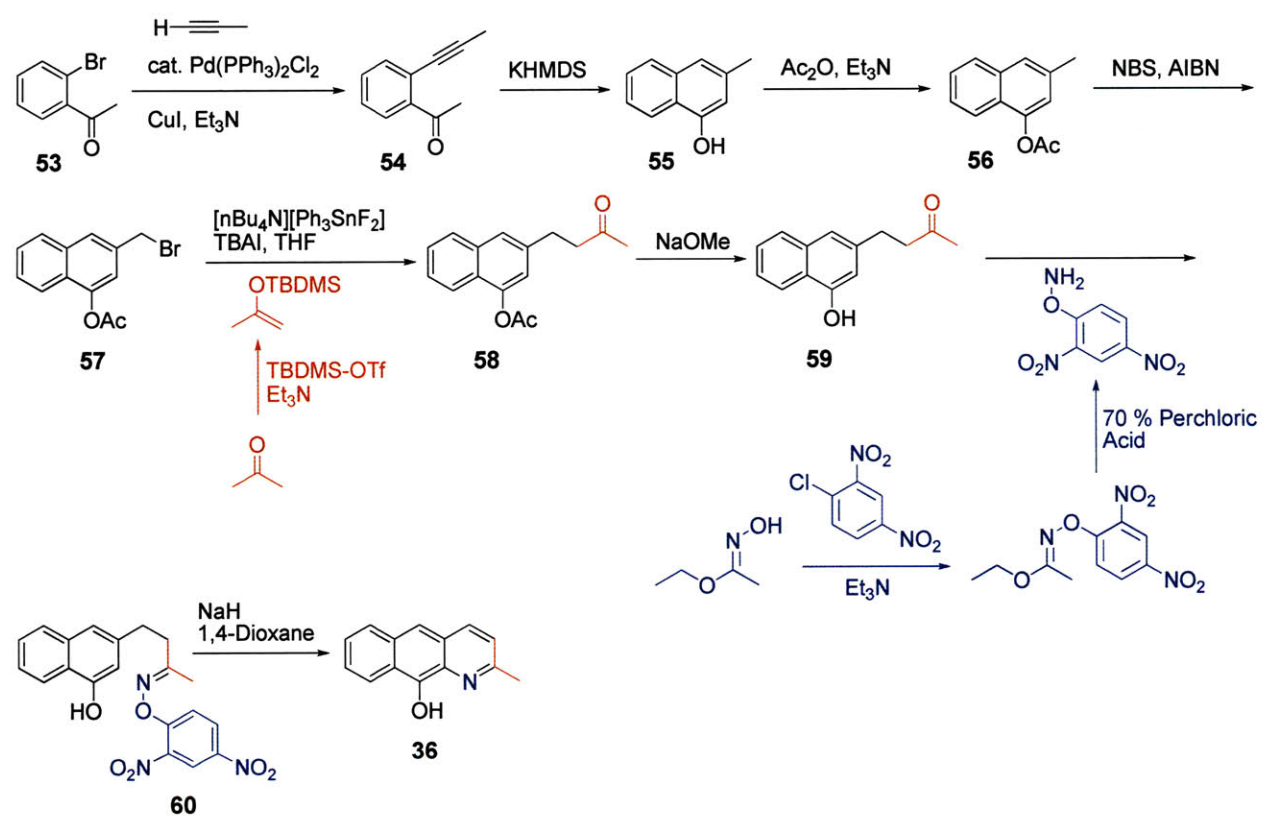
Most compounds were prepared using 1- or 2-step transformations from Oxn or one of its derivatives (Scheme 5-2). A notable exception is the tricyclic 10-hydroxy-2-methylbenzoquinoline (BOxn; **36**) (Scheme 5-3). Initial efforts toward the construction of this system using the well known Skraup/Dobner-von Miller reaction^{21, 22} were unsuccessful, even though the reaction afforded a related compound **52** (Scheme 5-3a) in modest yield. Thus, three other routes were considered. First, the Narasaka group published several reports of quinoline synthesis through oxime intermediates (**60**).²³⁻²⁶ Following this approach, the synthesis was mapped out to contain at least 11 linear steps that included a problematic alkylation of acetone (Scheme 5-3b). The Combes synthesis^{21, 27} was also considered, but it would have yielded a product with the undesirable C4 substitution (**62**) (Scheme 5-3c). Finally, BOxn (**36**) was successfully accessed through the fourth option, the Friedlander method of quinoline synthesis,^{28, 29} that required a 6-step sequence by Dr. Carrico-Moniz (Scheme 5-3d).

Scheme 5-3. Synthesis of BOxn using a) the Skraup Reaction, b) Oxime Chemistry, c) the Combes Synthesis or d) the Friedlander Method

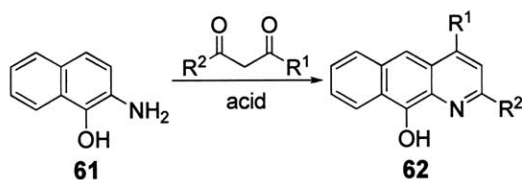
a) Skraup



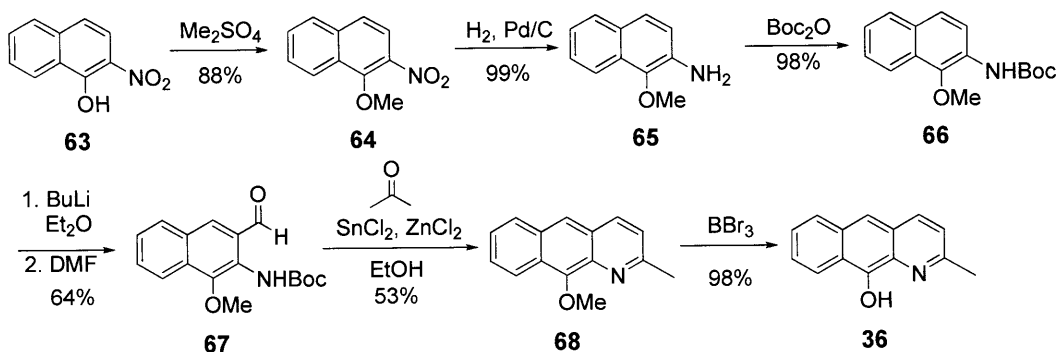
b) Oxine



c) Combes

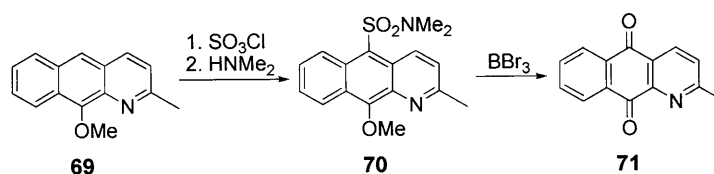


d) Friedlander



When compared to the parent compound **28** (Oxn: $\lambda_{em} = 360$ nm, $\lambda_{ex} = 530$ nm), BOxn (**36**) displayed greatly shifted excitation and emission wavelengths (460 nm and 590 nm, respectively). However, the fluorescence intensity was 10-fold lower. Since sulfonamide-substitution had substantially increased fluorescence intensity of the parent Oxn (**36**) molecule in our previous studies,¹³ sulfonamidation was also attempted on the tricyclic system. Unfortunately, while this moiety can be installed in the 5 position of the methyl-protected alcohol BOxn derivative **70**, upon deprotection the sulfonamide efficiently eliminated and the benzoquinoline oxidized to the corresponding quinone **71** (Scheme 5-4).

Scheme 5-4. Installation of Dimethylsulfonamide and Oxidation to Quinone upon Methoxy Deprotection



We also prepared several 9-hydroxy-acridine derivatives bearing the sulfonamide substitution in either the 6 or the 6 and 8 positions, compounds **35** and **34**, respectively in Scheme 5-2. Similarly to BOxn, acridine-based derivatives displayed red-shifted wavelengths, but greatly reduced fluorescence intensities when compared to Sox (Figure 5-3).

Bicyclic Derivatives of Oxn

Our attention was next directed toward the synthesis and photophysical evaluation of modified bicyclic derivatives. Most of the new compounds followed the trend observed with the tricyclic system: extension of wavelengths resulted in compromised brightness of the fluorophore (Figure 5-3). Photophysical properties of several of the more notable chromophores are summarized in Table 5-1. Indeed, only the aldehyde-substituted chromophore **39** showed an improved quantum yield, measured by standard methods.¹⁷ Nonetheless, this derivative was not appropriate for further studies since it exhibited shorter λ_{em} , and the easily oxidized aldehyde group was predicted to limit its use in biological systems.

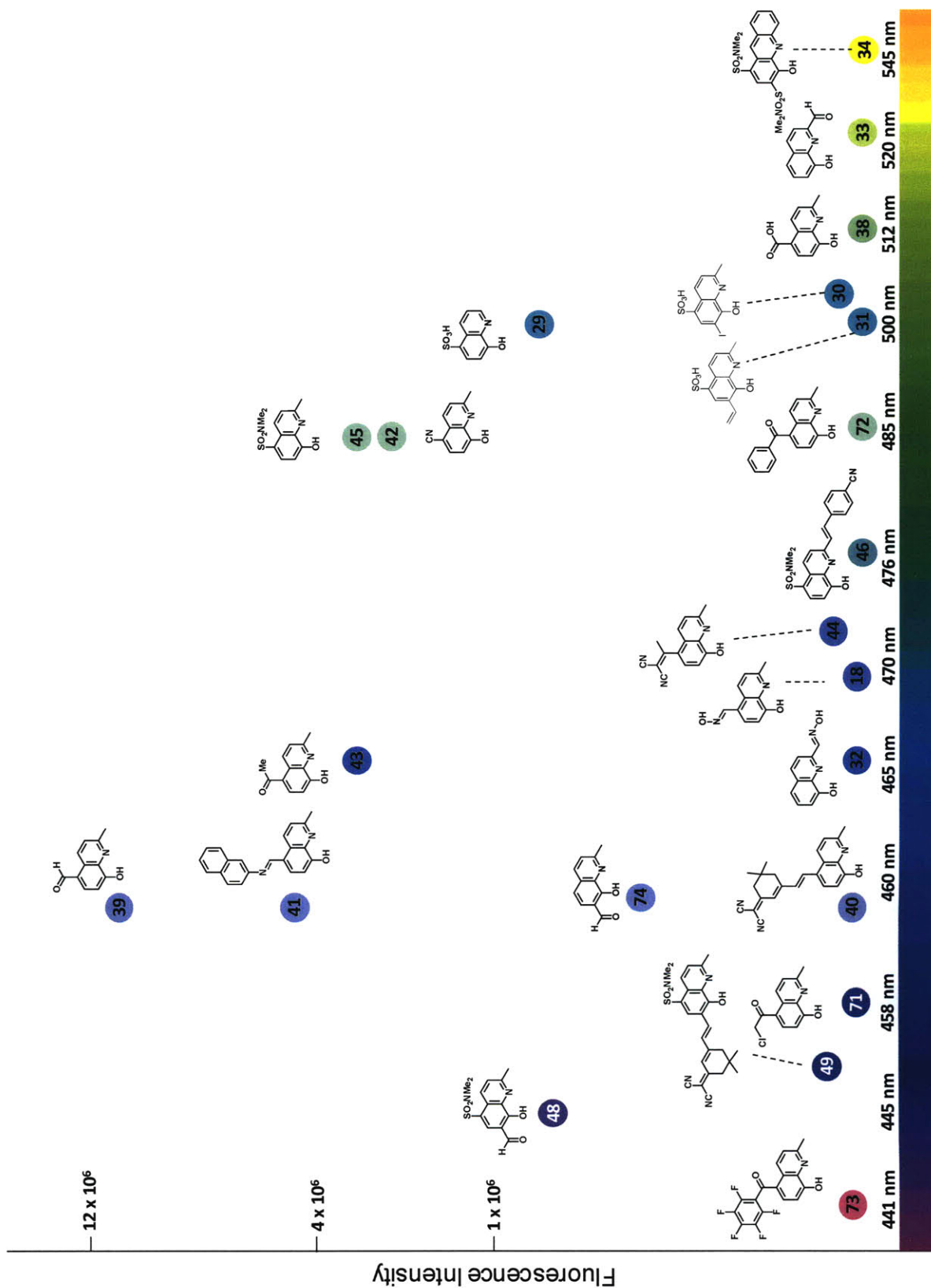
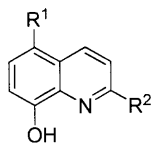


Figure 5-3. Visual comparison of emission wavelengths and fluorescence intensity for some Oxn derivatives (1.66 μM) when complexed with Mg^{2+} (242 mM).

Table 5-1. Relevant Spectroscopic Data for Selected Oxn Derivatives that Form Fluorescent Complexes with Mg²⁺



Compound	R ¹	R ²	λ_{ex} (nm)	λ_{em} (nm)	$\Phi^{a,b}$
45^c	SO ₂ N(CH ₃) ₂	CH ₃	360	485	0.342
39	CHO	CH ₃	373	460	0.597
42	CN	CH ₃	362	485	0.276
43	COCH ₃	CH ₃	370	465	0.168
72	COCH ₂ Cl	CH ₃	373	460	0.034
38	CO ₂ H	CH ₃	362	505	0.004
73	CO-Ph	H	375	485	0.002

^a Spectra were acquired in 150 mM NaCl, 50 mM HEPES (pH 7.4), 25 °C with 10 μ M **1-7** and 10 mM MgCl₂. ^b Excitation of all species is provided at λ_{max} (355-425 nm). Quantum yields were calculated with reference to a quinine sulphate standard (in 0.05 M H₂SO₄). ^c Extinction coefficient: $\epsilon_{355} = 8,247 \text{ cm}^{-1} \text{ M}^{-1}$.

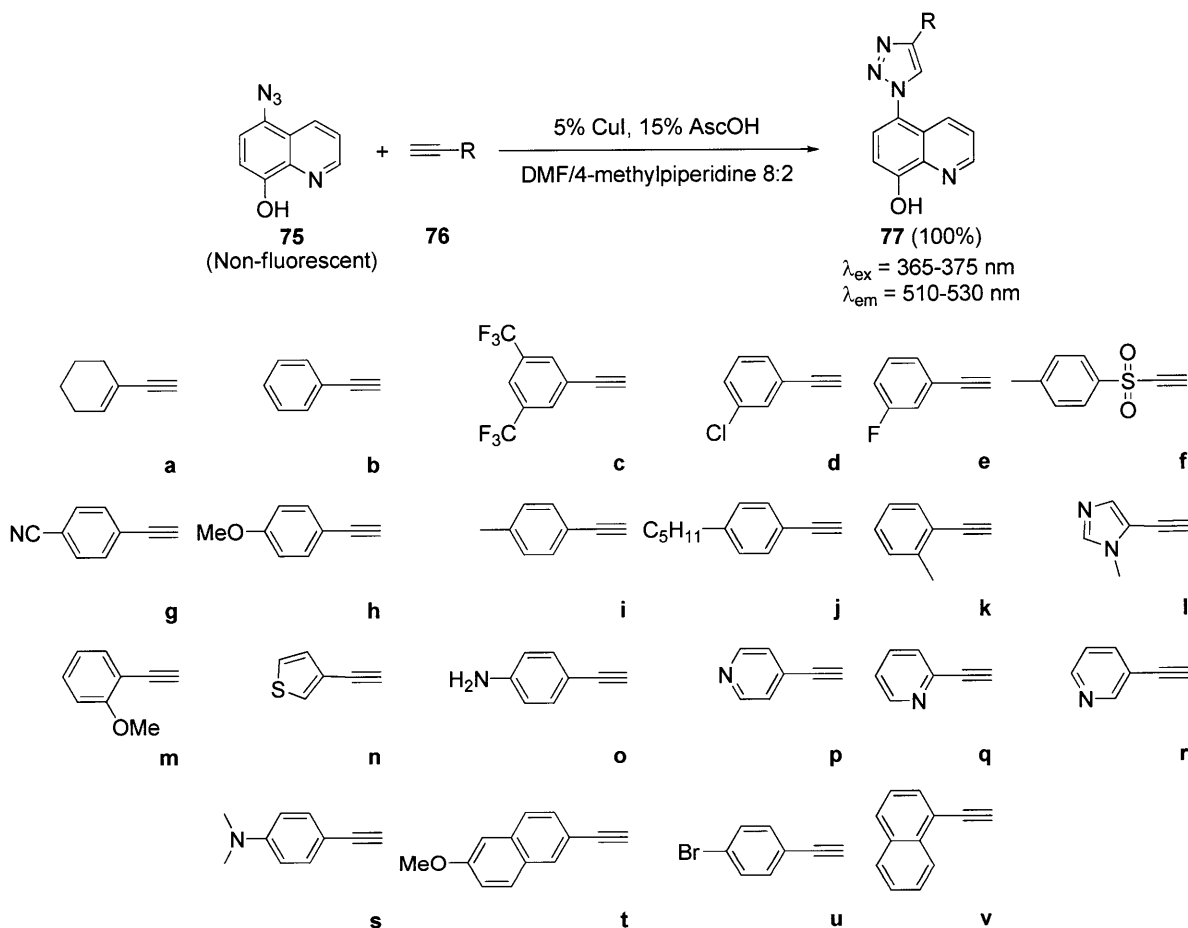
Synthesis and Screening of Triazole-substituted Oxn Derivatives

In light of these findings, we decided to focus on 8-hydroxyquinoline derivatives with triazole substitution at position 5. The triazole ring is a versatile and readily installed linkage that has been used to extend the conjugation of diverse aromatic systems.^{30, 31} Therefore, we envisioned that azide substitution at position 5 of the hydroxyquinoline would provide a non-fluorescent intermediate that could be readily subject to 1,3-dipolar cycloaddition with a variety of terminal alkynes using the Cu(I)-catalyzed Huisgen reaction.^{20, 32}

For this purpose azide **75** was prepared using previously reported methods (Scheme 5-5).³³ As expected, **75** showed no fluorescence due to the quenching effect from the electron-rich azido group.³⁰ In the presence of catalytic Cu(I) and ascorbic acid **75** reacts readily at room temperature with 1-ethynylcyclohexene (**76a**) in DMF/4-methylpiperidine (8:2) to afford the cycloaddition product **77a** in excellent yield. Quinoline **77a** has a λ_{ex} of 371 nm and a λ_{em} of 522 nm due to the elimination of azide quenching after formation of the triazole ring. Despite the

poor quantum yield ($\Phi = 0.033$), this initial result encouraged us to screen for improved fluorescence properties of the triazole substituted quinolines by investigating the properties of products from the 1,3-dipolar cycloaddition reaction of **75** with 21 additional alkynes (**76b-v**).

Scheme 5-5. 1,3-Dipolar Cycloaddition Reactions of **75** with **76a-v**



The cycloaddition reactions were generally complete in 12 h at room temperature and were monitored by TLC and mass spectrometry. The formation of the fluorescent triazole derivatives could be easily established upon exposure to a hand-held UV lamp ($\lambda_{\text{ex}} = 365\text{ nm}$). The fluorophores were then qualitatively compared in a 96-well plate format (transilluminator; $\lambda_{\text{ex}} = 365\text{ nm}$) to identify promising compounds (Figure 5-4) and were further subjected to

quantitative analysis in a fluorescence plate reader (see the Experimental Methods). The excitation and emission wavelengths of the triazole products (**77b-v**, $\lambda_{\text{ex}} = 360\text{-}375\text{ nm}$, $\lambda_{\text{em}} = 510\text{-}530\text{ nm}$) were improved compared to those for Sox (**45**, $\lambda_{\text{ex}} = 360\text{ nm}$, $\lambda_{\text{em}} = 485\text{ nm}$, $\Phi = 0.342$, $\epsilon_{355} = 8,247\text{ cm}^{-1}\text{ M}^{-1}$). Based on the preliminary screening, selected targets were then synthesized in larger quantities and the quantum yields of the corresponding hydroxyquinoline derivatives were determined. Compared to **77a** ($\Phi = 0.033$) a 3.5-fold improvement in quantum yield was obtained in the case of the bromide **77u** ($\lambda_{\text{ex}} = 375\text{ nm}$, $\lambda_{\text{em}} = 525\text{ nm}$, $\Phi = 0.111$, $\epsilon_{355} = 7,905\text{ cm}^{-1}\text{ M}^{-1}$). In view of the fluorescent properties of this derivative, we chose to use it as a chelation-sensitive fluorophore to prepare probes for mitogen-activated protein kinase-activated protein kinase-2 (MK2),³⁴ and sarcoma kinase (Src),³⁵⁻³⁷ used as models of Ser/Thr and Tyr kinases, respectively. For the purposes of comparison, the analogous fluorescent peptides containing the original Sox chromophore were also prepared as previously described.³

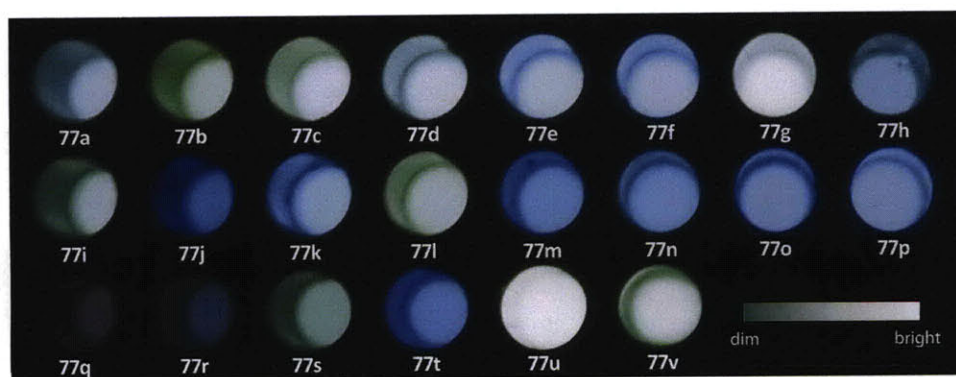


Figure 5-4. Qualitative comparison of emission wavelengths of **77a-v**. The colors shown here do not represent the true fluorescent wavelengths (shown in the Supporting Information). The fluorophores (10 μM dissolved in DMSO) were illuminated ($\lambda_{\text{ex}} = 365\text{ nm}$) in 50 mM HEPES (pH 7.4), 150 mM NaCl, 10 mM MgCl_2 at 25 $^\circ\text{C}$.

Synthesis and Biophysical Evaluation of Clk-based Peptidyl Kinase Substrates

The synthesis of the probes, outlined in Scheme 5-6, was performed using a strategy similar to that used for the preparation of the Sox-based recognition-domain focused (RDF) chemosensors.³ Diazotization of 5-amino-2-methylquinolin-8-ol (**52**, prepared from 8-hydroxyquinoline using literature methods)³⁸ followed by treatment of the diazonium salt with NaN₃ gave the corresponding azide **53** (66% yield). Protection of the phenolic hydroxyl group as a *tert*-butyldiphenylsilyl ether produced **54** (98%), which was then brominated under free radical conditions to afford the bromide **55** (30%). To avoid dibromination, the reaction was stopped after 20 min, thereby providing a mixture of the desired product (**55**) and the starting material (**54**), which could not be separated using standard chromatographic methods and was used in the next step without purification. Fmoc-based solid phase peptide synthesis (SPPS) was utilized to assemble the intact peptide that included an appropriately placed cysteine residue protected with monomethoxytrityl (Mmt), which is a hyper acid-labile protecting group (Scheme 5-6). After selective on-resin sulfhydryl deprotection, the free thiol was alkylated with **55**. Then a 1,3-dipolar cycloaddition reaction with 1-bromo-4-ethynylbenzene in the presence of catalytic Cu(I) gave the corresponding triazole-substituted peptide. Standard TFA cleavage from the resin and concomitant removal of all side-chain protecting groups revealed the desired chemosensor with excellent conversion to the final product (> 95%).

Scheme 5-6. Synthesis of the Clk RDF Chemosensors

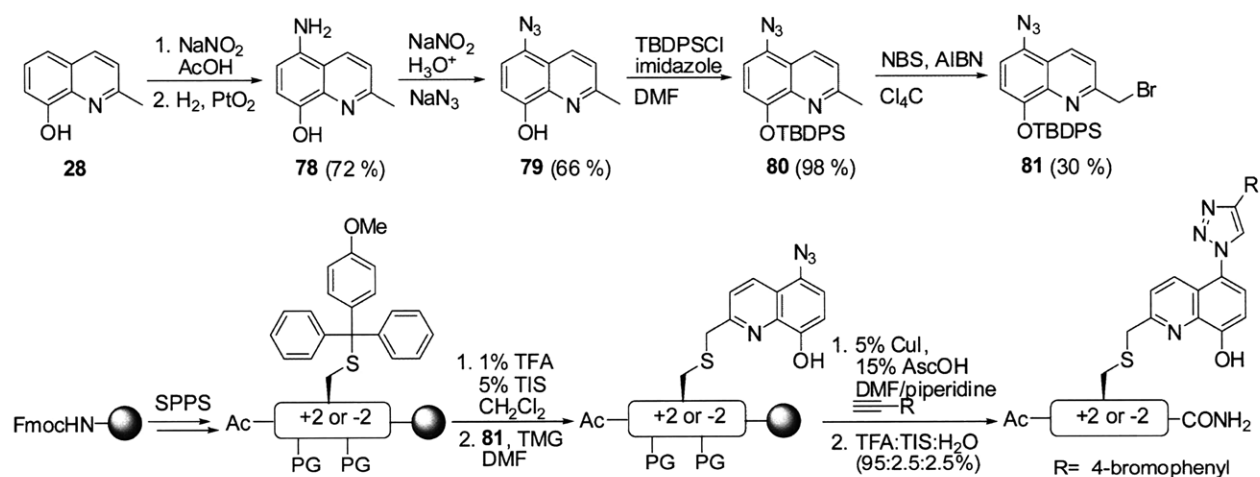


Table 5-2 shows the substrate sequences of the Sox- and click (Clk)-based RDF probes for MK2 and Src kinases, as well as the fluorescence increases that were observed with the corresponding phosphopeptides. The difference in fluorescence was determined by comparison of the fluorescence intensity at the maximum emission wavelength (485 nm for Sox and 525 nm for Clk) of phosphorylated and unphosphorylated peptides in the presence of Mg^{2+} . The fluorescence increases of the click peptides are between 2- and 2.5-fold, which are still significant changes that are useful in enzymatic assays (*vide infra*). More specifically, the click-based RDF peptides exhibited larger fluorescence increases than the Sox-based RDF peptides in the case of Src (entries 3 and 4) while this trend is reversed in the case of MK2 (entries 1 and 2).

Table 5-2. Substrate Sequences of the RDF Chemosensors and Their Fluorescence Increases

Entry	Name	Target kinase	Location of the chromophore ^a	Peptide Sequence ^b	Fold Fluorescence Increase ^c
1	P1	MK2	C	Ac-AH <u>LQRQLS</u> *I-C(Sox)-HH-CONH ₂	4.4 ± 0.2
2	P2	MK2	C	Ac-AH <u>LQRQLS</u> *I-C(Clk)-HH-CONH ₂	2.1 ± 0.3
3	P3	Src	N	Ac-AEE-C(Sox)-IY* <u>GEFEAKKKK</u> -CONH ₂	2.0 ± 0.1
4	P4	Src	N	Ac-AEE-C(Clk)-IY* <u>GEFEAKKKK</u> -CONH ₂	2.4 ± 0.2

^a Location determined in reference to the chromophore. C denotes C-terminus and N stands for N-terminus. ^b Asterisk (*) denotes the residue that is phosphorylated. In cases where it has been determined, residues important in kinase recognition are underlined. ^c Measured in triplicate as a quotient of fluorescence intensity at 485 nm (for Sox peptides) or 525 nm (for Clk peptides) of phosphopeptide and substrate in 20 mM HEPES (pH 7.4), 10 mM MgCl₂, and 10 μM peptide (for Sox peptides $\lambda_{\text{ex}} = 360$ nm; for Clk peptides $\lambda_{\text{ex}} = 375$ nm).

As an example, Figure 5-5a shows a comparison between the fluorescence spectrum of the synthetically-obtained phosphopeptide MK2(Sox) [**P1**] and that of the analogous MK2(Clk) [**P2**]. The results were essentially the same for the Src sensors (see the Experimental Methods). Neither species was fluorescent at pH 7.0 (50 mM HEPES, 150 mM NaCl) in the absence of the metal ion. Upon addition of Mg²⁺ the fluorescence spectra of Mg²⁺-bound **P1** and Mg²⁺-bound **P2** exhibited emission maxima of 485 and 525 nm, respectively, indicating a red-shift of 40 nm. On the other hand, in the corresponding excitation spectra the Mg²⁺-bound **P1** reached a maximum at 360 nm and Mg²⁺-bound **P2** emission peaked at 375 nm, representing a bathochromic shift of 15 nm.

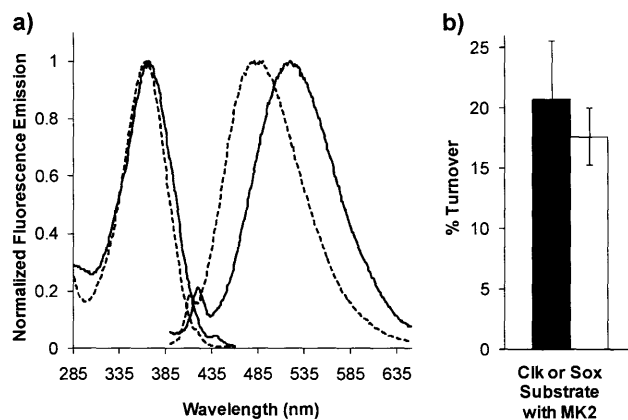


Figure 5-5. Spectral characterization and enzymatic evaluation of Clk-based substrates. (a) Fluorescence excitation and emission spectra of P1 (--) and P2 (—) with Mg^{2+} . Samples were prepared in 50 mM HEPES (pH 7.4) and 150 mM NaCl. Spectra were acquired at 25 °C and were baseline-corrected using a sample of the buffer solution. (b) Percentage of turnover of the Clk-based (■, entry 2) or Sox-based (□, entry 1) substrate with MK2 after 10 min. Assays were performed in 20 mM HEPES (pH 7.4), 10 mM $MgCl_2$, 0.1 mM EGTA, 0.01% Brij 35, 0.1 mg/mL BSA, 1 mM DTT, 1 mM ATP, 5 μ M substrate and 10 ng MK2 at 30 °C. Plotted values indicate the mean \pm s.e.m. for triplicate measurements.

Evaluation of Clk-based Substrates in Enzymatic Assays

Having validated the utility of the new fluorophore alone and in peptides through photophysical characterization, we also evaluated its efficacy in reporting kinase activity in biochemical assays. Following established protocols,³ Sox- and Clk-based substrates (entries 1 and 2, respectively, in Table 5-2) were subjected to MK2 kinase assays under identical conditions and then the overall turnover of each substrate was compared. As shown in Figure 5-5b, MK2 phosphorylated the Clk-substrate just as efficiently as the Sox-substrate indicating that the size of Clk chromophore does not adversely influence reaction kinetics. Based on previous work, which has shown that Sox-based substrates had at least comparable, if not better kinetics than parent peptides, we believe that the Clk-based reporters will also follow the same

trend for Src and other kinases. However, kinase substrate kinetics are highly empirical and, thus, new substrates will have to be experimentally evaluated. If unsuitable for the kinase of interest, the sensors can be also improved using our high-throughput, mass spectrometry-based method (Chapter 3).³⁹

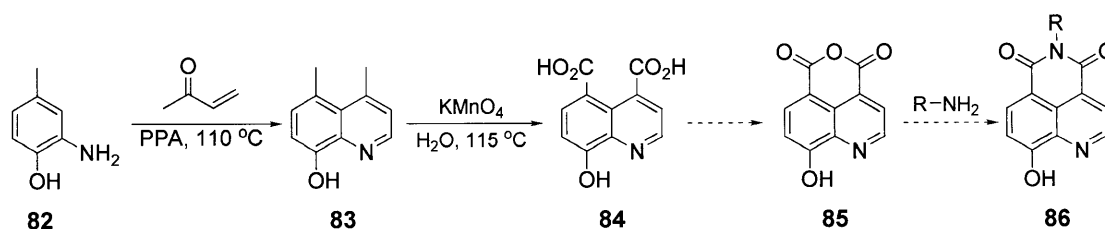
Conclusions

In conclusion, several tricyclic and bicyclic derivatives of 8-hydroxyquinoline were prepared and screened for favorable photophysical properties (e.g., extended excitation and emission wavelengths and increased quantum yield and extinction coefficient). While we were able to induce a significant bathochromic shift (e.g., with 9-hydroxy-2-methylbenzoquinoline (**36**)), in all cases this shift was accompanied by a decrease in the brightness of the chromophore. On the other hand, the extension of conjugation via triazolyl substitution of Oxn at C5 yielded encouraging fluorescent properties. We explored this avenue by synthesizing a library of 1,3-triazole-substituted 8-hydroxyquinolines (**76a-v**). Specifically, when Oxn was modified with the *p*-bromophenyl-substituted triazole (Clk, **77u**) it exhibited significant red-shifts in excitation (15 nm) and emission maxima (40 nm) when complexed to Mg²⁺ compared to Sox. The Clk chromophore was then incorporated into peptide phosphorylation chemosensors for MK2 and Src kinases. When evaluated with MK2, the chromophore does not inhibit the ability of the enzyme to recognize and phosphorylate the Clk probe, and effectively reports kinase activity. Together, these results effectively expand the potential capabilities of the hydroxyquinoline-based kinase sensing strategy.

Future Directions and Perspectives

Following the successful screening of the triazolyl-substituted Oxn library for improved chromophores, an additional platform yielding efficient access to multiple derivatives should be explored. For example, installation of a third ring, a cyclic anhydride fused in the 4 and 5 positions of Oxn, would allow us to couple a host of amines to the anhydride core (**85**), giving a library of Oxn-imide derivatives (**86**) (Scheme 5-7). Synthesis efforts toward the final product **86** have been initiated. Multiple conditions were attempted in the Skraup reaction, but only in the presence of polyphosphoric acid was the pyridine ring assembled to give **83** (Scheme 5-7). Subsequently, we were able to fully oxidize the benzylic methyl groups, but the resulting diacid **84** remains to be closed either as the anhydride **59** or by direct amine coupling to yield imide-Oxn (**86**). Access to this core would provide an opportunity to quickly construct a library of new Oxn-based derivatives that are quite different from oxines reported so far. The resulting compounds would be screened for bathochromic shifts in wavelengths and enhancement in brightness.

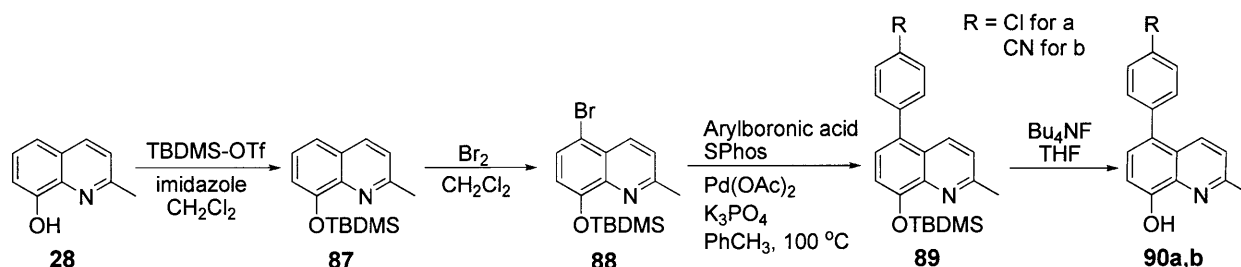
Scheme 5-7. Synthesis of an Alternative Tricyclic Core



Since the Azenbacher group reported extended excitation and emission wavelengths through the Suzuki-Miyaura coupling of EWG or EDG to the Oxn core,¹⁷ we synthesized two of those derivatives (**90a** and **90b**) (Scheme 5-8). The syntheses were done following reported protocols and the fluorescence properties of the purified products should now be tested in the

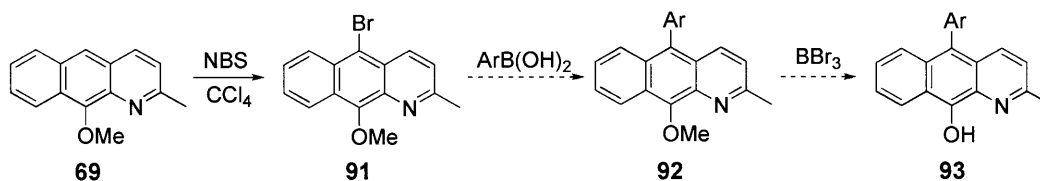
presence of Mg^{2+} . If these compounds display useful properties, fine-tuning can be achieved with numerous arylboronic acids.

Scheme 5-8. Synthesis of 5-ArylOxn Derivatives



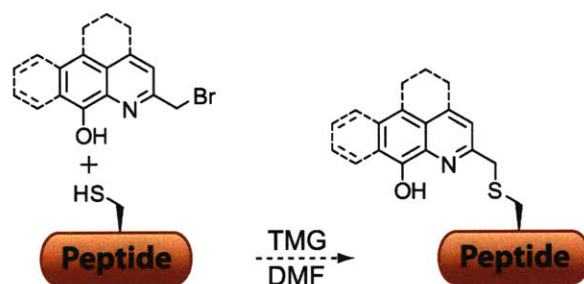
Furthermore, if arylation at C5 turns out to be a fruitful approach to improving the quantum yield for bicyclic derivatives, it should also be applied to the BOxn fluorophores. The derivatization of the 5 position of these linear tricyclic compounds was attempted with dimethylsulfonamide, but without much success due to oxidation of the middle ring to the corresponding quinone upon methoxy deprotection (Scheme 5-4). However, bromination of **69** is quite facile, thus giving a ready handle for installation of an aryl substituent through the Suzuki-Miyaura reaction (Scheme 5-9). The C-C bond at C5 should prevent quinone formation during the subsequent alcohol deprotection of **92** and may increase the quantum yield and the extinction coefficient of the target product **93**.

Scheme 5-9. Preparation of C5 Aryl-substituted BOxn



Lastly, some of the more hydrophobic Oxn derivatives should be incorporated into peptides through the previously developed on-resin cysteine alkylation (Scheme 5-10). This facile transformation will resolve the solubility problems that were encountered with a number of fluorophores and will also facilitate more accurate measurement of photophysical properties.

Scheme 5-10. Peptide Incorporation of Oxn Derivatives



Together, these derivatives should expand our arsenal of CHEF-based chromophores that could be useful in cells or in multiplexed and multi-colored kinase assays.

Acknowledgements

I am grateful to have worked with Dr. Dora Carrico-Moniz and Dr. Juan Antonio Gonzalez Vera on this project. Dora synthesized the tricyclic compounds presented here and Juan Antonio prepared various other bicyclic Oxn derivatives. I also thank Juan Antonio for providing Figure 5-2. This research was supported by the NIH Cell Migration Consortium (GM064346). I also acknowledge the Department of Chemistry Instrumentation Facility (NIH-1S10RR013886-01) and the Biophysical Instrumentation Facility (NSF-0070319).

Experimental Methods

General Information

All solvents and reagents were obtained commercially and used without further purification, unless otherwise noted. N^α-Fmoc-protected amino acids [Fmoc-Ala-OH, Fmoc-Arg(Pbf)-OH, Fmoc-Cyc(Mmt)-OH, Fmoc-Glu(OtBu)-OH, Fmoc-Gln(Trt)-OH, Fmoc-His(Trt)-OH, Fmoc-Ile-OH, Fmoc-Leu-OH, Fmoc-Lys(Boc)-OH, Fmoc-Phe-OH, Fmoc-Ser(tBu)-OH, Fmoc-Ser(PO(OBn)OH)-OH, Fmoc-Tyr(tBu)-OH, Fmoc-Tyr(PO(OBn)OH)-OH] were purchased from Novabiochem. Whenever anhydrous and/or degassed CH₂Cl₂ was necessary it was distilled from calcium hydride under an argon atmosphere. Analytical TLC was performed on silica gel 60 F₂₅₄ precoated plates (EMD Chemicals Inc.) and visualized by UV. Flash column chromatography was performed as previously described⁴⁰ using forced flow of the indicated solvent on AdTech Flash Silica Gel (32-60 μm packing, 60 Å pore diameter, Adedge Technologies). Organic solutions were concentrated *in vacuo* by rotary evaporation at ~10 Torr (house vacuum) at 25-40 °C, then at ~0.5 Torr (vacuum pump), unless otherwise indicated. Peptides were purified *via* preparative reverse-phase C18 HPLC employing a gradient of solvents A (H₂O with 0.1% v/v TFA) and B (CH₃CN with 0.1% v/v TFA). Compounds were characterized by ¹H, ¹³C NMR and mass spectrometry. Peptide purity was determined by analytical reverse-phase HPLC.

Instrumentation and Materials

NMR: ¹H and ¹³C NMR spectra were recorded on a Bruker 400 MHz Avance spectrometer. Chemical shifts (δ) are reported in parts per million (ppm) and referenced to CDCl₃ (7.26 ppm

for ^1H and 77.0 ppm for ^{13}C). Coupling constants (J) are reported in Hertz (Hz) and multiplicities are abbreviated as singlet (s), doublet (d), doublet of doublets (dd), triplet (t) and multiplet (m).

HPLC: HPLC was carried out on Waters Prep LC 4000 System or Waters Delta 600 System equipped with Waters 2487 dual wavelength absorbance detectors. Columns used: C_{18} analytical (flow rate = 1 mL/min), Beckman Ultrasphere ODS, 5 μm , 150 x 4.6 mm; C_{18} preparatory (flow rate = 15 mL/min), YMC-Pack Pro, 5 μm , 250 x 20 mm.

ESI-MS: Applied Biosystems Mariner mass spectrometer.

MALDI-TOF MS: PerSeptive Biosystems Voyager MALDI-TOF instrument.

HRMS: Provided by the Department of Chemistry Instrumentation Facility (DCIF), MIT.

UV-Vis Spectrophotometer: Shimadzu UV-2401PC.

Fluorometer: Fluoromax 3 from Jobin Yvon. Cuvette: Starna Cells (16.100F-Q-10) 100 μL sub-micro cuvette, 1 cm path length.

Fluorescence Plate Reader: HTS 7000 Bio Assay Reader from Perkin Elmer or SpectraMax GeminiXS Dual Scanning Microplate Spectrofluorometer from Molecular Devices. Plate: Corning assay plate, 96-well, half area, no lid, flat bottom, non-binding surface, non-sterile, white polystyrene.

Synthesis and Characterization of Oxine derivatives

Compounds **45**¹³, **39**⁴¹, **42**⁴¹, **43**⁴², **38**⁴³ and **73**⁴⁴ were prepared by previously described methods. Characterization of each compound was consistent with literature.

*5-Carbaldehyde-8-Hydroxy-2-methylquinoline (39)*⁴¹

Yield: 64 %, ¹H NMR (500 MHz, CDCl₃) δ ppm: 2.75 (s, 3H), 7.24 (d, *J* = 8 Hz, 1H), 7.51 (d, *J* = 8 Hz, 1H), 7.90 (d, *J* = 8 Hz, 1H), 9.51 (d, *J* = 8 Hz, 1H), 10.01 (s, 1H). ¹³C NMR (125 MHz, Cl₃CD) δ ppm: 24.6, 108.8, 123.6, 124.6, 125.4, 134.6, 137.4, 139.0, 157.4, 158.0, 191.6. HRMS (ESI): calcd for C₁₁H₉NO₂ [M + H]⁺: 188.0706, found: 188.0711.

*5-Carbonitrile-8-Hydroxy-2-methylquinoline (42)*⁴¹

Yield: 79 %, ¹H NMR (500 MHz, CDCl₃) δ ppm: 2.77 (s, 3H), 7.15 (d, *J* = 8.5 Hz, 1H), 7.52 (d, *J* = 8.5 Hz, 1H), 7.83 (d, *J* = 8.5 Hz, 1H), 8.37 (d, *J* = 8.5 Hz, 1H). ¹³C NMR (125 MHz, Cl₃CD) δ ppm: 23.7, 27.6, 106.3, 121.1, 124.5, 125.2, 134.0, 137.6, 157.0, 158.9. HRMS (ESI): calcd for C₁₁H₈N₂O [M + H]⁺: 185.0709, found: 185.0704.

*1-(8-Hydroxy-2-methylquinolin-5-yl)ethanone (43)*⁴²

Yield: 66 %, ¹H NMR (500 MHz, CDCl₃) δ ppm: 2.70 (s, 3H), 2.75 (s, 3H), 7.13 (d, *J* = 8 Hz, 1H), 7.46 (d, *J* = 9 Hz, 1H), 8.10 (d, *J* = 8 Hz, 1H), 9.45 (d, *J* = 9 Hz, 1H). ¹³C NMR (125 MHz, Cl₃CD) δ ppm: 24.5, 28.6, 108.3, 124.5, 125.0, 125.2, 133.0, 136.5, 156.0, 157.2, 199.1. HRMS (ESI): calcd for C₁₂H₁₁NO₂ [M + H]⁺: 202.0863, found: 202.0856.

2-Chloro-1-(8-hydroxy-2-methylquinolin-5-yl)ethanone (72)

Compound **72** was prepared with 2-chloroacetyl chloride following the same procedure used to obtain **43**. Yield: 71 %, ¹H NMR (500 MHz, CDCl₃) δ ppm: 2.76 (s, 3H), 4.78 (s, 2H), 7.15 (d, *J* = 8 Hz, 1H), 7.51 (d, *J* = 9 Hz, 1H), 8.06 (d, *J* = 8 Hz, 1H), 9.39 (d, *J* = 9 Hz, 1H). ¹³C NMR (125 MHz, Cl₃CD) δ ppm: 24.6, 46.9, 108.3, 121.3, 125.4, 125.5, 132.7, 135.9, 157.0, 157.7, 191.4. HRMS (ESI): calcd for C₁₂H₁₀ClNO₂ [M + H]⁺: 236.0473, found: 236.0479.

General Synthesis of the Triazolyl Derivatives 77a-v

5-Azido-8-hydroxyquinoline (**75**, 50 mg, 0.26 mmol) and the corresponding alkyne (**76a-v**) (0.26 mmol) were suspended in a 8:2 mixture of DMF/4-methylpiperidine (2 mL). Ascorbic acid (7.1 mg, 0.04 mmol) and copper iodide (2.5 mg, 0.01 mmol) were added suspended in a 8:2 mixture of dimethylformamide/4-methylpiperidine (1 mL) and the heterogeneous mixture was stirred vigorously overnight in the dark at room temperature. TLC analysis indicated complete consumption of the reactants in 12 h. The mixture was dissolved in ethyl acetate (40 mL), was washed with H₂O (5 mL), brine (5 mL), dried over Na₂SO₄, and evaporated to yield the corresponding triazolyl derivatives 10a-v.

8-Hydroxy-5-(4-cyclohexenyl-1H-1,2,3-triazol-1-yl)quinoline (77a)

1-Ethynyl-1-cyclohexene (**76a**) was used as the starting material. ¹H NMR (500 MHz, CD₃OD) δ ppm: 1.71-1.79 (m, 2H), 1.82-1.86 (m, 2H), 2.26-2.28 (m, 2H), 2.48-2.49 (m, 2H), 6.62 (m, 1H), 7.36 (d, *J* = 8.5 Hz, 1H), 7.79 (d, *J* = 8.5 Hz, 1H), 7.83 (dd, *J* = 4 and 8.5 Hz, 1H), 8.22 (s, 1H), 8.39 (d, *J* = 8.5 Hz, 1H), 9.02 (d, *J* = 4 Hz, 1H). ¹³C NMR (125 MHz, CD₃OD) δ ppm: 23.4, 23.7, 26.4, 27.5, 113.1, 123.7, 124.7, 126.0, 126.6, 127.0, 127.7, 128.3, 136.0, 137.4, 148.6, 150.9, 154.4. HRMS (ESI): calcd for C₁₇H₁₆N₄O [M + H]⁺: 293.1397, found: 293.1394.

8-Hydroxy-5-(4-phenyl-1H-1,2,3-triazol-1-yl)quinoline (77b)

Ethynylbenzene (**76b**) was used as the starting material. ¹H NMR (500 MHz, CD₃OD) δ ppm: 7.30 (d, *J* = 8.5 Hz, 1H), 7.41 (dd, *J* = 1.5 and 7.5 Hz, 1H), 7.49 (t, *J* = 7.5 Hz, 2H), 7.70 (dd, *J* = 4.5 and 9.5 Hz, 1H), 7.77 (d, *J* = 8.5 Hz, 1H), 7.96 (dd, *J* = 1.5 and 8.5 Hz, 2H), 8.21 (d, *J* = 8.5 Hz, 1H), 8.74 (s, 1H), 8.97 (dd, *J* = 1.5 and 4.5 Hz, 2H). ¹³C NMR (125 MHz, CD₃OD) δ ppm: 111.7, 127.0, 127.1, 129.8, 130.2, 131.5, 134.3, 138.4, 149.2, 149.9, 155.9. HRMS (ESI): calcd for C₁₇H₁₂N₄O [M + H]⁺: 289.1084, found: 289.1076.

8-Hydroxy-5-(4-(3,5-bis(trifluoromethyl)phenyl)-1H-1,2,3-triazol-1-yl)quinoline (77c)

1-Ethynyl-3,5-bis(trifluoromethyl)benzene (**76c**) was used as the starting material. ¹H NMR (500 MHz, CD₃OD) δ ppm: 7.38 (d, *J* = 8.5 Hz, 1H), 7.84 (dd, *J* = 4.5 and 8.5 Hz, 1H), 7.87 (d, *J* = 8.5 Hz, 1H), 7.99 (s, 1H), 8.52 (dd, *J* = 1.5 and 8.5 Hz, 1H), 8.57 (s, 1H), 9.03 (dd, *J* = 1.5 and 4.5 Hz, 1H), 9.07 (s, 1H). ¹³C NMR (125 MHz, CD₃OD) δ ppm: 113.2, 122.8, 123.8, 124.6, 124.8, 125.7, 125.9, 126.6, 127.0, 127.9, 133.6, 134.4, 146.4, 148.6, 154.5. HRMS (ESI): calcd for C₁₉H₁₀F₆N₄O [M + H]⁺: 425.0832, found: 425.0836.

8-Hydroxy-5-(4-(3-chlorophenyl)-1H-1,2,3-triazol-1-yl)quinoline (77d)

1-Chloro-3-ethynylbenzene (**76d**) was used as the starting material. ¹H NMR (500 MHz, CD₃OD) δ ppm: 7.34 (d, *J* = 8.5 Hz, 1H), 7.41 (d, *J* = 8 Hz, 1H), 7.48 (t, *J* = 8 Hz, 1H), 7.77 (dd, *J* = 4.5 and 8.5 Hz, 1H), 7.81 (dd, *J* = 8 Hz, 1H), 7.90 (d, *J* = 8 Hz, 1H), 8.01 (s, 1H), 8.32 (dd, *J* = 1.5 and 8.5 Hz, 1H), 8.82 (s, 1H), 9.01 (dd, *J* = 1.5 and 4.5 Hz, 1H). ¹³C NMR (125 MHz, CD₃OD) δ ppm: 112.3, 124.7, 125.2, 125.6, 125.7, 126.4, 126.8, 127.4, 129.6, 131.8,

133.6, 135.6, 136.2, 137.4, 147.9, 149.4, 155.4. HRMS (ESI): calcd for C₁₇H₁₁ClN₄O [M + H]⁺: 323.0621, found: 323.0625.

8-Hydroxy-5-(4-p-tolyl-1H-1,2,3-triazol-1-yl)quinoline (77i)

1-Ethynyl-4-methylbenzene (**76i**) was used as the starting material. ¹H NMR (500 MHz, CD₃OD) δ ppm: 2.40 (s, 3H), 7.31 (d, *J* = 8.5 Hz, 1H), 7.41 (d, *J* = 8.5 Hz, 1H), 7.83-7.88 (m, 2H), 7.84 (d, *J* = 8 Hz, 1H), 7.88 (d, *J* = 8 Hz, 1H), 8.50 (d, *J* = 8.5 Hz, 1H), 8.72 (s, 1H), 9.04 (dd, *J* = 1.5 and 4.5 Hz, 1H). ¹³C NMR (125 MHz, CD₃OD) δ ppm: 21.4, 113.4, 124.6, 124.7, 126.0, 126.7, 126.9, 128.0, 128.6, 130.8, 138.0, 140.0, 148.4, 149.5, 154.2. HRMS (ESI): calcd for C₁₇H₁₁ClN₄O [M + H]⁺: 323.0694, found: 323.0702.

8-Hydroxy-5-(4-(4-bromophenyl)-1H-1,2,3-triazol-1-yl)quinoline (77u)

1-Bromo-4-ethynylbenzene (**76u**) was used as the starting material. ¹H NMR (500 MHz, Cl₃CD) δ ppm: 7.28 (d, *J* = 8 Hz, 1H), 7.56 (dd, *J* = 4 and 8.5 Hz, 1H), 7.60-7.64 (m, 2H), 7.61 (d, *J* = 8 Hz, 1H), 7.81-7.83 (m, 1H), 7.82 (d, *J* = 8.5 Hz, 1H), 8.11 (s, 1H), 8.16 (d, *J* = 8.5 Hz, 1H), 8.90 (d, *J* = 3.5 Hz, 1H). ¹³C NMR (125 MHz, Cl₃CD) δ ppm: 108.9, 122.2, 122.5, 123.5, 124.2, 124.3, 125.1, 127.4, 129.0, 132.1, 132.2, 137.7, 146.9, 148.9, 153.9. HRMS (ESI): calcd for C₁₇H₁₁BrN₄O [M + H]⁺: 367.0189, found: 367.0187.

5-Azido-8-hydroxy-2-methylquinoline (79)

5-Amino-8-hydroxy-2-methylquinoline (**78**; 723 mg, 4.2 mmol) was dissolved in a solution of concentrated hydrochloric acid (0.4 mL) and water (5 mL), cooled to -3 °C in a salt-ice bath, stirred for 10 min, then treated dropwise with a cold solution of sodium nitrite (0.50 g, 7.2 mmol)

in water (5 mL). The mixture was stirred for 20 min, then treated dropwise with sodium azide (0.60 g, 9.2 mmol) in water (40 mL), stirred at 0 °C for a further 1.5 h, then allowed to warm to room temperature over 24 h in the dark. Isolation by extraction with diethyl ether gave a dark brown solid, which was recrystallized from light petroleum to yield **13** as light brown crystals (554 mg, 66%). ¹H NMR (500 MHz, CD₃OD) δ ppm: 3.31 (s, 3H), 7.06 (d, J = 8.5 Hz, 1H), 7.15 (d, J = 8.5 Hz, 1H), 7.36 (d, J = 8.5 Hz, 1H), 8.21 (d, J = 8.5 Hz, 1H). ¹³C NMR (125 MHz, CD₃OD) δ ppm: 24.9, 111.8, 115.6, 121.6, 123.7, 127.9, 132.6, 139.6, 151.1, 159.7. HRMS (ESI): calcd for C₁₀H₈N₄O [M + H]⁺: 201.0771, found: 201.0773.

5-Azido-8-tert-butyl-diphenylsilyloxy-2-methylquinoline (80)

A 100-mL flask was successively loaded with dry DMF (10 mL), **79** (200 mg, 1 mmol), imidazole (68.08 mg, 1 mmol), and tert-butyl-diphenylsilyl chloride (302 mg, 1.1 mmol). The solution was stirred at room temperature for 10 h, diluted with ethyl acetate (500 mL), washed with aqueous HCl (0.1 M, 50 mL), brine (100 mL), water (100 mL), dried over Na₂SO₄ and evaporated under reduced pressure to afford 8.41 g (96%) of protected product as a colorless oil (428 mg, 98%). ¹H NMR (500 MHz, CDCl₃) δ ppm: 1.19 (s, 9H), 2.33 (s, 3H), 6.98 (d, J = 8.5 Hz, 1H), 7.06 (d, J = 8.5 Hz, 1H), 7.10 (d, J = 8.5 Hz, 1H), 7.38-7.26 (m, 6H), 7.81-7.79 (m, 4H), 8.11 (d, J = 8.5 Hz, 1H). ¹³C NMR (125 MHz, CDCl₃) δ ppm: 20.1, 24.3, 26.8, 113.5, 116.7, 120.6, 121.8, 127.3, 128.4, 129.2, 130.6, 134.3, 135.1, 140.9, 148.9, 157.9. HRMS (ESI): calcd for C₂₆H₂₆N₄OSi [M + H]⁺: 438.1876, found: 438.1879.

5-Azido-2-bromomethyl-8-tert-butyl-diphenylsilyloxyquinoline (81)

NBS (165.5 mg, 0.93 mmol) and AIBN (152.7 mg, 0.93 mmol) were added to a solution of **80** (371 mg, 0.85 mmol) in Cl_4C (4.5 mL), and the mixture was refluxed 20 min and evaporated to dryness. The residue was dissolved in CH_2Cl_2 (20 mL), the solution was washed with H_2O (5 mL) and brine (5 mL), dried over Na_2SO_4 , and evaporated. The residue was purified by flash chromatography, using 20-50% gradient of EtOAc in hexane as eluent, to yield the unresolved (3:1) mixture of **80** and **81** (131.6 mg, 30%). ^1H NMR (500 MHz, CDCl_3) δ ppm: 1.16 (s, 9H), 4.24 (s, 2H), 6.97 (d, $J = 8.5$ Hz, 1H), 7.03 (d, $J = 8.5$ Hz, 1H), 7.09 (d, $J = 8.5$ Hz, 1H), 7.26-7.43 (m, 6H), 7.76-7.78 (m, 4H), 8.24 (d, $J = 8.5$ Hz, 1H). HRMS (ESI): calcd for $\text{C}_{26}\text{H}_{25}\text{BrN}_4\text{OSi}$ $[\text{M} + \text{H}]^+$: 517.1054, found: 517.1050.

Peptide Synthesis

a. General Protocol

All peptides were synthesized using the standard Fmoc-based amino acid protection chemistry. Peptides were synthesized on Fmoc-PAL-PEG-PS resin (Applied Biosystems, 0.19 mmol/g) using on-resin alkylation. The resin was swelled in CH_2Cl_2 (5 min.) and then DMF (5 min) prior to synthesis. All the amino acids were coupled according to the following procedure: Fmoc deprotection (20% 4-methylpiperidine in DMF, 3 x 5 min), rinsing step (DMF, 5 x), coupling step (amino acid/PyBOP/HOBt/DIEA, 6:6:6:6, 0.15 M in DMF, 30-45 min), rinsing step (DMF, 5 x; CH_2Cl_2 , 5 x). The coupling was repeated if necessary as determined by the TNBS test. At the end of the synthesis, the Fmoc group was removed with 20% 4-methylpiperidine in DMF (3 x 5 min.) and the resin was rinsed with DMF (5 x). The resin-attached free amines were capped by exposure to Ac_2O (20 equiv.) and pyridine (20 equiv.) in DMF for 30 min. The resin was

rinsed with DMF (5 x), CH₂Cl₂ (5 x) and subjected to 20% 4-methylpiperidine in DMF (3 x 5 min.). The resin was finally washed with DMF, CH₂Cl₂, MeOH (5 x each) and dried under vacuum.

b. On-resin Alkylation of Peptides with 15

Resin-attached peptides (50 mg, 0.0095 mmol, 1 equiv.) incorporating Cys(Mmt) were swelled in CH₂Cl₂, then DMF. The Mmt protecting group was removed from the resin-bound peptide by bubbling N₂ through a solution of 1% TFA, 5% TIS in CH₂Cl₂ (4 x 20 min). The resin was washed with CH₂Cl₂ (5 x) and DMF (5 x). Anhydrous DMF (200 μL) was added to the resin followed by freshly distilled tetramethylguanidine (5.96 μL, 0.0475 mmol, 5 equiv.). The mixture was incubated for 2-3 min. Compound **15** (17 mg, 0.0285 mmol, 3 equiv.) was dissolved in anhydrous DMF (150 μL) and added to the resin. After ca. 12 hours of reaction time, the excess reagents were drained and the resin washed with DMF, CH₂Cl₂, MeOH, CH₂Cl₂ (5 x).

c. On-resin Click Chemistry of Azido-Oxn Peptides with 76u

Resin-attached peptides (50 mg, 0.0095 mmol, 1 equiv.) incorporating 5-Azido-8-Hydroxyquinoline were swelled in CH₂Cl₂, then DMF (5 min). A mixture of 1-bromo-4-ethynylbenzene (**76u**; 34.4 mg, 0.19 mmol), ascorbic acid (0.75 mg, 0.0043 mmol) and copper iodide (0.27 mg, 0.0014 mmol) was added to the resin suspended in a 8:2 mixture of DMF/4-methylpiperidine (1.5 mL). After ca. 12 hours of reaction time, the excess reagents were drained and the resin washed with DMF, CH₂Cl₂, MeOH, CH₂Cl₂ (5x). The resin cleavage and protecting group removal was achieved by exposing the resin-bound peptides to TFA/H₂O/TIS (95:2.5:2.5% v/v). The resulting solution was concentrated under a stream of N₂ and precipitated by addition of cold Et₂O. The pellet was triturated with cold Et₂O, redissolved in water, filtered

and lyophilized. The peptides were purified by preparative reverse-phase HPLC using UV detection at 228 nm (amide bond absorption) and 316 nm (8-hydroxyquinoline absorption). Only fractions showing a single peak of correct mass by analytical HPLC were used in further experiments.

d. Characterization data for peptides

Kinase	Peptide	Peptide Sequence	Mol. Formula	HPLC t_R (min) ^b	[M] Calcd.	[M+H] ⁺ found ^c
MK2	P1 ^a	Ac-AHLQRQLSI-CSox-HH-CONH ₂				
		Ac-AHLQRQLpSI-CSox-HH-CONH ₂				
	P2	Ac-AHLQRQLSI-CClk-HH-CONH ₂	C ₈₁ H ₁₁₃ BrN ₂₈ O ₁₇ S	21.32	1862.91	1863.38
Src	P3 ^a	Ac-AHLQRQLpSI-CClk-HH-CONH ₂	C ₈₁ H ₁₁₄ BrN ₂₈ O ₂₀ PS	23.45	1942.89	1943.22
		Ac-AEE-CSox-IYGEFEAKKKK-CONH ₂				
	P4	Ac-AEE-CSox-IpYGEFEAKKKK-CONH ₂				
		Ac-AEE-CClk-IYGEFEAKKKK-CONH ₂	C ₉₉ H ₁₃₉ BrN ₂₄ O ₂₆ S	22.00	2193.28	2194.45
		Ac-AEE-CClk-IpYGEFEAKKKK-CONH ₂	C ₉₉ H ₁₄₀ BrN ₂₄ O ₂₉ PS	21.86	2273.26	2274.96

^a The synthesis and characterization of peptides P1 and P3 has been described.³ ^b Reported retention times (t_R) and HPLC conditions are from analytical runs. Method: 5 % B (5 min) followed by an increase to 15 % B (1 min) and a linear gradient to 15–45 % B (30 min). ^c The data was collected on a MALDI-TOF mass spectrometer.

Stock solutions

Due to the affinity of the phosphorylated peptides for selected transition metal ions,^{1, 3} only reagents of the highest purity and lowest metal content were used to avoid the need to remove metal ion impurities after preparation.

1. Stock solutions of the peptides were prepared in doubly deionized water and concentrations were determined by UV-Vis (based on the determined extinction coefficient of the fluorophore moiety, either **28** (Sox), $\epsilon_{355} = 8247 \text{ M}^{-1} \text{ cm}^{-1}$ or **77u** (Clk), $\epsilon_{360} = 7905 \text{ M}^{-1} \text{ cm}^{-1}$ in 0.1 M NaOH with 1 mM Na₂EDTA).¹ An average of the values from three separate solutions, each prepared using a different volume of the stock solution, was read on UV-Vis

spectrophotometer. Purified peptide stock solutions could be stored at 4 °C for at least 6 months or -20 °C for longer periods.

2. 500 mM HEPES (SigmaUltra) was prepared and adjusted to pH 7.4 with NaOH (99.998+%, Aldrich) solution.
3. 10 mM DTT (Biotechnology grade, Mallinckrodt) was prepared in degassed ultrapure water and stored in aliquots at -80 °C.
4. 500 mM EGTA (SigmaUltra) was prepared in 2 M NaOH and stored at 4 °C.
5. A magnesium chloride stock solution of 2.66 M was prepared using Alfa Aesar Puratronic grade salts. Most commercially available salts contain Zn^{2+} as significant impurities and should not be used due to the high affinity of the phosphorylated peptides for Zn^{2+} . The Mg^{2+} concentration was determined by titration with a standardized solution of EDTA (Aldrich) in the presence of an Eriochrome Black T (Aldrich) as described previously.¹
6. 500 mM HEPES (SigmaUltra) was prepared and adjusted to pH 7.4 with NaOH (99.998+%, Aldrich) solution.
7. 20 mg/mL BSA (Heat Shock Fraction V, Roche) was prepared in ultrapure water, filtered through a 0.45 micron syringe filter to remove particulates and stored at 4 °C.
8. 100 mM ATP (Disodium salt, Low Metals Grade, Calbiochem) was prepared in ultrapure water. The solution was stored in aliquots at -80 °C.

Fluorescence experiments

a. Fluorescence analysis of 8-hydroxyquinoline click products

A 96-well plate was used in the experiments for preliminary examination of fluorescence properties. The overall volume in each well was 200 μ L. Individual reactions contained the crude

product from the click chemistry reaction (10 μ M dissolved in DMSO), MgCl₂ (10 mM), NaCl (150 mM) and HEPES (50 mM) at 25 °C (pH 7.4). The fluorescence spectra were recorded with fixed excitation at 370 nm and emission at 525 nm. The excitation and emission wavelengths for each fluorophore are summarized in the table below. Based on the preliminary screening, selected products were then synthesized in larger quantities and the quantum yields of the corresponding hydroxyquinoline derivatives were determined.

Compound	λ_{ex} (nm)	λ_{em} (nm)	Φ^a
77a	371	522	0.033
77b	370	525	0.041
77c	367	523	0.043
77d	365	525	0.071
77e	365	520	-
77f	365	525	-
77g	365	525	-
77h	365	510	-
77i	375	525	0.067
77j	365	525	-
77k	365	525	-
77l	360	520	-
77m	360	525	-
77n	365	515	-
77o	360	510	-
77p	360	520	-
77q	365	515	-
77r	360	520	-
77s	360	530	-
77t	360	525	-
77u^b	375	525	0.111
77v	365	520	-

^a Quantum yields of selected fluorophores were calculated with reference to quinine sulphate (in 0.05 M H₂SO₄) as a standard (vide infra). ^b Extinction coefficient: $\epsilon_{355} = 7905 \text{ cm}^{-1} \text{ M}^{-1}$ (vide infra).

b. Extinction coefficient determination

Extinction coefficients of **28** and **77u** were measured in 50 mM HEPES (pH 7.0), 150 mM NaCl. The ϵ_{max} values were determined by plotting absorbance at 360 nm versus concentration for four chromophore solutions with concentrations between 20 and 60 μM and including 1 mM MgCl_2 .

c. Quantum yield determination

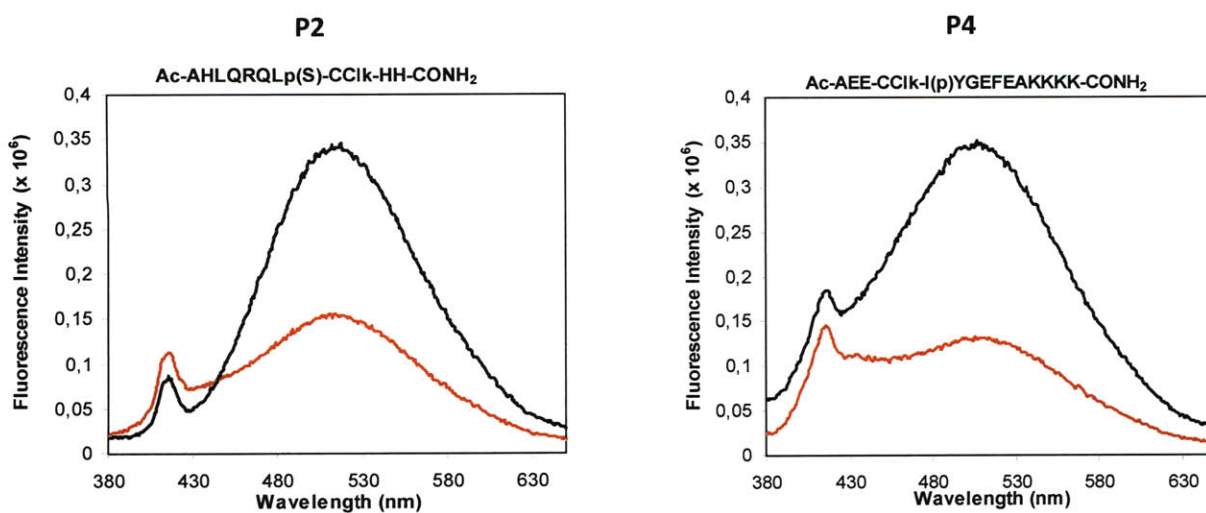
The quantum yield (Φ) was determined in 20 mM HEPES (pH 7.4). Quinine sulphate dihydrate (QS, Fluka, puriss. for fluorescence) in 0.1 M H_2SO_4 was used as a standard ($\Phi = 0.55$). A 4 μM solution of the corresponding oxine derivative with 50 mM MgCl_2 was compared to a 4 μM solution of quinine sulfate to assure that the absorbance (A_{360}) is less than 0.05 at identical excitation wavelengths. The following equation was used to calculate the quantum yield:

$$\Phi = \frac{IA_{\text{QS}} \Phi_{\text{QS}}}{AI_{\text{QS}}}$$

where $A = A_{360}$ and $I =$ integrated fluorescence intensity ($\lambda_{\text{ex}} = 360$ nm). The calculated Φ assumes that the refractive index of 0.1 M H_2SO_4 is identical to that of 20 mM HEPES (pH 7.4). The error associated with the Φ of quinine sulfate is at least 10%, the error in Φ is no less than 10%.

d. Spectral comparison of phosphorylated and unphosphorylated peptides

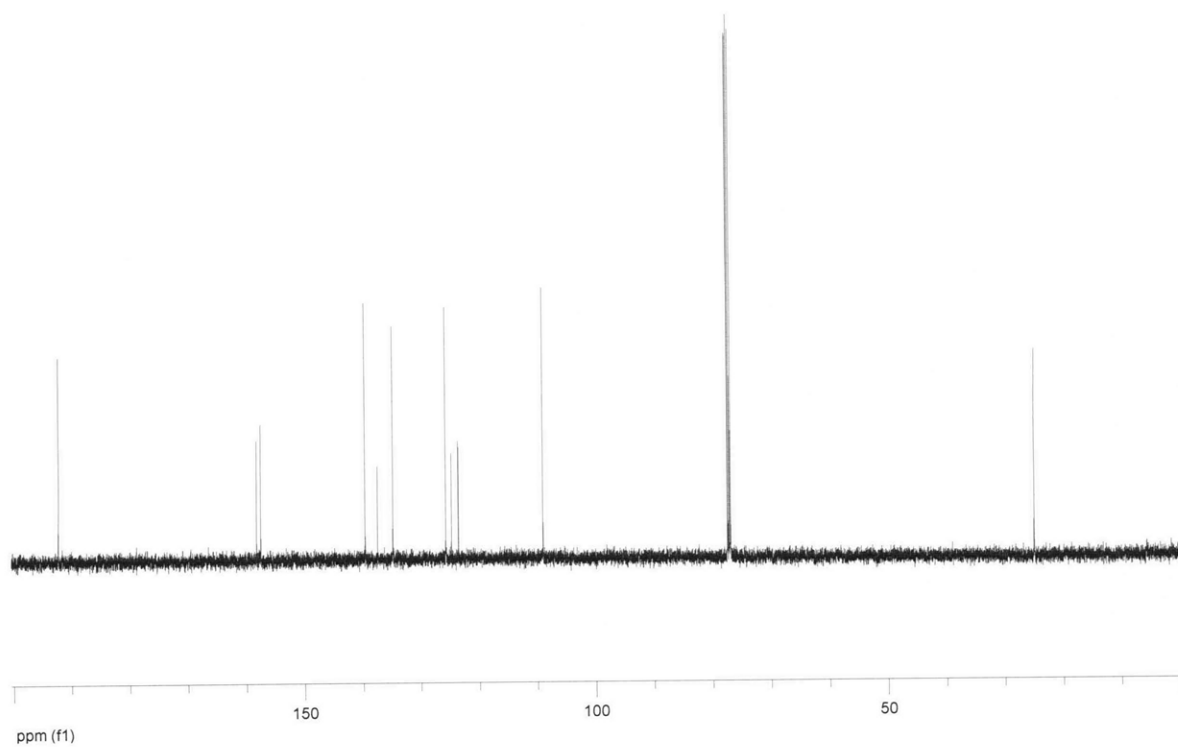
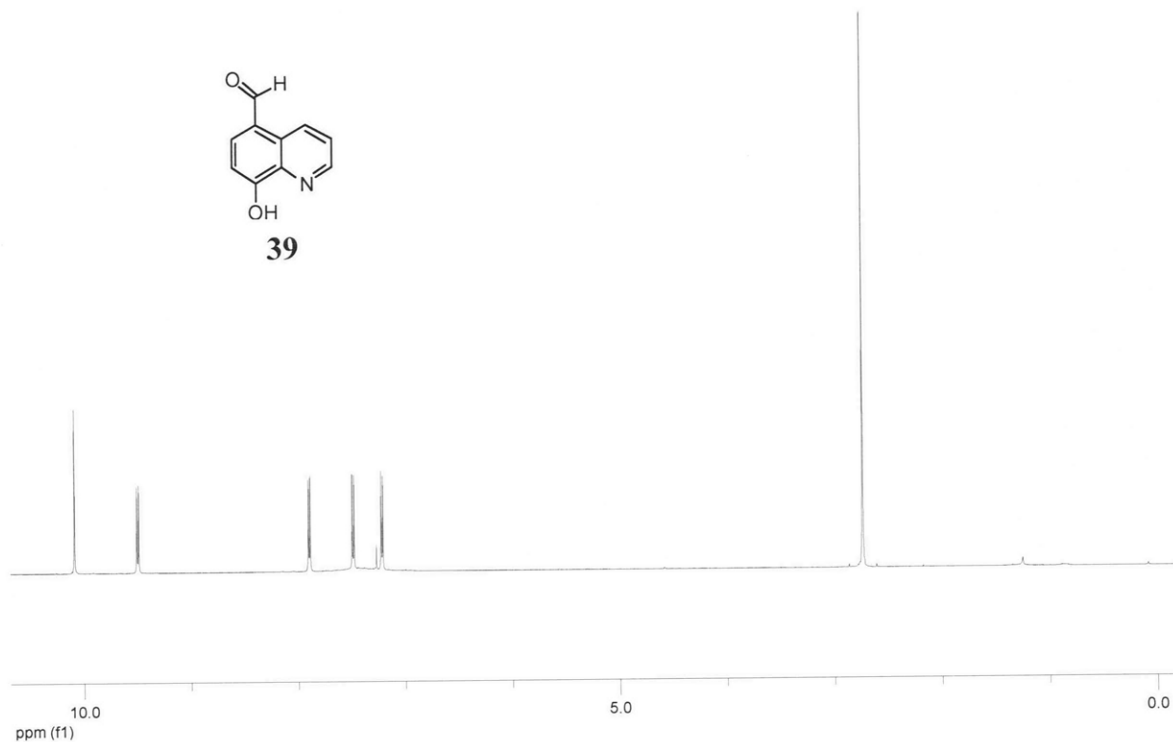
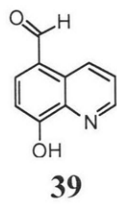
The fluorescence spectra of 10 μM phosphorylated (black line) and unphosphorylated (red line) peptides in 20 mM HEPES (pH 7.4) and 10 mM MgCl_2 were recorded in the fluorometer (slit widths: $E_m = 5$ nm, $E_x = 5$ nm; $\lambda_{\text{ex}} = 360$ nm, $\lambda_{\text{em}} = 380$ -650 nm) in a quartz microcuvette (120 μL).

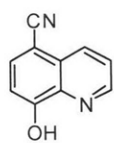


e. Enzyme Experiments with MK2 and C-Sox- or C-Clk-based Substrates

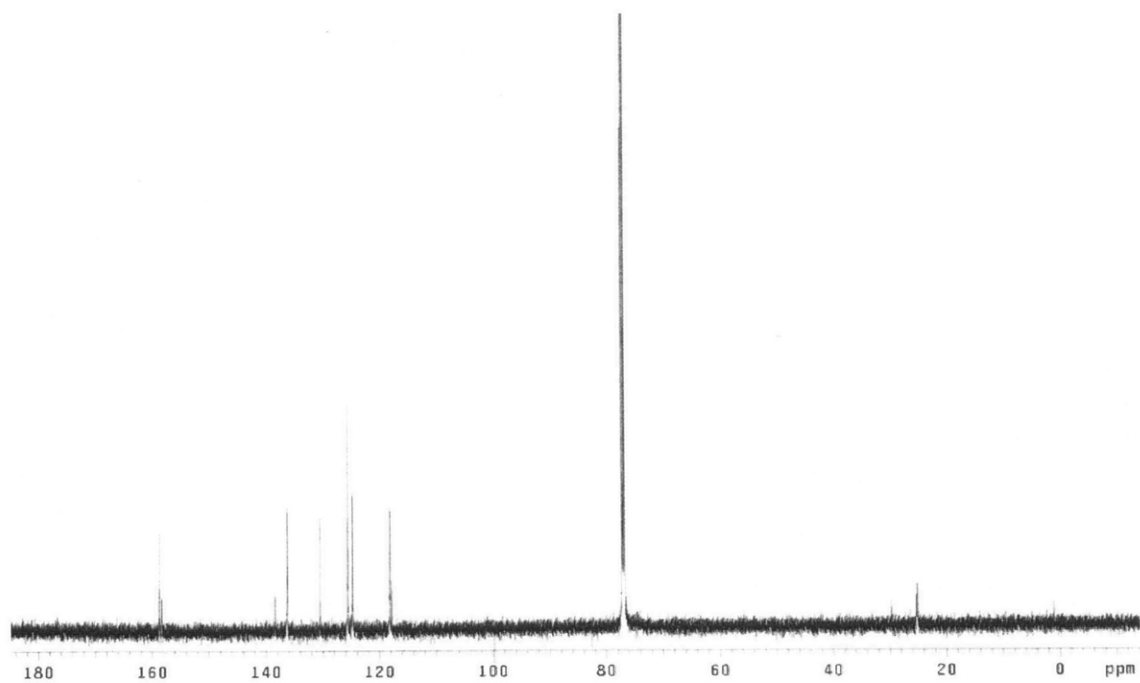
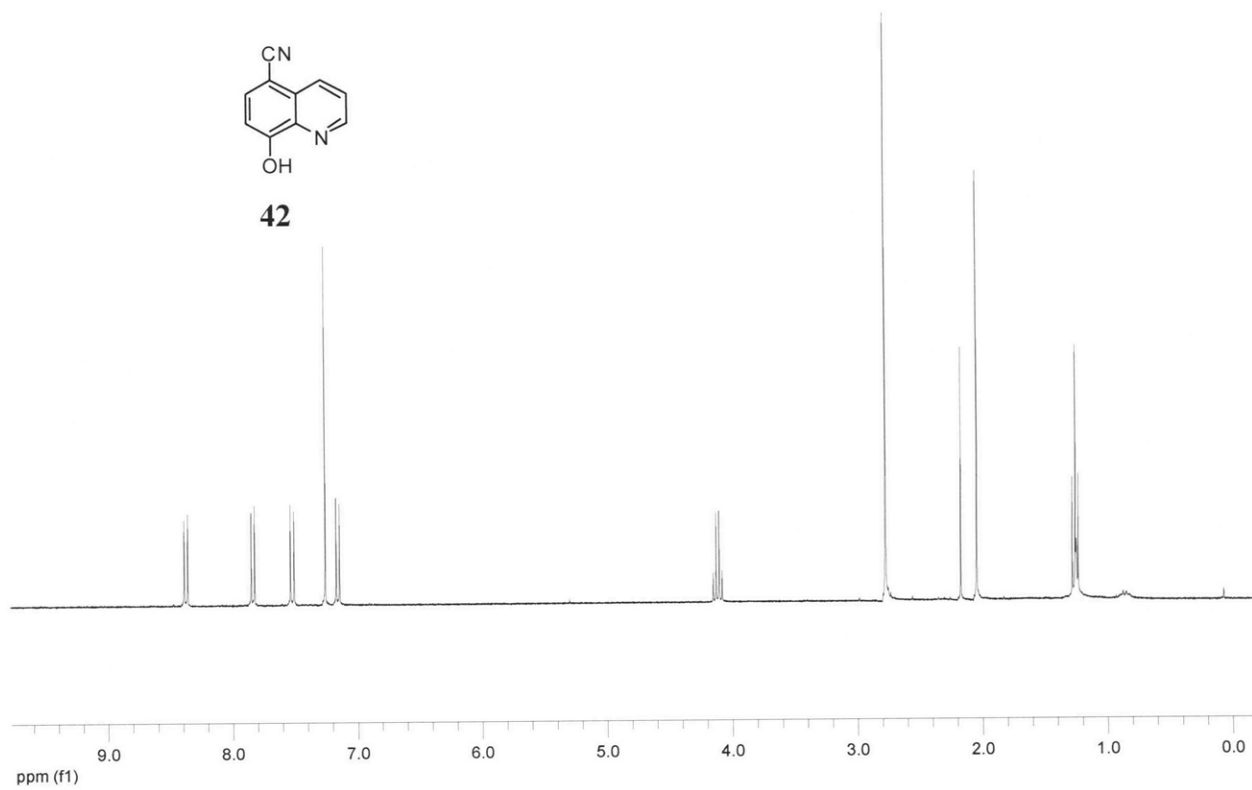
Recombinant MK2 (Upstate, appropriately diluted with 20 mM HEPES [pH 7.4], 1 mM DTT, 0.1% Brij-35, and 1 mg/mL BSA) was added to initiate each reaction. The assays were performed in the fluorometer (slit widths: Em = 5 nm, Ex = 5 nm; $\lambda_{\text{ex}} = 360$ nm, $\lambda_{\text{em}} = 485$ nm) using a quartz microcuvette (120 μL) at 30 °C for 10 min. Standard assay conditions were as follows: 20 mM HEPES (pH 7.4), 10 mM MgCl₂, 1 mM ATP, 1 mM DTT, 0.1 mM EGTA, 0.01% Brij-35, 0.1 mg/mL BSA, 1 ng MK2. The percent turnover (% TO) for C-Sox- and C-Clk-based peptides was then calculated from fluorescence intensity after 10 min of reaction time and using previously described protocols.^{1,3}

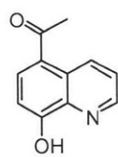
NMR Spectra



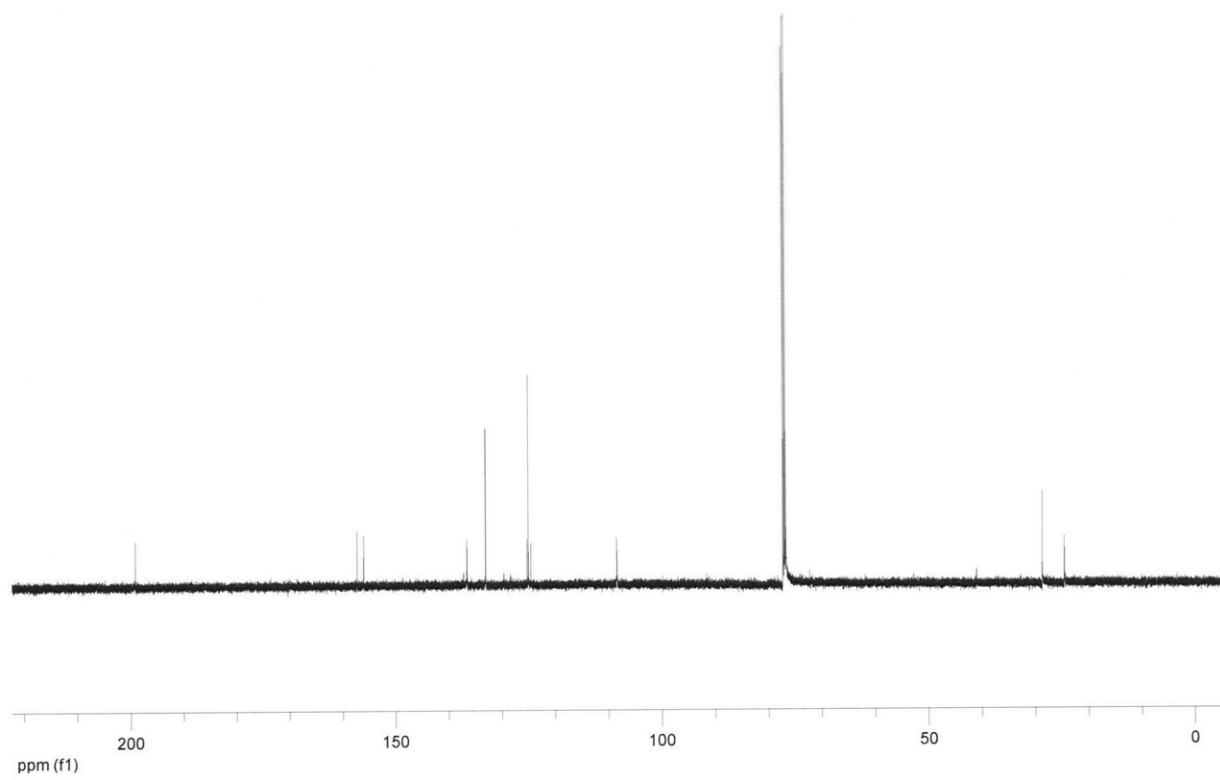
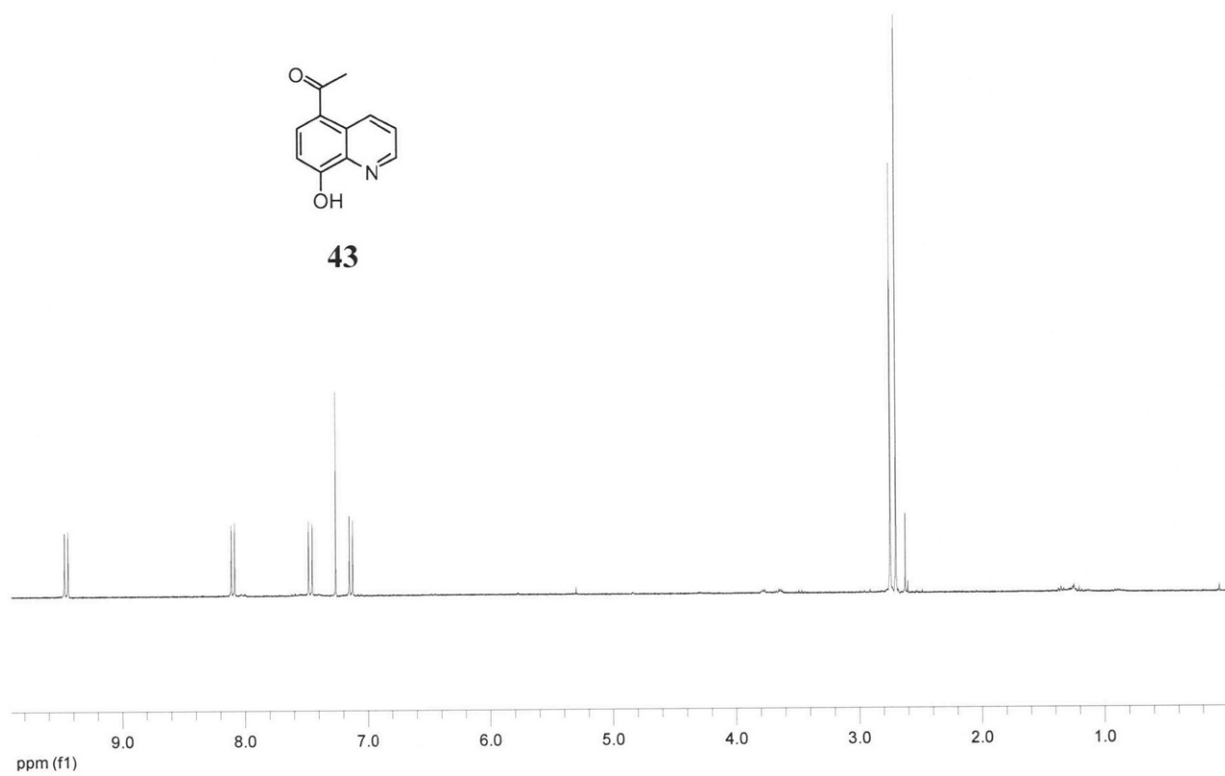


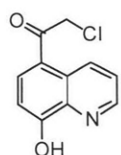
42



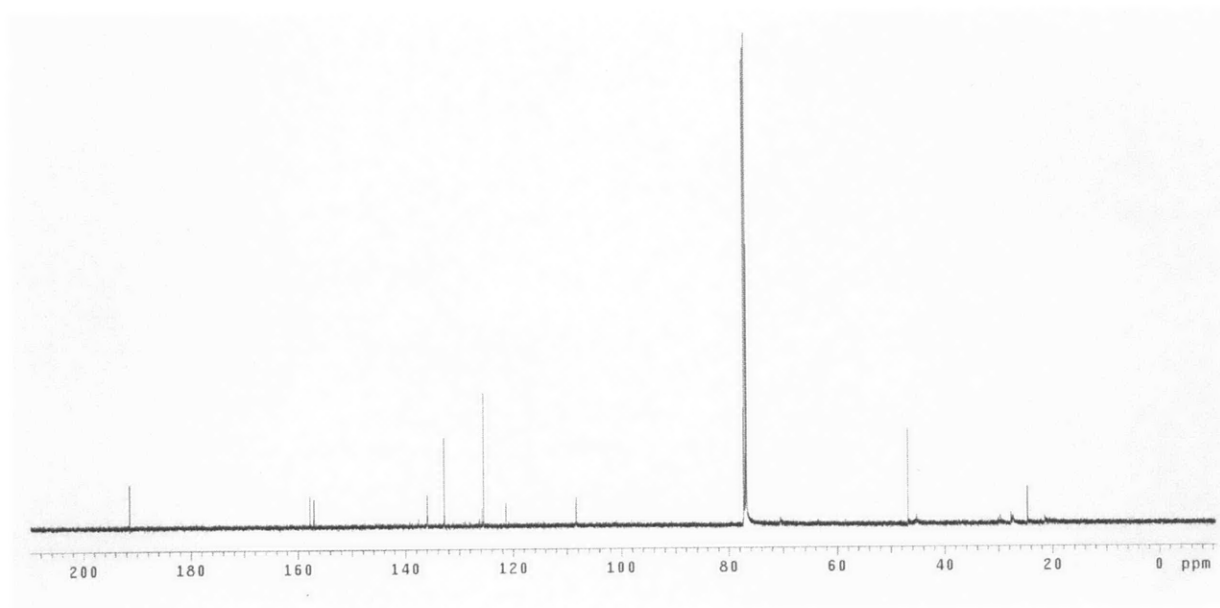
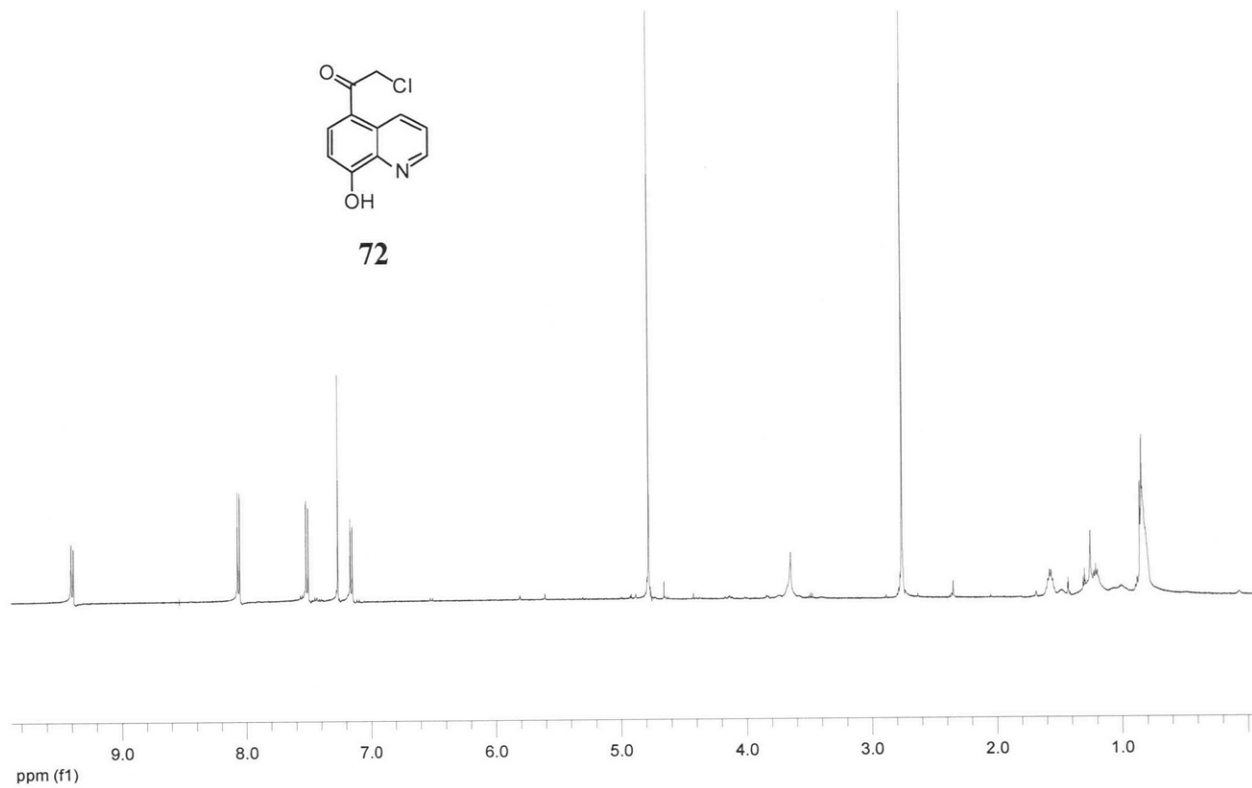


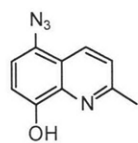
43



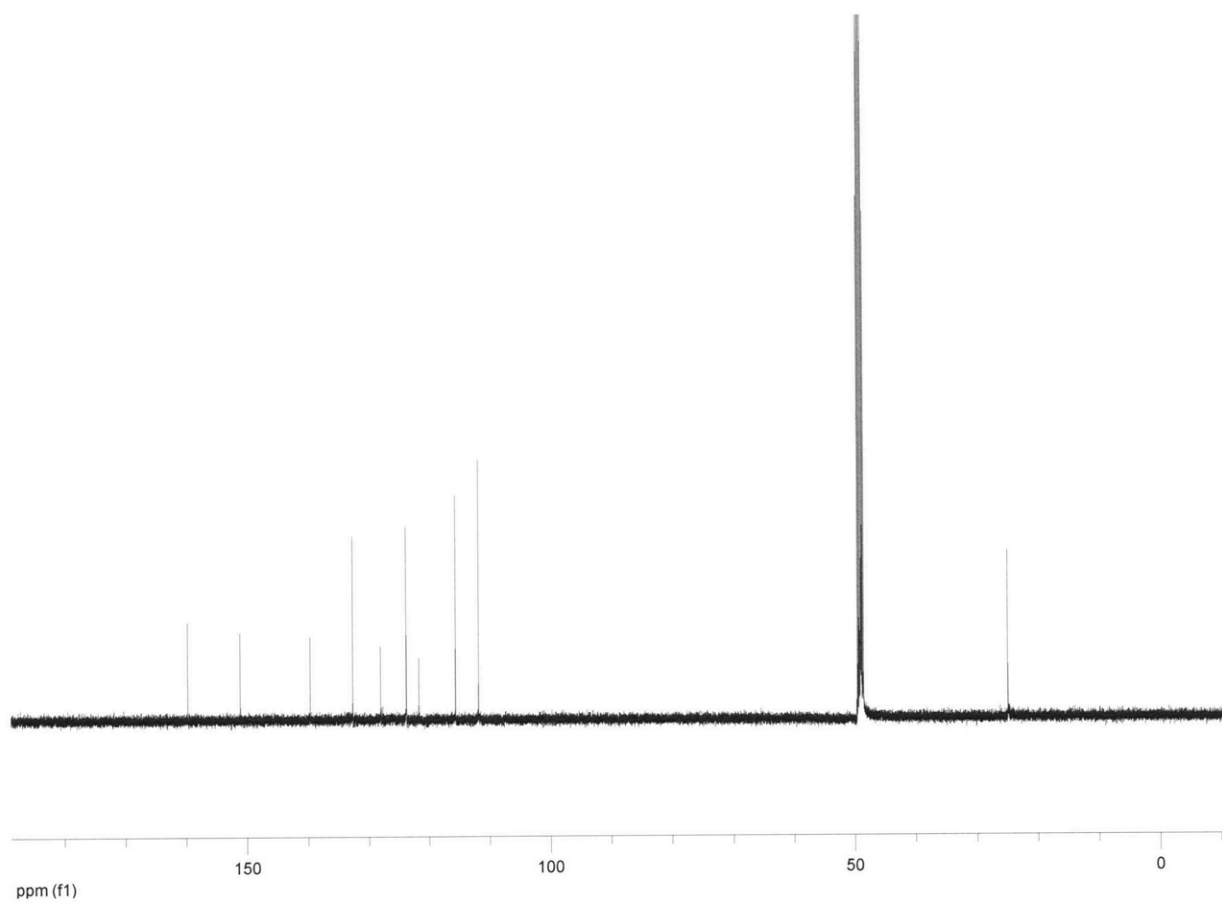
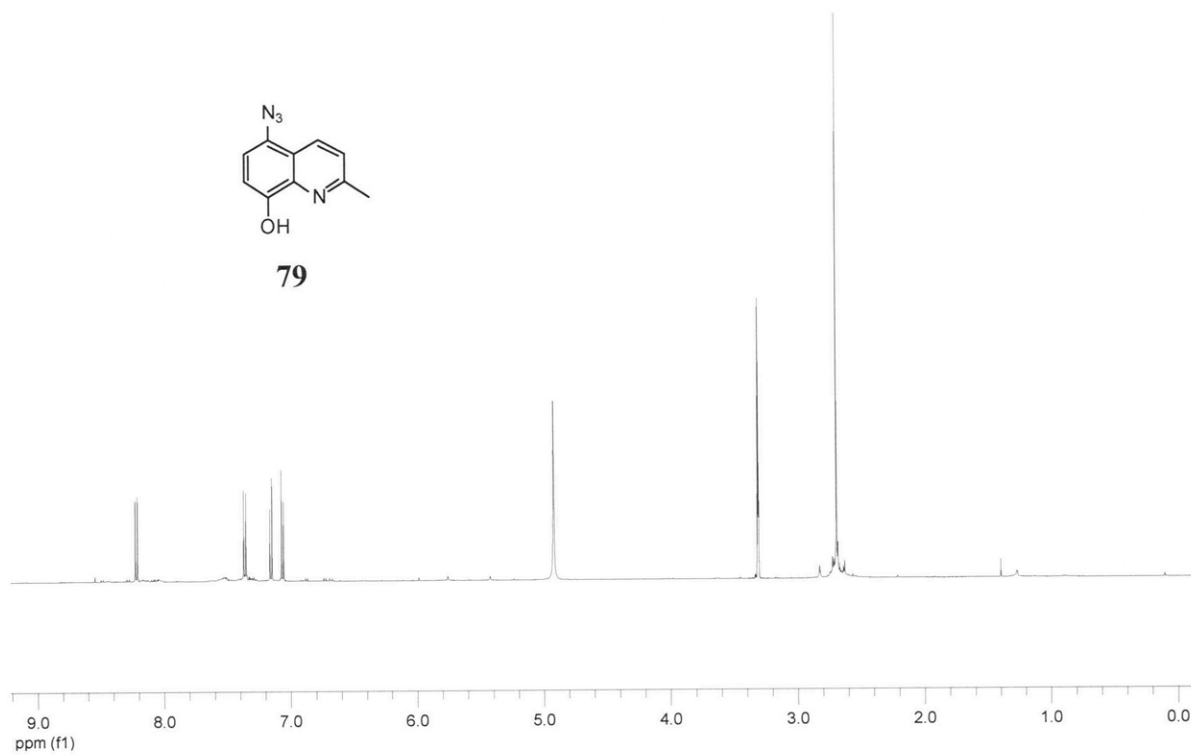


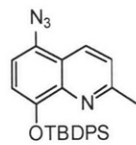
72



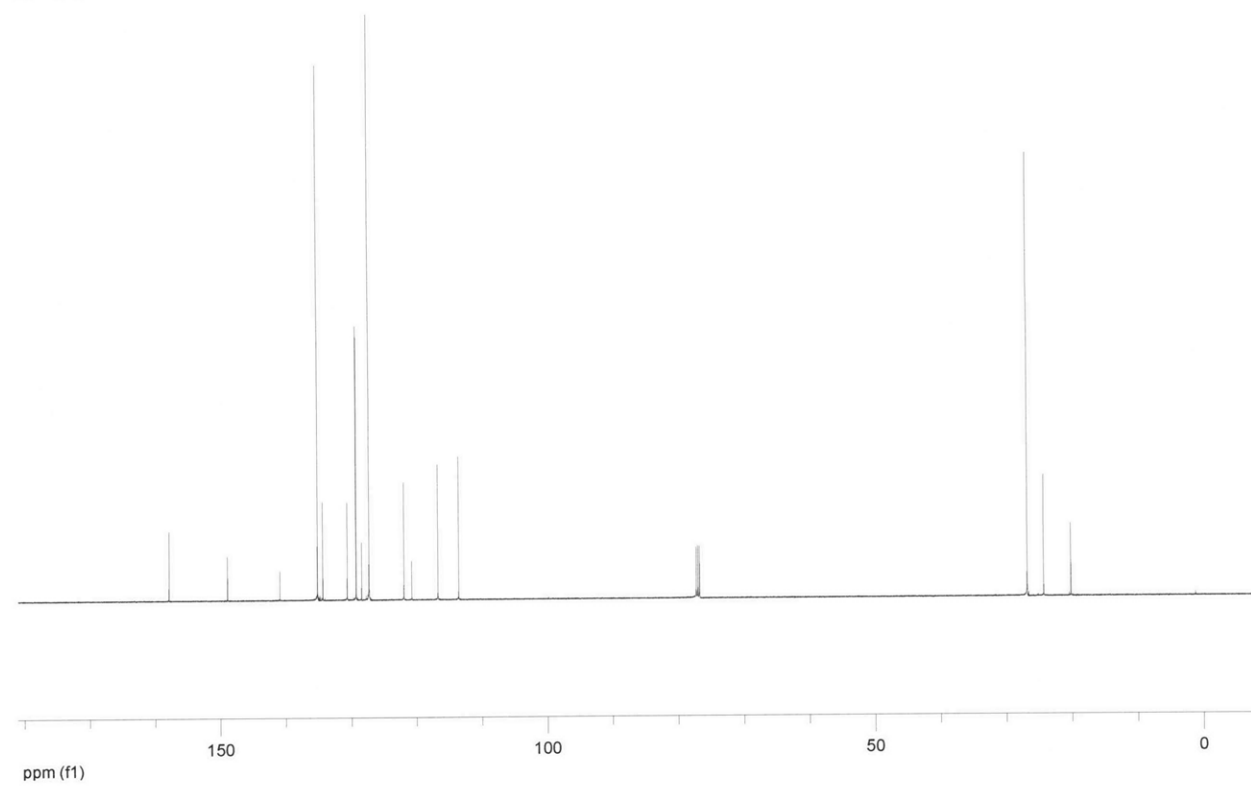
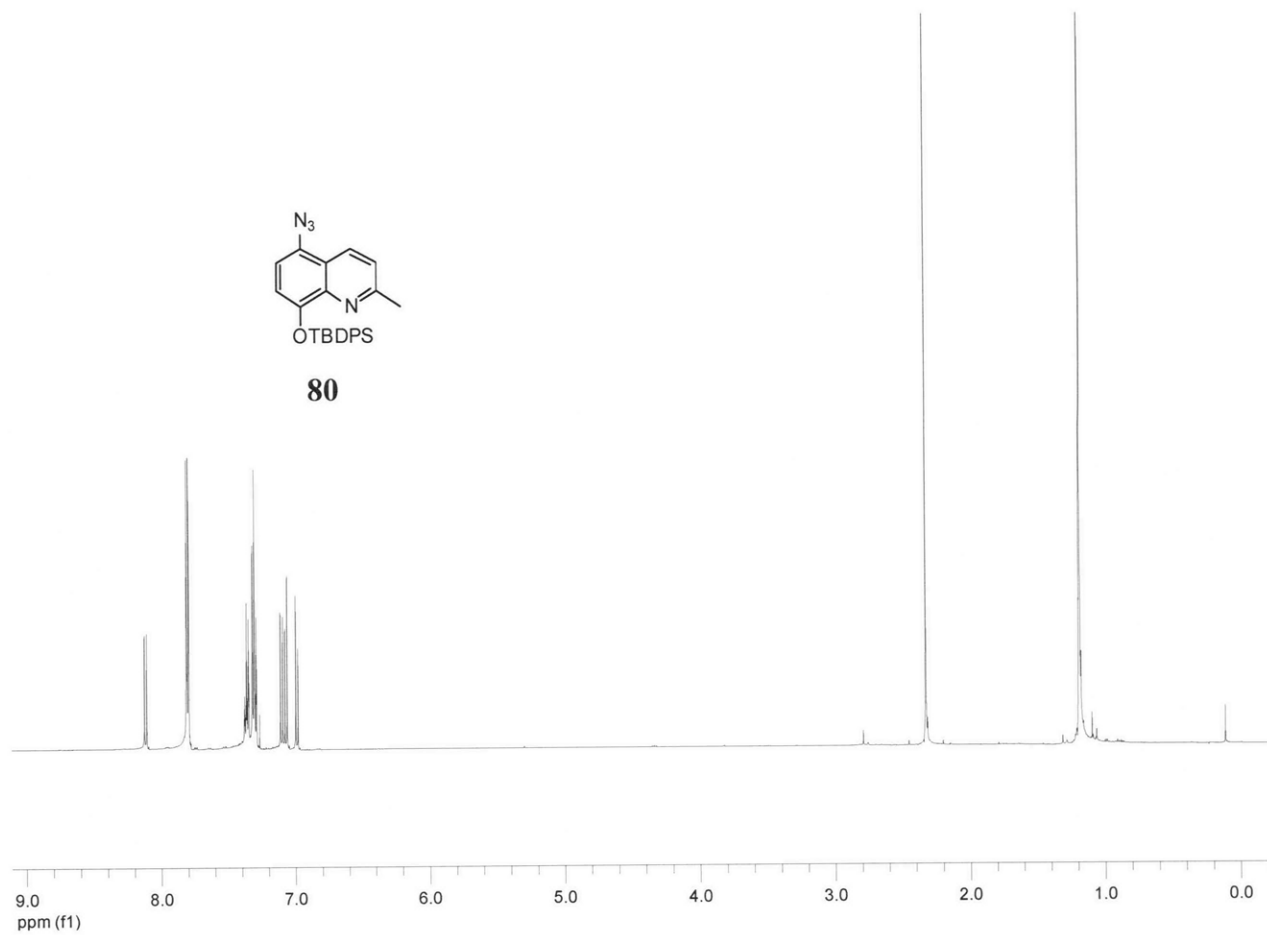


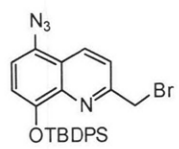
79



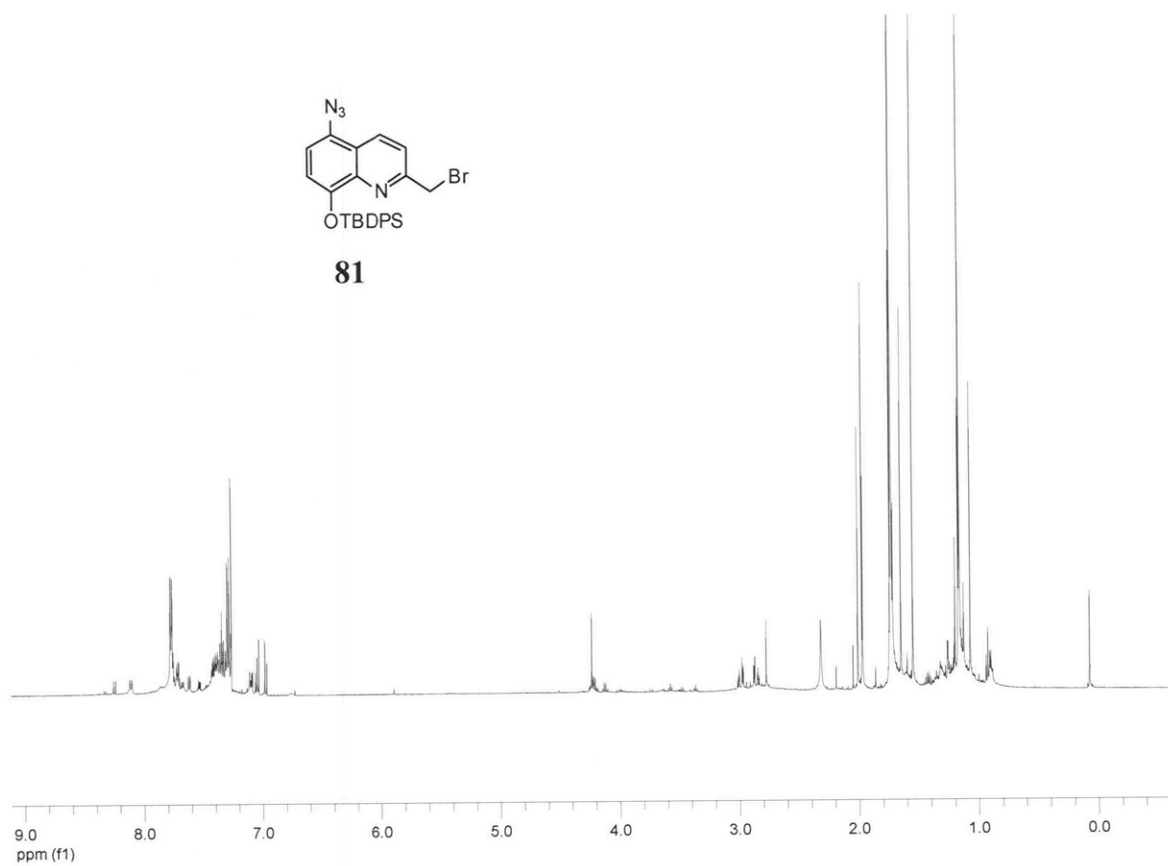


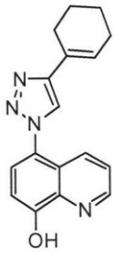
80



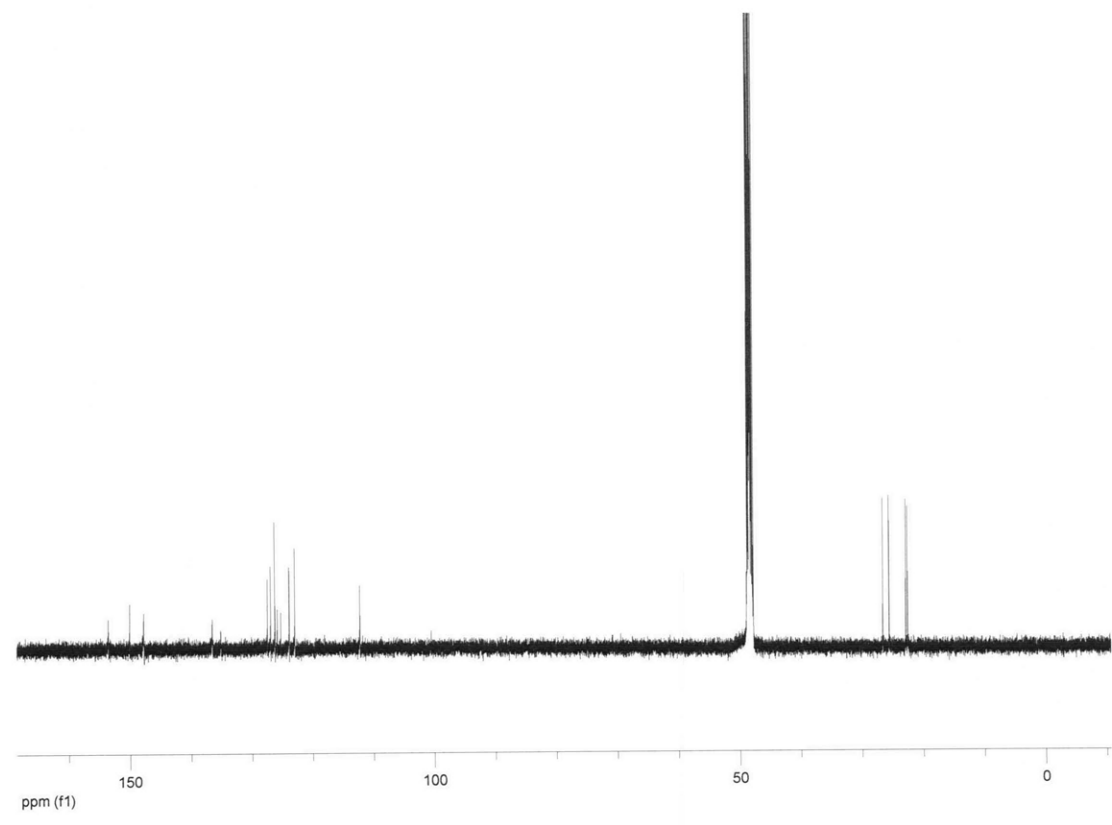
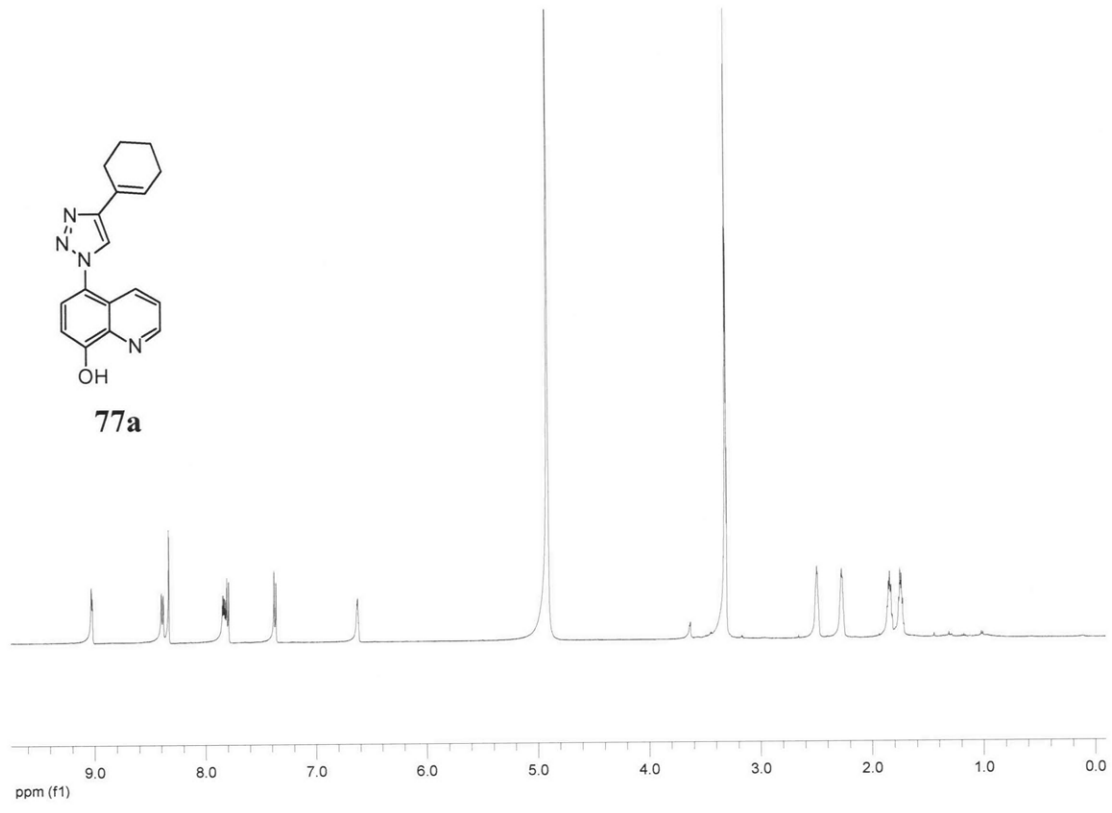


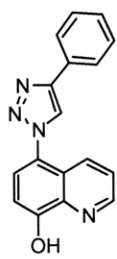
81



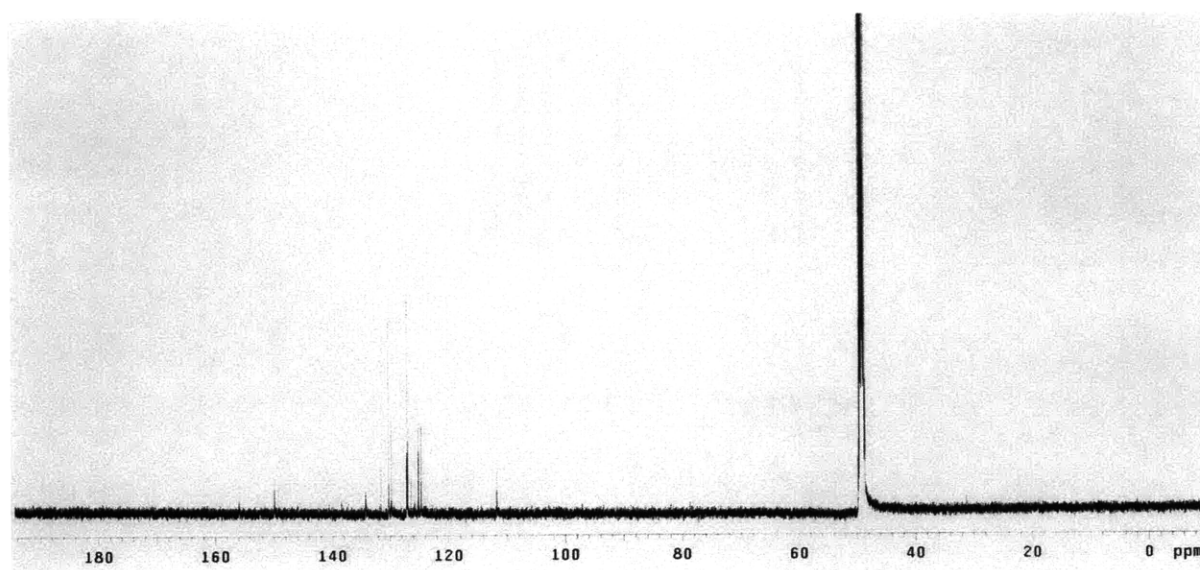
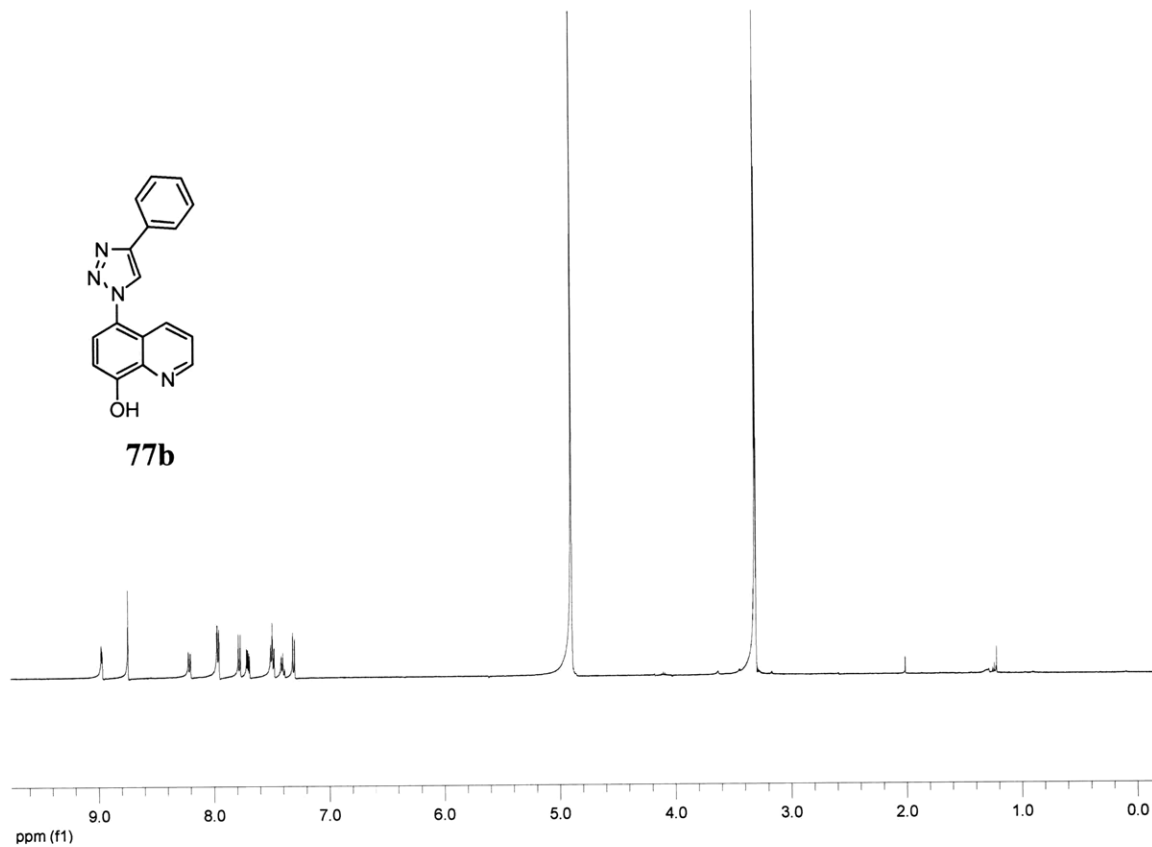


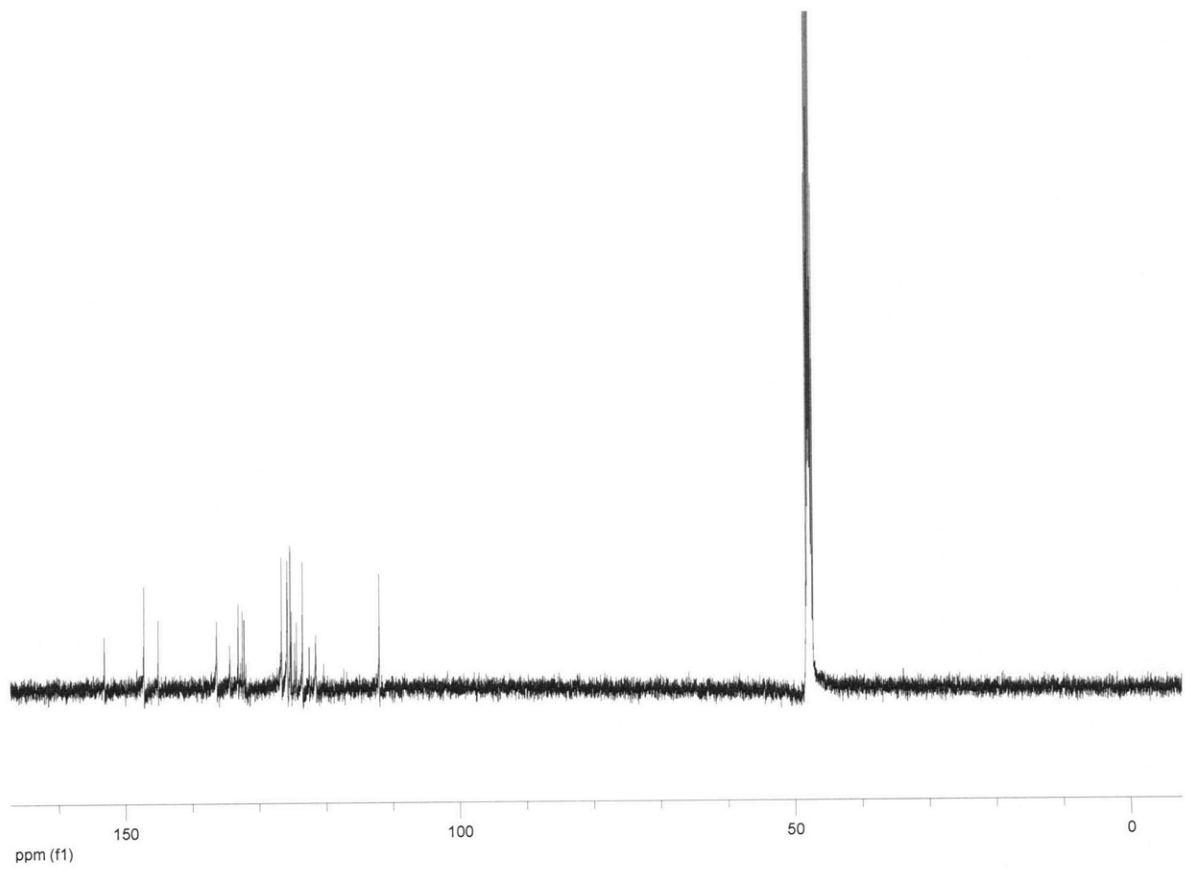
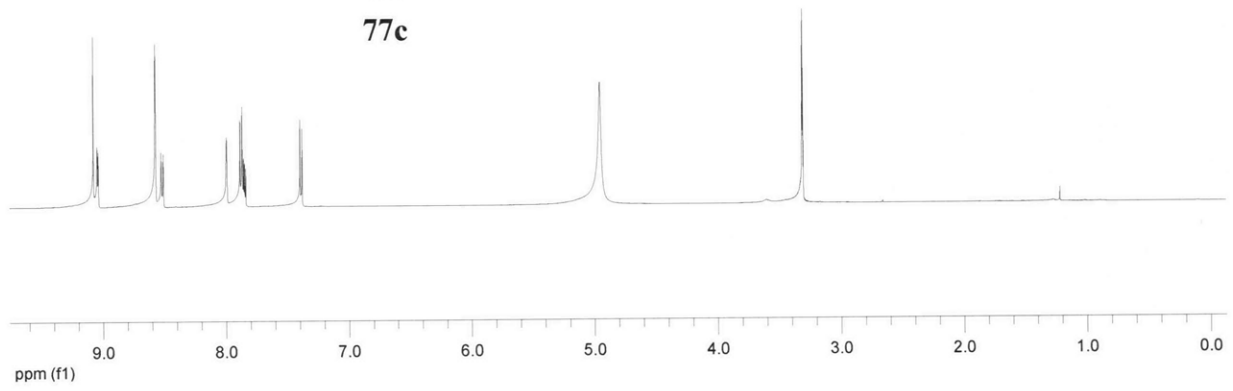
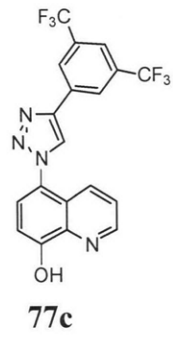
77a

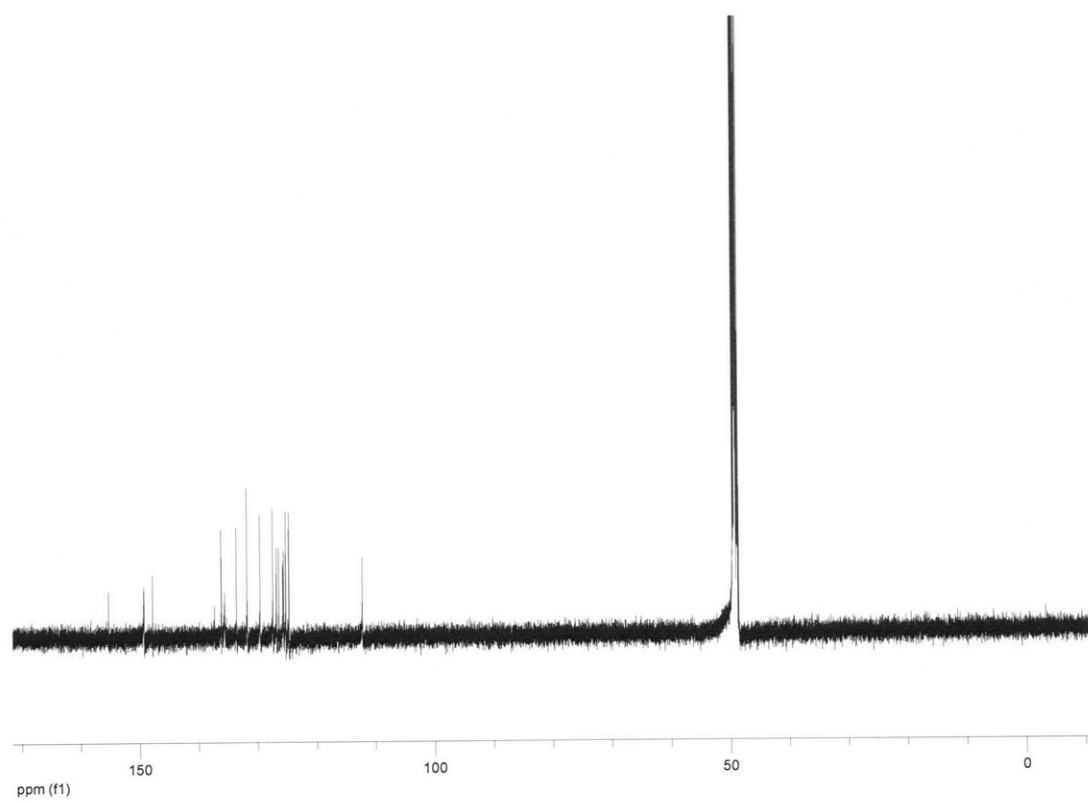
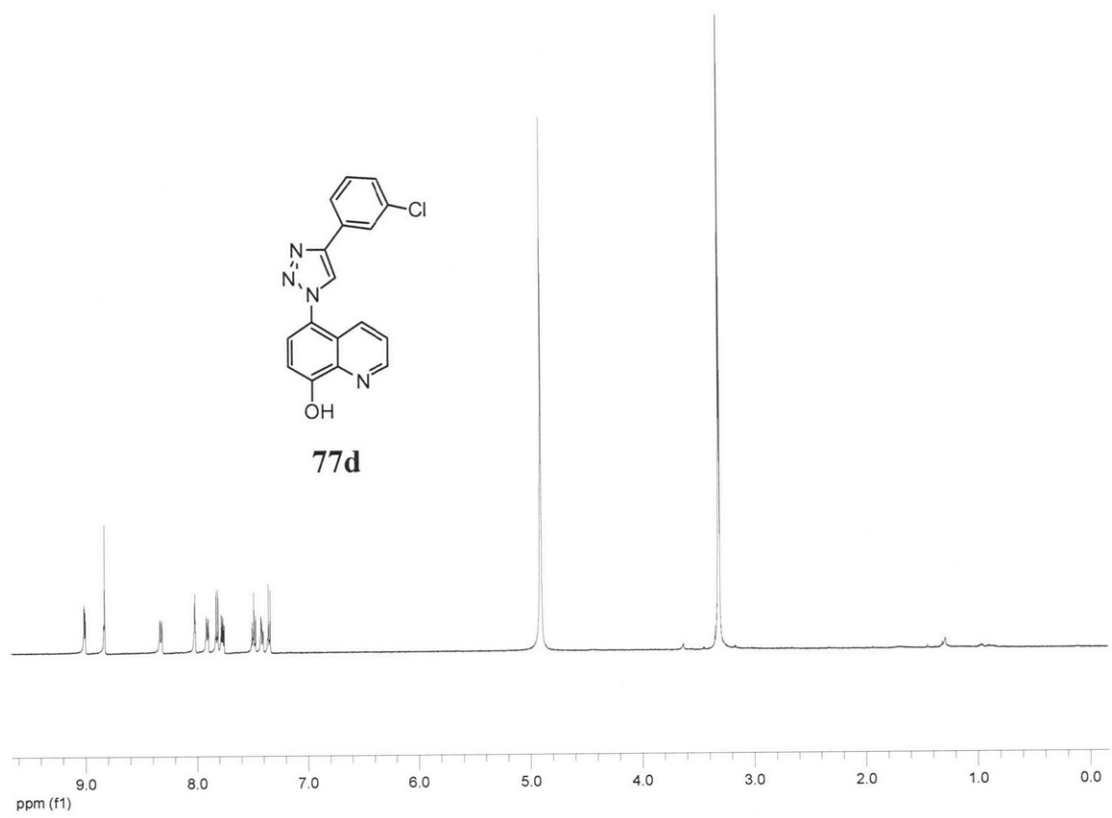


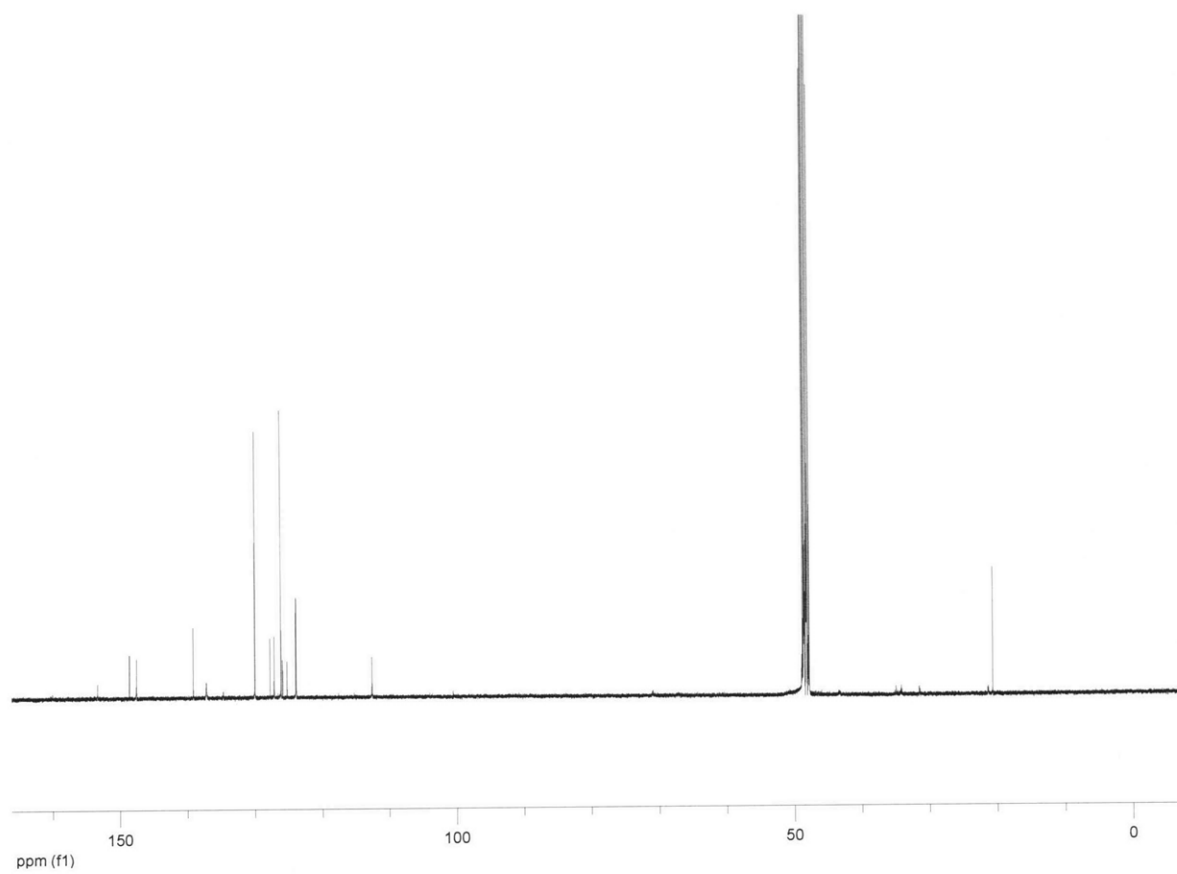
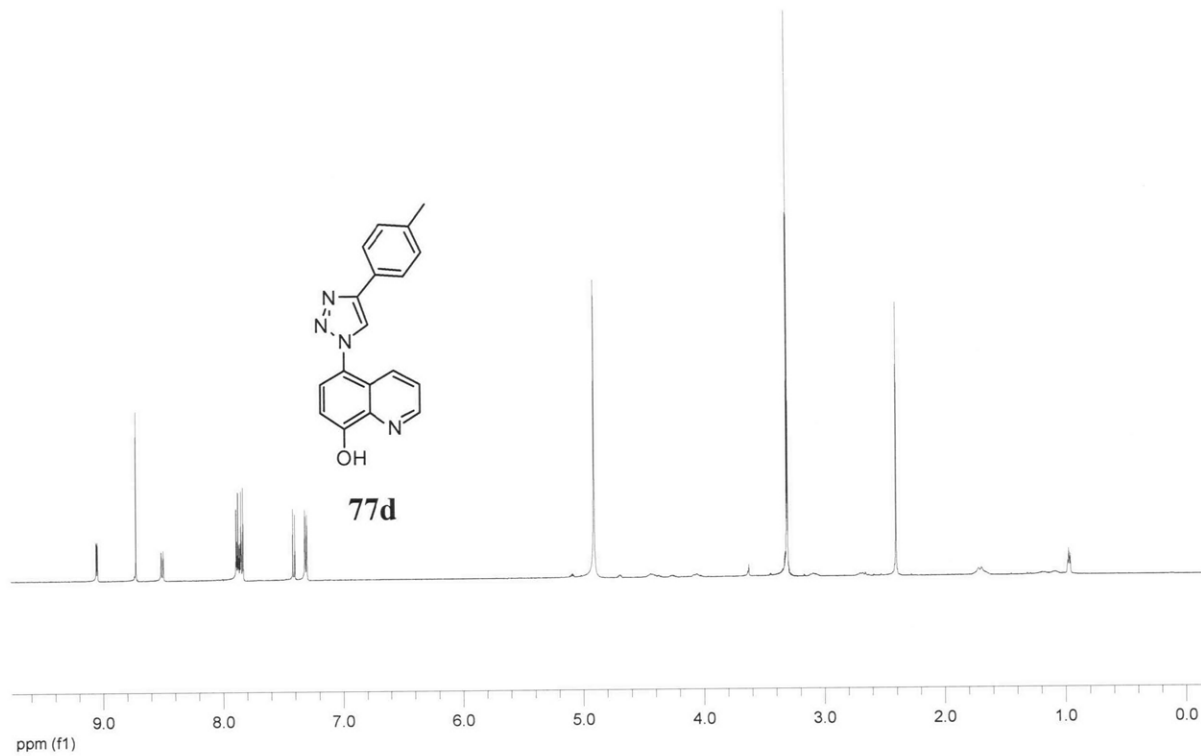


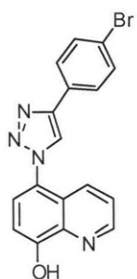
77b



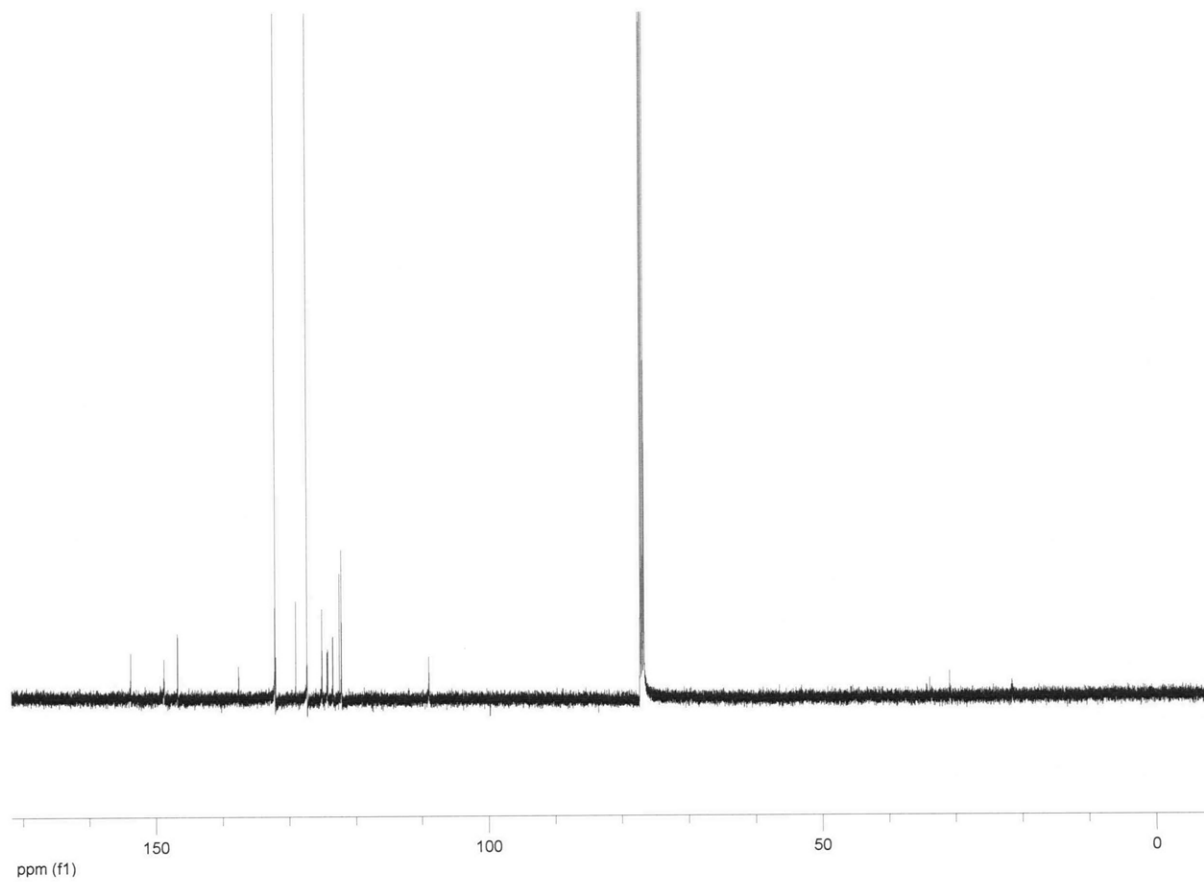
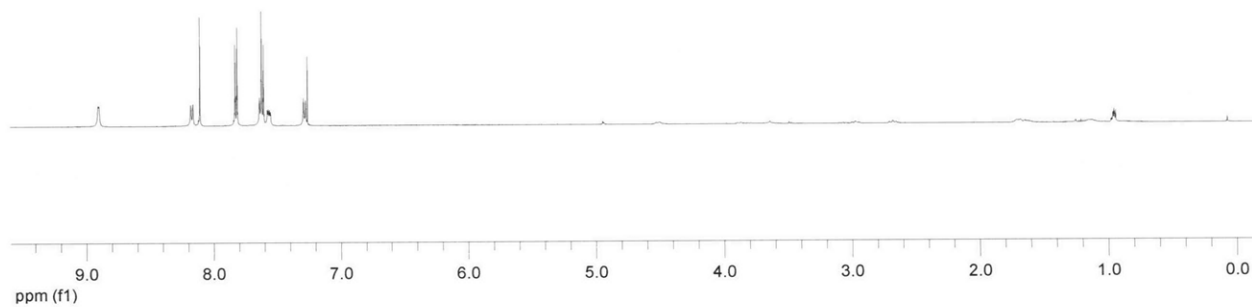








77u



References

1. Shults, M. D.; Imperiali, B. Versatile Fluorescence Probes of Protein Kinase Activity. *J. Am. Chem. Soc.* **2003**, *125*, 14248-14249.
2. Shults, M. D.; Carrico-Moniz, D.; Imperiali, B. Optimal Sox-based fluorescent chemosensor design for serine/threonine protein kinases. *Anal. Biochem.* **2006**, *352*, 198-207.
3. Lukovic, E.; Gonzalez-Vera, J. A.; Imperiali, B. Recognition-domain focused chemosensors: Versatile and efficient reporters of protein kinase activity. *J. Am. Chem. Soc.* **2008**, *130*, 12821-12827.
4. Shults, M. D.; Janes, K. A.; Lauffenburger, D. A.; Imperiali, B. A multiplexed homogeneous fluorescence-based assay for protein kinase activity in cell lysates. *Nat. Methods* **2005**, *2*, 277-283.
5. Lukovic, E.; Taylor, E. V.; Imperiali, B. Monitoring Protein Kinases in Cellular Media with Highly Selective Chimeric Reporters. *Angew. Chem. Int. Ed. Engl.* **2009**, Accepted.
6. Tsien, R. Y. New calcium indicators and buffers with high selectivity against magnesium and protons: design, synthesis, and properties of prototype structures. *Biochemistry* **1980**, *19*, 2396-2404.
7. Seitz, W. R. Fluorescence Derivatization. *CRC Cr. Rev. Anal. Chem.* **1980**, *8*, 367-405.
8. Goldman, M.; Wehry, E. L. Environmental effects upon fluorescence of 5- and 8-hydroxyquinoline. *Anal. Chem.* **1970**, *42*, 1178-1185.
9. Bardez, E.; Devol, I.; Larrey, B.; Valeur, B. Excited-state processes in 8-hydroxyquinoline: Photoinduced tautomerization and solvation effects. *J. Phys. Chem. B* **1997**, *101*, 7786-7793.
10. Bronson, R. T.; Montalti, M.; Prodi, L.; Zaccheroni, N.; Lamb, R. D.; Dalley, N. K.; Izatt, R. M.; Bradshaw, J. S.; Savage, P. B. Origins of 'on-off' fluorescent behavior of 8-hydroxyquinoline containing chemosensors. *Tetrahedron* **2004**, *60*, 11139-11144.
11. Walkup, G. K.; Imperiali, B. Stereoselective synthesis of fluorescent alpha-amino acids containing oxine (8-hydroxyquinoline) and their peptide incorporation in chemosensors for divalent zinc. *J. Org. Chem.* **1998**, *63*, 6727-6731.
12. Jotterand, N.; Pearce, D. A.; Imperiali, B. Asymmetric synthesis of a new 8-hydroxyquinoline-derived alpha-amino acid and its incorporation in a peptidylsensor for divalent zinc. *J. Org. Chem.* **2001**, *66*, 3224-3228.
13. Pearce, D. A.; Jotterand, N.; Carrico, I. S.; Imperiali, B. Derivatives of 8-hydroxy-2-methylquinoline are powerful prototypes for zinc sensors in biological systems. *J. Am. Chem. Soc.* **2001**, *123*, 5160-5161.
14. Shults, M. D.; Pearce, D. A.; Imperiali, B. Modular and Tunable Chemosensor Scaffold for Divalent Zinc. *J. Am. Chem. Soc.* **2003**, *125*, 10591-10597.
15. Perez-Bolivar, C.; Montes, V. A.; Anzenbacher, P., Jr. True blue: blue-emitting aluminum(III) quinolinolate complexes. *Inorg. Chem.* **2006**, *45*, 9610-9612.
16. Palacios, M. A.; Wang, Z.; Montes, V. A.; Zyryanov, G. V.; Anzenbacher, P., Jr. Rational design of a minimal size sensor array for metal ion detection. *J Am Chem Soc* **2008**, *130*, 10307-14.
17. Montes, V. A.; Pohl, R.; Shinar, J.; Anzenbacher, P., Jr. Effective manipulation of the electronic effects and its influence on the emission of 5-substituted tris(8-quinolinolate) aluminum(III) complexes. *Chem. Eur. J.* **2006**, *12*, 4523-4535.

18. Pohl, R.; Montes, V. A.; Shinar, J.; Anzenbacher, P., Jr. Red-green-blue emission from tris(5-aryl-8-quinolinolate)Al(III) complexes. *J. Org. Chem.* **2004**, *69*, 1723-1725.
19. Ghedini, M.; La Deda, M.; Aiello, L.; Grisolia, A. Fine-tuning the luminescent properties of metal-chelating 8-hydroxyquinolines through amido substituents in 5-position. *Inorg. Chim. Acta* **2004**, *357*, 33-40.
20. Rostovtsev, V. V.; Green, L. G.; Fokin, V. V.; Sharpless, K. B. A stepwise Huisgen cycloaddition process: copper(I)-catalyzed regioselective "ligation" of azides and terminal alkynes. *Angew. Chem. Int. Ed. Engl.* **2002**, *41*, 2596-2599.
21. Bergstrom, F. W. Heterocyclic N compounds. IIA. Hexacyclic compounds: pyridine, quinoline and isoquinoline. *Chem. Rev.* **1944**, *35*, 77-277.
22. Manske, R. H. F.; Kulka, M. The Skraup synthesis of quinolines. *Org. React.* **1953**, *7*, 59-98.
23. Kitamura, M.; Yoshida, M.; Kikuchi, T.; Narasaka, K. Synthesis of quinolines and 2H-dihydropyrroles by nucleophilic substitution at the nitrogen atom of oxime derivatives. *Synthesis* **2003**, 2415-2426.
24. Kusama, H.; Yamashita, Y.; Narasaka, K. Synthesis of Quinolines via Intramolecular Cyclization of Benzylacetone Oxime Derivatives Catalyzed with Tetrabutylammonium Perrhenate(VII) and Trifluoromethanesulfonic Acid. *Chem. Lett.* **1995**, 5-6.
25. Kusama, H.; Uchiyama, K.; Yamashita, Y.; Narasaka, K. Synthesis of Azaspirodienones via Intramolecular Cyclization of p-Hydroxybenzylactone Oximes and Their Transformation into Quinolines. *Chem. Lett.* **1995**, 715-716.
26. Kusama, H.; Yamashita, Y.; Uchiyama, K.; Narasaka, K. Transformation of oximes of phenethyl ketone derivatives to quinolines and azaspirotrienones catalyzed by tetrabutylammonium perrhenate and trifluoromethanesulfonic acid. *Bull. Chem. Soc. Jpn.* **1997**, *70*, 965-975.
27. West, A. P.; Vanengen, D.; Pascal, R. A. Attempted synthesis of a 1,2,3,4-tetraphenylfluoreno[1,9-gh]quinoline. *J. Org. Chem.* **1992**, *57*, 784-786.
28. Manske, R. H. F. The chemistry of quinolines. *Chem. Rev.* **1942**, *30*, 113-144.
29. Cheng, C. C.; Yan, S. J. The Friedlander synthesis of quinolines. *Org. React.* **1982**, *28*, 37-201.
30. Sivakumar, K.; Xie, F.; Cash, B. M.; Long, S.; Barnhill, H. N.; Wang, Q. A fluorogenic 1,3-dipolar cycloaddition reaction of 3-azidocoumarins and acetylenes. *Org. Lett.* **2004**, *6*, 4603-4606.
31. Sawa, M.; Hsu, T. L.; Itoh, T.; Sugiyama, M.; Hanson, S. R.; Vogt, P. K.; Wong, C. H. Glycoproteomic probes for fluorescent imaging of fucosylated glycans in vivo. *Proc. Natl. Acad. Sci. U.S.A.* **2006**, *103*, 12371-12376.
32. Kolb, H. C.; Finn, M. G.; Sharpless, K. B. Click chemistry: Diverse chemical function from a few good reactions. *Angew. Chem. Int. Ed.* **2001**, *40*, 2004-2021.
33. Dunkin, I. R.; ElAyeb, A. A.; Gallivan, S. L.; Lynch, M. A. 4H-Azepin-4-ones from 4-azidophenols in low-temperature matrices. *J. Chem. Soc., Perkin Trans. 2* **1997**, 1419-1427.
34. Roux, P. P.; Blenis, J. ERK and p38 MAPK-activated protein kinases: a family of protein kinases with diverse biological functions. *Microbiol. Mol. Biol. Rev.* **2004**, *68*, 320-44.
35. Martin, G. S. The hunting of the Src. *Nat. Rev. Mol. Cell Biol.* **2001**, *2*, 467-475.
36. Frame, M. C. Src in cancer: deregulation and consequences for cell behaviour. *Biochim. Biophys. Acta* **2002**, *1602*, 114-130.

37. Schlessinger, J. New roles for Src kinases in control of cell survival and angiogenesis. *Cell* **2000**, 100, 293-296.
38. Gershon, H.; McNeil, M. W. 5- and 7-Substituted 2-Methyl-8-quinolinols. *J. Heterocycl. Chem.* **1972**, 9, 659-667.
39. Gonzalez-Vera, J. A.; Lukovic, E.; Imperiali, B. A rapid method for generation of selective Sox-based chemosensors of Ser/Thr kinases using combinatorial peptide libraries. *Bioorg. Med. Chem. Lett.* **2009**, 19, 1258-1260.
40. Still, W. C.; Kahn, M.; Mitra, A. Rapid Chromatographic Technique for Preparative Separations with Moderate Resolution. *J. Org. Chem.* **1978**, 43, 2923-2925.
41. Fiedler, H. Synthesis of methyl-8-hydroxyquinoline aldehydes. *Arch. Pharm.* **1960**, 293/65, 609-621.
42. Manecke, G.; Aurich, H. P. *Makromol. Chem.* **1970**, 133, 83-100.
43. Zouhiri, F.; Danet, M.; Benard, C.; Normand-Bayle, M.; Mouscadet, J. F.; Leh, H.; Thomas, C. M.; Mbemba, G.; d'Angelo, J.; Desmaele, D. HIV-1 replication inhibitors of the styrylquinoline class: introduction of an additional carboxyl group at the C-5 position of the quinoline. *Tetrahedron Lett.* **2005**, 46, 2201-2205.
44. Sharma, P. K.; Khanna, R. N. Photo-Fries Rearrangement - Rearrangement of Benzoyloxy Compounds. *Monatsh. Chem.* **1985**, 116, 353-356.

Curriculum Vitae
for
ELVEDIN LUKOVIĆ
Department of Chemistry, 18-544
Massachusetts Institute of Technology
77 Massachusetts Ave.
Cambridge, MA 02139
Tel: 617-452-2826
elvedin@mit.edu

Education

- 2009 Ph.D. Organic Chemistry
 Massachusetts Institute of Technology, Cambridge, MA
- 2002 B.A. Chemistry with a Concentration in Biochemistry (Honors)
 Haverford College, Haverford, PA

Research Experience

- 2003-2009 **Massachusetts Institute of Technology**, Cambridge, MA
 Graduate Research Assistant
 Thesis Title: Development of Selective Peptide- and Protein-Based Reporters of
 Kinase Activity Utilizing Chelation-Enhanced Fluorescence
 Advisor: Professor Barbara Imperiali
- 2002-2003 **Massachusetts Institute of Technology**, Cambridge, MA
 Research Assistant
 Title: Development of Lanthanide Binding Tags (LBTs)
 Advisor: Professor Barbara Imperiali
- 2001-2002 **Haverford College**, Haverford, PA
 HHMI Research Fellow
 Thesis Title: Synthesis of Tethered Alamethicin Ion Channels
 Advisor: Professor Karin Åkerfeldt
- 2000 **Haverford College**, Haverford, PA
 Summer Research Fellow
 Title: Toward the Synthesis of Ripostatin A
 Advisor: Professor Fran Blase

Awards and Fellowships

- 2008 Morse Travel Grant, Massachusetts Institute of Technology
2005-2006 Cancer Training Grant Fellow, Massachusetts Institute of Technology
2003-2004 Chemistry Department Award for Outstanding Teaching by a Graduate Student, Massachusetts Institute of Technology
2003 Honorable Mention for a Predoctoral Fellowship, National Science Foundation
2002 The Colin MacKay Award; Academic Honor Roll, Haverford College
2001-2002 Howard Hughes Medical Institute Interdisciplinary Scholar, Haverford College

Publications

- 2009 González-Vera, J. A.; Luković, E.; Imperiali, B. Synthesis of Red-Shifted 8-Hydroxyquinoline Derivatives Using Click Chemistry and Their Incorporation into Phosphorylation Chemosensors. *J. Org. Chem.* **2009**, in press.
- 2009 Luković, E.; Vogel Taylor, E.; Imperiali, B. Monitoring Protein Kinases in Cellular Media with Highly Selective Chimeric Reporters. *Angew. Chem. Int. Ed. Engl.* **2009**, in press.
- 2009 González-Vera, J. A.; Luković, E.; Imperiali, B. A Rapid Method for Generation of Selective Sox-Based Chemosensors of Ser/Thr Kinases Using Combinatorial Peptide Libraries. *Bioorg. Med. Chem. Lett.* **2009**, *19*, 1258-1260.
- 2008 Luković, E.; González-Vera, J. A.; Imperiali, B. Recognition-Domain Focused Chemosensors: Versatile and Efficient Reporters of Protein Kinases Activity. *J. Am. Chem. Soc.* **2008**, *130*, 12821-12927.

Patents

- 2006 Imperiali, B.; Luković, E.; Carrico-Moniz, D. Sox-Based Kinase Sensors. U.S. Patent Application Filed August 16, 2006.

Presentations

- 2007 E. Luković, B. Imperiali. Development and Application of the Branched Sox-Based Peptides as Fluorescent Kinase Activity Reporters. 234th National ACS Meeting: Boston, MA, U.S.A.
- 2003 E. Luković, A. Wassner, J. Hurt, A. Woolley, V. Borissenko, K. Åkerfeldt. Tethered Alamethicin Channels. The Fifth European Symposium of the Protein Society: Florence, Italy.
- 2002 E. Luković, A. Wassner, J. Hurt, J. Lear, K. Åkerfeldt, Templated Alamethicin Ion Channels. The Lise Meitner Symposium, Lund University: Lund, Sweden.
- 2001 E. Luković, A. Wassner, J. Hurt, J. Lear, K. Åkerfeldt, Tetrameric Alamethicin Channels. The Protein Society 15th Symposium: Philadelphia, PA, U.S.A.

Teaching Experience

Department of Chemistry, Massachusetts Institute of Technology

2005 Teaching Assistant, Bioorganic Chemistry 5.55

2004 Teaching Assistant, Organic Chemistry 5.12

2003 Teaching Assistant, General Chemistry 5.111

Department of Chemistry, Haverford College

1999-2002 Chemistry Question Center Tutor

2000-2001 Laboratory Assistant, Organic Chemistry and General Chemistry

Future Plans

2009- Medical Student at **SUNY Downstate College of Medicine**, Brooklyn, NY